CARBON-CARBON BOND FORMATION REACTIONS USING SOLID POROUS CATALYSTS

A THESIS

SUBMITTED TO THE

UNIVERSITY OF PUNE

FOR THE DEGREE OF

DOCTOR OF PHILOSOPHY

IN

CHEMISTRY

BY

PRANJAL KALITA

Dr. RAJIV KUMAR
(RESEARCH GUIDE)

CATALYSIS DIVISION
NATIONAL CHEMICAL LABORATORY
PUNE 411 008
INDIA

OCTOBER 2007

डॉ. राजीव कुमार

उपनिदेशक

प्रमुख,उत्प्रेरक एवम् अकार्बनिक रसायन प्रभाग

Dr. Rajiv Kumar
Deputy Director
Head, Catalysis & Inorganic Chemistry Division

DECLARATION BY RESEARCH SUPERVISOR

Certified that the work incorporated in the thesis entitled: "**CARBON-CARBON BOND FORMATION REACTIONS USING SOLID POROUS CATALYSTS**", submitted by Mr. Pranjal Kalita, for the Degree of *Doctor of Philosophy*, was carried out by the candidate under my supervision at Catalysis Division, National Chemical Laboratory, Pune 411008, India. Such material as has been obtained from other sources has been duly acknowledged in the thesis.

Dr. Rajiv Kumar   Date:

(Research Guide)   Place: Pune

Tel. : 91 - 20 - 2590 2631 / 2590 2009   E-mail : r.kumar@ncl.res.in   Resi.: 91 - 20 - 27293074
(D) : 91 - 20 - 2590 2762   Web   : www.ncl-india.org
Fax : 91 - 20 - 2590 2633 / 2590 2634

DECLARATION BY RESEARCH SCHOLAR

I hereby declare that the thesis entitled "**CARBON-CARBON BOND FORMATION REACTIONS USING SOLID POROUS CATALYSTS**", submitted for the Degree of *Doctor of Philosophy* to the University of Pune, has been carried out by me at Catalysis Division, National Chemical Laboratory, Pune 411 008, India, under the supervision of Dr. Rajiv Kumar. The work is original and has not been submitted in part or full by me for any other degree or diploma to this or any other University.

Pranjal Kalita   Date:

(Research Scholar)   Place: Pune

Dedicated to MY

Mother

&

Late Father

ACKNOWLEDGEMENTS

Baag, Dr. Subramaniyam, Dr. Mukulesh, Dr. Anirban, Dr. Dhananjoy and all other research scholars for such a friendly and cheerful working atmosphere, for their constant support, love and care throughout my stay in NCL.

I should not forget my beloved friends- Sanjeev, Innamul, Rahul, Bichitra, Biva, Dr.(Mrs) Gitanjali, Dr. Manoj, Rupak, Dr. Himadri, Dhruba, Trailokya, Dr. Dignata da, Dr. Kaktai da, Maumita, Purabi, Dr.(Mrs) Smriti, Sanchay, Gautam, Bhanita, Dr. Rabin, Dr. Balen da, Debojit, Rupankar for their individual support during my carrier.

It gives me immense pleasure to thank Dr. Manash, Dr. Sasank, Dr. Jadav, Dr. Arindam, Dr. Pranjal, Sanjiv, Khirud, Lakshi, Diganta, Rahul, Ankur, Upendra, Sofia, Gitali, Pankaj, Anshuman, Ananta, Dr. Siddtharth, for their direct and indirect contributions in my personal and professional life during tenure in NCL.

I take this opportunity to express my earnest respect to my teachers throughout my carrier, Dr. D. C. Deka, Department of Chemistry, Gauhati University, who is the key inspiration and help to build up my research career in science.

I am very much grateful to my eldest brother in law because of whom I am here today. Not only he, obviously my enormous mother who had shown finger print power to stand in the earth. Of course my admiration also goes to sisters-Sashi ba, Swarna ba, Dulu ba, Mamani ba, high opinion brothers-Bapa da, Gautam da, deference brother in laws-Ananta, Bhupen, Chitraranjan, sister in law-Dangar bau, and finally my esteem unforgettable cousins, nephews, nieces—Sona, Hiya, Lucky, Jupi, Neha, Raaj, Silpi and Babu, for their love, understanding and encouragement throughout my life. Their blessings and encouragement have always made me an optimist in any unknown areas I had ventured.

Finally, my thanks are due to Council of Scientific and Industrial Research, Government of India, for awarding the junior and senior research fellowships and Dr. S. Sivaram, Director, and Dr. B. D. Kulkarni, Deputy Director, National Chemical Laboratory to carry out my research works, extending all infrastructural facilities and to submit this work in the form of a thesis for the award of Ph. D degree.

October 2007   Pranjal Kalita

Table of Contents

BENZYLATION REACTION

Abbreviations

AAS	Atomic Absorption Spectrometry
BA	Benzyl Alcohol
BC	Benzyl Chloride
BET	Brunauer-Emmett-Teller
BJH	Barret-Joyner-Halenda
BMBB	1-Benzyl-3-(4-methyl benzyl) Benzene
Conv.	Conversion
CP MAS NMR	Cross Polarization Magic Angle Spinning Nuclear Magnetic Resonance
CTMABr	Cetyltrimethylammonium Bromide
DBE	Dibenzyl Ether
DCM	Dichloromethane
DMF	N, N-Dimethylformamide
EPR	Electron Paramagnetic Resonance
FID	Flame Ionization Detector
FTIR	Fourier Transform Infrared
FSM	Folded Sheet Materials
GC	Gas Chromatography
GC-MS	Gas Chromatography-Mass Spectrometry
HCl	Hydrochloric Acid
HMS	Hexagonal Mesoporous Silica
HRTEM	High-Resolution Transmission Electron Microscopy
K	Kelvin
LCT	Liquid Crystal Template
LLC	Lyotropic Liquid Crystals
MeCN	Acetonitrile
MDPM	Methyldiphenylmethane
MPBA	Methylphenylbenzyl Alcohol
MPBC	Methylphenylbenzyl Chloride
$MeNO_2$	Nitromethane
MS41	Family of Mesoporous Materials

Na$_2$SO$_4$	Sodium Sulphate
P123	Poly(ethylene glycol)-block-poly(propylene glycol)- poly(ethylene glycol)
PXRD	Powder X-Ray Diffraction
SBA	Santa Barbara Amorphous
SEM	Scanning Electron Microscopy
SLC	Silicatropic Liquid Crystal
TBD	1,5,7-Triazabicyclo[4.4.0] dec-5-ene
TCD	Thermal Conductivity Detector
TEM	Transmission Electron Microscopy
TEOS	Tetraethyl Orthosilicate
TFA	Trifluoromethanesulfonic Acid
THF	Tetrahydrofuran
TLC	Thin Layer Chromatrography
TMAOH	Tetramethylammonium Hydroxide
TON	Turn Over Number
TPD	Temperature Programmed Desorption
UV-Vis	Ultraviolet-visible
XPS	X-ray Photoelectron Spectroscopy
Zr(OC$_4$H$_9$)$_4$	Zirconium (IV) Butoxide
Zr-TMS	Zirconium Based Transition Metal Oxide Mesoporous Molecular Sieves

<div style="border: 2px solid black; padding: 20px; text-align: center;">

CHAPTER 1

INTRODUCTION AND LITERATURE SURVEY

</div>

1.1 ZEOLITES AND MESOPOROUS MATERIALS

Zeolites are microporous crystalline aluminosilicates consist of silicon (Si), aluminum (Al) and oxygen (O), where Si and Al are tetrahedrally coordinated through oxygen in a three-dimensional open network.[1,2] These intersesting materials have definite crystalline structure with uniform cavities and pores.[1] Zeolites posses regular, well-defined microporous channel structures with high surface area (as high 700 m^2/g) and tunable adsorption capacity.

The various features of zeolites and related materials, such as (i) shape-selectivities (product, reactant and transition state),[3] (ii) the relative high chemical and thermal stabilities and (iii) strong acidity, make these materials as attractive solid catalysts for oil refining, petrochemistry and in the production of fine chemicals. Furthermore, microporous zeolitic materials have earned the reputation of environmentally benign catalysts due to several factors like waste minimization, simple operation, easy work-up and regenerability of the catalysts.[4] However, the main restriction of microporous zeolitic materials is the size constraints of ca. 0.75nm and therefore not suitable for catalytic transformations involving organic molecules having kinetic diameters above 0.75nm.

The synthesis of mesoporous molecular sieves called M41S is one of the most exciting discoveries in the field of materials synthesis.[5] The discovery of hexagoanally ordered mesoporous silicate structures by Mobil Corporation (M41S materials) and by Kuroda et al. (FSM-16 materials) pioneered a new era in material science.[5] These materials possess extremely high surface areas and easily accessible, well-defined mesopores, which broke pore size constraint of microporous zeolites. The M41S family is classified into three members: MCM-41, MCM-48 and MCM-50, with hexagonal 'honeycomb', cubic 'gyroid' and lamellar structures, respectively.[5-7]

Recently, neutral nonionic surfactants (block copolymers) were used as templates to prepare mesoporous materials with large pores (HMS, SBA-11, -12, -15, -16 and FDU-1, -2, -5, etc.)[8-14] through hydrogen bonding or electrostatic interactions. The use of anionic surfactants produced only lamellar or disordered silica based mesophases. The synthesis of these materials opens new possibilities for preparing catalysts with uniform pores in the mesoporous region, which will allow the access to relatively larger organic molecules for catalytic transformations.[15]

1.2. SYNTHESIS AND MECHANISM OF FORMATION OF MESOPOROUS MATERIALS

The M41S family of mesoporous materials is synthesized using a silica source and different organic structure directing agents, *e.g.*, cationic surfactants containing long alkyl chain (10-20 carbons) quaternary ammonium compounds, often followed with addition of co-surfactants. The different phases of M41S mesoporous materials were found depending upon the various synthesis parameters such as surfactant / silica molar ratio, silica source (tetraethyl orthosilicate, fumed silca), cetyltrimethylammonium ($C_{16}TMA^+$) cations and water.[16]

A number of models have been proposed to rationalize the mechanism of formation of mesoporous materials by various synthesis routes. All these models are based on the role of surfactants in solution to direct the formation of silicate mesostructure. In solution, the surfactants have a hydrophilic head group and a long chain hydrophobic tail group within the same molecule, which will aggregate and self-organize in such a way so as to minimize the contact between the incompatible ends. Different mechanisms of formation of mesoporous materials, postulated taking into consideration different types of interaction between the surfactant and the inorganic precursor under different synthesis conditions, are discussed briefly below.

1.2.1. Liquid Crystal Templating (LCT) Mechanism

The Mobil researchers proposed two synthesis mechanisms.[5,17] In the first route, the $C_nH_{2n+1}(CH_3)_3N^+$ surfactant species organize into lyotropic liquid crystal (LLC) phase, which can serve as template for the formation of hexagonal MCM-41 structure. Firstly, the surfactant micelles aggregate into a hexagonal array of rods, followed by interaction of silicate or aluminate anions present in the reaction mixture with the surfactant cationic head groups. Thereafter condensation of the silicate species occurs leading to the formation of an inorganic polymeric species. After combusting off the surfactant template by calcination, hexagonally arranged inorganic hollow cylinders are produced (Scheme 1.1). However, the drawbacks of this synthesis pathway was pointed out by Cheng *et al.*,[18] according to whom the hexagonal liquid-crystal phase does not form below 40 % of surfactant concentration. It is known that MCM-41 may be formed at low surfactant concentrations (1 wt %) with respect to water content, and *in situ* [14]N NMR spectra indicated that the hexagonal liquid-crystalline phase was not present anytime during formation of MCM-41.[19]
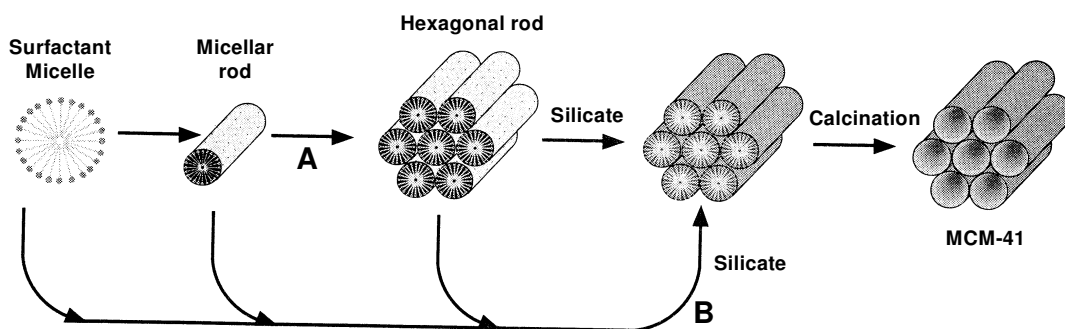
Scheme 1.1. Liquid crystal templating (LCT) mechanism proposed for the formation of MCM-41; (A) liquid crystal phase initiated and (B) silicate anion initiated. **[Source: Ref. 5b]**

In the second route, the hexagonal ordering is initiated by the presence of silicate species in the reaction mixture.[5a,b] Chen *et al.* explained that randomly distributed surfactant micelles with rod-like morphology are formed initially, and their interaction with silicate oligomers generate randomly oriented surfactant micelles surrounded by two or three silica monolayers.[19] The presence of rod-like micelles in solution was supported by isotropic *in situ* [14]N NMR.[19] Further condensation between silicate species on adjacent rods occurs on heating, initiating the long-range hexagonal ordering (Scheme 1.2).
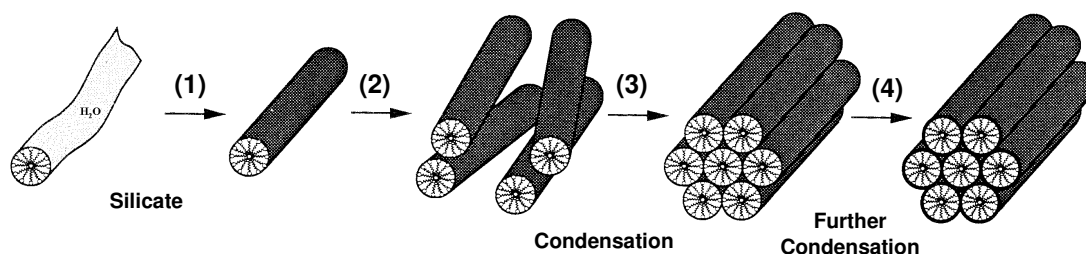
Scheme 1.2. Silicate rod assembly proposed for the formation of MCM-41; (1) and (2) random ordering of rod-like micelles and interaction with silicate species, (3) spontaneous packing of the rods, and (4) remaining condensation of silicate species on further heating. **[Source: Ref. 19]**

1.2.2. Charge Density Matching

The charge density matching model proposed by Stucky *et al.* suggested that condensation occurs between initially formed silicate species by the electrostatic interaction between the anionic silicates and the cationic surfactant head groups.[20] This eventually reduces the charge density and therefore, curvature was introduced into the layers to maintain the charge density balance with the surfactant head groups, which leads to transformation of the lamellar mesostructure into the hexagonal one

(Scheme 1.3.A). Although, this silica-initiated synthesis mechanism has been widely accepted, the presence of an intermediate lamellar species has been disputed.
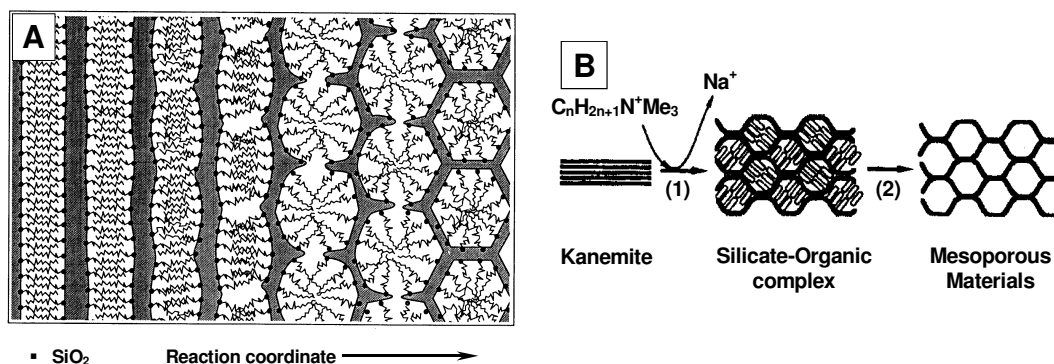
Scheme 1.3. Transformation of surfactant-silicate systems from lamellar to hexagonal mesophases; (A) hexagonal mesophase obtained by charge density matching, and (B) folding of kanemite silicate sheets around intercalated surfactant molecules. **[Source: Refs. 20 and 5d]**

1.2.3. Folded Sheet Mechanism

The "folded-sheet mechanism" postulated by Inagaki *et al*. indicated the presence of intercalated silicate phases in the synthesis medium of the reaction products (Scheme 1.3.B).[5d] The flexible silicate layers of kanemite fold around the surfactant cations, and cross-linking of the interlayer occurs by condensation of silanol groups on adjacent silicate sheets. On increase of pH, the amount of occluded $C_nH_{2n+1}(CH_3)_3N^+$ cations in kanemite increases resulting in expansion of the kanemite interlayers to form another class of regular hexagonal structure called FSM-16.

1.2.4. Silicatropic Liquid Crystals

Firouzi *et al*. have developed a model based on cooperative organization of inorganic and organic molecular species into 3D structured arrays.[21] According to this model, the physicochemical properties of a particular system were not determined by the organic arrays having long-range preorganized order, but by the dynamic interplay

among ion-pair inorganic and organic species, so that different phases can readily be obtained through small variation of controllable synthesis parameters. The exchange of silicate anions with the surfactant halide counter ions formed the "silicatropic liquid crystal" (SLC) phase (Scheme 1.4), which exhibited very similar behavior to that of typical lyotropic systems and finally condensed irreversibly into MCM-41.

1.2.5. Generalized Liquid Crystal Templating Mechanism

1.2.5.1. Ionic Route (Electrostatic Interaction)

Huo *et al*. proposed a generalized mechanism for the formation of mesostructures, which was based on specific types of electrostatic interaction between an inorganic precursor (I) and a surfactant head group (S).[22] In this concept, four different approaches were proposed to synthesize transition metal oxide mesostructures.[22a] The first route involves the charge density matching between surfactant cations and inorganic anions (S^+I^-). The second route deals with the charge-reversed situation, *i.e.*, anionic surfactant and cationic inorganic species (S^-I^+). Both, the third and the fourth routes are counterion-mediated pathways. The third one demonstrates the assembly of cationic species *via* halide ions ($S^-X^+I^-$), while the fourth one depicts the assembly of anionic species *via* alkali metal ions ($S^+X^-I^+$). These synthesis strategies are acceptable for the formation of a wide variety of hexagonal, cubic or lamellar, mesophases. However, a general problem encountered very often is the poor stability of the inorganic framework, which frequently collapses after removal of the surfactant.
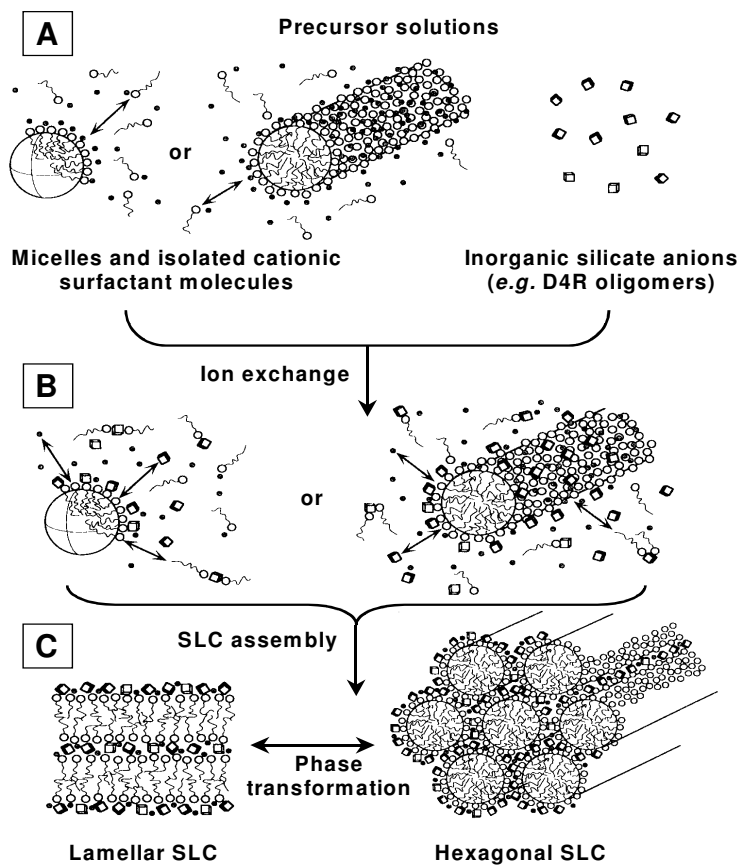
Scheme 1.4. Cooperative organization for the formation of silicatropic liquid crystal phase / silicate-surfactant mesophases; (A) organic and inorganic precursor solutions, (B) preliminary interaction of the two precursor solutions after mixing, and (C) multidentate interaction of the oligomeric silicate units with the surfactant molecules. **[Source: Ref. 21]**

1.2.5.2. Neutral Templating Route (Hydrogen Bonding Interaction)

Tanev and Pinnavaia proposed another route to synthesize hexagonal mesoporous silicas (HMS) having thicker pore walls, high thermal stability and smaller crystallite size but having higher amounts of interparticle mesoporosity and lower degree of long-range ordering of pores than MCM-41 materials.[8,23] This route is essentially based on hydrogen bonding between neutral primary amines (S^0) and

neutral inorganic precursors (I^0), wherein hydrolysis of tetraethyl orthosilicate (TEOS) in an aqueous solution of dodecylamine yields neutral inorganic precursor. Using the same approach, porous lamellar silicas with vesicular particle morphology have been synthesized with the aid of double headed alkylamines linked by a hydrophobic alkyl chain (α,ω-dialkylamine).[23b]

1.2.5.3. Ligand-Assisted Templating Route (Covalent Interaction)

Antonelli and Ying have proposed a ligand-assisted templating mechanism for the synthesis of hexagonally packed mesoporous metal oxide completely stable to surfactant removal.[24] In a typical synthesis, the surfactant was dissolved in the metal alkoxide precursor before addition of water to allow nitrogen–metal covalent bond formation between the surfactant head group and the metal alkoxide precursor. The existence of this covalent interaction was confirmed by ^{14}N NMR spectroscopic studies. In this approach, the structure of the mesophases could be controlled by adjustment of the metal / surfactant ratio, which led to a new class of mesoporous transition metal oxides analogous to M41S family.

1.3. METAL-SUBSTITUTED MESOPOROUS MOLECULAR SIEVES

In order to generate potential catalytic activities, the incorporation of heteroatoms into the inert silica framework or walls of pure siliceous mesoporous materials is an important route to modify the nature of the framework and make them catalytically active. The advantages of using ordered mesoporous solids in catalysis are due to their relatively large pores, which facilitate mass transfer, and the very high surface area, which allows a high concentration of active sites per unit mass of material.[25] In fact, the initial catalytic studies with mesoporous molecular sieves were focused on metal-substituted MCM-41 materials for mainly acid catalyzed and oxidation reactions.[25]

Modification of the framework composition of mesoporous materials can be done either by the direct synthesis or through post synthesis method. It is well reported that a variety of heteroatoms are incorporated into the pore channels of mesoporous supports. The incorporation of trivalent metal ions such as Al,[26] B,[27] Ga,[28] Fe,[29] *etc* in the silica frame-work produces negative charges that can be compensated by protons providing acid sites and hence serve as important materials in acid catalysis. The substitution of various transition metals like Ti,[30] V,[31] Cr,[32] Mn,[33] Co,[34] Sn,[35] Mo,[36] Zr,[37] and lanthanide metal like Ce[38] can be incorporated into the mesoporous materials, with important redox catalytic properties.

While, there are large numbers of reports on the incorporation of single hetero metal ion in mesoporous silica, relatively very few reports are available on simultaneous double incorporation of two or more hetero metals in such M41S materials. For instance, Ti, Co, Fe, Zn, Ni, Cr or Cu-containing Al-MCM-41 materials were prepared by direct synthesis method using cetyltrimethylammonium bromide as a surfactant.[38-41] These materials are catalytically active for carbon-carbon bond formation reactions such as Friedel-Crafts alkylation, Mukaiyama-Michael, Mukaiyama-aldol, oxidation reactions, hydroamination reaction.[38-41] Moreover, Ti and Al-containing hexagonal mesoporous silicas (Ti-Al-HMS) were prepared through a sol-gel reaction procedure using dodecylamine as a surfactant, catalytically active for gas-phase epoxidation of propylene by molecular oxygen.[42]

1.4. ORGANO FUNCTIONALIZED MESOPOROUS MATERIALS

In order to utilize the unique properties of the mesoporous material for specific applications in catalysis, sorption, *etc*, introduction of reactive organic functional groups, by the incorporation of organic components as part of the silicate walls to form organic-inorganic hybrid materials is quite important.[25,43] The advantages of

organic-inorganic hybrid materials arise from the fact that inorganic components can provide mechanical, thermal or structural stability, while the organic features can be readily modified for various specific applications.[44]

Through the development of organic-inorganic hybrid mesoporous solids, much progress has been made in the last few years towards their application in a variety of fields. Such mesoporous solids have been functionalized at precise sites and were demonstrated to exhibit improved activity and selectivity in a large number of catalytic reactions and sorption processes.[44a,45] The synthesis procedures of organic-inorganic hybrid materials, developed so far, effectively utilize the large amount of silanol groups resting on the surface of M41S related materials.[44] Another advantage of these materials is that the hydrophilic-hydrophobic properties can be tailored by the judicious choice of the organo alkoxy silanes.[15,46,47] The pore walls of mesoporous materials are easily modified with either purely inorganic or with hybrid, semiorganic functional groups and can be successfully used as catalysts for green chemistry.[44] Grafting method has been widely used in the field of catalysis for functionalization of surface hydroxyl groups as anchor points by organosilanes in silica network. Important applications of these modified and functionalized systems include selective heterogeneous catalysis and photocatalysis involving bulky grafted catalysts and / or the conversion of large substrates. The following section briefly highlights the possible ways of surface modifications over mesoporous materials for the formation of organic-inorganic hybrid mesoporous materials.

1.4.1. Post Synthesis Grafting Methods

In this method, the organic functional groups are introduced to the surface of mesoporous silica as the terminal groups of an organic monolayer by post synthesis modification of pre-synthesized mesoporous materials. This can be done usually after

removal of surfactant from the inorganic matrix (Scheme 1.5).[48] Mesoporous silicas possess high concentration of silanol groups (Si-OH) at the surface. These silanol groups are well-situated anchoring points for functionalization of organic group to the silica network.[49]
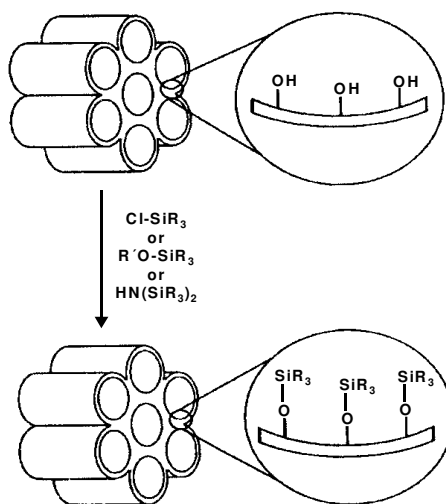
Scheme 1.5. Functionalization of inner walls of mesoporous silicates by grafting. **[Source: Ref. 45 d]**

1.4.1.1. Grafting with Passive Surface Groups

Organic functional groups with lower reactivity could be grafted to enhance the hydrophobicity of the surface and protecting the material towards hydrolysis. Further, the pore diameter of mesoporous materials can also be adjusted by varying the alkyl chain length of the silylating agent or by increasing the quantity of the silylating agent.[50] Surface modifications are generally carried out by using trimethyl chlorosilane (Me$_3$SiCl),[5d,51] trimethyl ethoxysilane (Me$_3$Si(OC$_2$H$_5$)) and hexamethyldisilazane [(Me$_3$Si)$_2$NH].[49,52] Out of these, hexamethyldisilazane was extensively used for functionalization of surface silanol groups to passivate the

surface silanols and also to depolarize the surface for selective adsorption experiments.[52a.b]

1.4.1.2. Grafting with Reactive Surface Groups

Grafting of the mesopore surfaces with reactive functional groups like olefin, cyanide, thiol, amine, halide, epoxide etc. permits functionalization of the surface. After modification of these materials with the desired functional groups, catalytically active homogenous transition metal complexes as well as organometallic complexes can be anchored over this organic-inorganic hybrid materials.[53]

1.4.1.3. Site-Selective Grafting

For grafting of organic functional groups, the external surface of the mesoporous materials is kinetically more accessible than the internal surface.[54] To minimize the grafting on the external surface, it is necessary to passivate the silanol groups on the external surface before functionalizing those on the internal surface.[54] Basically there are two approaches for selective external surface passivation as follows.

(i) In the first approach, external surface silanols of the mesoporous material are passivated with dichlorodiphenylsilane (Ph_2SiCl_2). There after, 3-aminopropyl triethoxy silane (3-APTS) can be grafted inside the channels. The high-resolution transmission electron microscopy (HRTEM) and FTIR spectroscopy were used to verify amine functional groups in the inner pore channels of MCM-41.[55]

(ii) In the second approach, grafting of Me_3SiCl was carried out predominantly at the external surface without removing the surfactants from the as-synthesized MCM-41 materials. In this case, surfactant was then removed by solvent extraction method, which resulted in the materials having free silanol groups predominantly inside the channels while the external surface silanol groups are passivated. The main

advantages of this method are that it reduced two-step synthesis procedure and that the grafting of reactive organic moieties predominantly occurs inside the channels.[56]

1.4.2. Direct co-condensation Method

Organo-functionalized mesoporous materials can be prepared by one-step co-condensation method between tetraalkoxy silanes ($Si(OR)_4$, R = Et, Me) with one or more organoalkoxy silanes (R-$Si(OR^1)_3$, R^1 = Et, Me), through the sol-gel process in the presence of a structure orientor and the auxillary chemicals.[57] Depending on the nature of the R groups, a variety of organofunctionalized mesoporous materials can be synthesized where organic moiety is attached covalently through Si-C bond on the surface of mesoporous material. The advantages of this method over the grafting procedures include the stability of the inorganic framework even at relatively higher organic loadings, homogenous distribution of the organic groups in the pore channels as well as the single step preparation procedures.[58] An acidic-alcohol mixture for solvent extraction is used to remove the occluded surfactants from the product to obtain the organofunctionalized ordered mesoporous material (Scheme 1.6).[58a,59] Since organic pendant groups are present in as-prepared materials along with surfactant, the surfactant can not be removed by calcination as it will also decompose the pendant organic moieties, thus defeating the purpose of organic functionalization of mesoporous silicas itself.
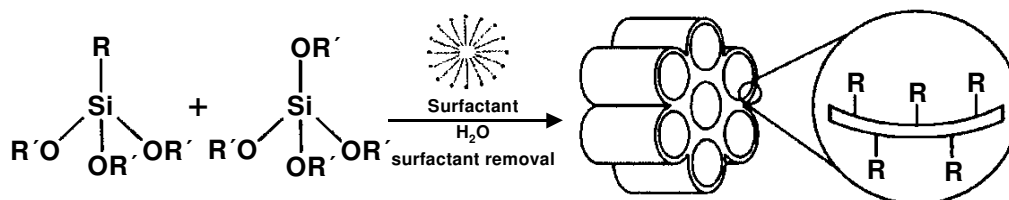
Scheme 1.6. Synthesis of organo-functionalized mesoporous silicates by co-condensation. **[Source: Ref. 45d]**

1.5. MESOPOROUS ZIRCONIA IN CATALYSIS

After the discovery of the MCM-41 materials, various researchers employed an idea of non-silica-based mesoporous oxide materials. For instance, the oxides of titanium,[60] zirconium,[61] niobium,[62] tantalum[63] aluminum,[64] hafnium,[65] tin,[66] and manganese[67] have been synthesized using ionic or neutral templates as structure directing agents. Although, most of them were comprised of mainly non-porous framework thereby limiting their effectiveness in catalytic applications. Stucky et al. then synthesized mesoporous metal oxides with a semi crystalline framework by block copolymer templating materials.[68]

The first zirconium-based mesoporous materials were synthesized by Hudson and Knowels using cationic surfactant as a template by adopting the scaffolding mechanism where the preparation of mesoporous zirconium (IV) oxide samples was obtained by surfactant exchanged hydrous zirconium (IV) oxide.[61a] The scaffolding mechanism was proposed by Ciesla et al.[61b,c] (Scheme 1.7) where they observed the formation of porous zirconium oxo phosphate by a surfactant-assisted synthesis, leading to zirconia compounds with high surface areas and regular pore systems. Here, either zirconium sulfate or zirconium propoxide were used as zirconia source with cationic surfactant to obtain sulfate containing material. Another approach was reported by Blin et al.[61d] for the synthesis of mesoporous zirconia where they used cationic surfactant and zirconyl chloride as zirconia source.

Hydrous zirconium (iv) oxide
exchanged with ammonium cations
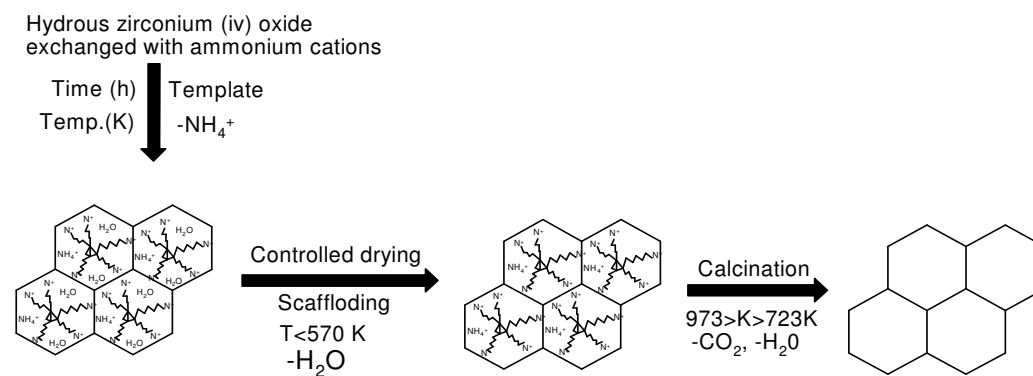
Time (h)   Template
Temp.(K)   -NH$_4$$^+$

Controlled drying

Scaffloding
T<570 K
-H$_2$O

Calcination

973>K>723K
-CO$_2$, -H$_2$0

Scheme 1.7. Synthesis of mesoporous zirconia using zirconium (IV) oxide with cationic surfactant via scaffolding mechanism. **[Source. Ref. 61a]**

Recently, Antonelli reported the synthesis and mechanistic studies of sulfated mesoporous zirconia with chelating carboxylate surfactants having long chain acid as surfactant (Scheme 1.8).[61e] Similarly, Wong and Ying reported mesostructured zirconium oxide prepared via amphiphilic templating mechanism with a variety of head groups (anionic and nonionic) and tail group chain lengths (1-18 carbons).[61f] They claimed the mesoporous material based on zirconia as Zr-TMS (zirconium oxide with a mesostructured framework) and in this thesis the same name is used. They further proposed two types of interaction between the surfactants and zirconium source (Scheme 1.9).

COOH $\xrightarrow[\text{-ROH}]{\text{Zr(OH)}_4}$ COOZr(OR)$_3$ $\xrightarrow[\text{2. MeOH/H}_2\text{ SO}_4]{\text{1. H}_2\text{ O/Heating}}$

Scheme 1.8. Synthetic strategy for mesoporous zirconia. In the first step the metal alkoxide is combined with the carboxylic acid prior to addition of water. After addition of water and aging form ambient to 423 K over several days the mesostructure is obtained. **[Source: Ref. 61e]**

Scheme 1.9. Representative schematic drawings of (A) the anionic amphiphile-zirconium n-propoxide interaction, and (B) the nonionic amphiphile-zirconium isopropoxide interaction. **[Source: Ref. 61f]**

The mesoporous sulfated zirconia synthesized by Larsen et al., is quite useful material as catalyst and catalyst support,[61g] where mesoporous zirconia was prepared through a template-assisted mechanism. After the formation of pore structure, the template is removed by extraction or calcination at 823 K. If the temperature is raised above 873 K, the zirconia starts to transform from the metastable (tetragonal) phase to the stable monoclinic phase. This phase transformation is accompanied by a dramatic change in pore structure of zirconia. At temperatures lower than phase transformation temperature, the pore structure of zirconia also changes, but to a lesser extent, as a result of sintering and grain growth. Metal oxides like yttria, ceria, magnesia or lanthana can stabilize the tetragonal phase through doping.

Transition metal oxides are widely used as industrial catalysts and as catalysts supports. Unfortunately they usually have poorly defined pore structures. The synthesis of mesoporous silica partially substituted by zirconium has been attempted to circumvent the difficulty of preparing stable mesoporous zirconia.   Zirconium

oxide is of particular interest because it contains both acidic and basic surface sites. In the recent years SO_4^{2-}/ZrO_2 has attracted attention as it catalyzes various industrially important reactions such as: isomerization, condensation and Friedel-Crafts acylation reactions.[69] However, its non-uniform pore size, low porosity, and low surface area limit its potential application for catalyzing reactions of bulky molecules. Despite these limitations zirconia has a high melting point, low thermal conductivity, high corrosion resistance, and amphoteric behavior, all of which can be useful properties for a support material. Parvulescu et al. studied the synthesis of mesoporous zirconium oxide using cationic surfactant and claimed that the synthesis occurred via a scaffolding mechanism.[70] The possibility of obtaining such material with a mesoporous texture has made this oxide even more interesting.

1.6. PHYSICOCHEMICAL CHARACTERIZATION

The mesoporous and inorganic–organic hybrid mesostructured materials can be characterized by various techniques, which provide important information about different physicochemical features. Commonly used characterization techniques are:

1. Powder X-ray diffraction (PXRD)

2. Ultraviolet-visible (UV-Vis) spectroscopy

3. Fourier transform infrared (FTIR) spectroscopy

4. Nuclear magnetic resonance (NMR) spectroscopy

5. X-ray photoelectron spectroscopy (XPS)

6. Atomic absorption spectrometry (AAS)

7. Scanning electron microscopy (SEM)

8. Transmission electron microscopy (TEM)

9. Porosity measurements by nitrogen (N_2) adsorption (BET method)

10. Temperature programmed desorption of ammonia.

1.6.1. Powder X-Ray Diffraction

It is well recognized that X-ray diffraction, based on wide-angle elastic scattering of X-rays, has been the single most important tool to determine the structure of the materials characterized by long-range ordering. The X-ray diffraction patterns are obtained by measurement of the angles at which an X-ray beam is diffracted by the sample. Bragg's equation relates the distance between two *hkl* planes (*d*) and the angle of diffraction (2θ) as: $n\lambda = 2d\sin\theta$, where λ = wavelength of X-rays, n = an integer known as the order of reflection (*h*, *k* and *l* represent Miller indices of the respective planes).[71] From the diffraction patterns, the uniqueness of structure,[72] phase purity,[73] degree of crystallinity and unit cell parameters of the crystalline materials can be determined.

The identification of phase is based on the comparison of the set of reflections of the sample with that of pure reference phases distributed by International Center for Diffraction Data (ICDD). Unit cell parameter (a_0) of a cubic lattice can be determined by the following equation: $a_0 = d_{hkl}\sqrt{(h^2 + k^2 + l^2)}$, where d = distance between two consecutive parallel lattice planes having Miller indices *h*, *k* and *l*.

1.6.2. Diffuse Reflectance UV-VIS Spectroscopy

UV-Vis spectroscopy deals with the study of electronic transitions between orbitals or bands of atoms, ions or molecules in gaseous, liquid and solid state. In the case of transition metal ions or atoms, any change in their coordination sphere may affect their optical properties and therefore can be characterized by UV-Vis.[74] For solid substances like transition metal containing mesoporous materials, diffuse reflectance UV-Vis spectroscopy (DRUV-Vis) is applied to determine the ligand field symmetry and oxidation state of the metal inside the solid matrices. Thus, DRUV-Vis spectroscopy is a sensitive probe to examine the coordination sphere of metal ions via

ligand to metal charge transfer bands. Generally, as the coordination number of metal ion decreases the "ligand to metal charge transfer band" shifts towards lower wave number (blue shift).[75]

1.6.3. Fourier Transform Infrared Spectroscopy

Fourier transform infrared (FTIR) spectroscopy deals with the vibration of chemical bonds in a molecule at various frequencies depending on the elements and types of bonds. After absorbing electromagnetic radiation the frequency of vibration of a bond increases leading to transition between ground state and several excited states. The energy of these transitions corresponds to the infrared region (4000–400 cm^{-1}) of the electromagnetic spectrum. The term Fourier transform (FT) refers to a recent development in the manner in which the data are collected and converted from an interference pattern to an infrared absorption spectrum that is like a molecular "fingerprint".[76]

In the case of porous silicates, the FTIR spectra in 400–1300 cm^{-1} region provide information about the structural details including isomorphous substitution in framework, whereas the bands in 3000–4000 cm^{-1} region allow to determine different Bronsted and Lewis acid sites[77] and silanol groups.[78] Acidic and basic properties as well as their strength can also be estimated using carbon dioxide (CO_2), ammonia (NH_3), pyridine, triphenylphosphine (PPh_3) *etc*. as probe molecules and their quantitative estimation by FTIR.[79]

1.6.4. Nuclear Magnetic Resonance Spectroscopy

With the advent of sophisticated solid-state Magic Angle Spining (MAS) NMR techniques, it has become possible to obtain NMR spectra of solids with spectral resolution nearly comparable to that of liquids.[80-82] High-resolution NMR spectra of solid samples with narrow line width can be obtained by magic angle

spinning (MAS), where the solid sample is fast rotated about an axis inclined at a "magic" angle $\theta = 54°44'$ to the direction of B_0.[82] Modern high-resolution solid-state MAS-NMR spectroscopy allows one to elucidate the chemical and structural environment of several atoms (*e.g.* [13]C, [27]Al, [29]Si, ^{19}F, ^{31}P, [51]V *etc.*) in a solid matrix like that of porous materials.[81]

Cross-polarization (CP) technique does not affect the line width of the spectra, but is applied to improve the sensitivity, *i.e.*, the signal to noise ratio (SNR) of the spectra of nuclei with low natural abundance (*e.g.* [13]C, [29]Si, [31]P *etc.*), and to monitor the spatial proximity of nuclei.[82] CP involves indirect excitation of the less abundant nucleus through magnetization transfer from an abundant spin system (*e.g.* [1]H).

1.6.5. X-Ray Photoelectron Spectroscopy

X-ray photoelectron spectroscopy (XPS) is widely used for probing the electronic structure of atoms, molecules and condensed matter. When an X-ray photon of energy $h\nu$ is incident on a solid matter, the kinetic energy (E_k) and the binding energy (E_b) of the ejected photoelectrons can be related as follows: $E_k = h\nu - E_b$.

This kinetic energy distribution of the photoelectrons is fabricated by a series of discrete bands, which symbolizes for the electronic structure of the sample.[83] The core level binding energies of all the elements (other than H and He) in all different oxidation states are unique, which provides instant detection of the chemical composition of the sample after a full range scan.[84] However, to account for the multiplet splitting and satellites accompanying the photoemission peaks, the photoelectron spectra should be interpreted in terms of many-electron states of the final ionized state of the sample, rather than the occupied one-electron states of the neutral species.[85]

1.6.6. Atomic Absorption Spectroscopy

The principle of atomic absorption is based on energy absorbed during transitions between electronic energy levels of an atom. When some sort of energy is provided to an atom in ground state by a source such as a flame (temperature ranging from 2100–2800 °C), outer-shell electrons are promoted to a higher energy excited state. The radiation absorbed as a result of this transition between electronic levels can be used for quantitative analysis of metals and metalloids present in solid matrices, which have to be dissolved by appropriate solvents before analysis. The basis of quantitative analysis depends on measurement of radiation intensity and the assumption that radiation absorbed is proportional to atomic concentration. Analogy of relative intensity values for reference standards is used to determine elemental concentrations.[86]

1.6.7. Scanning Electron Microscopy

Scanning electron microscopy (SEM) is an important tool for morphological characterization of mesoporous molecular sieve materials. A scanning electron microscope can generate an electron beam scanning back and forth over a solid sample. The interaction between the beam and the sample produces different types of signals providing detailed information about the surface structure and morphology of the sample. When an electron from the beam encounters a nucleus in the sample, the resultant Coulombic attraction leads to a deflection in the electron's path, known as Rutherford elastic scattering. A fraction of these electrons will be completely backscattered, reemerging from the incident surface of the sample. Since the scattering angle depends on the atomic number of the nucleus, the primary electrons arriving at a given detector position can be used to produce images containing topological and compositional information.[87]

The high-energy incident electrons can also interact with the loosely bound conduction band electrons in the sample. However, the amount of energy given to these secondary electrons as a result of the interactions is small, and so they have a very limited range in the sample. Hence, only those secondary electrons that are produced within a very short distance from the surface are able to escape from the sample. As a result, high-resolution topographical images can be obtained in this detection mode.[88]

1.6.8. Transmission Electron Microscopy

Transmission electron microscopy (TEM) is typically used for high resolution imaging of thin films of a solid sample for microstructural and compositional analysis. The technique involves: (i) irradiation of a very thin sample by a high-energy electron beam, which is diffracted by the lattices of a crystalline or semicrystalline material and propagates along different directions, (ii) imaging and angular distribution analysis of the forward-scattered electrons (unlike SEM where back scattered electrons are detected), and (iii) energy analysis of the emitted X-rays.[89] The topographic information obtained by TEM in the vicinity of atomic resolution can be utilized for structural characterization and identification of various phases of mesoporous materials, *viz.*, hexagonal, cubic or lamellar.[90] TEM also provides real space image on the atomic distribution in the bulk and surface of a nanocrystal.[91]

1.6.9. Porosity Measurement by N_2 Adsorption

Despite of some theoretical limitations, the Brunauer-Emmett-Teller (BET) method continues to be the most widely used method for the evaluation of surface area, pore volumes and pore size distributions of porous solids from N_2 physisorption isotherm data. The BET equation can be represented as follows:

$$\frac{p}{v(p_0 - p)} = \frac{1}{v_m c} + \frac{c-1}{v_m c}\frac{p}{p_0}$$, where v = volume of N_2 adsorbed by the sample under

pressure p, p_0 = saturated vapor pressure at the same temperature, v_m = volume of N_2

adsorbed when the surface is covered with a unimolecular layer, and c = constant for a

given adsorbate.[92]

The equation suggests that the plot of $\dfrac{p}{v(p_0 - p)}$ versus $\dfrac{p}{p_0}$ should be linear,

and from the intercept $\dfrac{1}{v_m c}$ and slope $\dfrac{c-1}{v_m c}$, the values of v_m and c can be determined

as follows: $v_m = (\text{slope} + \text{intercept})^{-1}$.

Thus the specific surface area (S) of a sample can be determined as follows:

$$S = \frac{N_0 v_m A}{22414 m}$$, where N_0 = Avogadro number, m = amount of solid adsorbent, A =

cross-section of the gas molecules (16.2 Å^2 for N_2), and S is expressed in $\text{cm}^2\ \text{g}^{-1}$ unit.

Several computational procedures are available for the derivation of pore size

distribution of mesoporous samples from physisorption isotherms. Most popular

among them is the Barrett-Joyner-Halenda (BJH) model, which is based on

speculative emptying of the pores by a stepwise reduction of p/p_0, and allowance

being made for the contraction of the multilayer in those pores already emptied by the

condensate.[93] The mesopores size distribution is usually expressed as a plot of

$\Delta V_p/\Delta r_p$ versus r_p, where V_p = mesopore volume, and r_p = pore radius. It is assumed

that the mesopores volume is completely filled at high p/p_0.

1.6.10. Temperature Programmed Techniques: TPD of Ammonia

Temperature programmed desorption (TPD) technique can be used to

characterize the acidity of the catalyst. First the catalyst is contacted with a base

molecule like ammonia to neutralize the acid sites present. Then, the catalyst is

heated slowly and the evolved gas (*e.g.* ammonia) is quantitatively measured continuously by GC using a thermal conductivity detector (TCD).[94] Instrumentation for temperature-programmed investigations consists of a reactor charged with catalyst in a furnace that can be temperature programmed and TCD to measure the concerned active gas of the gas mixture before and after interaction.

1.7. CATALYTIC APPLICATIONS AND PROSPECTS

While homogeneous catalysts are generally very active, they suffer from some inherent short comings, *viz.*, (i) complicated work-up of the reaction mixture, (ii) preparation of the pure products not contaminated with catalysts or constituents there of, and (iii) isolation of the valuable catalyst or its constituents, which can be achieved only with high technical complexity and expenditure.[95] The most feasible way to circumvent this problem is to "heterogenize" the homogeneous catalyst, by means of immobilization, anchoring, or encapsulation on an inorganic (zeolites or mesoporous materials)[45a] or organic (polymeric) solid support.[96]

The concept of heterogenization provides the prospective for extending the benefits of homogeneous systems to heterogeneous catalysis. These benefits include easier separation of catalyst and reaction products leading to shorter work up times, improved process efficiency, the potential for reactivation and reuse of the supported catalyst comprising of expensive ligands. However, the prime requirement of the heterogenization approach is to maintain the stability of the heterogenized complex, such that it does not decompose or leach out from the solid matrix to the liquid phase during the course of reaction, and at the same time retains high activity and selectivity.

In this section, the catalytic applications and prospects of metal-containing mesoporous materials and organo-modified mesoporous materials for different types

of carbon-carbon bond formation reactions studied, and are reported in the present dissertation, are briefly reviewed below:

1.7.1. CARBON-CARBON BOND FORMATION REACTIONS

Although, the condensation of aldehydes and ketones over zeolites has been studied extensively under vapor-phase, fixed-bed reaction conditions,[97] liquid-phase carbon-carbon bond formation reactions catalyzed by zeolite are less common.[98] Here, in the present section some of the carbon-carbon bond formation reactions, relevant to the present dissertation, are described briefly.

1.7.1.1. Friedel-Crafts Benzylation Reaction

Electrophilic alkylation of aromatics can be carried out by variety of reactants such as olefins, alcohols, and halogenated hydrocarbons.[99] Usually, diphenylmethane and its derivatives have been prepared typically by Friedel–Crafts benzylation reaction in liquid phase homogeneous system using strong Lewis acids, such as $AlCl_3$, $FeCl_3$ and $ZnCl_2$[100] and Brönsted acids such as polyphosphoric acid, H_2SO_4, HF, CF_3SO_3H as catalysts.[100-101] The products are industrially important compounds used as pharmaceutical intermediates[102] and fine chemicals.[103] In the fragrance industry diphenylmethane has been used as both a fixative and a scenting soap, as a synergist in some insecticides[104] and as a plastisizer,[105] dyes[106] etc.

Many solid bases have recently been found useful in the production of alkylated products. Several alkali doped silica, zeolites, mesoporous silica have been recently reported for base catalyzed alkylation reactions[107] Macquarrie et al have reported KF supported on natural phosphate as a green base catalyst.[108] Base catalyzed selective side chain monoalkylation of methylene active compounds is important industrial process for the formation of intermediates.[109] Alkali metal

carbonates and organic bases have been studied in the selective monomethylation of arylacetonitriles and methyl aryl acetates in detail using reactor.[110]

1.7.1.2. Mukaiyama-Michael Reaction

Organosilicon reagents are widely used in modern organic synthesis because of their unique and moderate reactivity, which enables highly efficient and selective organic reactions, their ready availability, and their relatively low toxicity.[111] As a result, several synthetically valuable reactions using organosilicon reagents, viz., Mukaiyam-aldol condensation and Mukiayama-Michael reaction with silyl enolates,[112] the Hosomi-Sakurai reaction with allysilanes[113] and the Hiyama coupling with alkenyl, alkynyl, and arylsilanes[114] have been developed. These reagents act as stable synthetic equivalents of the corresponding carbanions and efficiently react with a variety of carbon electrophiles, with the aid of a catalyst such as a Lewis acid or transition metal catalyst.

In 1974, Mukaiyama and co-workers reported the first examples of Lewis acid catalyzed Michael reaction between enol silanes and α,β-unsaturated carbonyl acceptors.[115] This reaction provides an important method for the preparation of δ-dicarbonyl compounds (1,5- dicarbonyl compounds) under neutral, mild conditions using a catalytic amount of Lewis acid[115] or a fluoride ion source.[116] This reaction variant is an attractive alternative to the conventional metalloenolate process due to the mild reaction conditions and superior regiocontrole (1,4-versus 1,2-addition).

To date, there are only few reports available for the Mukaiyama-Michael reaction using heterogeneous catalyst.[38d,98,117]

1.7.1.3. Mukaiyama-Aldol Condensation

In 1973, Mukaiyama and coworkers reported that in the presence of $TiCl_4$, ketone trimethylsilyl enolates react smoothly with aldehydes to give aldol

products.[111a,118] Since the discovery of the so-called Mukaiyama-aldol condensation, the use of silyl enolates as enolate equivalent had received much attention from synthetic organic chemist. At the present time, silyl enolates are well recognized as very valuable reagents for highly efficient and selective carbon-carbon bond formation and functionalization introducing a carbonyl group. The original methods for the directed aldol and aldol-type condensations of aldehydes and acetals with silyl enolates require a stoichiometric amount of a Lewis acid such as $TiCl_4$, BF_3. OEt_2, or $SnCl_4$.[118] In addition, it has been found that fluoride ion sources also work as effective catalysts of the aldol condensation.[119] In the last decade, much attention has been paid for the development of diastero- and enantioselective aldol condensation,[120] aqueous aldol condensations using water stable Lewis acid,[121] novel types of silyl enolates with unique reactivity. However, only few literature reports are available for Mukaiyama-aldol condensation using heterogeneous catalysts.[117c,122,123]

1.7.1.4. Michael-Addition of Indoles to α, β-Unsaturated Carbonyl Compounds

The Michael-addition of indole to enone consists of conjugate addition reaction of nucleophiles (indole) to unsaturated carbonyl (enone) compounds in either basic[124] or acidic reaction condition.[125] The investigation of the chemistry of indoles has been, and continues to be, one of the most active area in heterocyclic chemistry.[126] In particular, β-indoylketones have received much attention as important building blocks for the synthesis of many natural products, alkaloid, fine chemicals and biologically active compounds including anticancer agents, like β-lactum.[127,128] The other heterocyclics such as indole alkaloid, harmicine, tryptophan, etc are used in a wide range of medicinal purposes.[127]

In general, Michael-addition of indoles to enones occurs in both Lewis and Brönsted acid reaction conditions.[127] However, the acid-catalyzed conjugate addition

of indoles requires careful control of the acidity to prevent unwanted side reactions, including dimerization and polymerization.[129] So far, extensive efforts have been made in developing homogeneous catalysts for the Michael-addition of indole to enone. But, there are limited reports in the literature for the Michael-addition of indole to enone using heterogeneous catalyst.[130]

1.7.1.5. Synthesis of Coumarins by Pechmann Reaction

Coumarins and their derivatives have been investigated widely in synthetic organic chemistry. Coumarins are structural units of various natural products and feature widely in pharmacology and biologically active compounds.[131] For instance, the Pechmann reaction has been used for the synthesis of natural products like rotenone and cannabinol.[132] The Pechmann reaction is extensively used for the synthesis of coumarin and its derivatives.[133]

Pechmann reactions consist of reacting derivatives of phenol and β-keto ester to produce hydroxy derivatives of coumarins.[133b] In this reaction, coumarins have been synthesized by using different condensing agents such as $FeCl_3$, $ZnCl_2$, $AlCl_3$, $TiCl_4$, $SnCl_4$, H_2SO_4, P_2O_5, $POCl_3$, HCl, H_3PO_4, $NaOC_2H_5$, sodium acetate and trifluoroacetic acid as well as boric anhydride, etc.[133b]

For acid-catalyzed organic reactions, the covalent attachment of alkylsulfonic acid groups to the surface of mesoporous molecular sieves based on silica has been reported by various authors and successfully implemented in acid catalyzed reactions, including esterification, condensation reactions, acetalization and acetylation.[134] Up till now, very few metallosilicate molecular sieves with different topologies and organic inorganic hybrid materials have been investigated as heterogeneous catalysts for synthesis of coumarins by Pechmann reaction.[135]

1.7.1.6. Michael-Addition of β-Nitrostyrene to Malonate

The Michael-addition ractions of nitroalkenes to malonates have been developed as a powerful tool in organic synthesis because Michael adducts are versatile building blocks for agricultural and pharmaceutical compounds.[136,137]

Solid bases such as alkaline-substituted zeolites, alkaline-earth oxides, hydrotalcites, AlPOs have been used successfully for nucleophilic reactions involving carbanion-type species for the formation of new carbon-carbon bonds through aryl-ring side chain alkylation, Knoevenagel condensation, aldol condensation, Michael additions, etc.[107,108] To date, there are no reports of this reaction being carried out using solid catalyst and to the best of my knowledge this thesis will most probably report the first example of Michael-addition of nitroalkenes to malonates using a heterogeneous catalyst system.

1.8. OBJECTIVES OF THE THESIS

The objectives of the present study are the following:

(1) To prepare and characterize mesoporous materials by incorporation of Ce and Al in MCM-41 networks, and use these new materials as catalyst for different carbon-carbon bond formation reactions such as benzylation of toluene, Mukaiyama-Michael addition and Mukaiyama-aldol condensation.

(2) To anchor homogeneous catalyst (trifluoromethanesulfonic acid) over solid Zr-TMS material, and to employ this catalyst for the different carbon-carbon bond formations reactions such as Michael-addition of indoles to α, β-unsaturated carbonyl compounds and synthesis of coumarins by Pechmann reaction.

(3) To immobilize 1,5,7-triazabicyclo [4.4.0] dec-5-ene over MCM-41 and SBA-15 mesoporous materials, and examine for the carbon-carbon bond formation reaction

such as Michael-addition of nitrostyrene to malonate. The work conducted in this thesis aims to contribute towards green and sustainable catalytic processes.

1.9. OUTLINE OF THE THESIS

The thesis will be presented in **SIX** chapters, as summarized below:

Chapter 1 presents a general introduction to various aspects of zeolites, mesoporous aluminosilicates and their physicochemical properties. Salient features of certain metal oxides catalysts are discussed. Various instrumentation technique adopted for characterization of these catalysts are also described in brief. A detailed description is also given to various carbon-carbon bond formation reactions pertaining to the present study. The objectives of the present thesis research have also been highlighted.

Chapter 2 presents the synthesis of Ce-containing mesoporous Al-MCM-41, synthesis of Zr-TMS catalyst and organofunctionalized by trifluoromethanesulphonic acid (triflic acid, TFA) on Zr-TMS catalyst, synthesis of Si-MCM-41 and SBA-15 materials and then immobilization of 1,5,7-triazabicyclo [4.4.0] dec-5-ene (TBD) on Si-MCM-41 and SBA-15 materials. The different techniques have been used for characterization of synthesized materials such as XRD, N_2 adsorption, UV-visible, TPD-NH$_3$, FT-IR, XPS, ^{13}C, ^{29}Si, and ^{27}Al CP MAS NMR, SEM, TEM, AAS analysis and microanalysis.

Chapter 3 deals the catalytic acitivity of Ce-MCM-41, Al-MCM-41 and Ce-Al-MCM-41 catalysts. In this chapter various parameters have been studied, such as reaction time with different MCM-41 samples, different temperatures and solvents, recycle study and different substrates. Following are the main topics discussed.

(a) Friedel-Crafts benzylation reaction under solvent free condition over Ce-MCM-41, Al-MCM-41 and Ce-Al-MCM-41 catalysts.

(b) Preparation of 1, 5-dicarbonyl compounds by Mukaiyama-Michael reaction over Ce-MCM-41, Al-MCM-41 and Ce-Al-MCM-41 catalysts.

(c) Preparation of β-hydroxy carbonyl compounds by Mukaiyama-aldol condensation under solvent free condition over Ce-MCM-41, Al-MCM-41 and Ce-Al-MCM-41 catalysts.

Chapter 4 presents the catalytic activity of Zr-TMS and Zr-TMS-TFA catalyst. In this chapter various parameters have been studied, such as reaction time with different Zr-TMS-TFA samples, different amount of catalyst, temperatures, recycle study and different substrates. This chapter is divided into two parts-

(a) Michael-addition of indoles to α, β-unsaturated carbonyl compounds over triflic acid loaded Zr-TMS catalyst.

(b) Synthesis of coumarin and its derivatives over triflic acid loaded Zr-TMS catalyst by Pechmann reaction.

Chapter 5 describes the catalytic properties of MCM-41 / SBA-15-TBD (1, 5, 7-triazabicyclo [4.4.0] dec-5-ene) mesoporous materials for the Michael-addition of β-nitrostyrene to malonate. In this chapter also various parameters have been studied, such as reaction time with different Zr-TMS-TFA samples, different amount of catalyst, temperatures, recycle study and different substrates.

Chapter 6 summarizes and concludes the results obtained and the basic findings of the present work.

1.10. REFERENCES

1.   J. M. Newsam, *Science* **1986,** 231, 1093.

2.   D. W. Breck, *Zeolite Molecular Sieves*, Wiley, New York, **1974**.

3.   (a) S. M. Csicsery, *Zeolites* **1984**, 4, 202. (b) S. M. Csicsery, *Pure Appl. Chem*. **1986**, 58, 841. (c) P. Ratnasamy, R. Kumar, *Stud. Surf. Sci. Catal*. **1995**, 97, 367.

4.   (a) P.-S. E. Dai, *Catal. Today* **1995**, 26, 3. (b) R. A. Sheldon, *J. Mol. Catal. A*: *Chem.* **1996**, 107, 75. (c) J. H. Clark, D. J. Macquarrie, *Chem. Soc. Rev*. **1996**, 25, 303.

5.   (a) C. T. Kresge, M. E. Leonowicz, W. J. Roth, J. C. Vartuli, J. S. Beck, *Nature* **1992**, 359, 710. (b) J. S. Beck, J. C. Vartuli, W. J. Roth, M. E. Leonowicz, C. T. Kresge, K. D. Schmitt, C. T. W. Chu, D. H. Olson, E. W. Sheppard, S. B. McCullen, J. B. Higgins, J. L. Schlenker, *J. Am. Chem. So*c. **1992**, 114, 10834. (c) T. Yanagisawa, T. Shimizu, K. Kuroda, *Bull. Chem. Soc. Jp*n. **1990**, 63, 988. (d) S. Inagaki, Y. Fukushima, K. Kuroda, *J. Chem. Soc. Chem. Commu*n. **1993**, 680.

6.   A. Corma, *Chem. Rev*. **1997**, 97, 2373.

7.   T. Linssen, K. Cassiers, P. Cool, E. F. Vansant, *Adv. Colloid Interface Sci.* **2003**, 103, 121.

8.   P. T. Tanev, T. J. Pinnavaia, *Science* **1995**, 267, 865.

9.   S. A. Bagshaw, E. Prouzet, T. J. Pinnavaia, *Science* **1995**, 269, 1242.

10.   D. Zhao, Q. Huo, J. Feng, B. F. Chmelka, G. D. Stucky, *J. Am. Chem. Soc.* **1998**, 120, 6024.

11.   C. Yu, B. Tian, J. Fan, G. D. Stucky, D. Zhao, *J. Am. Chem. Soc.* **2002**, 124, 4556.

12.   D. Zhao, J. Feng, Q. Huo, N. Melosh, G. H. Fredrickson, B. F. Chmelka, G. D. Stucky, *Science* **1998**, 279, 548.

13.   S. Shen, Y. Li, Z. Zhang, J. Fan, B. Tu, W. Zhou, D. Zhao, *Chem. Commun*. **2002**, 2212.

14.   X. Liu, B. Tian, C. Yu, F. Gao, S. Xie, B. Tu, R. Che, L.-M. Peng, D. Zhao, *Angew. Chem., Int. Ed.* **2002**, 41, 3876.

15.   K. Moller, T. Bein, *Chem. Mater.* **1998**, 10, 2950.

16.   J. C. Vartuli, K. D. Schmitt, C. T. Kresge, *Chem. Mater.* **1994**, 6, 2317.

17.   J. S. Beck, J. C. Vartuli, G. J. Kennedy, C. T. Kresge, W. J. Roth, S. E. Schramm, *Chem. Mater.* **1994**, 6, 1816.

18.   C. F. Cheng, H. He, W. Zhou, J. Klinowski, *Chem. Phys. Lett.* **1995**, 244, 117.

19.   C. -Y. Chen, S. L. Burkett, H. -X. Li, M. E. Davis, *Microporous Mater.* **1993**, 2, 27.

20.   (a) A. Monnier, F. Schuth, Q. Huo, D. Kumar, D. I. Margolese, R. S. Maxwell, G. D. Stucky, M. Krishnamurthy, P. Petroff, A. Firouzi, M. Janicke, B. F. Chmelka, *Science* **1993**, 261, 1299. (b) G. D. Stucky, A. Monnier, F. Schuth, Q. Huo, D. I. Margolese, D. Kumar, M. Krishnamurthy, P. Petroff, A. Firouzi, M. Janicke, B. F. Chmelka, *Mol. Cryst. Liq. Cryst.* **1994**, 240, 187.

21.   (a) A. Firouzi, D. Kumar, L. M. Bull, T. Besier, P. Sieger, Q. Huo, S. A. Walker, J. A. Zasadzinski, C. Glinka, J. Nicol, D. I. Margolese, G. D. Stucky, B. F. Chmelka, *Science* **1995**, 267, 1138. (b) A. Firouzi, F. Atef, A. G. Oertli, G. D. Stucky, B. F. Chmelka, *J. Am. Chem. Soc.* **1997**, 119, 3596.

22.   (a) Q. Huo, D. I. Margolese, U. Ciesla, P. Feng, P. Sieger, R. Leon, P. Petroff, F. Schuth, G. D. Stucky, *Nature* **1994**, 368, 317. (b) Q. Huo, D. I. Margolese, U. Ciesla, D. G. Demuth, P. Feng, T. E. Gier, P. Sieger, A. Firouzi, B. F. Chmelka, F. Schuth, G. D. Stucky, *Chem. Mater.* **1994**, 6, 1176.

23.   (a) P. T. Tanev, T. J. Pinnavaia, *Chem. Mater.* **1996**, 8, 2068. (b) P. T. Tanev, T. J. Pinnavaia, *Science* **1996**, 271, 1267.

24.   D. M. Antonelli, J. Y. Ying, *Angew. Chem. Int. Ed.* **1996**, 35, 426.

25.   (a) A. Sayari, *Chem. Mater.* **1996**, 8, 1840. (b) J. Y. Ying, C. P. Mehnert, M. S. Wong, *Angew. Chem. Int. Ed.* **1999**, 38, 56.

26.   (a) R. Ryoo, C. H. Ko, R. F. Howe, *Chem. Mater.* **1997,** 9, 1607. (b) Z. Luan, C. - F. Cheng, W. Zhou, J. Klinowski, *J. Phys Chem.* **1995,** 99, 1018. (c) M. Janicke, D. Kumar, G. D. Stucky, B. F. Chmelka, *Stud. Surf. Sci. Catal*.**199**4, 84, 243. (d) M. Hartmann, C. Bischof, *Stud. Surf. Sci. Catal*. **1998**, 117,249.

27.   A. Sayari, C. Danumah, I. L. Moudrakovski, *Chem. Mater.* **1995,** 7, 813.

28.   C.-F. Cheng, H. He, W. Zhou, J. Klinowski, J. A. S. Gonçalves, L. F. Gladden, *J. Phys. Chem.* **1996,** 100, 390.

29.   A. Tuel, S. Gontier, *Chem. Mater.* **1996,** 8, 114.

30.   (a) A. Corma, M. T. Navarro, J. P. Pariente, *J. Chem. Soc. Chem. Commun*. **1994**, 147. (b) P. T. Tanev, M. Chibwe, T. J. Pinnavaia, *Nature* **1994,** 368,

321.

31.   (a) K. M. Reddy, I. Moudrakovski, A. Sayari, *J. Chem. Soc. Chem. Commun*. **1994**, 1059. (b) S. C. Laha, R. Kumar, *Micropor. Mesopor. Mater.* **2002**, 53, 163.

32.   N. Ulagappan, C. N. Rao, *Chem. Commun*. **1996**, 1047.

33.   D. Zhao, D. Goldfarb, *J. Chem. Soc. Chem. Commun*. **1995**, 875.

34.   A. Jentys, N. H. Pham, H. Vinek, M. Englisch, L. A. Lercher, *Microporous Mater*. **1996,** 6, 13.

35.   (a) T. K. Das, K. Chaudhari, A. J. Chandwadkar, S. Sivasanker, *J. Catal.* **1999**, 183, 281. (b) T. Gaydhankar, P. N. Joshi, P. Kalita, R. Kumar, *J. Mol. Catal. A: Chem.* **2006,** 265, 306.

36.   R. K. Rana, B. Viswanathan, *Catal. Lett*. **1998,** 52, 25.

37.   A. Tuel, S. Gontier, R. Teissier, R., *J. Chem. Soc. Chem. Commun*. **1996,** 651.

38.   (a) S. C. Laha, P. Mukharjee, S. R. Sainkar, R. Kumar, *J. Catal.* **2002**, 207, 213. (b) M. D. Kadgaonkar, S. C. Laha, R. K. Pandey, P. Kumar, S. P. Mirajkar, R. Kumar, *Catal. Today* **2004**, 97, 225. (c) P. Kalita, N. M. Gupta, R. Kumar*, J. Catal.* **2007**, 245, 338. (d) P. Kalita, R. Kumar*, Stud. Surf. Sci. Catal.* **2007**, 170, 1161.

39.   H. Jing, Z. Guo, H. Ma, D. G. Evans, X. Duan, *J. Catal*. **2002,** 212, 22.

40.   S. K. Bhargava, D. B. Akolekar, *J. Colloid Interface Sci.* **2005**, 281, 171.

41.   G. V. Shanbhag, T. Joseph, S.B. Halligudi, *J. Catal*. **2007,** 250, 274.

42.   Y. Liu, K. Murata, M. Inaba, N. Mimura, *Appl. Catal. A: Gen.* **2006**, 309, 91.

43.   A. Sayari, S. Hamoudi, *Chem. Mate*r. **2001**, 13, 3151.

44.   (a) A. P. Wight, M. E. Davis, *Chem. Rev.* **2002**, 102, 3589. (b) A. Taguchi, F. Schuth, *Micropor. Mesopor. Mate*r. **2004**, 77, 1.

45.   (a) D. E. De Vos, M. Dams, B. F. Sels, P. A. Jacobs, *Chem. Rev.* **2002**, 102, 3605. (b) X. Feng, G. E. Fryxell, L. Q. Wang, A. Y. Kim, J. Liu, K. M. Kemner, *Science* **1997**, 276, 923. (c) D. Brunel, N. Bellocq, P. Sutra, A. Cauvel, M. Lasperas, P. Moreau, F. D. Renzo, A. Galarneau, F. Fajula, *Coord. Chem. Re*v. **1998**, 178, 1085. (d) A. Stein, B. J. Melde, R. C. Schroden, *Adv. Mate*r. **2000**, 12, 1403. (e) U. Schbert. *New. J. Chem.* **1994**, 18, 1049.

46.   (a) T. Yokoi, H. Yoshitake, T. Tatsumi, *J. Mater. Che*m. **2004**, 14, 951. (b) H-P. Lin, L-Y. Yang, C-Y. Mou, S-B. Liu, H-K. Lee, *New J. Che*m. **2000**, 24,

253. (c) H. Q. Yang, G. Y. Zhang, X. L. Hong, Y. Y. Zhu, *Micropor. Mesopor. Mate*r. **2004**, 68, 119.

47.   W. M. Van Rhijn, D. E. De Vos, F. Sels, W. D. Bossaert, P. A. Jacobs, *J. Chem. Soc. Chem. Commun*. **1998**, 317.

48.   P. M. Price, J. H. Clark, D. J. Macquarrie, *J. Chem. Soc. Dalton Tran*s. **2000**, 101.

49.   X. S. Zhao, G. Q. Lu, *J. Phys. Chem. B* **1998**, 102, 1556.

50.   T. Kimura, S. Saeki, Y. Sugahara, K. Kuroda, *Langmuir* **1999**, 15, 2794.

51.   J. S. Beck, D. C. Calabro, S. B. McCullen, B. P. Pelrine, K. D. Schmitt, J. C. Vartuli, *Method for Functionalizing Synthetic Mesoporous Crystalline Material*, Mobil Oil Corporation, USA, **1992**.

52.   (a) R. Anwander, C. Palm, J. Stelzer, O. Groeger, E. Engelhardt, *Stud. Surf. Sci. Catal*. **1998**, 117, 135. (b) R. Anwander, I. Nagl, M. Widenmeyer, G. Engelhardt, O. Groeger, C. Palm, T. Roser, *J. Phys. Chem. B* **2000**, 104, 3532. (c) V. Antochshuk, M. Jaroniec, *J. Phys. Chem. B* **1999**, 103, 6252. (d) C. P. Jaroniec, M. Kruk, M. Jaroniec, A. Sayari, *J. Phys. Chem. B* **1998**, 102, 5503.

53.   (a) P. Sutra, D. Brunel, *Chem. Commun.* **1996**, 2485. (b) Y. V. Subba Rao, D. E. De Vos, P. A. Jacobs, *Angew. Chem. Int. Ed.* **1997**, 36, 2661. (c) J. F. Diaz, K. J. Balkus Jr., F. Bedioui, V. Kurshev, L. Kevan, *Chem. Mater.* **1997**, 9, 61.

54.   M. H. Lim, A. Stein, *Chem. Mate*r. **1999**, 11, 3285.

55.   D. S. Shepherd, W. Zhou, T. Maschmeyer, J. M. Malters, C. L. Roper, S. Parsons, B. F. G. Johnson, M. J. Duer, *Angew. Chem. Int. Ed*. **1998**, 37, 2719.

56.   F. De Juan, E. R. Hitzky, *Adv. Mate*r. **2000**, 12, 430.

57.   C. Sanchez, F. Ribot, *New J. Che*m. **1994**, 18, 1007.

58.   (a) S. L. Burkett, S. D. Sims, S. Mann, *Chem. Commu*n. **1996**, 1367. (b) D. J. Macquairre, *Chem. Commu*n. **1996**, 1961. (c) Q. Huo, D. I. Margolese, G. D. Stucky, *Chem. Mate*r. **1996**, 8, 1147.

59.   M. H. Lim, C. F. Blanford, A. Stein, *J. Am. Chem. Soc*. **1997**, 119, 4090.

60.   (a) D. M. Antonelli, J. Y. Ying, *Angew. Chem., Int. Ed. Engl.* **1995**, 34, 201.
       (b) H. Yoshitake, T. Sugihara, T. Tatsumi, *Chem. Mater,* **2002**, 14, 1023.

61.   (a) J. A. Knowles, M. J. Hudson, *J. Chem. Soc. Chem. Commun.* **1995**, 2083. *J. Mater. Chem.* **1996**, 6, 89. (b) U. Ciesla, S. Schacht, G. D. Stucky, K. K. Unger, F. Schuth, *Angew. Chem.   Int. Ed.* **1996,** 35, 541. (c) U. Ciesla, M.

Froba, G. D. Stucky, K. K. Unger, F. Schuth, *Chem. Matet.* **1999**, 11, 227. (d) J. L. Blin, R. Flamant, B. L. Su, *Int. J. Inorg. Mater.* **2001**, 3, 959. (e) D. M. Antonelli, *Adv. Mater.* **1999**, 11, 487. (f) M. S. Wong, J.Y. Ying, *Chem. Mater.* **1998**, 10, 2067. (g) G. Larsen, E. Lotero, M. Nabity, L.M. Petkovic, D. S. Shobe, *J. Catal.* **1996**, 164, 246.

62.   B. Lee, D.L. Lu, J.N. Kondo, K. Domen, *J. Am. Chem. Soc.* **2002**, 124, 11256.

63.   D. M. Antonelli, J. Y. Ying, *Chem. Mater.* **1996**, 8, 874.

64.   S. A. Bagshaw, T. J. Pinnavaia, *Angew. Chem. Int. Ed.* **1996**, 35, 1102

65.   P. Liu, J. Liu, A. Sayari, *Chem. Commun.* **1997**, 577.

66.   K. G. Servin, T. M. AbdeFattah, T. J. Pinnavaia, *Chem. Commun.* **1998**, 1471.

67.   Z. Tian, W. Tong, J. Wang, N. Duan, V. V. Krishnan, S. L. Suib, *Science* **1997**, 276, 926.

68.   P. Yang, D. Zhao, D. I. Margolese, B. F. Chmelka, G. D. Stucky, *Nature* **1998**, 396, 152.

69.   G. D. Yadav, J. J. Nair, *Mircopor. Mesopor. Mater.* **1999**, 33, 1.

70.   V. I. Parvulescu, H. Bonnemann, V. Parvulescu, B. Endruschar, A. Ch. W. Rufinska, B. Tesche, G. Poncelet, *Appl. Catal. A: Gen.* **2001**, 214, 273.

71.   W. H. Bragg, W. L. Bragg, *The Crystalline State*, Vol. 1, McMillan, New York, **1949**.

72.   S. Biz, M. Occelli, *Catal. Rev. -Sci. Eng.* **1998**, 40, 329

73.   G. Bergeret, in *Handbook of Heterogeneous Catalysis*, Vol. 2, Eds: G. Ertl, H. Knozinger, J. Weitkamp, Wiley-VCH, Weinheim, **1997**, p. 464.

74.   C. K. Jorgensen, *Absorption Spectra and Chemical Bonding in Complexes*, Pergamon, New York, **1962.**

75.   G. Kortum, *Reflectance Spectroscopy*, Springer, Berlin, **1969.**

76.   P. R. Griffiths, J. A. De Haseth, *Fourier Transform Infrared Spectrometry*, John Wiley and Sons Inc., New York, **1986**.

77.   C. C. Freyhardt, M. Tsapatsis, R. F. Lobo, K. J. Balkus, M. E. Davis, *Nature* **1996**, 381, 295.

78.   P. A. Jacobs, W. Y. Martier, *Zeolites* **1982**, 2, 226.

79.   J. Ryczkowski, *Catal. Today* **2001**, 68, 263.

80.   M. Mehring, *High Resolution NMR Spectroscopy in Solids*, Springer-Verlag, Berlin, **1976**.

81.   G. Engelhardt, D. Michel, *High-Resolution Solid-State NMR of Silicates and Zeolites*, John Wiley and Sons Ltd., Chichester, **1987**.

82.   G. Engelhardt, in: *Handbook of Heterogeneous Catalysis*, Vol. 2, Eds: G. Ertl, H. Knozinger, J. Weitkamp, Wiley-VCH, Weinheim, **1997**, p. 525.

83.   C. S. Fadley, in: *Electron Spectroscopy: Theory, Techniques and Applications*, Vol. 2, Eds: C. R. Brundle, A. D. Baker, Academic Press, New York, **1978**, p.1.

84.   W. N. Delgass, T. R. Hughes, C. S. Fadley, *Catal. Rev.* **1970**, 4, 179.

85.   W. F. Egelhoff Jr., *Surf. Sci. Rep.* **1987**, 6, 253.

86.   J. W. Robinson, *Atomic Absorption Spectroscopy*, Marcel Dekker, New York, **1975**.

87.   G. Lawes, *Scanning Electron Microscopy And X-Ray Microanalysis*, John Wiley and Sons Ltd., Chichester, **1987**.

88.   D. E. Newbury, D. C. Joy, P. Echlin, C. E. Fiori, J. I. Goldstein, *Advanced Scanning Electron Microscopy and X-Ray Microanalysis*, Plenum Press, New York, **1986**.

89.   J. R. Fryer, *Chemical Applications of Transmission Electron Microscopy*, Academic Press, San Diego, **1979**.

90.   (a) J. M. Thomas, O. Terasaki, P. L. Gai, W. Zhou, J. Gonzalez-Calbet, *Acc. Chem. Res.* **2001**, 34, 583. (b) V. Alfredsson, M. Keung, A. Monnier, G. D. Stucky, K. K. Unger, F. Schuth, *J. Chem. Soc. Chem. Commun.* **1994**, 921.

91.   Z. L. Wang, in: *Characterization of Nanophase Materials*, Ed: Z. L. Wang, Wiley-VCH, Weinheim, **2000**, Chap. 3, p. 37.

92.   S. Brunauer, P. H. Emmett, E. Teller, *J. Am. Chem. Soc.* **1938**, 60, 309.

93.   E. P. Barrett, L. G. Joyner, P. P. Halenda, *J. Am. Chem. Soc.* **1951**, 73, 373.

94.   M. Chamumi, D. Brunel, F. Fajula, P. Geneste, P. Moreau, J. Solof, *Zeolites* **1994**, 14, 283.

95.   J. Manassen, in: *Catalysis, Progress in Research*, Eds: F. Basolo, R. E. Burwell Jr. Plenum Press, New York, **1973**, p. 177.

96.   P. Ermert, in: *Solid-Supported Combinatorial and Parallel Synthesis of Small-Molecular-Weight Compound Libraries*, Eds: D. Obrecht, J. M. Villalgordo, Elsevier, Oxford, **1998**, p. 44.

97.   (a) T. J. Huang, W. O. Haag, US Pat, 4 339 606 **1982**, EP 112 821 **1986**. (b) K.

Weissermel, H. J. Arpe, *Industrielle Organishe Chemie*, Verlag Chemie, Weinheim, **1978**, 108. (c) C. D. Chang, W. H. Lang, N. Morgan, EP 13 600 **1980**. (d) Y. Servotte. J. Jacobs, P. A. Jacobs, in "*Proc. Zeocat Symp.*" Siofok (Hungary) **1985**, *Acta. Phys. Chem*. (Szeged) **1985**, 1. (e) J. Shabati, R. Lazar, E. Biron, *J. Mol. Catal.* **1984**, 27, 35. (f) H. van Bekkum, H. W. Kouwenhoven, *React. Trav. Chim. Phy, Bas,* **1983**, 108, 283. (g) C. D. Chang, W. H. Lang, US Pat. 4 220 783 **1979**.

98.   M. Kawai, M. Onaka, Y. Izumi, *Bull. Chem. Soc. Jpn.* **1988**, 61, 1237.

99.   P. B. Venuto, *Micropor. Mater*. **1994,** 2, 297.

100.   (a) G. A. Olah, *Friedel–Crafts Chemistry*, Wiley/Interscience, New York, **1973**. (b) G. A. Olah, G. K. S. J. Prakash, J. Sommer, *Superacids*, Wiley/Interscience, New York, **1985**.

101.   R. D. Howells, J. D. Mc Cown, *Chem. Rev*. **1977**, 77, 69.

102.   T. W. Bastock, J. H. Clark, *Speciality Chemicals,* Elsevier, London, **1991.**

103.   (a) B. M. Khadilkar, S. D. Borkar, *Chem. Technol. Biotechnol,* **1998***,* 71, 209. (b) R. Commandeur, N. Berger, P. Jay, J. Kervennal, *Eur. Pat. Appl.* EP 0 442 986 **1991** to Atochem S.A.

104.   (a) A. D. Harford, H.W. Vernon, *US Patent 2*, 897 112 **1956**. (b) A. Douglas, H.W. Vernon, *British Petroleum Co. Ltd*., DE-AS, 1 094 035 **1957**.

105.   N. K. Moshinskaya, V. S. Olifer, L. I. Zhuoiev, SU, 137993 **1960**.

106.   E. Siggel, *US Patent*, 2 710 849 **1952**.

107.   (a) H. Hattori, *Chem. Rev.* **1995,** 95, 537. (b) R. J. Davis, *J. Catal.* **2003,** 216**,** 396. (c) D. Barthomeuf, *Catal. Rev. Sci. Eng*. **1996,** 38, 521. (d) Z.-H. Fu, Y. Ono, *J. Catal.* **1994,** 145**,** 166. (e) D. Brunel, *Micropor. Mesopor. Mater*. **1999,** 27**,** 329. (f) R. Bal, K. Chaudhary, S. Sivasanker, *Catal. Lett*. **2000,** 70, 75.

108.   D. J. Macquarrie, R. Nazih, S. Sebti, *Green Chemistry* **2002,** 4, 56.

109.   (a) Y. Ono, *Appl. Catal. A: Gen.* **1997,** 155**,** 133. (b) P. Tundo, M. Selva, *Chem. Tech*. **1995,** 25, 31. (c) J-P. Rieu, A. Boucherle, H. Cousse, G. Mouzin, *Tetrahedron* **1986,** 42, 4095.

110.   (a) P. Tundo, G. Malagho, F. Trotta, *Ind. Eng. Chem. Res*. **1989,** 28, 881.(b) M.Selva, C.A. Marques, P. Tundo, *J. Chem. Soc. Perkins Trans.* **1994,** 1, 1323.

111.   (a) H. Yamamoto and K. Oshima, *Main Group Metals in Organic Synthesis*, **2002,** 2, 409. (b) I. Fleming, D. H. R. Barton, D. Ollis, J. D. Neville, *In Comprehensive Organic Chemistry* Eds. Pergamon Press: Oxford, **1979**, Vol. 3, Chap. 13, p. 539. (c) W. P. Weber, *Silicon Reagents in Organic Synthesis*; Springer, Berlin, **1983**. (d) E. W. Colvin, *Silicon Reagents in Organic Synthesis*; Academic Press: London, **1988**. (e) E. Langkope, D. Schinzer, *Chem. Rev*. **1995**, 95, 1375. (f) I. Fleming, A. Barbero, D. Walter, *Chem. Rev*. **1997**, 97, 2063. (g) Z. Rappoport, Y. Apeloig, *The Chemistry of Organic Silicon Compounds*; Eds; Wiley, Chichester, **1998**; Vol. 2; S. Patai, Z. Rappoport, Eds., **1989**; Vol. 1.

112.   (a) T. Mukaiyama, *In Organic Reactions*; Wiley, New York, **1982**; Vol. 28, p. 203. (b) C. Gennari, B. M. Trost, I. Fleming, *In Comprehensive Organic Synthesis,*   Eds. Peragamon Press, Oxford, **1991**; Vol. 2, Chap. 2.4, p. 629.

113.   (a) A. Hosomi, Acc. *Chem. Res*. **1988**, 21, 200. (b) I. Fleming, B. M. Trost, I. Fleming, *In Comprehensive Organic Synthesis* Eds. Peragamon Press, Oxford, **1991,** Vol. 2, Chap. 2.4, p. 563.

114.   T. Hiyama, *Metal-Catalyzed Cross-Coupling Reactions*, Wiley, Weinheim, **1998**, Chap. 10, p. 421.

115.   (a) K. Narasaka, K. Soai, T. Mukaiyama, *Chem. Lett.* **1974**, 1223. (b) K. Saigo, M. Osaki, T. Mukaiyama, *Chem. Lett.* **1976**, 163. (c) K. Narasaka, K. Soai, Y. Aikawa, T. Mukaiyama. *Bull. Chem. Soc. Jpn.* **1976**, 49, 779. (d) N. Iwasawa, T. Mukaiyama, *Chem. Lett.* **1987**, 463. (e) M. Hayashi, A. Inubushi, T. Mukaiyama, *Bull. Chem. Soc. Jpn*. **1988**, 61, 4037.

116.   (a) J. Boyer, R. J. P. Corriu, R. Perz, C. Reye, *Tetrahedron* **1983**, 39, 117. (b) R. Noyori, I. Nishida, J. Sakata, *J. Am. Chem. Soc*. **1983**, 105, 1598. (c) T. V. Rajan Babu, *J. Org. Chem*. **1984**, 49, 2083, (d) C. R. Brindaban, S. Manika, B. Sanjay, *Tetrahedron Lett*. **1993**, 34, 1989.

117.   (a) M. Kawai, M. Onaka, Y. Izumi, *J. Chem. Soc. Chem. Commun*. **1987,** 1203. (b) M. Sasidharan, R. Kumar, *Catal. Lett.* **1996,** 38, 251. (c) M. Sasidharan, R. Kumar, *J. Catal.* **2003**, 220, 326.

118.   (a) T. Mukaiyama, K. Narasaka, K. Banno, *Chem.Lett.* **1973**, 1011. (b) T. Mukaiyama, K. Banno, K. Narasaka, *Chem.Lett.* **1973**, 1011. (c) T. Mukaiyama, K. Banno, K. Narasaka, *J. Am. Chem. Soc.* **1974**, 96, 7503.

119.   (a) R. Noyori, K. Yokoyama, J. Sakata, I. Kuwajima, E. Nakamura, M. Shimizu, *J. Am. Chem. Soc.* **1977**, 99, 1265. (b) E. Nakamura, M. Shimizu, I. Kuwajima, J. Sakata, K, Yokoyama, R Noyori, *J. Org. Chem.* **1983**, 48, 932. (c) R. Noyori, I. Nishida, J. Sakata, *J. Am. Chem. Soc.* **1983,**105, 1598.

120.   (a) T. Bach, *Angew. Chem. Int. Ed.* **1994**, 33, 417. (b) S. G. Nelson *Tetrahedron: Asymmetry* **1998**, 9, 357. (c) H. Groger, E. M. Vogl, M. Shibashaki, *Chem. Eur. J*. **1998,** 4, 1137. (d) E. N. Jacobsen, A. Pfaltz, H. Yamamoto, *In Comprehensive Asymmetric Catalysis*, Eds; Springer, Heidelberg, **1999**, Vol. 3, p. 998. (e) R. Mahrwald, *Chem. Rev.* **1999**, 99, 1095. (f) T. D. Machajewski, C.-H. Wong, *Angew. Chem. Int. Ed.* **2000**, 39, 1352.

121.   (a) C.-J, Li, T. -H, Chan, *Organic Reactions in Aqueous Media*; Wiley, New Work, **1997**. (b) P. A. Grieco, *Organic Synthesis in Water*, Ed.; Blackie Academic and Professional, London, **1998**. (c) B. Cornils, W. A. Herrmann, *Aqueous-Phase Organometallic Chemistry: Concepts and Applications*; Wiley-VCH, Weinheim, **1998**.

122.   (a) M. Sasidharan, S. V. N. Raju, K. V. Srinivasan, V. Paul, R. Kumar, *Chem. Comm.* **1996**, 129. (b) T. Gaydhankar, P. N. Joshi, P. Kalita, R. Kumar, *J. Mol. Catal. A: Chem.* **2006,** 265, 306.

123.   R. Garro, M. T. Navarro, J. Primo, A. Corma, *J. Catal.* **2005**, 233, 342.

124.   (a) S. G. Davies, T. D. McCarthy, *Synlett* **1995**, 700. (b) S. D. Bull, S. G. Davies, S. Delgado-Ballester, G. Fenton, P. M. Kelly, A. D. Smith, *Synlett* **2000**, 1257.

125.   D. Rosenthal, G. Braundrup, K. H. Davis, M. E. Wall, *J. Org. Che*m. **1965**, 30, 3689.

126.   T. L. Gilchrist, *Heterocyclic Chemsistry*, Academic Press, London, **1997**, p. 231.

127.   (a) J. Szmuszkovicz, *J. Am. Chem. Soc*. **1957**, 79, 2819. (b) Z, Iqbal, A. H Jackson, K. R. N. Rao, *Tetrahedron Lett*. **1988**, 29, 2577 (c) P. E. Harrington, M. A. Kerr, *Synlett*, **1996**, 1047. (d) P. E Harrington, M. A Kerr, *Can. J. Chem.* **1998**, *76*, 1256. (e) M. Agnusdei, M. Bandini, A. Melloni, A. Umani-Ronchi, *J. Org.Chem*. **2003**, 68, 7126.

128.   (a) M. Tani, S. Matsumoto, Y. Aida, S. Arikawa, A. Nakane, Y. Yokayama, Y. Murakami, *Chem. Phar. Bull.* **1994**, 42, 443. (b) H.-C. Zhang, H.Ye, A. F.

Moretto, K. K. Brumfield, B. E. Maryanoff, *Org. Lett.* **2000**, 2, 89. (c) G. W. Gribble, *J. Chem. Soc. Perkin Trans.* **2000**, 1, 1045.

129.   (a) W. J. Houlihan, *Indoles*; John Wiley & Sons, Inc.: New York, **1972**; Vol. 1, p 71. (b) Z. Iqbal, A. H Jackson, K. R. Rao, *Tetrahedron Lett.* **1988**, 29, 21.

130.   (a) Z. Iqbal, A. H. Jackson, K. R. N. Rao, *Tetrahedron Lett*. **1985**, 29, 2577. (b) A. H Jackson, R. K. Pandey, K. R. N. Rao, E. Roberts, *Tetrahedron Lett*. **1985**, 26, 793. (c) P. Laszlo, *Acc. Chem. Res.* **1986**, 19, 121. (d) J. M. Adams, *Appl. Clay Sci*. **1987**, 2,309. (e) R. Tahir, K. Banert, A. Solhy, S. Sebti, *J. Mol. Catal. A: Chem.* **2006**, 246, 39.

131.   (a) J. R. Johnson, *Org. React.* **1942,** 1, 210. (b) R. L. Shirner, *Org. React.* **1942,** 1, 1. (c) G. Jones, *Org. React*. **1967,** 15, 204. (d) G. Brufola, F. Fringuelli, O. Piermatti, F. Pizzo, *Heterocycles* **1996**, 43, 1257. (e) R. O'Kennedy, R. D. Thornes, *Coumarins: Biology, Applications and Mode of Action,* Wiley and Sons, Chichester, **1997**. (f) I. Yavari, R. Hekmat-Shoar, A. Zonouzi, *Tetrahedron Lett*. **1998,** 39, 2391. (g) R. D. H. *Prog. Chem. Org. Nat. Prod.* **1991**, 58, 84.

132.   (a) W. Bridge, A. J. Crocker, T. Cubin, A. Robertson, *J. Chem. Soc.* **1937**. 1530. (b) Ghosh, Todd, and Wilkinson, *J. Chem. Soc.* **1940**. 1121. (c) R. Adams, B. R. Baker, *J. Am. Chem. Soc.* **1940**, 62, 2405.

133.   (a) H. von Pechmann, C. Duisberg, *Chem. Ber*. **1884**, 17, 929. (b) S. Sentha, R. Phadke, *Org. React*. Vol.7, chap. 1, **1953**, p. 1. (c) E. C. Horning, *Organic Synthesis, Coll.* Vol. III, John Wiley & Sons, New York, **1955**, p. 281.

134.   (a) W. D. Bossaert, D. E. De. Vos, W. M. Van Rhijim, J. Bullen, P. J. Grobet, P. A. Jacobs, *J. Catal.* **1999**, 182, 156. (b) I. Diaz, C. Marquez-Alvarez, F. Mohino, J. Perez-Pariente, E. Sastre, *J. Catal.* **2000**, 193, 295. (c) S. Shylesh, S. Sharma, S. P. Mirajkar, A. P. Singh, *J. Mol. Catal. A: Chem.* **2004**, 212, 219.

135.   (a) D. A. Chaudhari, *Chem. Ind*. **1983**, 568. (b) E. A. Gunnewegh, A. J. Hoefnagel, H. van Bekkum, *J. Mol. Catal. A: Chem.* **1995,** 100, 87. (c) B. M. Reddy, M. K. Patil, P. Lakshmann, *J. Mol. Catal. A: Chem.* **1995**, 256, 290. (d) T. Li, Z. Zhang, F. Yang, C. Fu, *J. Chem. Res*. **1998**, 38. (e) I. Rodriguez, S. Iborra, F. Rey, A. Corma, *Appl. Catal. A: Gen.* **2000**, 194-195, 241. (f) S. Fr`ere, V. Thi´ery, T. Besson, *Tetrahedron Lett*. **2001**, 42, 2791. (g) B. M.

Reddy, V. R. Reddy, D. Giridar, *Synth. Commun*. **2001**, 31, 3603. (h) M. C. Laufer, H. Hausmann, W. F. Holderich, *J. Catal.* **2003**, 218, 315. (i) J. C. Rodri-Dominguez, G. Kirsch, *Tetrahedron Lett.* **2006**, 47, 3279. (j) S. Selvakumar, M. Chidambaram, A. P. Singh, *Catal. Commun*. **2007**, 8, 777. (k) B. Tyagi, M. K. Mishra, R. V. Jasra, *J. Mol. Catal. A: Chem.* **2007**, 276, 47.

136.   (a) D. M. Barnes, J. Ji, M. G. Fickes, M. A. Fitzgerald, S. A. King, H. E. Morton, F. A. Plagge, M. Preskill, S. H. Wagaw, S. J. Wittenberger, J. Zhang, *J. Am. Chem. Soc*. **2002**, 124, 13097. 130. (b) M. Watanabe, A. Ikagawa, H. Wang, K. Murata, and T. Ikariya, *J. Am. Chem. Soc.* **2004**, 126, 11148.

137.   (a) J. Mulzer, R. Zuhse, R. Schmiechen, *Angew. Chem. Int. Ed.* **1992**, 31, 870. (b) J. Ji, D. M. Barnes, J. Zhang, S. A. King, S. J. Wittenberger, H. E. Morton, *J. Am. Chem. Soc.* **1999,** 121*,* 10215. (c) P. J. Nichols, J. A. DeMattei, B. R. Barnett, N. A. LeFur, T-H Chuang, A. D. Piscopio, K. Koch, *Org. Lett*. **2006**, 8, 1495.

CHAPTER 2

SYNTHESIS AND CHARACTERIZATION

2.1. INTRODUCTION

The syntheses of mesoporous silicate materials have opened-up new possibilities for preparing heterogeneous catalysts containing uniform pores with high surface area.[1] These mesoporous materials have great potential in a wide range of applications such as catalyst for the synthesis of fine chemicals, as support, sensor, etc.[2] Surface modification of M41S type mesoporous silicates by reactive organic functional groups have been investigated extensively.[3] This surface modification allows tailoring of the surface properties for variety of potential applications, *viz.*, catalysis, immobilization of catalytically reactive species, chemical sensing and fabrication of nanomaterials.[2,4] The inorganic part (polymeric silicate framework) of the surface modified hybrid mesoporous materials provides structural, thermal and mechanical stability; whereas the pendant organic species permit flexible control of interfacial properties to provide covalently linked anchoring site for catalytically important metals and metal complexes.

This chapter presents the experimental data regarding

(i) the synthesis of siliceous mesoporous Si-MCM-41 and in situ incorporation of Ce and Al in MCM-41 network, using our published procedure.[5-7]

(ii) the synthesis of Zr-TMS materials and surface modification of Zr-TMS materials by organic functional group *viz*. trifluoromethanesulphonic acid (triflic acid).[8]

(iii) the synthesis of Si-MCM-41[1] and SBA-15 materials,[9,10,11] and immobilization of 1,5,7-triazabicyclo [4.4.0] dec-5-ene (TBD) in MCM-41[12,13] and SBA-15 through post-synthesis routes.

2.2. CHARACTERIZATION TECHNIQUES

The powder X-ray diffractograms of as-synthesized and calcined samples were recorded on a Rigaku Miniflex diffractometer (Cu-K$_\alpha$ radiation, λ = 1.54054 Å) in 2θ range 1.5 –10° at a scanning rate of 1° min^{-1}, and 1.5-60° at a scanning rate of 2° and 4° min^{-1} for MCM-41 and Zr-TMS materials, respectively. The PXRD data for SBA-15 materials were collected on a PAN alytical X'pert Pro instrument using Bragg-Brentano geometry in 2θ range 0.5–5.0° at a scanning rate of 1° min^{-1} (λ = 1.5416 Å). The specific surface area (S$_{BET}$) and mesoporosity were checked by N$_2$ sorption at 77 K using NOVA 1200 Quantachrome equipment. The samples were evacuated at 573 K before N$_2$ sorption. The surface area was calculated from linear part of BET (Brunauer-Emmet-Teller) equation and the method of Barret-Joyner-Halenda (BJH) was employed to determine the pore-size distribution (PSD). The coordination of the metal ions was monitored by using diffuse reflectance UV-visible spectroscopy. A Shimadzu UV-2101 PC spectrometer equipped with a diffuse reflectance attachment was employed for this purpose using BaSO$_4$ as reference. Elemental analysis for C, H, N and S to measure the sulfonic acid and TBD loading in the catalysts were recorded by an EA 1108 elemental analyzer (Carloalysts were recorded by an EA 1108 elemental analyzer (Carloba instruments).

The solid state MAS and CP MAS NMR spectra were recorded on a Bruker MSL 300 NMR spectrometer. The finely powdered samples were placed in 7.0 mm zirconia rotors and spun at 7-8 kHz. The resonance frequencies of ^{29}Si, ^{27}Al, ^{13}C were 59.63, 78.2, 75.47 MHz, respectively. The chemical shifts were determined using aluminum sulphate (δ = 0 ppm from TMS), 3-(trimethylsilyl) propane-1-sulfonic acid (δ = 0 ppm from TMS) and adamantane (δ = 28.7 ppm from TMS) as the reference compounds for ^{27}Al, ^{29}Si and ^{13}C, respectively. The XPS analyses were conducted on

a Perkin-Elmer model 5300 X-ray photoelectron spectrometer equipped with MgK_α radiation.

Fourier transform infrared (FTIR) spectra recorded for functional group detection in the range of 400-4000 cm^{-1} on a Shimadzu FTIR 8201 PC and KBr pallet was taken as reference. The IR spectra were recorded at different temperatures and 300 scans were collected for each spectrum. To study the absorption of pyridine in mesoporous materials, Thermo Nicolet FTIR-instrument was used. A Thermo Nicolet (model-Nexus 870) FT-IR equipped with a high-pressure high-temperature stainless steel cell, fitted with water cooled CaF_2 windows and described earlier in detail,[14] was employed for recording of IR spectra in transmission mode. Self-supporting wafers ($\sim$ 50 mg) of 25 mm diameter, placed in a sample holder block, were in direct contact with a chromel-alumel thermocouple. Samples were heated *in-situ* for 8-10 h at a temperature of 550-575 K under vacuum ($\sim$1×10^{-3} Torr) for recording of the hydroxyl region bands, and also for carrying out pyridine adsorption experiments. For acidity measurements, samples were exposed at 420 K to multiple doses of pyridine (~9.5 µmol g^{-1} each) until it reached saturation coverage. A gas mixture containing nitrogen gas saturated with pyridine vapor was used for this purpose. The gas pressure in the IR cell was monitored with the help of a digital capacitance manometer. IR spectra were plotted at 420 K after equilibration time of 15-20 min for individual pulse injections. From these experiments calibration data were obtained for each sample, indicating a relationship between the area under spectral lines corresponding to Lewis and Brönsted acid sites and the amount of pyridine adsorbed. Final spectra were recorded under two different temperature conditions in order to distinguish between the weak and the strong adsorption sites: at 420 K after 10 min evacuation of the cell at the temperature of pyridine adsorption, or alternatively at room temperature

following post-exposure cooling of the sample and subsequent evacuation. A total of 300 scans were co-added for plotting of each spectrum at a resolution of 4 cm^{-1}. The absorbance values of individual vibrational bands, shown in parentheses in some of the figures, were taken as a measure of the relative intensities for gross inter-comparison.

The total acidity and acid strength of the catalysts were measured by temperature programmed desorption of NH$_3$(NH$_3$-TPD) using a micromeritics Autochem-2910 instrument. About 0.2 g of a fresh sample was placed in a U-shaped, flow-through, quartz micro-reactor for each experiment. The catalyst was activated at 775 K for 2 h under He flow (20 ml / min) and then cooled to 375 K before exposure to ammonia. The sample was flushed again in He for 1 h to remove any physisorbed ammonia and desorption profile was then recorded by increasing the sample temperature from 375 to 773 K at a ramp of 10 K min^{-1} by using TCD detector.

The scanning electron microscopic (SEM) images were recorded on a Philips Model XL 30 instrument. The samples were loaded on stubs and sputtered with thin gold film to prevent surface charging and also to protect from thermal damage from the electron beam, prior to scanning. The samples were dispersed on Holey carbon grids and Transmission Electron Microscopic (TEM) images were scanned on a Jeol Model 1200 EX instrument operated at an accelerating voltage of 100 kV.

2.3. SYNTHESIS OF MCM-41 MATERIALS

2.3.1. MATERIALS

Fumed silica (Surface area = 384 m^2 g^{-1}, Sigma Aldrich, USA), NaOH (Merck, India), sodium aluminate (NaAlO$_2$, 42.0 %, Al$_2$O$_3$, 39.0%, Na$_2$O and 19.0% H$_2$O; Loba Chemie, India), and cerium (IV) sulpahte (Ce(SO$_4$)$_2$.4H$_2$O) were

employed as starting material. Cetyltrimethylammonium bromide (CTMABr; Loba Chemie, India) was used as a structure directing agent.

2.3.1.1. Synthesis Procedure of Al-MCM-41, Ce-MCM-41 and Ce-Al-MCM-41 Materials

The syntheses of siliceous Si-MCM-41, Al-MCM-41, Ce-MCM-41 and Ce-Al-MCM-41 materials were carried out applying published procedure[5-7] The molar gel composition of Ce-containing Al-MCM-41 samples was: 1 SiO_2: x CeO_2: y Al_2O_3: 0.32 NaOH: 0.25 CTMABr: 125 H_2O where x was varied in the range of 0.0-0.04. The composition of the synthesis gel and the values of molar ratio Si/Al and Si/Ce in the final products are given in Table 2.1.

The hydrothermal syntheses of Si-MCM-41, Al-MCM-41, Ce-MCM-41 and various compositions of Ce-containing Al-MCM-41 (Ce-Al-MCM-41) samples with different Si/Ce ratios were carried out in a teflon-lined autoclave at a temperature of 383 K and over a period of 36 h. In a typical synthesis of a Ce-MCM-41 sample, 6.0 g of fumed silica was slowly added to 1.28 g of NaOH in 40.0 g of water under vigorous stirring for half an hour. Subsequently, an aqueous solution of sodium aluminate (accordingly required amount dissolved in 10.0 g of water) was added followed by the addition of 7.28 g of CTMABr dissolved in 40.0 g of water under vigorous stirring for half an hour. Finally, an aqueous solution of ceric sulphate (required amount dissolved in 10.0 g of water) was added to the gel mixture and the mass was stirred for half an hour. The remaining 125 g of water was then added and the stirring was continued further for half an hour. Finally, the synthesis gel was taken in a teflon-lined autoclave at 383 K for 36 h.

After the hydrothermal treatment, the samples were washed thoroughly first with distilled water and then with acetone, followed by drying (353 K) and

calcinations (775 K) for 8 h in air. The samples thus obtained were treated at room temperature with 0.5 M ammonium acetate solution twice to obtain the NH_4-form and then calcined again at 775 K for 7 h to finally obtain the H-form of MCM-41 samples. All the samples were of light yellow color.

Table 2.1. Chemical compositions of the synthesis gel mixtures

1 SiO_2: 0.32 NaOH: 0.25 CTMABr: 125 H_2O : x CeO_2: y Al_2O_3

Sample No	Sample	x	y	Si/Ce Gel	Si/Ce Solid[a]	Si/Al Gel	Si/Al Solid[a]
A	Si-MCM-41	0	0	0	0	0	0
B	Al-MCM-41 (25)[b]	0	0.04	0	0	25	30
C	Ce-MCM-41 (25, 0)[c]	0.04	0	25	30	0	0
D	Ce-Al-MCM-41(100, 25)[d]	0.01	0.04	100	108	25	32
E	Ce-Al-MCM-41 (75, 25)[d]	0.013	0.04	75	80	25	32
F	Ce-Al-MCM-41 (50, 25)[d]	0.02	0.04	50	59	25	33
G	Ce-Al-MCM-41 (25, 25)[d]	0.04	0.04	25	38	25	34
H	Amorphous SiO_2+ CeO_2+Al_2O_3(50,25)[d]	0.02	0.04	50	-	25	-
I	Pure CeO_2	-	-	-	-	-	-

[a] Calculated by AAS analysis.

[b] Numerical values in the parenthesis represents Si/Al ratio.

[c] Numerical values in the parenthesis represents Si/Ce ratio.

[d] Numerical values in the parenthesis represents Si/Ce and Si/Al ratio in gel, respectively.

2.3.2. CHARACTERIZATION

2.3.2.1. Powder X-Ray Diffraction

Figure 2.1 shows the powder X-ray diffraction (PXRD) patterns of calcined MCM-41 samples, exhibiting typical hexagonal phase (p6mm) and main (100) peak with (110), (200), (210) reflections in all samples. These results indicate ordered mesoporosity even after bi-metal incorporation of Al and Ce. As a representative case, the XRD pattern of calcined Ce-Al-MCM-41 (sample G with highest Ce contents) is shown in the Figure 2.2 in the range of 1.5-60° (2°/minute) along with the XRD patterns of physical mixture of 2.5 % of CeO_2 and calcined Al-MCM-41 (sample B) as well as pure CeO_2. These data clearly show the absence of any extra-network occluded CeO_2 phase in the Ce containing samples. These results are in agreement with our earlier reports on Ce-MCM-41.[5-7] The d_{100} values of different MCM-41 materials are given in Table 2.2 along with the corresponding unit cell parameter (a_o) of different samples, calculated from the peak with hkl (100) value and by using the equation $a_o = 2\ d_{100}/\sqrt{3}$. The slight increase in the d-values and increase in the hexagonal unit cell parameter can be taken as an indication of incorporation of cerium in the MCM-41 network. The observed increase in unit cell parameter on cerium incorporation in Al-MCM-41 may be attributed to the larger size of Ce^{4+} compared to that of Si^{4+}. Similar observations have been reported by earlier workers for incorporation of different transition and non-transition metal ions into framework of MCM-41.[15,16]
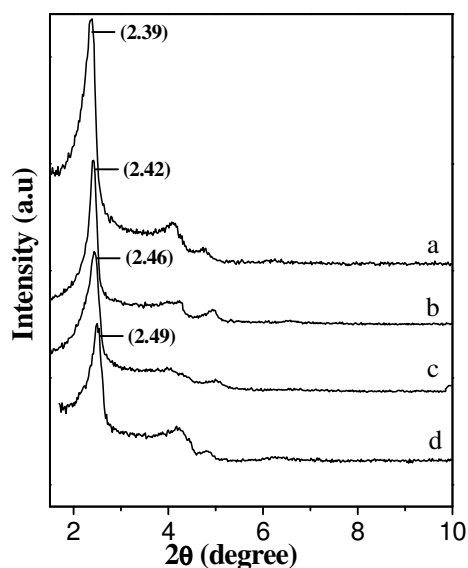
Figure 2.1. X-ray diffraction patterns of calcined (a) Si-MCM-41,(b) Al-MCM-41 (0, 30), (c) Ce-MCM-41 (30, 0), (d) Ce-Al-MCM-41 (38, 34) catalysts.
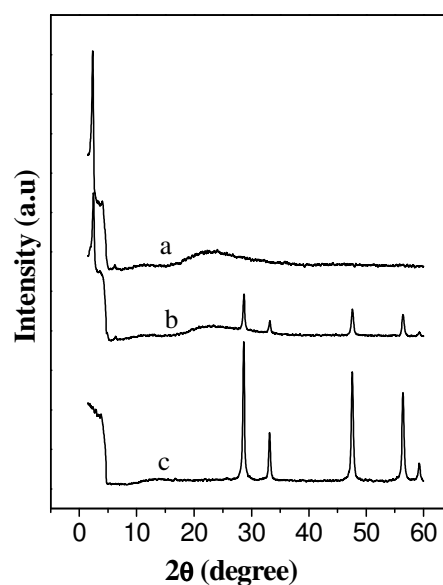
Figure 2.2. X-ray diffraction patterns of (a) Ce-Al-MCM-41 (sample G), (b) physical mixture of 2.5 % of CeO_2 in Al-MCM-41 (sample B) and (c) pure CeO_2.

2.3.2.2. Porosity Measurments

The porosity of the MCM-41 sample was evaluated by N_2 adsorption isotherms. Figure 2.3 shows N_2 adsorption-desorption isotherm and the corresponding pore size distribution curve (inset) for the sample Al-MCM-41 (sample B), Ce-MCM-41 (sample C), Ce-Al-MCM-41 (sample G). The data on specific surface area and pore diameter (BJH method) for different samples are shown in Table 2.2. All the samples showed type-IV isotherms with typical hysterisis loops,[17] having a sharp capillary condensation step at P/P_0 = 0.3-0.45 region, which is characteristic property of MCM-41 type ordered mesoporous materials.[18] In Table 2.2, a gradual decrease in BET surface area and an increase in average pore diameter as a function of increase in cerium content in MCM-41can be observed. These results are in agreement with our

XRD data and as mentioned above the increase in pore diameter with increase in cerium content may be attributed to the incorporation of larger size of Ce^{4+} cations in silica framework.
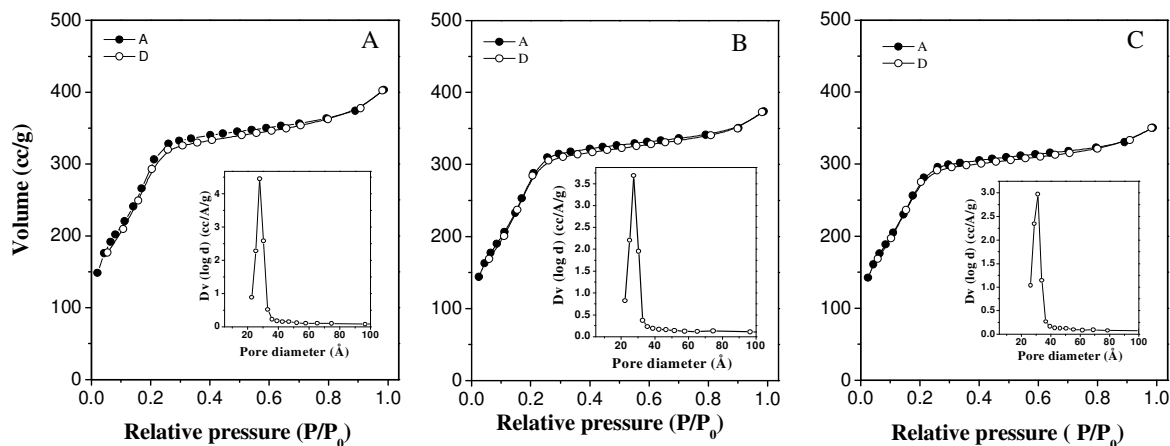

Figure 2.3. N_2 adsorption-desorption isotherms and corresponding pore size distribution curves (inset) for (A) Al-MCM-41 (sample B), (B) Ce-MCM-41 (sample C) and (C) Ce-Al-MCM-41 (sample G).

Table 2.2. Physicochemical characterization of MCM-41 samples.

Sample	Catalyst	Ce/Al Molar ratio	S_{BET} (m^2/g)	d_{100} (Å)	a_o[a] (Å)	Pore diameter (Å)
A	Si-MCM-41	-	1165	37.90	43.76	27.6
B	Al-MCM-41 (-, 30)	-	1104	37.88	43.74	27.9
C	Ce-MCM-41 (30, -)	-	850	37.63	43.32	27.1
D	Ce-Al-MCM-41 (108, 32)	0.3	995	38.45	44.39	28.9
E	Ce-Al-MCM-41 (80, 32)	0.4	989	38.44	44.38	29.5
F	Ce-Al-MCM-41 (59, 33)	0.6	971	38.43	44.37	30.85
G	Ce-Al-MCM-41 (38, 34)	0.9	940	38.41	44.35	31.14

[a] a_o, Unit cell parameter = 2 $d_{100}/\sqrt{3}$.

2.3.2.3. Diffuse Reflectance UV-Vis Spectroscopy

Curves C-G in Figure 2.4 represents the UV-Vis spectra of calcined $Ce_xAlMCM-41$ samples for different values of x. Curve H in this figure represents the spectrum of the physical mixture of silica, ceria and alumina powder. The Ce-Al-MCM-41 samples show a single symmetrical band at ca. 300 nm. It is well known that the position of the ligand to metal charge transfer ($O^{2-} \rightarrow Ce^{4+}$) spectra depends upon the ligand field symmetry surrounding the Ce centre. The tetra-coordinated Ce^{4+} requires higher energy than a hexa-coordinated one in electronic transitions from oxygen to cerium. It may therefore be concluded that the absorbance spectra of Ce-Al-MCM-41 at *ca.* 300 nm may arise, as shown in Figure 2.4 (curves C-G), due to the well-dispersed Ce^{4+} species (in tetra coordinated environment).
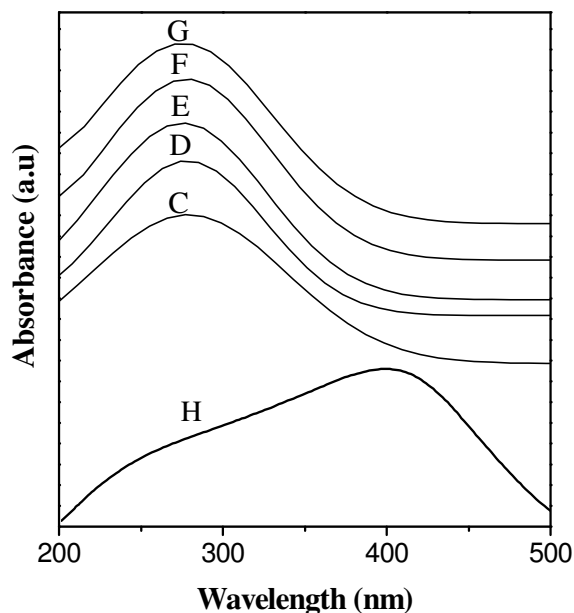

Figure 2.4. Diffuse reflectance UV-vis spectra of calcined samples (C) Ce-MCM-41 (30), (D) Ce-Al-MCM-41 (108, 32), (E) Ce-Al-MCM-41 (80, 32), (d) Ce-Al-MCM-41 (59, 33), (e) Ce-Al-MCM-41 (38, 34), and (H) SiO_2+ CeO_2+ Al_2O_3 (50, 25).

However, the sample prepared by physical mixture of silica, ceria and alumina powder (Figure 2.4, curve H) shows a red shift, where the absorption at wavelength ≈ 400 nm is known to occur due to hexa coordinated Ce^{4+} species.[5,6] Therefore, the comparison of spectral features of Ce-Al-MCM-41 and pure CeO_2 samples indicates the absence of secondary extra network phase of ceria in our samples, in agreement with XRD data. To confirm whether any Ce^{3+} phase is also present in Ce-MCM-41 and Ce-Al-MCM-41 samples, EPR measurements were carried out as Ce^{3+} is EPR active and Ce^{4+} is EPR inactive.[5,6] All Ce-containing samples were found to be EPR silent, clearly indicating the absence of any Ce^{3+} species. This became clear from the NMR studies where no effect of paramagnetic Ce^{3+} was seen. Further XPS data also supported the absence of Ce^{3+}.

2.3.2.4. Solid State ^{13}C CP MAS NMR Spectra

The solid state ^{13}C CP MAS NMR spectra of as-synthesized Ce-Al-MCM-41, Si-MCM-41 and CTA^+ ions in solution ($CDCl_3$) are shown in Figure 2.5. A comparison of the three spectra shows the presence of intact CTA^+ ions inside the pores of the MCM-41 channels. All the three ^{13}C NMR spectra are similar and therefore, the peak assignments are also same. The peaks at *ca*. 66 ppm in these spectra can be assigned to the CH_2 group of the cetyl chain neighboring the nitrogen atom. The peaks at *ca*. 53 ppm are due to the three CH_3 groups bonded to nitrogen atom, whereas the resonance between 32 and 22 ppm are due to different CH_2 carbon atoms of the cetyl chain. The peaks observed at *ca*. 14 ppm can be attributed to the terminal CH_3 group of the cetyl chain. The peaks (triplet) at *ca*. 77 ppm for CTA^+ in solution are due to solvent ($CDCl_3$).
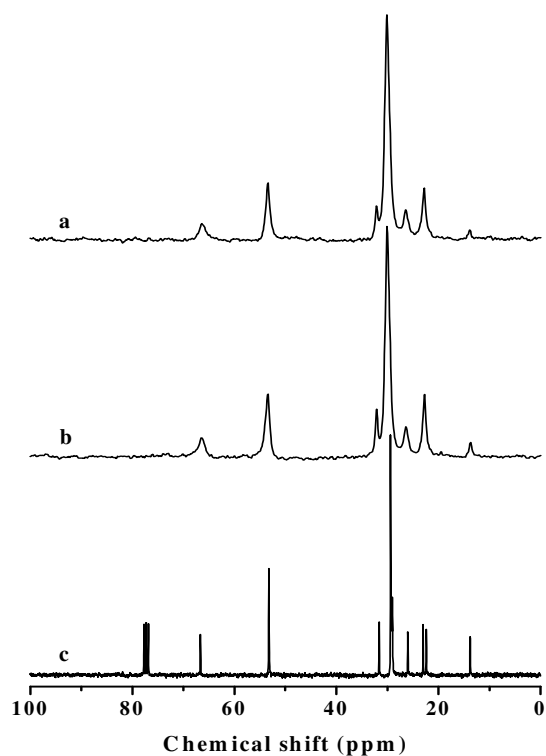
Figure 2.5. ^{13}C CP MAS NMR spectra of as-synthesized samples (a) Ce-Al-MCM-41 (38, 34), (b) Si-MCM-41 and (c) CTMA$^+$ ions in solution (CDCl$_3$).

2.3.2.5. Solid State ^{29}Si CP MAS NMR Spectra

Although, the ^{29}Si CP MAS NMR spectroscopy is a very sensitive probe for the characterization and identification of crystalline microporous zeolites and metallo-silicates, in MCM-41, which is an ordered array of amorphous material, the observed peaks are broad due to the flexibility and broad range of T-O-T angles. All calcined samples show characteristic peaks at around -102.2 and -110.2 ppm, which is usually assigned to Q^3 and Q^4 species, respectively. However, the peak due to Q^3 species is not observed distinctly for the calcined Si-MCM-41 sample (curve a, Figure 2.6). Instead, a broad peak centered at -109.6 ppm (Q^4 species) is observed, probably due to condensation of neighboring of Q^3 species to form Q^4 species during calcination.

Figure 2.6. ^{29}Si CP MAS NMR spectra of calcined samples (A) Si-MCM-41, (B) Al-MCM-41 (30), (E) Ce-Al-MCM-41 (80, 32), (F) Ce-Al-MCM-41 (59, 33) and (G) Ce-Al-MCM-41 (38, 34).

2.3.2.6. Solid State ^{27}Al MAS NMR Spectra

The solid state ^{27}Al MAS NMR spectra of Al-MCM-41 and Ce-Al-MCM-41 are shown in Figure 2.7, exhibiting a strong and sharp signal at 51-52 ppm. The signal at around 51-52 ppm could be assigned to tetrahedrally coordinated Al in the MCM-41 network. Near absence of any signal at around 0 ppm indicate these samples are substantially free from octahedrally coordinate nonframework Al in the MCM-41 network.
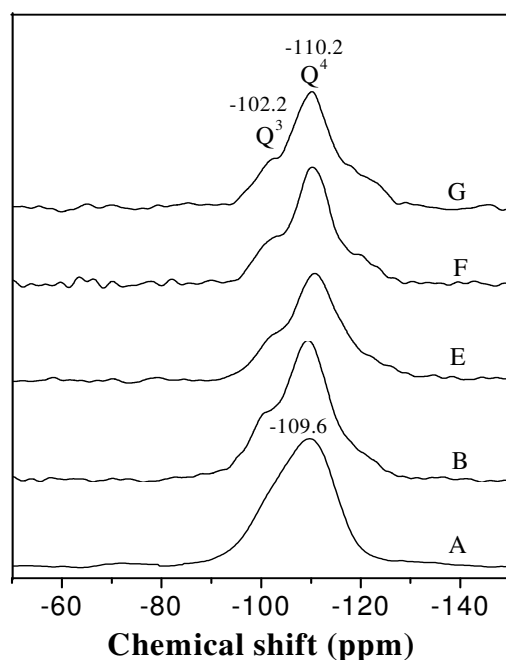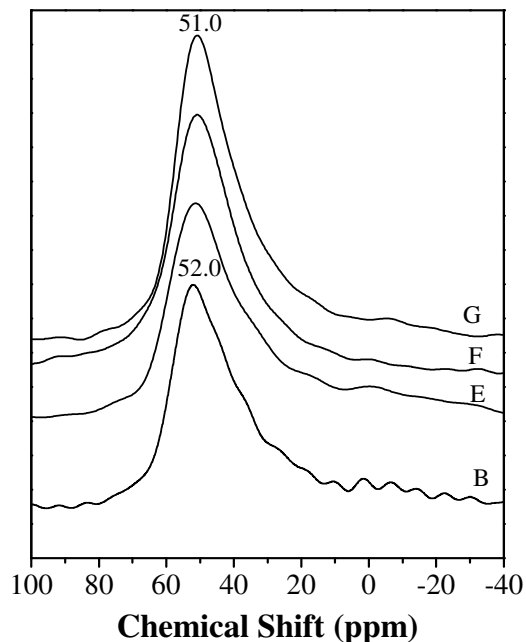
Figure 2.7. ^{27}Al MAS NMR spectra of calcined samples (B) Al-MCM-41 (30), (E) Ce-Al-MCM-41 (80, 32) and (F) Ce-Al-MCM-41 (59, 33) and (G) Ce-Al-MCM-41 (38, 34).

2.3.2.7. X-ray Photoelectron Spectroscopy

The Ce 3d XPS spectra of Ce-Al-MCM-41 are shown in Figure 2.8. The binding energies for different samples with varying Si/Ce and at comparable Si/Al ratios are summarized in Table 2.3. The binding energies of the Ce 3d, Si 2p and Al 2p core levels, found around 882.5 eV, 103.6 eV and 74.8 eV, respectively, agree well with the values reported in the literature.[19,20,21] The increase in binding energies of Si 2p, Al 2P and Ce $3d_{5/2}$ indicate the incorporation of cerium in the silica framework. The binding energies (882.5 eV and 916.0 eV) of Ce indicated that the only Ce (IV) species are present. The characteristic binding energy at 916 eV corresponds to tetravalent cerium Ce (IV).[22,23] This peak is not observed for Ce (III) and it is thus possible to differentiate the two-oxidation states.
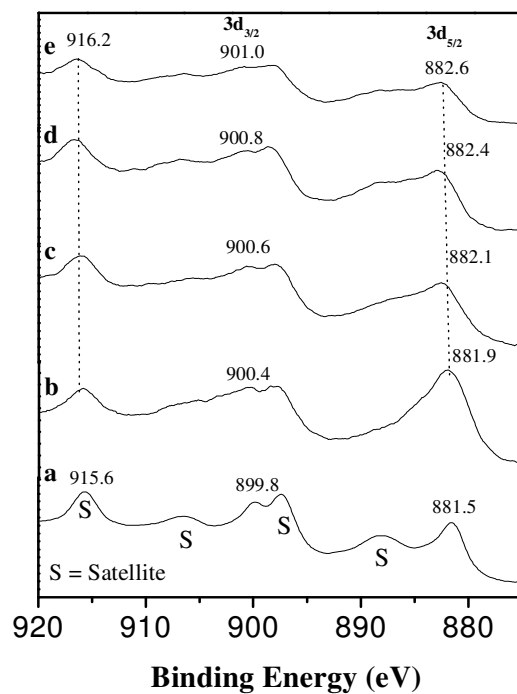
Figure 2.8. The Ce 3d XPS spectra of calcined (a) pure CeO_2, (b) Ce-MCM-41 (30), (c) Ce-Al-MCM-41 (80, 32), (d) Ce-Al-MCM-41 (59, 33) and (e) Ce-Al-MCM-41 (38, 34).

Table 2.3. Binding energies for Al-MCM-41, Ce-MCM-41 and Ce-Al-MCM-41 samples.

Serial no.	Catalysts	Binding energy (eV)		
		Si 2p	Al 2p	Ce $3d_{5/2}$
1	Al-MCM-41 (30)	103.4	74.6	-
2	Ce-MCM-41 (30)	103.4	-	881.8
3	Ce-Al-MCM-41 (108, 32)	103.5	74.7	882.0
4	Ce-Al-MCM-41 (80, 32)	103.6	74.8	882.2
5	Ce-Al-MCM-41 (59, 33)	103.7	74.9	882.5
6	Ce-Al-MCM-41 (38, 34)	103.8	75.0	882.7

2.3.2.8. Scanning Electron Microscopy

Figure 2.9 presents the scanning electron microscopy (SEM) micrographs of a representative Ce-Al-MCM-41 catalyst. In this figure two different kinds of particle morphology that are typical of MCM-41-type materials can be observed. One is winding worm type (Figure 2.9 A) and other one is a hexagonal type (Figure 2.9 B).[1a,b,15] The winding worm and hexagonal particles are of *ca.* 10 μm. The hexagonal morphology is indicative of long-range ordering of Ce-Al-MCM-41 samples.
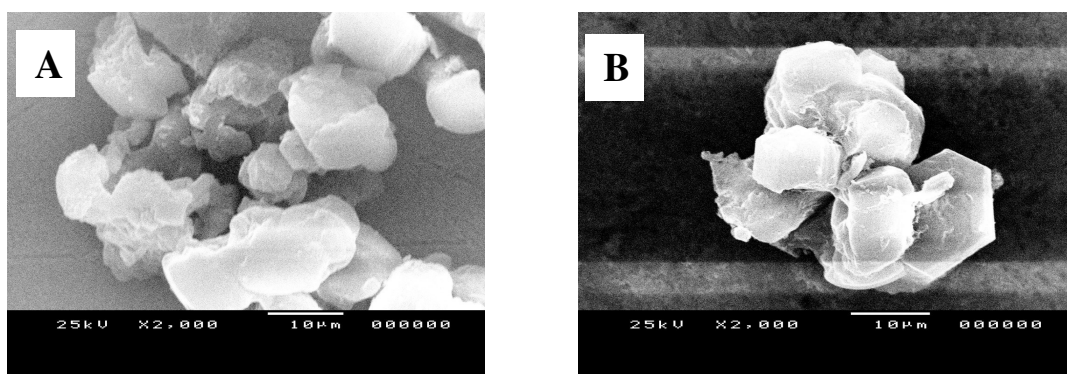

Figure 2.9. Scanning electron micrographs of calcined Ce-Al-MCM-41 sample having different types of particle morphology: (A) winding worm type and (B) hexagonal type.

2.3.2.9. Transmission Electron Microscopy

Figures 2.10 A and 2.10 B present the transmission electron microscopy (TEM) pictures of Ce-Al-MCM-41 parallel fringes corresponding to the side-on view of the long pores as well as a hexagonal system of lattice fringes along the pore direction. The equidistant parallel fringes of Ce-Al-MCM-41 (Figure 2.10 A) show unique feature of separate layers and the addition of such layers, one after one, resulting to the formation of a bunch of layers. Therefore, it supports that the formation of MCM-41 begins with the deposition of two to three monolayers of silicate precursor onto isolated surfactant micellar rods. Subsequently, these silicate-

encapsulated composite species spontaneously form the long-range order characteristic of MCM-41. [1a,b,24]
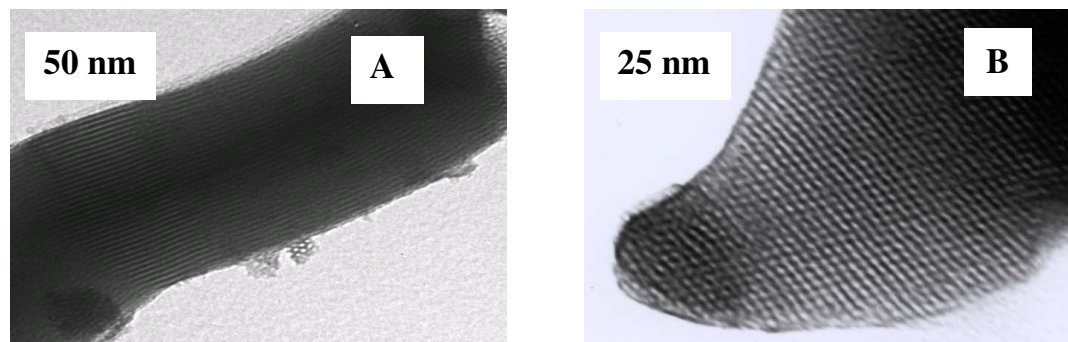

Figure 2.10. Transmission electron micrographs of calcined Ce-Al-MCM-41 (a) parallel fringes (side-on view) and (b) hexagonal array (viewed along the pore direction).

2.3.2.10. Infrared Spectroscopy Study

2.3.2.10.1. O−H Stretching Bands

Figure 2.11 presents the hydroxy region vibrational bands of $Ce_xAlMCM-41$ samples, containing similar Si/Al ratio (~ 25) but different amounts of Ce including a sample of Ce-MCM-41 where no Al is present (Figure 2.11, curve b). As seen in Figure 2.11 (curve b), the samples containing only Ce and no Al exhibit the presence of strong silanol groups ($\equiv$Si−OH, 3744 cm^{-1}) while a negligibly small absorbance was noticed in the lower frequency region. Presence of aluminum gave rise to a broad infrared band with a maximum at 3630 cm^{-1} (Figure 2.11, curve a), the value of full width at half maxima (FWHM) being ~ 140 cm^{-1}. Furthermore, a considerable increase in the intensity of this band was observed in case of the samples consisting of both Ce and Al. In addition, a broad absorbance band at frequency of *ca.* 3530 cm^{-1} and tailing towards lower wave number side was also observed in Ce-Al-MCM-41

samples (Figure 2.11, curves c and d). The presence of the low frequency vibrational band at *ca.* 3530 cm^{-1} becomes apparent on deconvolution of the ν (OH) bands, as shown in the plot given in the inset of Figure 2.11 as a typical case. A specific correlation is also noticeable in the intensity of different IR bands and the extent of heteroatom substitution in MCM-41. Thus, in the case of samples D-G containing comparable amount of Al (Table 2.2), the intensity of the silanol band at 3744 cm^{-1} was found to decrease progressively while that of the low frequency region bands increased with increasing Ce/Al content (Figure 2.11, curves a, c and d). These data are plotted in Figure 2.12. Further, the overall acid site concentration, as estimated from the area under ν (OH) region absorbance bands increased progressively as a function of Ce/Al ratio.

The hydroxy region vibrational bands of MCM-41 have been reported widely, and their frequency and concentration are found to depend on various factors, such as Si/Al ratio and the extent of dehydroxylation.[25,26,27] The 3744 cm^{-1} band arises due to isolated Si-OH groups. The band at 3660 cm^{-1}, observed for Al-MCM 41 and absent in Si-MCM-41 samples, is assigned to the hydroxy groups on coordinatively unsaturated aluminum oxide species that serve as Lewis acid sites. The lower frequency band at ~ 3530 cm^{-1} has also been reported earlier and has been assigned to hydrogen-bonded silanol groups.[26] The present study observes that intensity of lower frequency region bands, particularly the one at 3530 cm^{-1} increases considerably with increasing cerium content and also with increasing Ce/Al atom ratio (Figure 2.11 curves c and d). It is also observed that the increase in the intensity of these bands is normally accompanied by decease in the concentration of silanol groups (3744 cm^{-1} band) (Figure 2.12). The pyridine adsorption results, discussed later, have similarly demonstrated that the concentration of Brönsted and Lewis acid sites increases

considerably as a result of Ce incorporation in Al-MCM-41. The 3630 cm^{-1} band can therefore be assigned to bridge-bonded species, in agreement with the IR spectral features of microporous zeolites such as H/ZSM-5, FAU and BEA, where the O−H stretching bands at ∼3650 cm^{-1} is identified with the Al-(OH)-Si type species.[28]
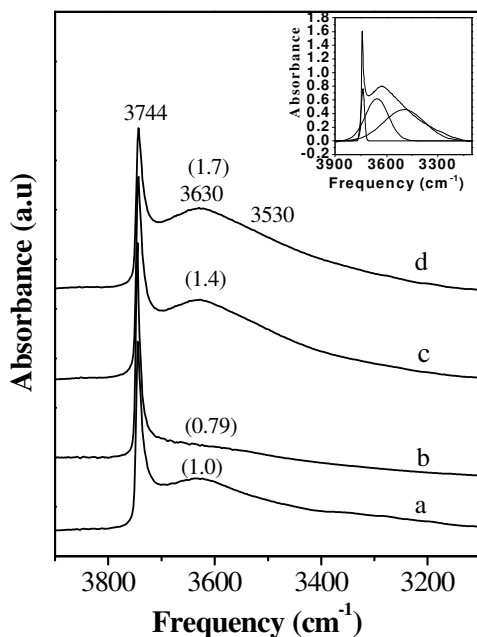
Figure 2.11. Hydroxy region IR spectra of activated Ce-Al-MCM-41 samples containing similar Si/Al ratio (∼ 25) but different Ce content. The absorbance values of individual bands are given in parentheses, curves (a) sample B, no Ce; (b) sample C, no Al; (c) Sample E, Ce/Al = 0.6; (d) sample F, Ce/Al = 0.9. Inset: Deconvolution of ν (OH) bands in Figure 11 d.

Figure 2.12. Variation of intensity (absorbance) of different O-H stretching bands in Figure 2.11, as a function of increasing Ce/Al ratio in Ce-Al-MCM-41 samples, curves (a) 3744; (b) 3630; and (c) 3520 cm^{-1}.

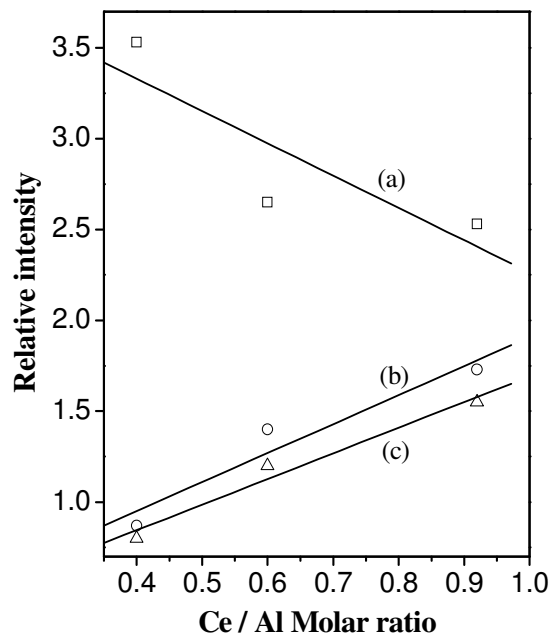In a recent IR study by Góra-Marek and Datka,[29] a similar low frequency band in H/MCM-41 and H/MCM-48 alumino-silicates has indeed been attributed to Si−(OH)−Al groups, giving rise to the Brönsted acidity in these mesoporous materials. The band at ~ 3530 cm^{-1}, with a negative shift of ~ 200 cm^{-1}, with respect to the vibrational band of silanol group, represents a weak bonding and may arise due to hydroxyl groups associated with isolated cerium sites (Figures 2.11, curve d).

2.3.2.10.2. Pyridine Adsorption

Figure 2.13 presents IR spectra of Al-MCM-41 (sample B), recorded at 420 K after exposure at this temperature to four consecutive pulses of pyridine vapor (9.5 μmol g^{-1} each). For a lower pyridine coverage (curve a), mainly a pair of bands at 1613 and 1452 cm^{-1}, arising due to 8a ν(C-C) and 19b ν(C-C) vibrations of pyridine adsorbed at Lewis acid (designated as L_1) site is clearly seen. Another pair of bands is observed at 1636 and 1545 cm^{-1} due to the vibrations of pyridine molecules bound at bridge-bonded Brönsted (B) sites. Yet another intense band in this spectrum at 1490 cm^{-1} arises due to contribution of both the Lewis and the Brönsted acid sites in pyridine adsorption. With increasing pyridine loading, a new pair of bands is observed at 1595 and 1444 cm^{-1} (referred to as L_2 sites), while the intensity of the other bands mentioned above also increased progressively, the ratio B/L_1 remaining almost the same (Figure 2.13, curves b-d). Cooling of the sample to ambient temperature (~300 K) resulted in a pronounced increase in the intensity of 1595 and 1444 cm^{-1} band, while the intensity of the other bands changed only marginally. Similarly, the intensity of the L_2 bands decreased to a greater extent on subsequent evacuation for 10-15 minutes of the IR cell, as compared to the intensity of all other bands mentioned above. These data are presented in Figure 2.14.
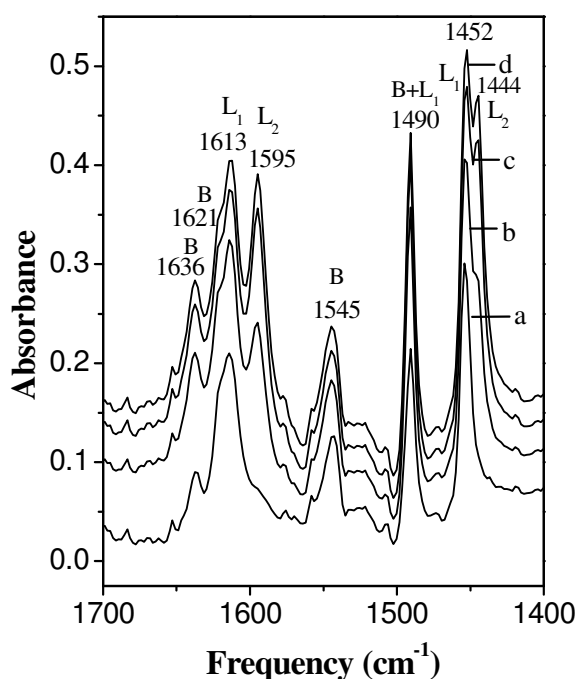
Figure 2.13. IR spectra of Al-MCM-41 (sample B) exposed to different doses of pyridine at 420 K, curves (a) 9.5; (b) 19.0; (c) 28.5; and (d) 38.0 μmol g^{-1}.

Figure 2.14. IR spectra of Al-MCM-41 (sample B) exposed at 420 K to saturation coverage of pyridine (curve a) followed by cooling to 300 K (curve b) and then evacuation (curve c).

Similarly, in the case of Ce-MCM-41 sample, the intensity of 1613 and 1452 cm^{-1} bands was very small and the ratio of 1444 and 1452 cm^{-1} bands increased progressively with increasing Ce-content. The intensity of the 1544 cm^{-1} and corresponding higher frequency bands at 1636 and 1623 cm^{-1} due to Brönsted acidity was considerably low in Ce-containing samples as compared to Al-MCM-41. The intensity of these bands was negligibly small for the samples even with higher Ce content. Typical IR spectra of Ce-MCM-41 as a function of pyridine loading at 420 K and on subsequent cooling to ambient temperature followed by pumping are shown in Figures 2.15 and 2.16. As seen from absorbance values given in parentheses in

Figures 2.13 to 2.16, the intensity of various IR bands particularly the bands at 1595 and 1444 cm^{-1} is much higher in the case of Ce-MCM-41sample, as compared to Al-MCM-41 sample.
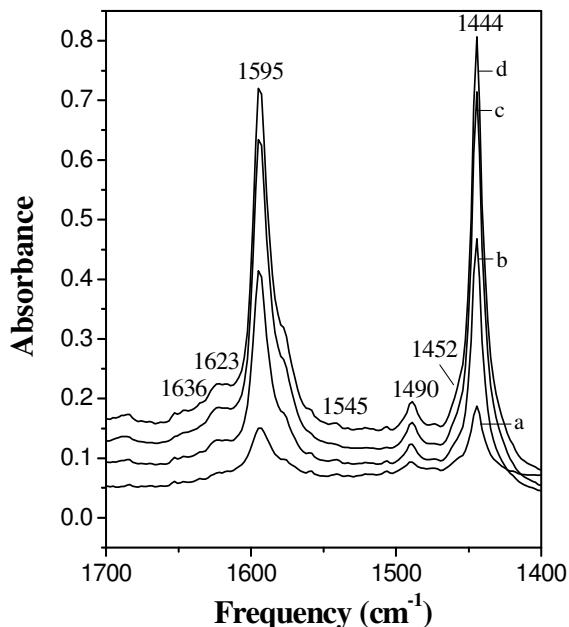
Figure 2.15. IR spectra of Ce -MCM-41(sample C) exposed to different doses of pyridine at 420 K. Curves (a) 9.5, (b) 19.0, (c) 28.5 and (d) 38.0 μmol g^{-1}.
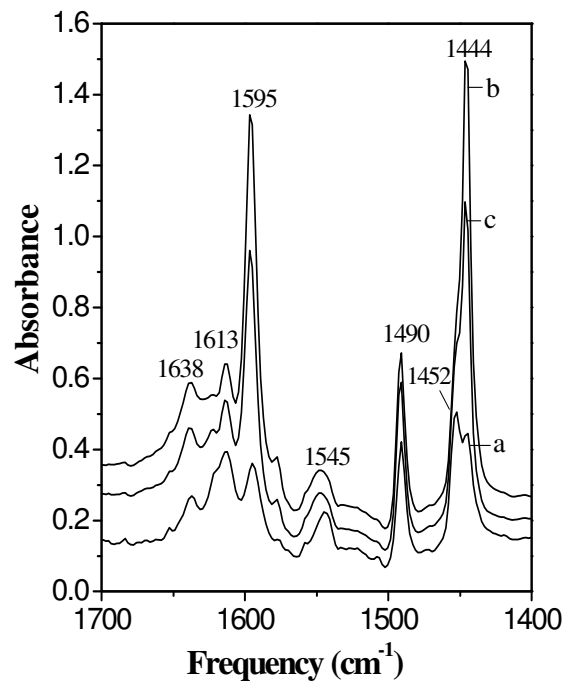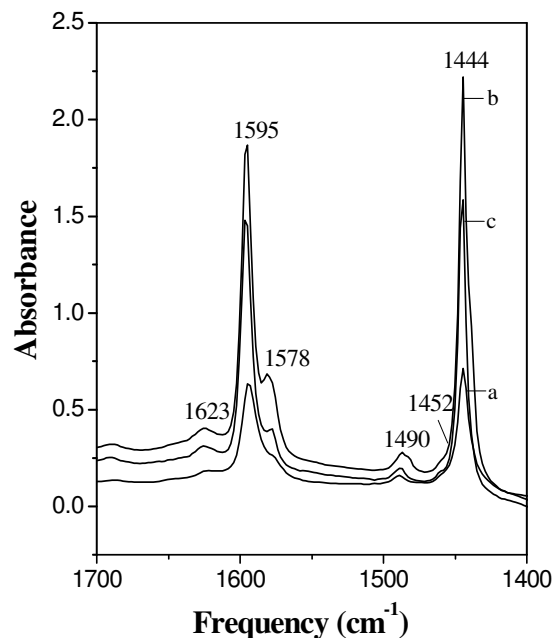
Figure 2.16. IR spectra of Ce-MCM-41 (sample C) exposed at 420 K to saturation coverage of pyridine (curve a), followed by cooling to 300 K (curve b) and then evacuation (curve c).

Figure 2.17 exhibits comparative IR spectra of different samples, recorded at 300 K after saturated adsorption of pyridine at 420 K followed by cooling to ambient temperature and subsequent pumping for 10-15 minutes. These results reveal that the relative intensity of IR bands is influenced differently when Ce alone or Ce + Al were substituted in a sample. In the case of Ce-MCM-41 (curve a), observe mainly a pair of strong bands at 1595 and 1444 cm^{-1}, while the intensity of the other bands due to adsorption of pyridine at above-mentioned L_1 and B sites was very small as compared

to Al-MCM-41 (spectrum b). In the case of samples having co-substituted Ce and Al (curves c-e), an important change to be noticed is a progressive increase in the intensity of the Brönsted site IR bands (1545, 1621 and 1636 cm^{-1}), as reflected in the absorbance values marked on these spectra. A progressive increase is also noticeable in the intensity of the 1444 and 1595 cm^{-1} band as a function of increasing Ce content.

Figure 2.17. IR spectra of Ce-Al-MCM-41samples, recorded at 300 K after exposure to saturation coverage of pyridine at 420 K followed by cooling to room temperature and subsequent evacuation.Curves (a) sample C, Ce-MCM-41; (b) sample B, Al-MCM-41; (c) sample E, Ce/Al = 0.4; (d) sample F, Ce/Al = 0.6; (e) sample G, Ce/Al = 0.9.
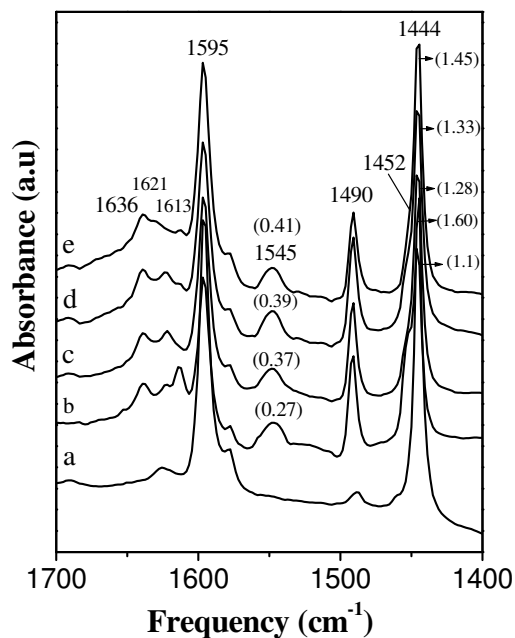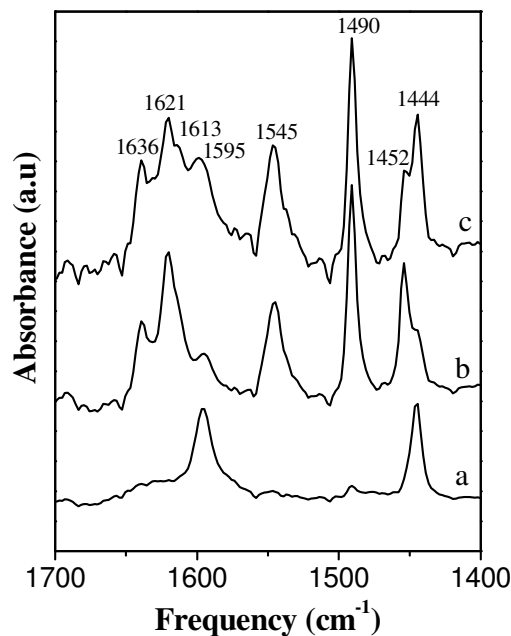
Figure 2.18. IR spectra of Ce-Al-MCM-41samples, recorded at 420 K after exposure to saturation coverage of pyridine at 420 K followed by evacuation for 10 min at same temperature. Curve (a) Ce-MCM-41; sample C, (b) Al-MCM-41, sample B and (c) Ce-Al-MCM-41, sample F, Ce/Al = 0.6.

Further, the relative intensity of above-mentioned IR bands was found to change considerably when the samples exposed to saturation coverage of pyridine were evacuated at 420 K instead of room temperature. Figure 2.18 presents such representative spectra recorded at 420 K. An important feature of these results is a considerable decrease in the relative intensity of L_2 (1444 cm^{-1}) bands as compared to that in Figure 2.17. The concentration of the individual acid sites in different Ce-Al-MCM-41 samples, calculated from the area under corresponding lines and using calibration values as mentioned in experimental (section). The change in their relative concentrations as a function of Ce and Al contents are given in Table 2.4 for comparison. The ratio of L_2/L_1 (1452/1444) was found to decrease further when the sample temperature was raised above 420 K indicating a weak binding of pyridine at L_2 acid sites.

The IR bands appearing at 1595 and 1444 cm^{-1} (L_2) in Figures 2.13-2.18 have been attributed earlier to different kinds of adsorption sites, i.e. to hydrogen-bonded pyridine because of the closeness of their frequency to that of the uncoordinated pyridine[27-30] and also to certain weak Lewis acid sites on the basis that similar pair of bands has been reported for the adsorption of pyridine over materials that exhibit a strong Lewis acid character, such as zeolites, metal oxides and clays.[31,32] In the present study, it observe that these bands are reasonably stable under evacuation at 420 K (Figure 2.17), a trend not expected from hydrogen-bonded pyridine. At the same time, the intensity of these bands is decreased considerably on rise in temperature (Table 2.4), thus indicating the weak bonding of pyridine at these sites. A similar pair of strong bands was observed in previous study on adsorption of pyridine over titania, which exhibited high catalytic activity for Lewis-acid catalyzed ortho-selective methylation of phenol.[33] In view of these observations, the pair of bands at

1595 and 1444 cm^{-1} (L$_2$ sites) may be attributed to weak Lewis acid sites. Based on the ratio of L$_2$/L$_1$ sites in different samples (Table 2.4), it can be concluded that the L$_2$ adsorption sites are promoted by the presence of Ce in a sample. These results are in consonance with the spectral feature in Figures 2.11. This interpretation finds support in the study of Yiu and Brown, reporting a similar pair of distinct Lewis acid sites in adsorption of pyridine over cation-exchanged mesoporous solid acid catalysts.[31]

Table 2.4. Concentration of Brönsted (B) and Lewis (L$_1$, L$_2$) acid sites and total acidity in Ce-Al-MCM-41 catalysts.

Sample[a]	Ce /Al mole ratio	Acid site concentration (μmol pyridine g^{-1})[b]				L$_2$ /L$_1$	B /L$_1$	L$_2$ /L$_1$	B /L$_1$	Total Acidity[d] (μmol NH$_3$ g^{-1})
		L$_2$ (1444 cm^{-1})	L$_1$ (1454 cm^{-1})	B (1545 cm^{-1})	Total	At 420 K[c]		At 300 K[c]		
B	-	62.4	140.2	120.0	322.6	0.4	0.85	1.6	0.4	334.5
C	-	169.7	40.0	0.0	209.7	4.2	0.0	13.7	0.0	160.6
D	0.3	53.2	95.6	170.5	319.3	0.5	1.7	1.8	0.4	338.6
E	0.4	58.6	101.1	190.0	349.7	0.6	1.9	2.3	0.6	365.7
F	0.6	120.3	110	154.0	384.3	1.1	1.5	2.5	0.7	419.7
G	0.9	140.0	115	207.0	462.0	1.2	1.8	3.5	1.1	468.3

[a]: B = Al-MCM-41 (0, 30); C = Ce-MCM-41(30, 0); D = Ce-Al-MCM-41 (108, 32); E = Ce-Al-MCM-41 (80, 32); F = Ce-Al-MCM-41 (59, 33) and G = Ce-Al-MCM-41 (38, 34).

[b] Spectra recorded at 420 K, on samples exposed to pyridine and then evacuated at same temperature. [c] Spectra recorded at 300 K, on samples exposed to pyridine at 420 K followed by cooling to room temperature and subsequence evacuation. [d] Measured by using TPD methods.

Curve (a) in Figure 2.19 shows IR spectrum of pyridine adsorbed (9.5 μmol g^{-1}) over Ce-Al-MCM-41 (Si/Ce = 59, Si/Al = 33, sample F) at 420 K, followed by cooling to room temperature and subsequent evacuation for 10 min. The L_2 sites, represented by a pair of IR bands at 1595 and 1444 cm^{-1}, and L_1 sites corresponding to weak bands appearing at 1613 and 1452 cm^{-1} in the form of shoulder bands and arising due to well reported 8a ν(C-C) and 19b ν(C-C) vibrations of strongly bonded pyridine.[7,27-30] The relative intensity of these two pairs of IR bands was found to change considerably on elevation of sample temperature subsequent to pyridine exposure. The spectra thus obtained at sample temperatures of 373, 423 and 473 K are shown as curves b, c and d, respectively, in Figure 2.19.

The intensity ratio L_2/L_1 decreases to a great extent on the rise of sample temperature, indicating a relatively weak binding of pyridine molecules at L_2 sites. Another pair of bands observed at 1636 and 1545 cm^{-1} corresponds to the well documented vibrations of pyridine bound at bridge-bonded Brönsted (B) sites.[31] However, another intense band appearing at 1490 cm^{-1} in these spectra arises due to participation of both the Lewis and Brönsted acid sites. The relative intensity of these bands was found to depend considerably on the Ce content in the Ce-Al-MCM-41 samples. For instance, plots a and b in Figure 2.20 show, respectively, the intensity ratios of 1545 cm^{-1} and 1444 cm^{-1} bands (B/L_2) and 1444 cm^{-1} and 1454 cm^{-1} bands (L_2/L_1) as a function of [(Ce+Al)/(Si+Ce+Al)] (at comparable Al contents) in different Ce-Al-MCM-41 samples. The same intensity ratios B/L_2 and L_2/L_1 are plotted against Ce/Al mole ratio in various Ce-Al-MCM-41 samples studied (Figure 2.21). These plots clearly suggest that with increasing Ce concentration in Ce-Al-MCM-41 samples, the concentration of Brönsted acid sites (vis-à-vis Lewis acid) and also that of the weak Lewis acid sites (L_2, due to Ce) compared to that of L_1 (due to Al

sites) also increase. As reported in our recent publication,[7] the probable new Brönsted

acid sites generated when both Ce and Al are present in silicate network is presented

in Scheme 2.1. It is plausible that the polarized ≡Ce-O-H bonds, due to hydrogen

bonded neighboring ≡Si-OH in the vicinity of ≡Ce- (OH)-Al≡ (Scheme 2.1 A) or

≡Si- (OH)-Al≡ (Scheme 2.1 B) moieties can impart additional Brönsted acid sites to

Ce-Al-MCM-41 samples. Since Ce^{4+} sites would possess more electropositive

character compared to that of Si^{4+}, the presence of Ce^{4+} in the vicinity of Al (≡Ce-

(OH)-Al≡ and / or ≡Si-(OH)-Al-Si-O-Ce≡) moiety may impart higher acid strength to

the bridging OH groups (Brönsted acid sites) via pull of electrons towards itself

thereby further leading to increased ease of deprotonation and therefore higher acid

strength. Furthermore, the Ce^{4+} cations in silica network also serve as independent

Lewis acid sites because of their ability to accept a loan pair of the electrons.[7]

    A   B
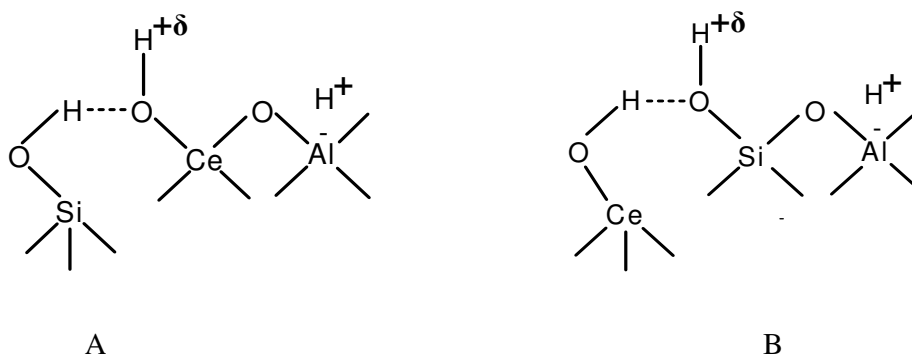
Scheme 2.1. Plausible new Brönsted acid sites generated due to simultaneous

incorporation of Ce and Al in Ce-Al-MCM-41 samples.[7]

       In conclusion, the data on acid site distribution in Table 2.4 clearly reveal that

the presence of Ce in Ce-Al-MCM-41 samples results in the increased concentration

of Brönsted acid sites and also that of the overall acid site concentration in these

samples. Also, the substitution of Ce promotes the development of L_2 Lewis acid

sites, where the binding of pyridine is weak as compared to the Lewis acid sites

associated with Al cations. Furthermore, the higher acidity of Ce-Al-MCM-41 samples as compared to that of Ce-MCM-41 or Al-MCM-41 (Table 2.4) provides a clear evidence of a kind of synergism that may exist between the Al and Ce cations in the dual-substituted samples. The higher values of B/L_1 ratio in case of the data collected at 420 K (Table 2.4) are indicative of a greater binding strength of Brönsted -bound pyridine, which may in turn influence the overall acid strength of dual-substituted samples, as is observed in the NH_3-TPD results described below.
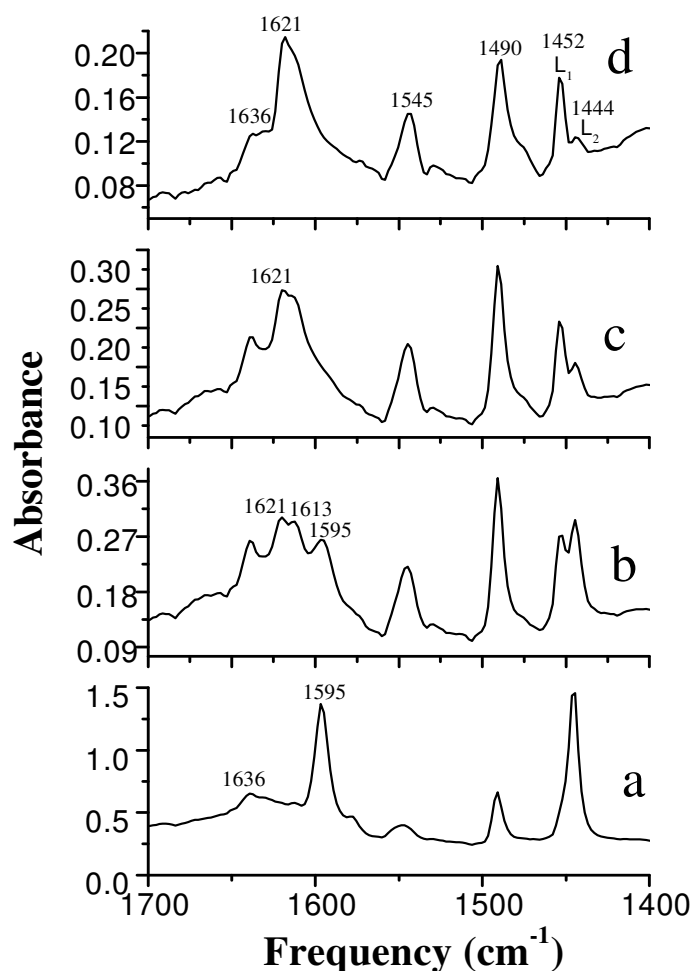

Figure 2.19. IR spectra of Ce-Al-MCM-41 (Si/Ce = 59, Si/Al = 33, sample F) sample, recorded at 300 K after exposure to saturation coverage of pyridine at 420 K followed by (a) cooling to room temperature and subsequent evacuation and different temperature, (b) 373 K, (c) 423 K and (d) 473 K.
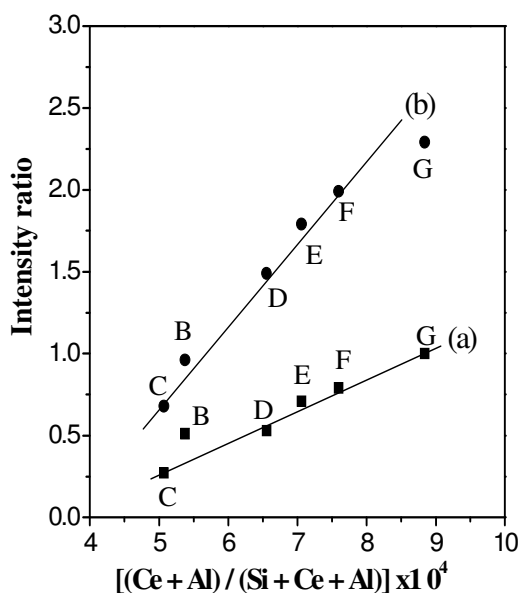
Figure 2.20. Plots of intensity ratio of different IR bands as a function of total metal content [(Ce+Al)/(Si+Ce+Al)] in the sample. Curves (a) 1545/1444 (B/L$_2$); (b) 1444/1452 (L$_2$/L$_1$) for adsorption at 420 K. The sample notations as per Table 2.1.
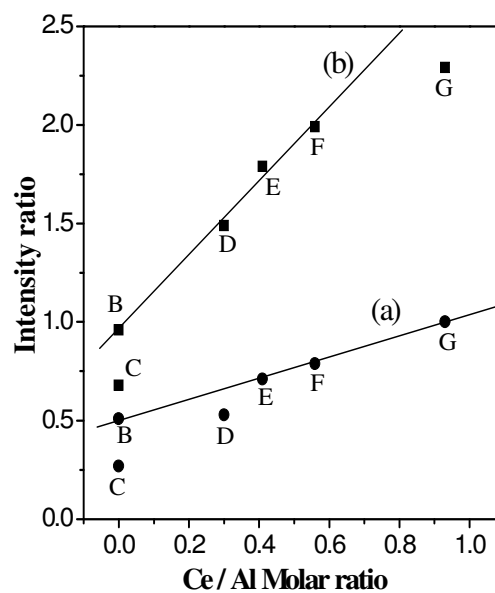
Figure 2.21. Plots of intensity ratio of different IR bands as a function of Ce/Al ratio. Curves (a) 1545/ 1444(B/L$_2$); (b) 1444/1452 (L$_2$/L$_1$) for adsorption at 420 K. The sample notations as per Table 2.1.

2.3.2.11. Temperature Programmed Desorption-Ammonia (TPD-Ammonia) Studies

The ammonia-TPD profiles of the catalysts with different MCM-41 samples are shown in Figure 2.22. As seen in this figure, all the samples show broad desorption signal in the region 400 to 600 K, indicating a wide distribution of the surface acid strength. The total amount of ammonia desorbed is listed in Table 2.4, and the data are plotted in the Figure 2.23 as a function of [(Ce+Al)/(Si+Ce+Al)] in different samples. These data reveal that as compared to individual acidity of Al-MCM-41 and Ce-MCM-41, the overall concentration of acid sites is higher in case of Ce-Al-MCM-41 and it varies almost linearly as a function of Ce content. The

ammonia-TPD data are thus in consonance with our IR results described above and confirm the Ce-induced enhancement in the total acidity in Ce-Al-MCM-41 samples. In addition to increase in the concentration of acid sites, also observe in Figure 2.22 a progressive increase in TPD peak maximum. These results are indicative of overall increase not only in the acid site concentration but also in the strength of these sites as a result of Ce incorporation
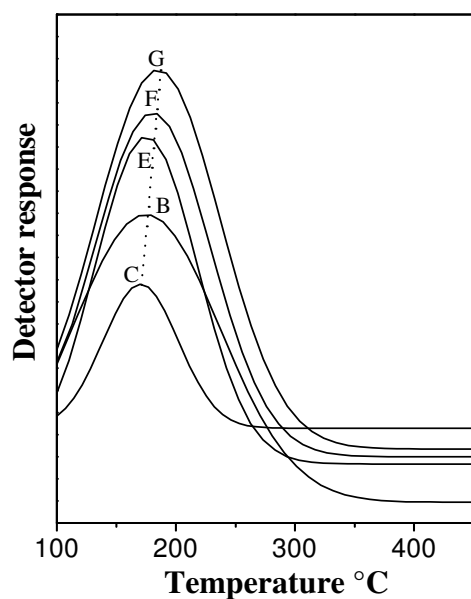

Figure 2.22. Comparative TPD–NH$_3$ spectra of activated Ce-Al-MCM-41 samples as a function of composition. The sample notations as per Table 2.1.
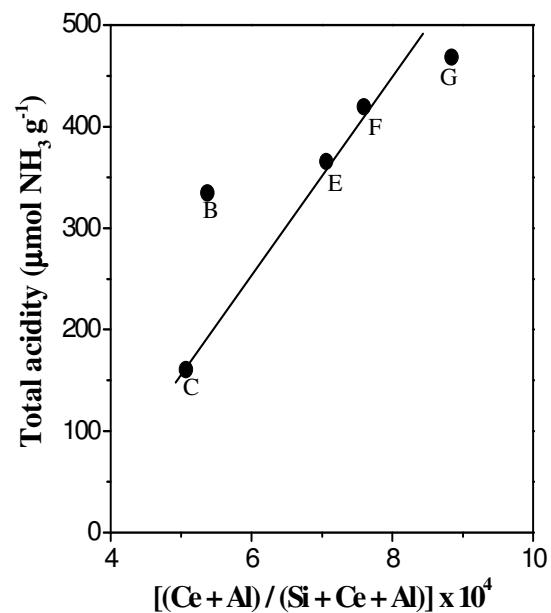
Figure 2.23. Plots of total acidity (μmol NH$_3$ g^{-1}) vs total metal content in Ce-Al-MCM-41 samples. The sample notations as per Table 2.1.

2.4. SYNTHESIS AND CHRACTERIZATION OF TRIFLIC ACID

FUNCTIONALIZED Zr-TMS CATALYST

2.4.1. MATERIALS

Zirconium (IV) butoxide (80 wt % solution in 1-butanol, Aldrich, USA), 25 wt % aqueous solution of tetramethylammonium hydroxide (TMAOH, Loba Chemie, India), 25 wt % aqueous solution of cetyltrimethylammonium bromide (CTMABr, Loba Chemie, India), and trifluoromethanesulphonic acid (CF_3SO_3H, triflic acid, Lancaster, UK),

2.4.1.1. Synthesis of Zr-TMS Catalyst

The Zr-TMS (Zr-TMS, zirconia based transition metal oxide mesoporous molecular sieves) material was synthesized in the following procedure and gel compositions as reported by earlier[8]: 0.07 $Zr(OC_4H_9)_4$: 1.4 BuOH: 0.02 CTMABr: 0.014 TMAOH: 1.7 H_2O.

A mixture of zirconium (IV) butoxide (80 wt % solution in butanol) and 1-butanol was stirred for 10 min. Then the required amount of water was added dropwise into this mixture under stirring to hydrolyze the zirconium (IV) butoxide to $Zr(OH)_4$. The precipitated $Zr(OH)_4$ mixture was added to an aqueous solution of CTMABr (25 wt % aqueous solution) and TMAOH (25 wt % aqueous solution) under continuous stirring. After further stirring for 2 h, the resulting synthesis gel (pH= 10.5-11.0) was transferred to a round-bottom flask, sealed, and refluxed for 48 h at 363 K under stirring. The solid product was recovered by filtration, washed with deionized water, acetone and dried at 373 K for 2 h. The surfactant was removed from the synthesized material by extraction with a mixture containing 100 g ethanol and 2.5

g of HCl (36 wt %) per gm of the solid material under reflux for 48 h.[34,35] The Zr-

TMS was washed with water and acetone and dried at 373 K for 6 h.

2.4.1.2. Synthesis of Zr-TMS-TFA Catalyst

The mesoporous solid Zr-TMS material was functionalized by triflic acid

(trifluoromethanesulfonic acid, CF_3SO_3H, TFA-triflic acid, Scheme 2.2) by known

procedure by using molar composition[8] of 0.07: Zr-TMS: 0.7 dry toluene: 0.03 triflic

acid.

The triflic acid (0.03 mol) was added to a mixture of toluene and Zr-TMS

under N_2 atmosphere and refluxed at 363 K for 2 h. Then the mixture was cooled,

filtered, washed with acetone, and dried at 373 K for 6 h. The unreacted triflic acid

was removed by soxhlet extraction using a mixture of dichloromethane (100g) and

diethyl ether (100 g) per gm of the catalyst for 24 h. Then the solid product was dried

at 393 K for 10 h. The synthesis of the catalyst is shown in Scheme 2.2. The different

loading of triflic acid (5 to 25 wt %) on Zr-TMS were synthesized.
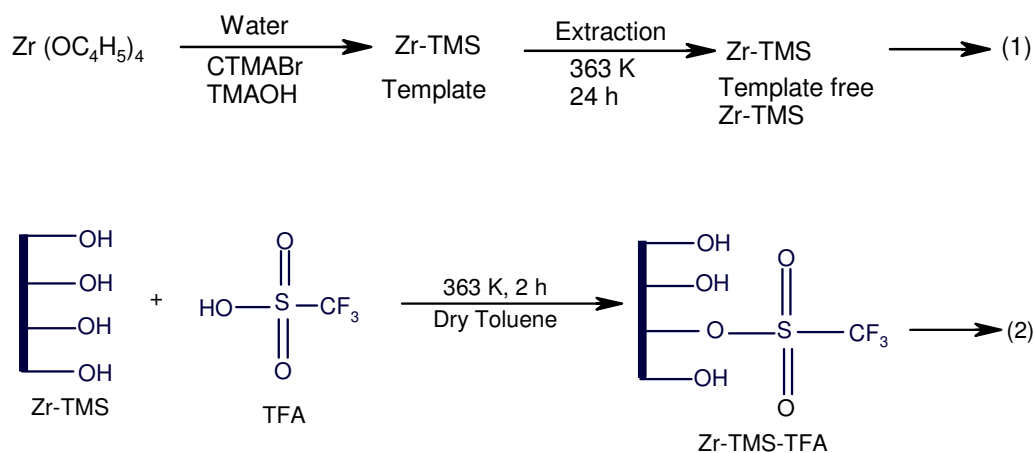
Scheme 2.2. Synthesis of triflic acid functionalized mesoporous zirconia (Zr-TMS-TFA) catalysts; (1) Synthesis and template removal of Zr-TMS material, (2) Functionalization of triflic acid over Zr-TMS material by post synthesis route.

2.4.1.3. Synthesis of Amorphous Zr-TMS-TFA-A Catalyst

The functionalized triflic acid amorphous Zr-TMS catalyst was prepared by the reported procedure[8] as follows. A mixture of 1-butanol (1.4 mol) and zirconium (IV) butoxide (0.07 mol) placed in a 3-necked 250 ml round-bottom flask equipped with a magnetic stirrer. The mixture was heated at 363 K for 10 min and then 0.28 mol of water was added dropwise into this mixture under stirring to hydrolyze the zirconium (IV) butoxide to get $Zr(OH)_4$. Now, the triflic acid (0.03 mol) was added slowly to the $Zr(OH)_4$ material and stirred at 363 K for 2 h. The mixture was cooled, filtered, washed with acetone and dried at 373 K for 6 h. The unreacted triflic acid removed by soxhlet extraction by using a mixture of dichloromethane (100 g) and diethyl ether (100 g) per gm of the catalyst for 24 h. Then the solid product was dried at 393 K for 10 h. The synthesized materials were white in color and functionalized amorphous material was designated as Zr-TMS-TFA-A (sample Q).

2.4.2. CHARACTERIZATION

2.4.2.1. Powder X-Ray Diffraction

The powder X-ray diffraction (XRD) patterns of all the synthesized catalysts are shown in Figure 2.24. The template free zirconia containing transition metal silicate (Zr-TMS) and triflic acid loaded (5-25 wt %) Zr-TMS catalysts exhibited a single, broad reflection at low angle 2theta (2.5-4.0°) and it is matched with the reported XRD pattern of ordered mesoporous ZrO_2.[36-42]

From Figure 2.24, it is seen that there is no high order reflection indicating absence of long range ordering. Other reflections observed at about 31° (broad) and at about 50° (small) in all the samples, are attributed to the tetragonal, monoclinic, and cubic phases of ZrO_2. They are readily formed after calcinations of the sample at higher temperature.[39] The broad reflection at $2\theta = 31°$ may also be due to the

presence of amorphous material as was reported in siliceous MCM-41.[43] The

crystallinity of the triflic acid loaded Zr-TMS materials decreased as the triflic acid

loading increased. Moreover, low intensity and the absence of high order reflections

indicates the order and mesostructure were different from that measured for the

mesopoporous silica.[36] The amorhous triflic acid loaded Zr-TMS catalyst also

showing low intensity reflections at about 5, 31 and 50° (2θ).
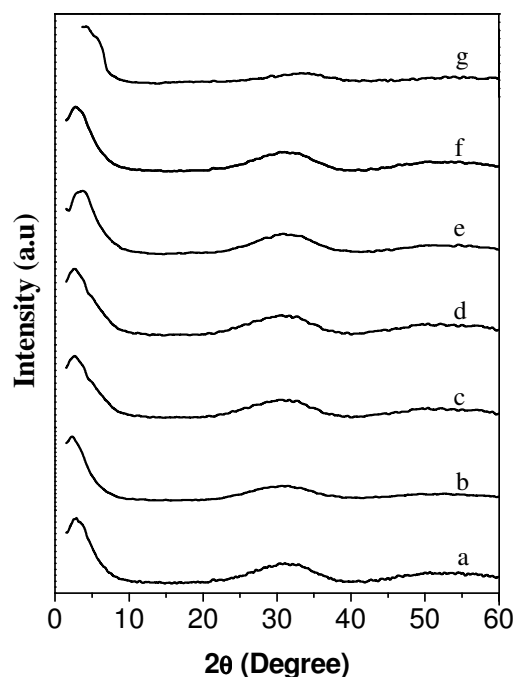
Figure 2.24. XRD pattern of (a) Zr-TMS, (b) Zr-TMS-TFA-5, (c) Zr-TMS-TFA-10,

(d) Zr-TMS-TFA-15, (e) Zr-TMS-TFA-20, (f) Zr-TMS-TFA-25 and (g) Zr-TMS-

TFA-25-A catalysts.

2.4.2.2. Porosity Measurements

The BET isotherms of Zr-TMS (A) and Zr-TMS-TFA-25 (B) are shown in

Figure 2.25. The inset shows the corresponding pore-size distributions. These two

graphs show the type IV isotherm which indicates the chararcteristics behavior of

ordered mesoporous materials.[36,37] The BET surface area of the Zr-TMS and triflic

acid functionalized Zr-TMS catalysts are given in Table 2.5. The surface area of Zr-TMS decreased by different loading of triflic acid as is observed in Table 2.5 and in accordance with the reported literature.[8,35,44,45] The specific surface area, pore volume and average pore diameter of Zr-TMS are 382 m^2g^{-1}, 0.38 cm^3g^{-1}, 45.3 Å (sample J), respectively. The corresponding values for functionalized Zr-TMS were 285 m^2g^{-1}, 0.24 cm^3g^{-1}, 34.3 Å (sample P), respectively which are comparable to synthesized Zr-TMS material using surfactant CTMABr (cetyltrimethylammonium bromide).[36,37] From Table 2.5, it is clear that decrease in surface area, pore diameter and pore volume of Zr-TMS-TFA-25 may attribute to the functionalization of Zr-TMS by triflic acid. The pore size distributions and isotherms of Zr-TMS confirm the retention of mesopores. These results are comparable with those previously reported for a mesoporous zirconia.[37]
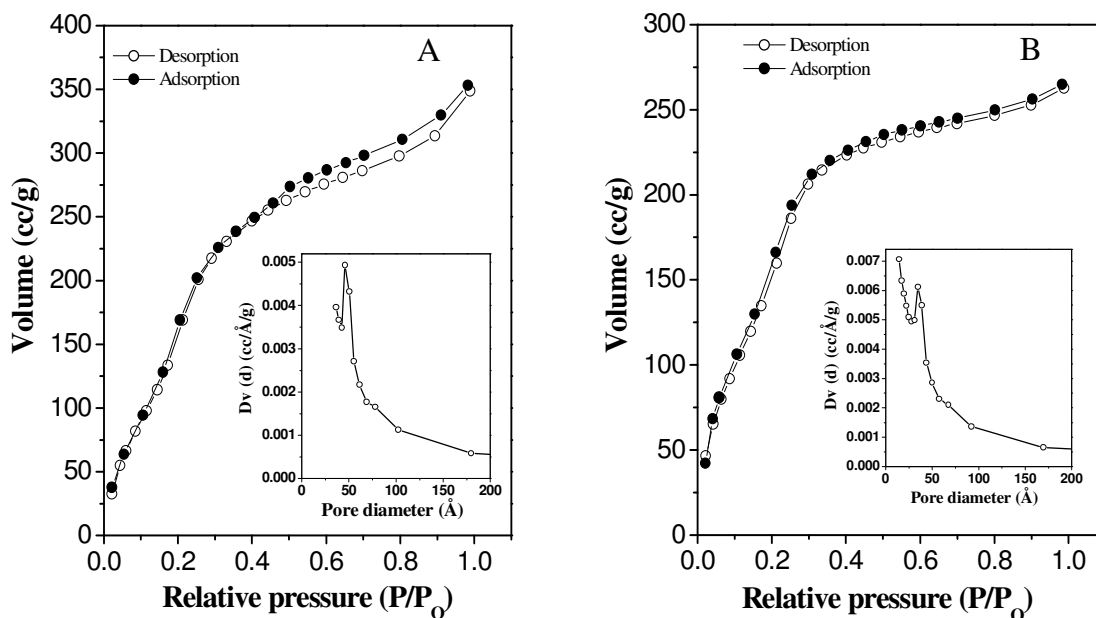

Figure 2.25. N_2 adsorption-desorption isotherms and corresponding pore size distribution curves (inset) for (A) Zr-TMS (sample J) and (B) Zr-TMS-TFA-25 (sample P).

2.4.2.3. Elemental Microanalyses

The results microanalyses of carbon and sulfur contents of the catalysts are shown in Table 2.5. The sulfur content was assigned to the loading of triflic acid and it was seen that acid loading over Zr-TMS increased with increasing in the amount of triflic acid introduced.

Table 2.5. Physiochemical properties of the Zr-TMS catalysts.

Sample name	Catalyst	Elemental analysis output (wt %)		Loading of Triflic acid (wt %)		BET surface area (m^2g^{-1})	Total pore volume (cm^3g^{-1})	Average pore diameter (Å)	Total acidity [c] (mmol/ g^{-1})
		C	S	Input	Output				
J	Zr-TMS	-	-	-	-	382	0.38	45.3	0.47
K	Zr-TMS-TFA-5 [a]	0.82	0.9	5.0	4.3	365	0.35	41.2	0.72
L	Zr-TMS-TFA-10	1.4	1.8	10.0	8.5	340	0.32	39.6	0.87
M	Zr-TMS-TFA-15	1.5	2.7	15.0	12.7	327	0.29	37.4	0.98
N	Zr-TMS-TFA-20	1.7	3.6	20.0	16.9	298	0.26	35.6	1.33
P	Zr-TMS-TFA-25	1.9	4.9	25.0	22.9	285	0.24	34.3	1.44
Q	Zr-TMS-TFA-25-A [b]	2.2	5.2	25.0	24.3	54	0.21	31.0	1.48
R	CF$_3$SO$_3$H	-	-	-	-	-	-	-	-

[a] Numbers denote wt % (input) of triflic acid loading over Zr-TMS.

[b] A denotes amorphous.

[c] Measured by using TPD-NH$_3$ method.

2.4.2.4. FTIR-Spectroscopy

The infrared spectra of Zr-TMS, Zr-TMS-TFA and Zr-TMS-TFA-A catalysts are shown in Figures 2.26. The strong and broad band between 3600-3200 cm^{-1} corresponds to the stretching mode of hydroxyl groups present on the surface (as Zr(OH)$_4$). The weak unresolved band between 850-700 cm^{-1} is attributed to Zr-O stretching modes. The sharp band in the region 1650-1600 cm^{-1} is due to the bending mode of associated water molecules. The IR-spectra of Zr-TMS-TFA (Figures 2.26, curves b-d) and Zr-TMS-TFA-25-A (Figure 2.26, curve e) show additional bands (at 1273, 1180, 1038 and 615 cm^{-1}) that are absent in Zr-TMS (Figure 2.26, curve a). The broad and intense band at 1273 cm^{-1} and medium band at 1180 cm^{-1} are due to S=O stretching mode of the incorporated triflic acid. [46,47]
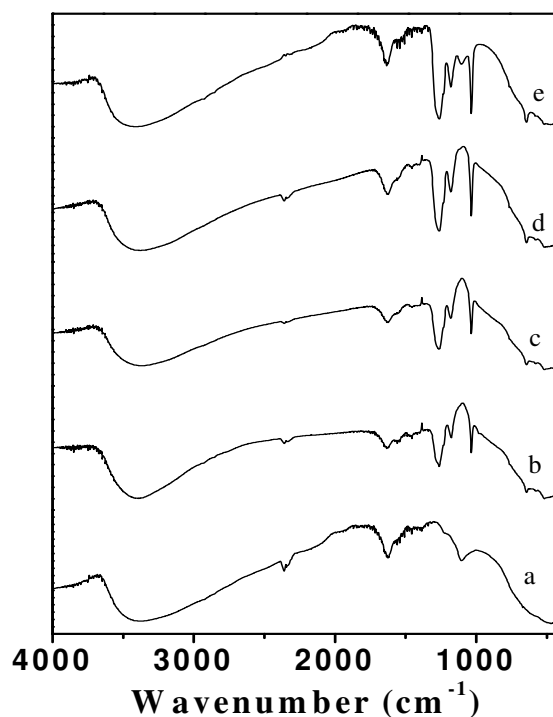

Figure 2.26. FTIR spectra of (a) Zr-TMS, (b) Zr-TMS-TFA-5, (c) Zr-TMS-TFA-15, (d) Zr-TMS-TFA-25 and (e) Zr-TMS-TFA-25-A catalysts.

The C-S link in Zr-TMS-TFA also gives a medium band at 615 cm^{-1}. This band is assigned to the SO_2 deformation mode and a sharp band at 1038 cm^{-1} is assigned to C-F band.[46,47] Moreover, the spectra of Zr-TMS-TFA and Zr- TMS-TFA-A are similar to the reported silver triflate spectrum.[48] Further, from the Figure 2.26, it can be seen that the stretching (3200-2800 cm^{-1}) and bending (1500-1300 cm^{-1}) modes of the methyl groups of CTMABr completely disappear after 48 h of extraction.[37,39] Thus, all these results indicate that the final material was free from surfactant and that the Zr-TMS was functionalized with TFA.

2.4.2.5. Temperature Programmed Desorption-Ammonia (TPD-Ammonia) Studies

The total acid strength of the functionalized Zr-TMS as well as amorphous Zr-TMS catalysts are shown in Table 2.5. Since, the functionalized materials are covalently bonded to the solid support, the same could not be treated above 573 K otherwise above this temperature triflic acid will be decomposed and lost from the solid support.[34,44,45,49] The total number of acid sites on the catalysts was found to increase proportionally with increased loading of triflic acid supported on Zr-TMS. The observed total acid strength of the amorphous catalyst (Zr-TMS-TFA-25-A) was comparable than that of mesoporous catalysts (Zr-TMS-TFA-25, Table 2.5).

2.4.2.6. UV-Visible Spectroscopy

The diffuse reflectance UV spectra of Zr-TMS, Zr-TMS-TFA catalyst are shown in Figure 2.27 An absorption at about 206 nm is attributed to the ligand-to-metal charge transfer involving isolated Zr(IV) atoms in tetrahedral coordination (curves a and b).[50,51] There is an increase in the intensity of 206 nm band in Zr-TMS-TFA-A materials with increasing Zr content. Similar observation were observed in the case of Zr-BEA.[52] These electronic transitions are clearly distinguishable from those in Zr-TMS-TFA-25 (curve b) and ZrO_2 (monoclinic symmetry) which show

absorptions at about 206 and 240 nm, respectively. However, no band was observed at 240 nm corresponding to zirconia (ZrO_2) in our samples.
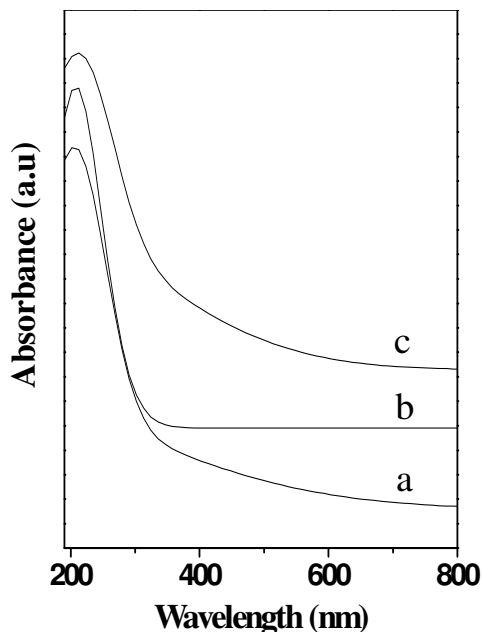
Figure 2.27. UV-Vis spectra of (a) Zr-TMS, (b) Zr-TMS-TFA-25 and (c) Zr-TMS-TFA-A-25 catalysts.

The absorption edge of zirconium oxide based powders is due to O^{2-} (Zr^{4+}) charge transfer transitions, corresponding to the excitation of electrons from the valence band (having O 2p character) to the conduction band (having Zr 4d character). The coordination of zirconium in oxides varies generally from six-fold to eight-fold, with examples provided by perovskite-type $SrZrO_3$ (6-fold), baddeleyite-type zirconia (7-fold) and cubic zirconia $ZrSiO_4$ (8-fold). The position of the edge shifts is located at lower energy for octahedral Zr^{4+} (inflection point near 300 nm for the perovskite), than for the heptacoordinated Zr^{4+} of monoclinic ZrO_2 (inflection point near 240 nm).[40] For Zr^{4+} in 8-coordination the edge is at the highest energy

(inflection point near 220 nm). These data refer to bulk polymorphs, while different positions of the absorption bands are expected for isolated Zr polyhedra.

2.4.2.7. X-ray Photoelectron Spectroscopy

The X-ray photoelectron spectrum of Zr-TMS-TFA-25 (sample P, Table 2.5) is shown in Figure 2.28. The samples exhibit the same environment of zirconium showing binding energy at about 179.0 eV for $3d_{5/2}$ and 181.5 eV for $3d_{3/2}$ species,[53] confirming the formation of stable zirconium. A hump observed at about 170.5 eV is due to the satellite peak of zirconium. Zr-TMS-TFA-25 shows a line broadening at about 165.0 eV characteristic for the S^{2-} of the thiol group of TFA.
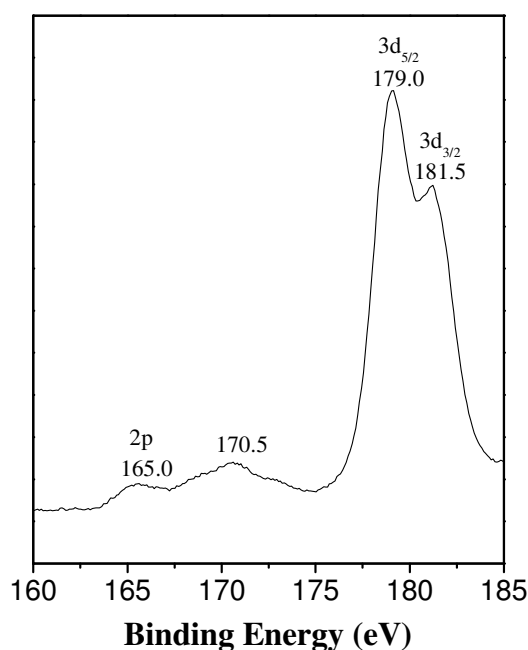
Figure 2.28. X-ray photoelectron spectra of Zr-TMS-TFA-25 catalyst (sample P, Table 2.5).

2.4.2.8. Solid State ^{13}C CP MAS NMR Spectrum

To confirm the presence of –CF$_3$ group in the material, the solid state ^{13}C CP MAS NMR spectrum (Figure 2.29) was recorded at 75.47 MHz with a rotational speed of 8 KHz for Zr-TMS-TFA-25 (sample P, Table 2.5). The quartet nature of the ^{13}C spectrum, arising due to the ^{13}C-^{19}F scalar coupling (J$_{C-F}$ ≈ 310 MHz), unambiguously shows the presence of CF$_3$ group. Moreover, the chemical shift observed at ≈ 123.1 and 115.3 ppm is very close to that reported for Na-O-SO$_2$–CF$_3$ (≈ 120 ppm),[54] indicating that the –CF$_3$ group is intact in the sample.

Figure 2.29. Solid-state ^{13}C CP MAS NMR spectrum of Zr-TMS-TFA-25 catalyst (sample P, Table 2.5).

2.5. SYNTHESIS AND CHARACTERIZATION OF MCM-41 AND SBA-15 MATERIALS, AND IMMOBILIZATION OF 1, 5, 7-TRIAZABICYCLO [4.4.0] DEC-5-ENE IN MCM-41 AND SBA-15 MATERIALS THROUGH POST-SYNTHESIS ROUTES
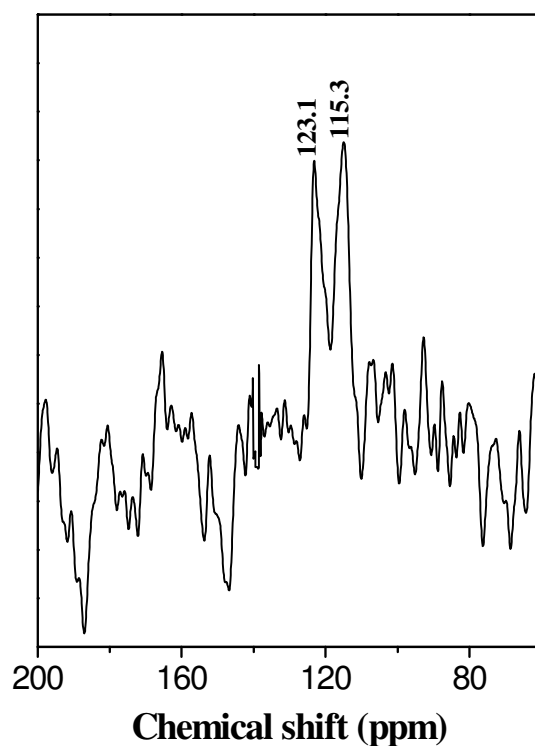
2.5.1. MATERIALS

Fumed silica (Surface area = 384 m^2 g^{-1}, Sigma Aldrich, USA), poly(ethylene glycol)-block-poly(propylene glycol)- poly(ethylene glycol) (P123, average molecular weight 5800, Aldrich, USA), tetraethyl orthosilicate (TEOS, Aldrich, USA) were employed as a starting material. Cetyltrimethylammonium bromide (CTMABr; Loba Chemie, India) was used as a structure directing agent, a 25 wt % aqueous solution of tetramethylammonium hydroxide (TMAOH, Loba Chemie, India), 3-glycidoxypropyl trimethoxysilane (Aldrich, USA), 1,5,7-triazabicyclo [4.4.0] dec-5-ene (TBD, Aldrich, USA) were used without further purification.

2.5.1.1. Synthesis of Si-MCM-41 Material

The hydrothermal synthesis was carried out in autoclave according to reported procedure.[1a,b] The molar gel compositions of the synthesis gel was: 1 SiO$_2$: 0.30 TMAOH: 0.25 CTMABr: 125 H$_2$O. In a typical synthesis of a Si-MCM-41 sample, 3.0 g of fumed silica was slowly added to 5.47 g of TMAOH (25 wt %) in 10.0 g of water under vigorous stirring. Subsequently, an aqueous solution of 4.55 g of CTMABr dissolved in 30.0 g of water. The remaining 72.5 g of water was added and the stirring was continued for 15 min. Finally, the synthesis gel was taken in teflon-lined auto-clave for 48 h. The materials thus obtained were filtered, washed thoroughly first with deionized water and then with acetone, and dried at 353 K. All the samples were calcined at 773 K for 8 h in the presence of air.

2.5.1.2. Synthesis of SBA-15 Material

Mesoporous silica SBA-15 was synthesized according to the reported procedure.[9,10] In a typical synthesis, 10 g of amphiphilic triblock copolymer, poly(ethylene glycol)-block-poly(propylene glycol)-block-poly(ethylene glycol) (average molecular weight = 5800, Aldrich Co.), was dispersed in 75 ml of water and 300 ml of 2M HCl solution while stirring. 21.25 g of tetraethyl orthosilicate (TEOS, Aldrich Co.) was added to it. The gel was continuously stirred at 313 K for 24 h, and then finally crystallized in a teflon-lined autoclave at 373 K for 48 h. After hydrothermal treatment, the solid product was filtered, washed with deionized water, acetone and dried in air at room temperature. The solid product (SBA-15) was calcined in air at 773 K for 6 h.

2.5.1.3. Immobilization of 1, 5, 7-Triazabicyclo [4.4.0] dec-5-ene in MCM-41 and SBA-15 Material

Silicous SBA-15 and MCM-41 were obtained by the above procedure and the solid residual templates were removed by calcinations. In a typical procedure for immobilization of 1, 5, 7-triazabicyclo [4.4.0] dec-5-ene in MCM-41 and SBA-15 material,[12,13] 3 g of vacuum dried MCM-41 and SBA-15 was allowed to react with 4.5 mmol of 3-glycidoxy propyl trimethoxy silane (Scheme 2.3) in dry toluene at refluxing temperature for 24 h. Then, the samples were cooled to room temperature, filtered, washed with acetone and dried. This material is designated as glycidylated MCM-41/SBA-15 (Scheme 2.3). Now, the glycidylated MCM-41/SBA-15 (1.0 g) was allowed to react with 2.2 mmol of 1, 5, 7-triazabicyclo [4.4.0] dec-5-ene (TBD) in dry toluene (15 ml) at 298 K for 10 h. The excess TBD was removed by soxhlet extraction with DCM. The sample was designated by MCM-41/SBA-15-TBD (Scheme 2.3) and stored under vacuum.
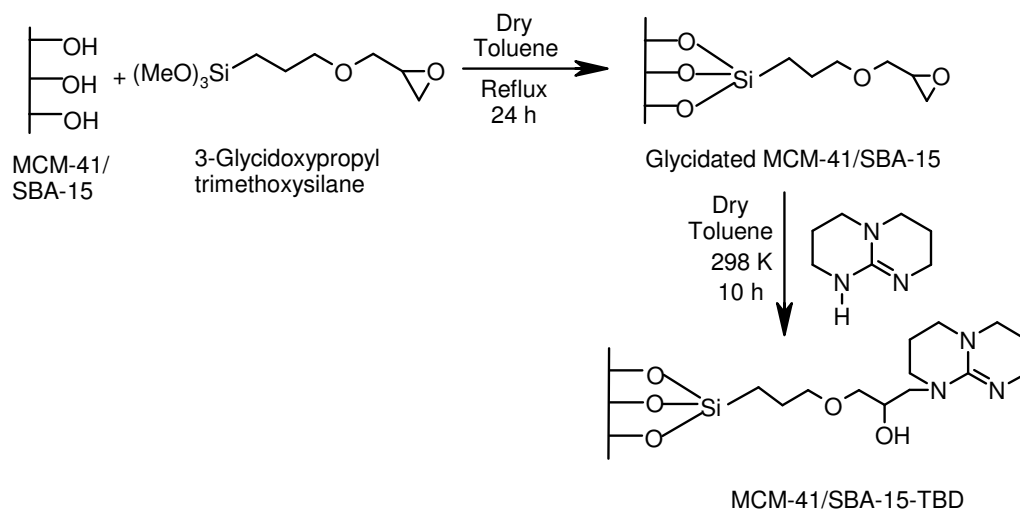
Scheme 2.3. Guanidine modified MCM-41 and SBA-15 material. **[Source. Ref. 21]**

2.5.2. CHARACTERIZATION

2.5.2.1. Powder X-Ray Diffraction

The X-ray diffraction patterns of (a) MCM-41 and (b) MCM-41-TBD materials are shown in the Figure 2.30. The typical hexagonal phase (*p6mm*) of MCM-41 [main (100) peak with weak (110), (200) and (210) reflections] is clearly visible in all the samples. These results indicate the reflection of highly ordered mesoporosity even after incorporation of organic functional group. However, a slight decrease in the peak intensities was observed in the case of the organo base functional group (TBD) loaded samples, which might be due to partial filling of organic group inside the mesopores.

Figure 2.30 shows the XRD profiles of pure SBA-15 and organo base functionalized SBA-15 materials. All the samples showed very similar XRD patterns. The samples showed three well-resolved diffraction peaks due to (1 0 0), (1 1 0) and (2 0 0) reflection in the 2θ range of 0.5–5° that could be indexed according to a 2D hexagonal *p6mm* symmetry.[9,10] Organic base incorporation did not alter the long-range ordering of the mesoporous structure. Inter-planar spacing (d_{100}) and unit cell

parameter (a_0) of various functionalized SBA-15 materials are listed in Table 2.6. The

d-spacing ($d_{1\ 0\ 0}$), estimated from the position of the low-angle peak is in the range of

9.8 to 10.4 nm. The unit cell parameter calculated using the equation $a_0 = 2d_{100}\ /\sqrt{3}$

(Table 2.6) is in good agreement with the values reported by others authors.[9,10]
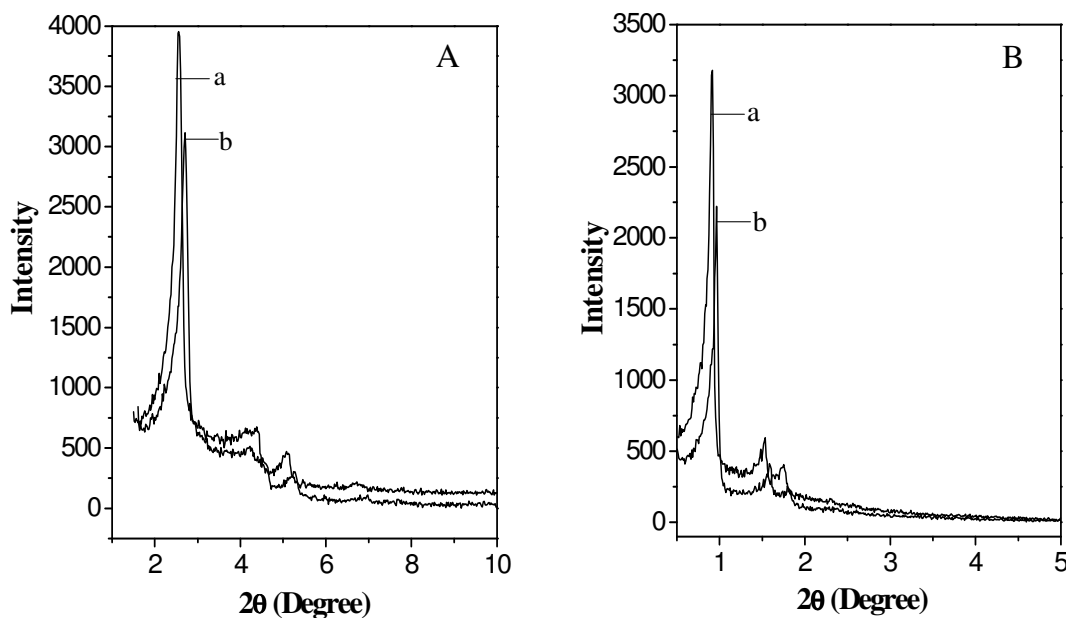
Figure 2.30. Powder X-ray diffraction pattern of (a) MCM-41 and (b) MCM-41-TBD

and (a) SBA-15 and (b) SBA-15-TBD catalysts.

2.5.2.2. Porosity Measurements

Figure 2.31 shows N_2 adsorption-desorption isotherm and the corresponding

pore size distribution curve for the calcined SBA-15 and SBA-15-TBD samples. The

nitrogen adsorption / desorption isotherms of both the samples are of type IV isotherm

(Figure 2.31) and exhibit a H1 hysteresis loop, which is typical of mesoporous

solids.[9,10,55,56] Furthermore, the adsorption branch of each isotherm showed a sharp

inflection at a relative partial pressure value of about 0.55 to 0.64. This is the

characteristic of capillary condensation within uniform pores. The position of the

inflection point indicates mesopore structure, and the sharpness of these steps

indicates the uniformity of the mesopore size distribution. A good match between the points of inflection on the adsorption branch of both isotherms suggests that samples have similar pore sizes (Figure 2.31). The low mesopore volume was observed in case of SBA-15-TBD because the mesopores were partially blocked by functionalized organic base (Table 2.6). The organic-functionalized materials show some loss of surface area and a pronounced reduction in the pore volume. The calculated 'pore diameter' is reduced from a value of 27.6 and 67.1 Å in the parent MCM-41 or SBA-15 to about 26.0 and 58.5 Å in the MCM-41-TBD or SBA-15-TBD catalysts, respectively.
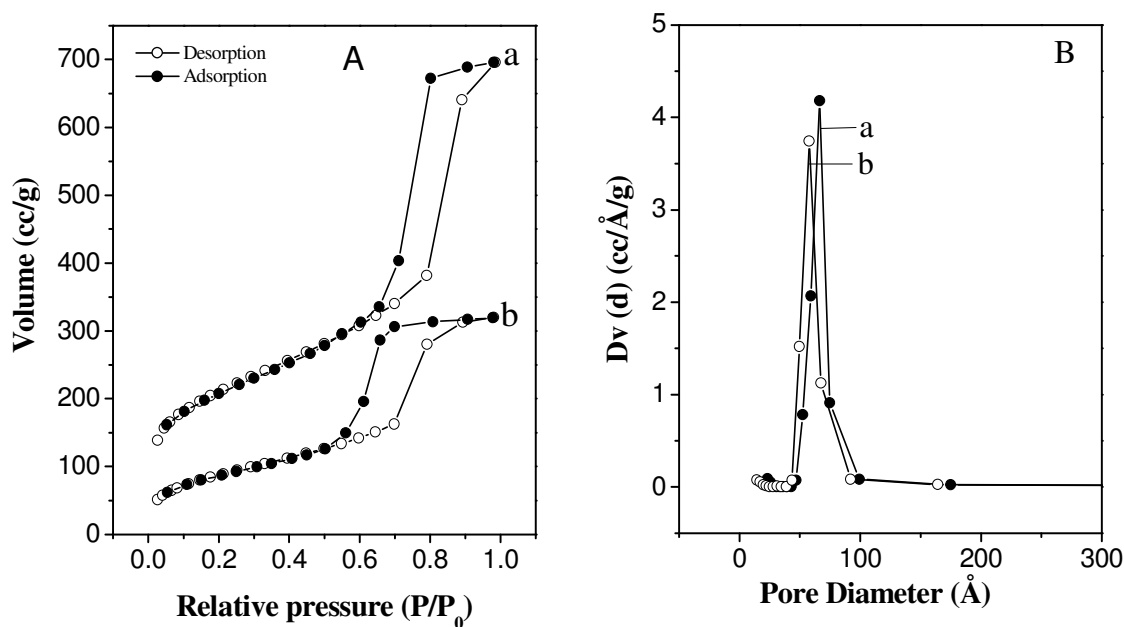

Figure 2.31. (A) N_2 adsorption-desorption isotherms and (B) corresponding pore size distribution curves for (a) calcined SBA-15 and (b) SBA-15-TBD catalysts.

Table 2.6. Physiochemical properties of MCM-41 / SBA-15 TBD catalysts.

Catalysts	TBD (mmol input)	Elemental analysis			TBD (mmol) (output)	S_{BET} (m^2/g)	d_{100} (Å)	a_o[a] (Å)	Pore diameter (Å)	Pore volume (cm^3/g)
		C	H	N						
MCM-41	-		-		-	980	37.9	43.8	27.6	1.01
MCM-41-TBD	2.2	11.9	3.3	3.9	0.92	363	37.5	43.4	26.0	0.25
SBA-15	-		-		-	733	96.6	111.7	67.1	0.95
SBA-15-TBD	2.2	16.0	3.8	4.1	0.97	391	91.6	105.9	58.5	0.52

[a] $a_{0,}$ unit cell parameter = $2d_{100}/\sqrt{3}$

2.5.2.3. Elemental Microanalyses

The results microanalyses of carbon, hydrogen and nitrogen contents of the catalysts are shown in Table 2.6. The nitrogen content was assigned to the loading of TBD over MCM-41/SBA-15 materials. The output amount was calculated with respect to nitrogen content.

2.5.2.4. FTIR-Spectroscopy

Figure 2.32 represent the FTIR spectra of (a) SBA-15, (b) glycidated SBA-15 and (c) SBA-15-TBD catalysts. The FTIR spectroscopy confirms the presence of the organic groups. The peaks around 1230, 1090, 804 and 465 cm^{-1} are the typical Si-O-Si band attributed to the condensed silica network present in all samples. The Si–OH vibration band at 970 cm^{-1} decreases after the first grafting suggesting the successful anchoring reaction between Si-OH and 3-glycidoxypropyl trimethoxysilane. The vibrational frequency of Si-OH decreases from 970 to 952 cm^{-1} by organo-functionalization of 3-glycidoxypropyl trimethoxysilane and TBD over calcined SBA-15 sample. The IR peaks at 3325 and 3300 cm^{-1} are due to free N-H bond. In the case of TBD functionalized SBA-15 sample, these peaks are absent indicating that TBD is attached with porous material. Characteristic peaks, due to C–H stretching vibrations

of propyl spacer and cycloalkane ring, were appeared in the range of 2863–2950 cm^{-1}. The spectrum c displays two new peaks at 1541 and 1465 cm^{-1} which are attributed to C=C and C=N bands, respectively. The peak of C–N is usually observed at 1000–1300 cm^{-1}. In the 1236-1310 cm^{-1} regions, the dominant contribution to the frequencies of the vibrational forms in which the different deformations of C–H bonds of methylene groups occurs are located. The stretching modes of C–C and C–N bonds mixed with the C–H bending modes of methylene groups appear in the 1400–1270 cm^{-1} range. The absorption bands in the 1100–880 and 800–450 cm^{-1} regions are connected with stretching and deformational skeleton modes of rings and O-H deformation mode at 1300-1400 cm^{-1}.
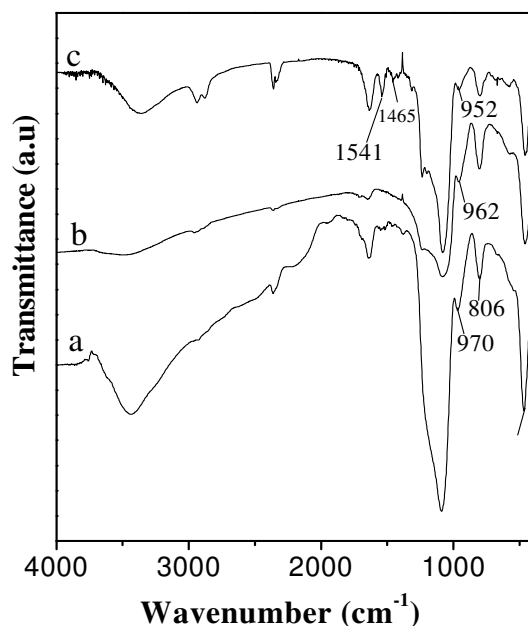

Figure 2.32. FTIR spectra of (a) SBA-15, (b) glycidated SBA-15 and (c) SBA-15-TBD catalysts.

2.5.2.5. Scanning Electron Microscopy

Figure 2.33 represent the scanning electron microscopy (SEM) images of calcined SBA-15 sample (A) and TBD immobilized SBA-15 sample (B). It consists

of many rope-like domains with relatively uniform sizes, which are aggregated into grain-like macrostructures.[9,57,58] After organofunctionalization by TBD, SBA-15 shows a similar particle morphology, which reflects the stability of the macroscopic structure.
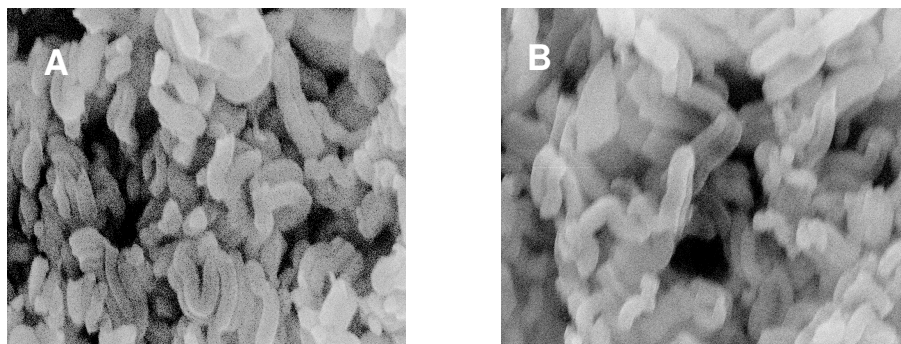
Figure 2.33. SEM micrographs of (A) calcined SBA-15, and (B) SBA-15-TBD catalysts.

2.5.2.6. Transmission Electron Microscopy

Transmission electron microscopy (TEM) images of calcined (A) SBA-15 and (B) SBA-15-TBD samples show well-ordered hexagonal arrays of mesopores with 2D *p*6*mm* hexagonal structure (Figure 2.34). The ordered mesoporous structure of the SBA-15 was slightly affected by functionalization of TBD over calcined SBA-15 sample. [9,57,58]
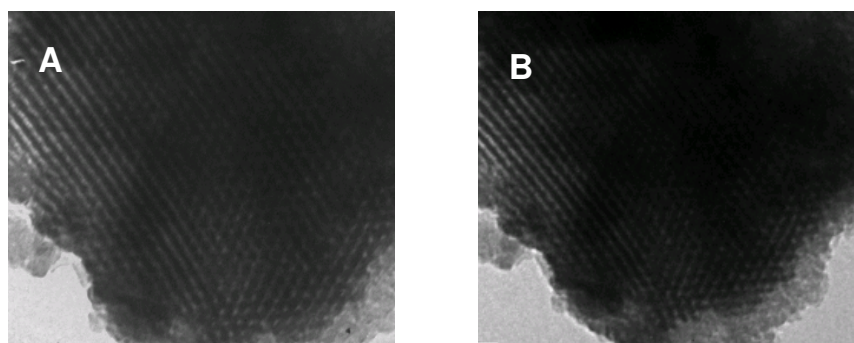

Figure 2.34. TEM micrographs of (A) calcined SBA-15, and (B) SBA-15-TBD catalysts.

2.5.2.7. Solid State ^{29}Si CP MAS NMR Spectrum

Figure 2.35 shows the ^{29}Si MAS NMR spectrum of the SBA-15-TBD. It was observed from NMR spectrum that the strong resonances at $\delta \approx -102$ and -110 ppm are due to the presence of of Q^3 [(SiO)$_3\equiv$Si–OH] and Q^4 [(SiO)$_3\equiv$Si–O–Si$\equiv$] species, respectively, present in the silicate framework of SBA-15-TBD materials. The presence of close-packed conformation of organic group is also manifested from the spectrum of the SBA-15-TBD sample. The two additional signals at $\delta \approx -59$ and -68 ppm are assigned to terminal (T^2) and cross-linked (T^3) siloxane groups, respectively, attached with pendant organic groups. These results suggest that the co-condensation process, the organic functional groups are anchored to the surface walls.
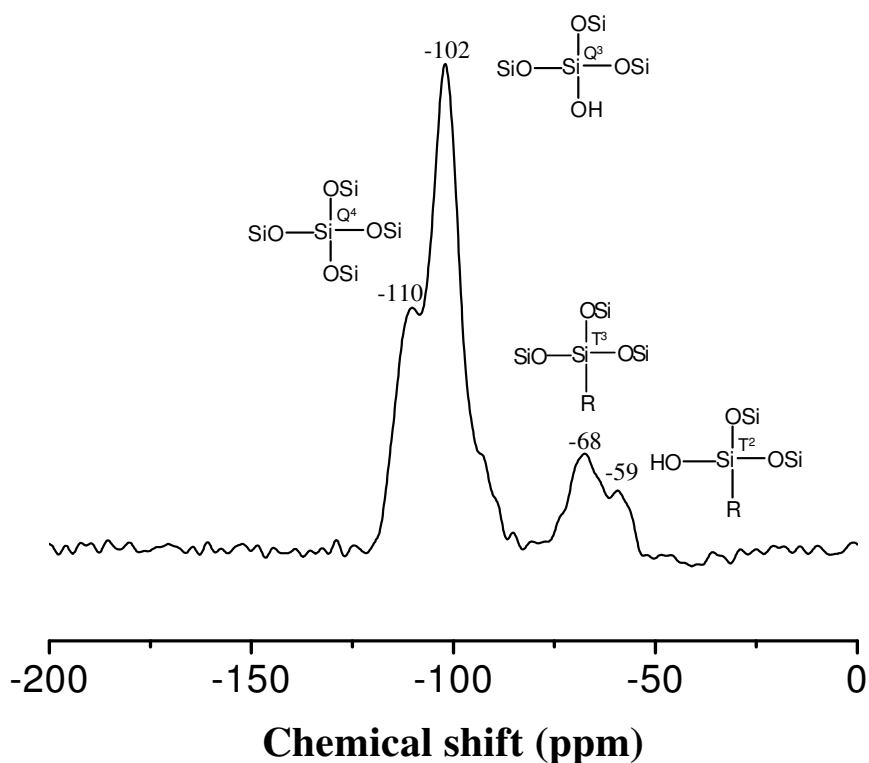
Figure 2.35. ^{29}Si CP MAS NMR spectrum of SBA-15-TBD catalyst.

2.5.2.8. Solid State ^{13}C CP MAS NMR Spectrum

The ^{13}C CP MAS NMR spectrum of SBA-15-TBD catalyst is shown in Figure 2.36. The three distinct ^{13}C signals observed at $\delta \approx 9$, 22 and 41 ppm, were assigned to C_1, C_2 and C_3 atoms, respectively, of the propyl chain attached with SBA-network (Scheme 2.3). The characteristic peaks in the cycloalkane viz. C=N ($\delta = 158$ ppm (C_{10})), C-N bond ($\delta = 73$ ppm, (C_6, C_4), $\delta = 46$ ppm (C_7, C_9)) and C-C bond ($\delta = 22$ ppm (C_8)) were also observed (Figure 2.36).

Figure 2.36. ^{13}C CP MAS NMR spectrum of SBA-15-TBD catalyst.

2.6. REFRENCES

1. (a) C. T. Kresge, M. E. Leonowicz, W. J. Roth, J. C. Vartuli, J. S. Beck, *Nature,* **1992**, 359, 710. (b) J. S. Beck, J. C. Vartuli, W. J. Roth, M. E. Leonowicz, C. T. Kresge, K. D. Schmitt, C. T.-W. Chu, D. H. Olson, E. W. Sheppard, S. B. McCullen, J. B. Higgins, J. L. Schlenker, *J. Am. Chem. Soc.* **1992**, 114, 10834. (c) A. Corma, *Chem. Rev.* **1997**, 97, 2373.
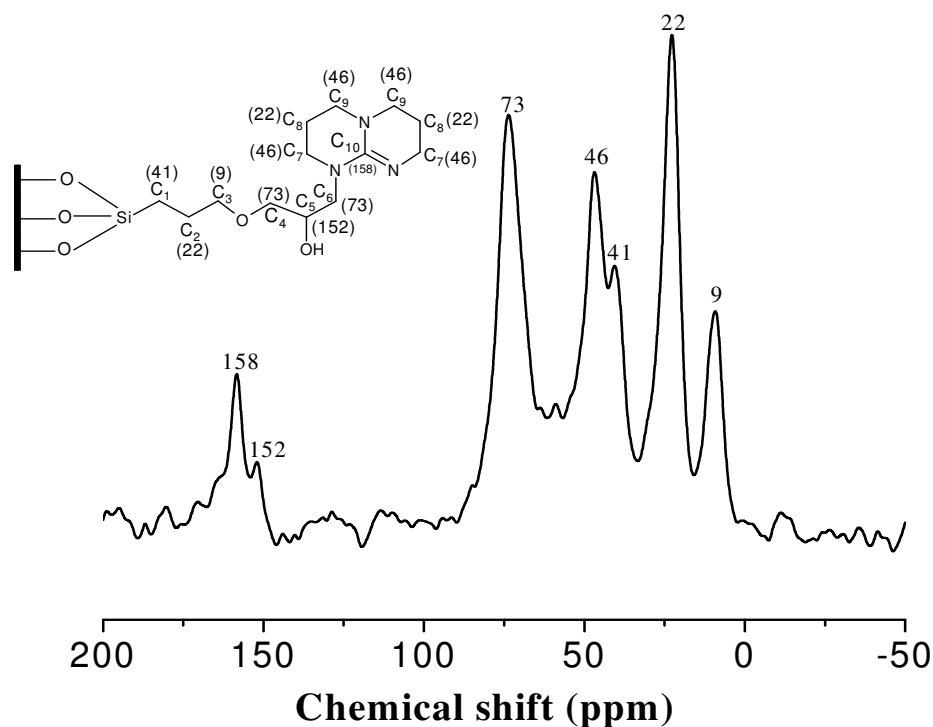
2. A. P. Wight, M. E. Devis, *Chem. Rev.* **2002**, 102, 3589.

3. A. Stein, B. J. Melde, R. C. Schroden, *Adv. Mater.* **2000**, 12, 1403.

4. K. Moller, T. Bein, *Chem. Mater.* **1998**, 10, 2950.

5. S. C. Laha, P. Mukharjee, S. R. Sainkar, R. Kumar, *J. Catal.* **2002**, 207, 213.

6. M. D. Kadgaonkar, S. C. Laha, R. K. Pandey, P. Kumar, S. P. Mirajkar, R. Kumar, *Catal. Today* **2004**, 97, 225.

7. P. Kalita, N. M. Gupta, R. Kumar, *J. Catal.* **2007**, 245, 338.

8. M. Chidambaram, D. Curulla-Ferre, A. P. Singh, B. G. Anderson, *J. Catal.* **2003**, 220, 442.

9. D. Zhao, J. Feng, Q. Huo, N. Melosh, G. H. Fredrickson, B. F. Chmelka, G. D. Stucky, *Science* **1998**, 279, 548.

10. D. Zhao, Q. Huo, J. Feng, B. F. Chmelka, G. D. Stucky, *J. Am. Chem. Soc.* **1998,** 120*, 6024.

11. J. Xu, Z. Luan, H. He, W. Zhou, L. Kevan, *Chem. Mater.* **1998**, 10, 3690.

12. Y. V. S. Rao, D. E. De Vos, P. A. Jacobs, *Angew. Chem. Int. Ed.* **1997**, 36, 2661.

13. D. E. De Vos, M. Dams, B. F. Sels, P. A. Jacobs, *Chem. Rev.* **2002,** 102, 3615.

14. N. M. Gupta in *'Catalysis: Principles and Applications"* Eds. B.Viswanathan, S. Sivasanker and A.V. Ramaswamy, Narosa, New Delhi **2002**, p. 127.

15. W. A. Carvalho, P. B. Varaldo, M. Wallau, U. Schuchardt, *Zeolites* **1997**, 18, 408.

16. D. Trong On, D. Desplanier-Giscard, C. Danumah, S. Kaliaguine, *Appl. Catal. A: Gen.* **2003**, 253, 545.

17. S. J. Gregg, K. S. W. Sing, *Adsorption, Surface Area and Porosity*, Academic Press, London, **1967**, p. 121.

18. C. -Y. Chen, H. -X. Li, M. E. Davis, *Microporous Mater.* **1993**, 2, 17.

19. D. B. Akolekar. *J. Chem. Soc. Faraday Trans.* **1994**, 90, 1041.

20. H. Hung, A. Adnot, S. Kaliaguine, *J. Catal.* **1992**, 137, 322.

21. R. M. Navarro, M. C. Alvarez-Galvan, M. Cruz Sanchez-Sanchez, F. Rosa, J. L. G. Fierro, *Appl. Catal. B Environ*. **2005**, 55, 22.

22. J. Z. Shyu, K. Otto, W. L. H. Watkins, G. W. Graham, R. K. Belitz, H. S. Gandhi, *J. Catal.* **1988**, 114, 239.

23. A. Mekki, *J. Electron. Spectrosc. Relat. Phenom*. **2005**, 142, 75.

24. C.-Y. Chen, S. L, Burkett, H.-X. Li, M. E. Davis, *Microporous Mater.* **1993,** 2, 27.

25   A. Jentys, N. H. Pham and H. Vinek, *J. Chem. Soc, Faraday Trans*. **1996**, 92, 3287.

26. J. Chem, Q. Li, R. Xu and F. Xiao, *Angew. Chem. Int. Ed*. **1995**, 34, 2694.

27. S. Kawi, S. C. Shen and P. L. Chew, *J. Mater. Chem*. **2002**, 12, 1582.

28. A. Corma, *Chem. Rev*. **1995**, 95, 559.

29. K. Gora-Marek and J. Datka, *Appl. Catal. A: Gen.* **2006,** 302, 104.

30. M. Selvaraj, B. R. Min, Y. G. Shul and T. G. Lee, *Micropor. Mesopor. Mater*. **2004**, 74, 143.

31. H. H. P. Yiu and D.R. Brown, *Catal. Lett*. **1998**, 56, 57.

32. A. R. Gandhe, J. B. Fernades., S. Varma and N. M. Gupta, *J. Mol. Catal. A: Chem*. **2005**, 238, 63.

33. M. Ziolek, I. Nowak, J. C. Lavalley, *Catal. Lett*. **1997**, 45, 259.

34. R. D. Howells, J. D. Mc Cown, *Chem. Rev*. **1977**, 77, 69.

35. A. O. Bianchi, M. Champanati, P. M. Tores, E. R. Castellon, A. J. Lopez, A. Vaccari, *Appl. Catal. A: Gen.* **2001**, 220, 105.

36. V. I. Parvulescu, H. Bonnemann, V. Parvulescu, B. Endurschat, A. Ch. W. Rufinska, B. Tesche, G. Poncelet, *Appl. Catal. A: Gen.* **2001**, 214, 273.

37. M. J. Hudson, J. A. Knowels, *J. Mater. Chem.* **1996**, 6, 89.

38. G. Pacheco, E. Zhao, E. D. Valdes, A. Garcia, J. J. Fripiat, *Micropor. Mesopor. Mater.* **1999**, 32, 175.

39. J. L. Blin, R. Flamant, B. L. Su, *Int. J. Inorg. Mater*. **2001**, 3, 959.

40. Y. Y. Huang, T. J. Mccarth, W. M. H. Sachtler, *Appl. Catal. A: Gen*. **1996**, 148, 135.

41. G. Larsen, E. Lotero, M. Nabity, L. M. Petkovic, D. S. Shobe, *J. Catal*. **1996**, 164, 246.

42. E. Zhao, S. E. Hardcastle, G. Pacheco, A. Garcia, A. L. Blumenfeld, J. J. Fripiat,

Micropor. Mesopor. Mater. **1999**, 31, 9.

43. U. Ciesla, S. Schacht, G. D. Stucky, K. K. Unger, F. Schuth, *Angew. Chem. Int. Ed. Engl*. **1996**, 35, 541.

44. A. N. Parvulescu, B. C. Gagea, M. Alifanti, V. Parvulescu, V. I. Parvulescu, S. Nae, A. Razus, G. Poncelet, P. Grange, *J. Catal*. **2001**, 202, 319.

45. N. C. Marziano, L. D. Ronchin, C. Tortato, A. Zingales, A.A. Sheikh-Osman, *J. Mol. Catal. A: Chem.* **2001**, 174, 265.

46. G. Herzberg, *Infrared and Raman Spectra of Polyatomic Molecules*, Van Nostrand, New York, **1945**, 285.

47. L. J. Bellamy, *The Infrared Spectra of Complex Molecules*, Wiley, New York, **1960**, 328.

48. C. J. Pouchert, *The Aldrich Library of IR Spectra*, 3rd Ed, **1981**, 533.

49. D. Q. Zhou, J. H. Yang, G. M. Dong, M. Y. Huang. Y. Y. Jiang, *J. Mol. Catal. A: Chem.* **2000**, 159, 85.

50. M. A. Camblor, A Corma, A. Mifsud, J, P´erez-Pariente, *Stud. Surf. Sci. Catal.* **1997,** 105, 341.

51. G. R Wang, X. Q. Wang, X. S. Wang, S. X Yu, *Stud. Surf. Sci. Catal.* **1994,** 83, 67.

52   A Tuel, S. Gontier, R. Teissier, *Chem. Commun.* **1996**, 651.

53. C. D. Wagner, W. M. Riggs, L. E. Davis, J. F. Mounder, G. E. Muilenberg, *Hand Book of X-ray Photoelectron Spectroscopy,* Perkin-Elmer Corp. **1979**.

54. C. J. Pouchert, J. Behnke, *The Aldrich Library of ^{13}C and ^{1}H FT NMR Spectra*, **1993**, Vol. 1. p. 1431.

55. R. Srivastava, D. Srinivas, P. Ratnasamy, *J. Catal*. **2005**, 233, 1.

56. R. Srivastava, D. Srinivas, P. Ratnasamy, *Micropor. Mesopor. Mater*. **2006**, 90, 314.

57. D. P. Sawant, A. Vinu, N. E. Jacob, F. Lefebvre, S. B. Halligudi, *J. Catal*. **2005,** 235, 314.

58. R. I. Kureshy, I. Ahmad, N. H. Khan, S. H. R. Abdi, K Pathak, R. V. Jasra, *J. Catal.* **2006**, 238, 134.

CHAPTER 3

3.1. METHODOLOGY FOR THE PREPARATION OF SUBSTITUTED DIPHENYL METHANE BY FRIEDEL-CRAFTS BENZYLATION OF TOLUENE BY BENZYL CHLORIDE AND BENZYL ALCOHOL UNDER SOLVENT FREE SYSTEM OVER Ce-MCM-41, Al-MCM-41 AND Ce-Al-MCM-41 CATALYSTS

3.1.1. INTRODUCTION

Ce-incorporated MCM-41 exhibited high activity for various catalytic reactions, such as: acylation of alcohols, vapor phase dehydrogenation of cyclohexanol to cyclohexane, hydroxylation of 1-naphthol with peroxides, and alkylation of naphthalene.[1,2] Similarly, Ce-incorporation in silica network of MCM-41 has been found to impart catalytic activity in the oxidation of cyclohexane[3] and n-heptane.[4] While Ce-MCM-41 has been found to be quite promising catalyst for Lewis acid–induced acylation reactions,[2] H/Al-MCM-41 can catalyze both, the Lewis and Brönsted acid catalyzed reactions owing to its Lewis and Brönsted acidity. Further, Ce-Al-MCM-41 samples, with simultaneous incorporation of Ce and Al in MCM-41, was found to exhibit higher catalytic activity for Brönsted acid catalyzed isopropylation of naphthalene and benzylation of benzyl alcohol as compared to Al-MCM-41 with comparable Al contents.[2,5] How such dual incorporation of Ce and Al can enhance the Brönsted acidity as well as the total acidity of these Ce-Al-MCM-41 catalysts is an aspect that has been discussed in (Chapter 2, Section 2.3.2.10 and 2.3.2.11) detailed using FTIR and TPD (ammonia) techniques.

The benzylation of toluene with benzyl chloride and benzyl alcohol, the reactions catalyzed by Lewis and Brönsted acid sites, respectively,[6,7] are chosen as model catalytic reactions for studying Lewis acidity and Brönsted acidity in the Ce-Al-MCM-41 catalysts. Schemes 3.1.1 and 3.1.2 depict the reaction products that would form when benzyl chloride and benzyl alcohol is used as alkylating agent, respectively. The main products in both the cases are 1, 4-methyldiphenylmethane (1, 4-MDPM) and 1, 2-methyldiphenylmethane (1, 2-MDPM). However, in the case of Lewis acid catalyzed route (Scheme 3.1.1) a small amount of 1-benzyl-3- (4-methyl benzyl) benzene (BMBB) and methylphenylbenzyl chloride (MPBC) is also obtained,

whereas in the case of Brönsted acid catalyzed benzylation of toluene the main side product formed is dibenzyl ether (DBE) along with minor amount of methylphenylbenzyl alcohol (MPBA) (Scheme 3.1.2).
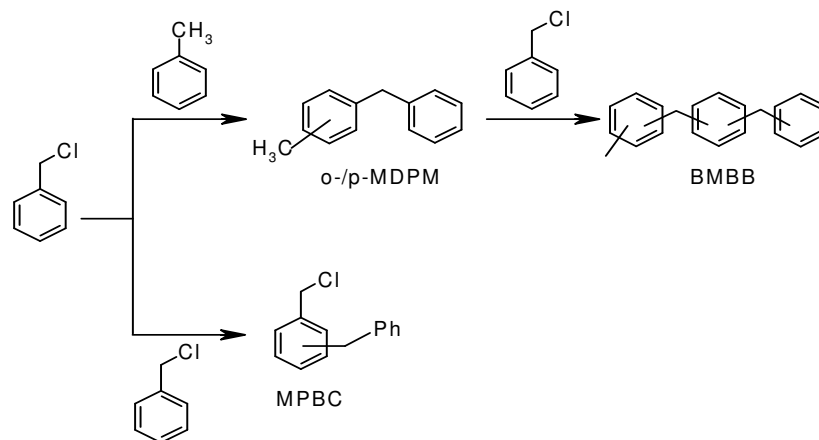
Scheme 3.1.1. Lewis acid catalyzed benzylation of toluene using benzyl chloride.
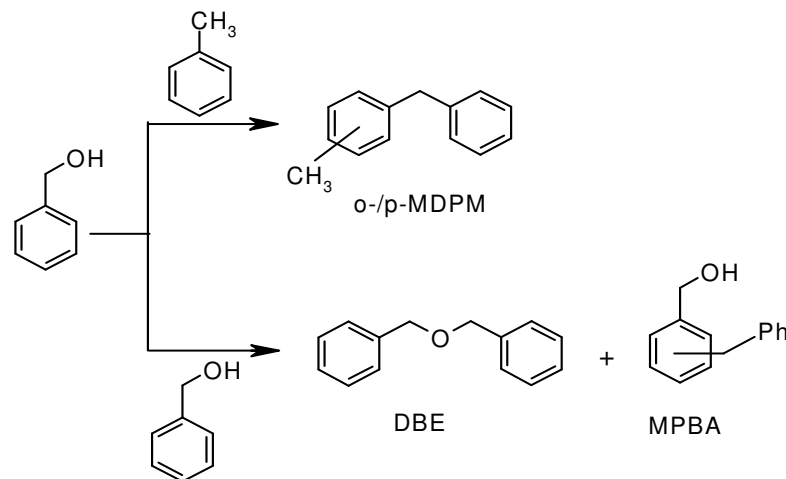
Scheme 3.1.2. Brönsted acid catalyzed benzylation of toluene using benzyl alcohol.

Hence, in the present section (3.1.1), systematic studies on the benzylation of toluene using benzyl chloride as well as benzyl alcohol catalyzed by different Ce-Al-MCM-41 samples are reported. For comparative purpose Ce-MCM-41 and Al-MCM-41 catalysts are also included in the study.

3.1.2. PROCEDURE FOR FRIEDEL-CRAFTS BENZYLATION REACTION

The reactions were performed in liquid phase batch-mode using a glass reactor. Prior to activity measurement, a catalyst sample (0.1g) was activated in air (423 K, 2h) and then cooled to room temperature. Benzylation of toluene was carried out by using two alkylating agents, i.e. benzyl chloride and benzyl alcohol. The substrate to alkylating agent molar ratio was ~20:1. The reactions were carried out in the absence of any solvent. The progress of the reaction was followed for duration of 6 h, by which time a complete conversion of the substrate was obtained in each experiment. The reaction mixture was centrifuged after cooling to room temperature. The separated organic layer was diluted with dichloromethane and the product was analyzed with the help of a Varian model-CP-3800 gas chromatograph equipped with a capillary column. The product identity was also confirmed by using a GC-MS.

3.1.3. RESULTS AND DISCUSSION

3.1.3.1. Catalytic Activity in Friedel-Crafts Benzylation Reaction

Table 3.1.1 presents the data obtained for reaction of toluene and benzyl chloride (Lewis catalyzed route) over Ce_x-Al-MCM-41 samples at two different temperatures. The main products are 1, 2- and 1, 4-MDPM. In addition, two other products formed by (i) benzylation of benzylchloride to methylphenylbenzyl chloride (MPBC) (Scheme 3.1.1) and (i) further benzylation of MDPM to 1-benzyl-3- (4-methyl benzyl) benzene (BMBB) were also obtained (Scheme 3.1.1), particularly at lower temperature.

The conversion increases significantly by increasing the reaction temperature from 363 K to 373 K (Table 3.1.1). The results in this table also reveal that the Ce-MCM-41 (Si/Ce = 30) and Al-MCM-41 (Si/Al = 30) samples exhibit comparable catalytic activity at both the reaction temperatures, confirming that the incorporation

of Ce in MCM-41 gave rise to a significant number of Lewis acid sites (L_2). It is of further interest to note that the presence of both the Ce and Al resulted in significant increase in substrate conversion, the extent of which increased with the increase in Ce/Al mol ratio at comparable Al contents. The selectivity for *o-* and *p-* isomers of the main reaction product remained unaffected of Ce content at both the reaction temperatures (Table 3.1.1). However, at the same time a progressive increase in the yield of MDPM as a function of increasing Ce content with a consequent decrease in the yield of BMBB and MPBC was also observed. This is more clearly seen from Figure 3.1.1 A and B.

Table 3.1.1. Liquid-phase benzylation of toluene with benzyl chloride at two reaction temperatures.[a]

Sample	Catalysts	Temp. (K)	BC Conv. (mole %)	Product Selectivity [b] (%)			
				o- MDPM	*p-* MDPM	BMBB	MPBC
B	Al-MCM-41	363	39	34	38	12	16
	(-, 30)	373	64	45	47	8	0
C	Ce-MCM-41	363	42	37	38	13	12
	(30, -)	373	68	44	48	8	0
E	Ce-Al-MCM-41	363	53	38	44	8	10
	(80, 32)	373	75	45	49	6	0
F	Ce-Al-MCM-41	363	59	41	45	6	8
	(59, 33)	373	81	45	51	4	0
G	Ce-Al-MCM-41	363	60	41	45	9	5
	(38, 34)	373	83	48	50	2	0

[a] Reaction condition: Catalyst = 0.1 g; reaction time: 6 h; toluene: benzyl chloride (BC): 20: (1 mole/ mole). [b]MDPM = 1, 4-methyldiphenylmethane; BMBB = 1-benzyl-3-(4-methyl benzyl) benzene; MPBC = methylphenylbenzyl chloride.
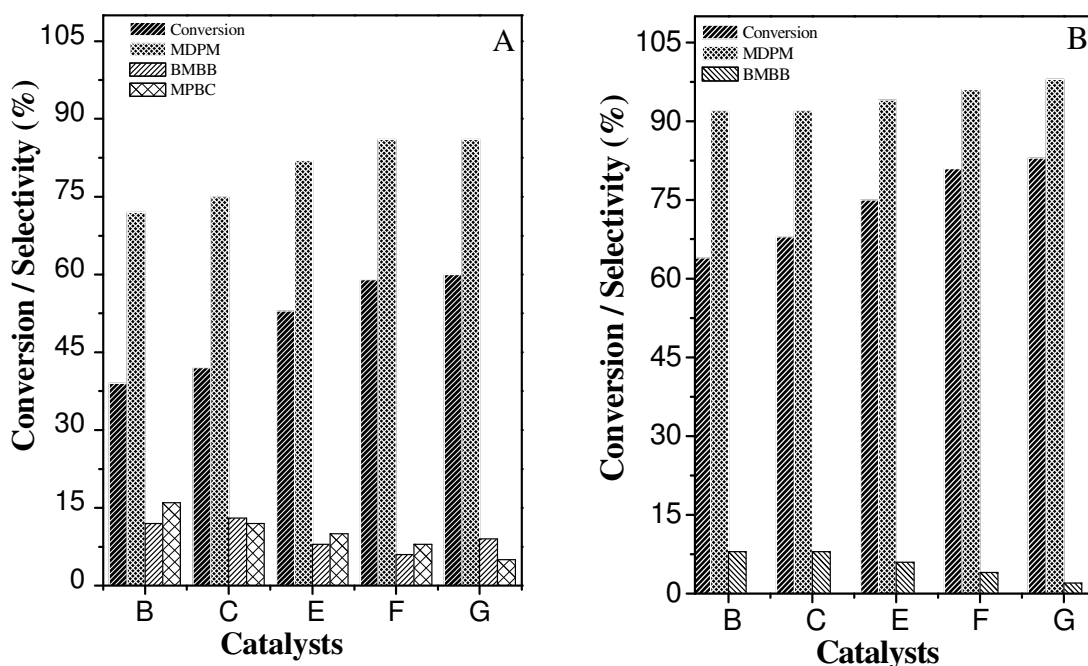
Figure 3.1.1. Liquid-phase benzylation of toluene with benzyl chloride at (A) 363 K and (B) 373 K two reactions temperatures.

Table 3.1.2 summarizes the results obtained using benzyl alcohol via Brönsted acid catalyzed route. As expected in the light of above-mentioned FTIR results (Chapter 2, Figures 2.15, 2.16, 2.17 and 2.18), the Ce-MCM-41 sample exhibited no activity at all for Brönsted acid catalyzed alkylation of toluene using benzyl alcohol. On the other hand, Al-MCM-41 shows considerably high activity, giving rise to the formation of methyldiphenylmethane (MDPM) as a major product. As in the case of benzyl chloride, here also two side products, namely methylphenylbenzyl alcohol (MPBA) formed by the benzylation of benzyl alcohol and dibenzyl ether (DBE) which is formed by etherification via self-condensation of benzyl alcohol, as shown in Scheme 3.1.2, were also obtained. The rise in reaction temperature from 363 to 373 K resulted in increased conversion even though the selectivity for MDPM remained almost the same. However, as in the case of data presented in Table 3.1.1, the incorporation of Ce along with Al resulted in increased conversion of the substrate and also in the increased yield of MDPM (Table 3.1.2). An increase in the selectivity

for DBE as a result of rise in temperature is also observed (Table 3.1.2). These results clearly suggest a synergistic effect of Ce incorporation in Al-MCM-41 in enhancing the acidity and consequently catalytic activity in both Lewis and Brönsted acid catalyzed reactions. In this case also, it is clearly seen from Figure 3.1.2 A and B.

Table 3.1.2. Liquid-phase benzylation of toluene with benzyl alcohol at two reaction temperatures.[a]

Sample	Catalysts	Temp. (K)	BA Conv. (mole %)	Product Selectivity [b] (%)			
				o- MDPM	*p-* MDPM	DBE	MPBA
B	Al-MCM-41 (-, 30)	373	22	37	39	13	11
		383	62	37	39	24	0
C	Ce-MCM-41 (30, -)	373	0	0	0	0	0
		383	0	0	0	0	0
E	Ce-Al-MCM-41 (80, 32)	373	29	41	43	9	7
		383	70	40	42	18	0
F	Ce-Al-MCM-41 (59, 33)	373	32	44	45	7	4
		383	76	40	42	18	0
G	Ce-Al-MCM-41 (38, 34)	373	33	43	45	5	7
		383	78	45	43	12	0

[a] Reaction condition: Catalyst: 0.1 g; reaction time: 6 h; toluene: benzyl alcohol (BA): 20: 1 (mole/mole) [b] MDPM = 1,4-methyldiphenylmethane; DBE = dibenzyl ether; MPBA = methylphenylbenzyl alcohol.
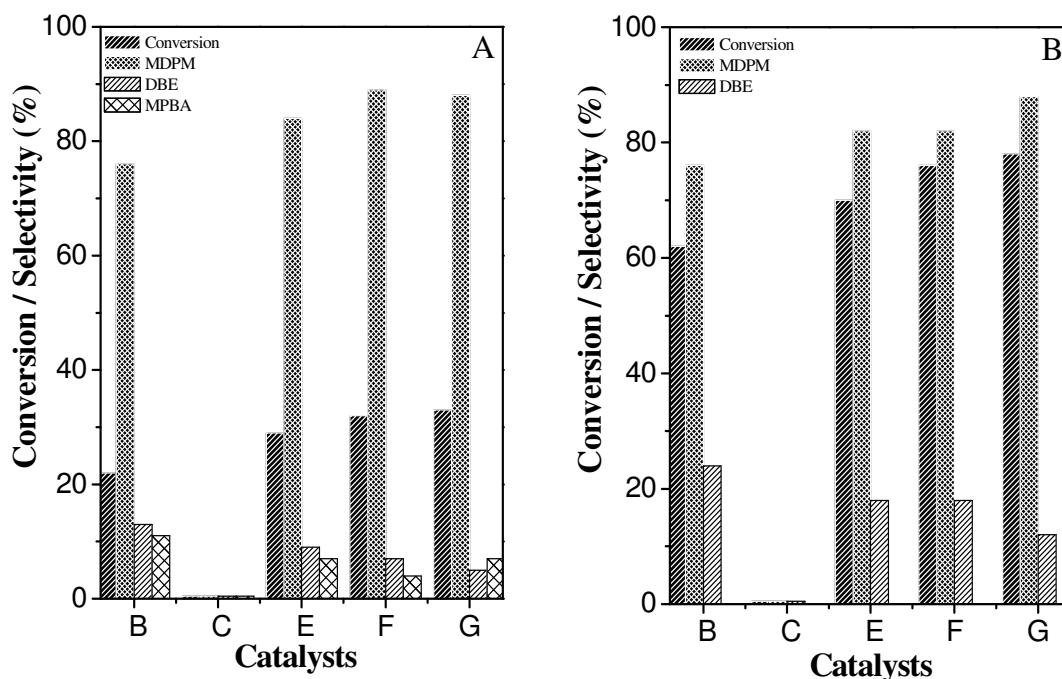
Figure 3.1.2. Liquid-phase benzylation of toluene with benzyl alcohol at (A) 373 K and (B) 383 K two reactions temperatures.

It is pertinent to emphasize that no enhancement at all was observed in the catalytic activity of Ce-exchanged or Ce-impregnated Al-MCM-41 vis-à-vis H/Al-MCM-41, either in Lewis or Brönsted acid catalyzed reactions.[2,5] Hence, the Ce-induced enhancement in the catalytic activity cannot be attributed to the presence of extra-network Ce^{4+} species, either at the exchange site or possibly existing as occluded CeO_2 moieties.

3.1.4. CONCLUSIONS

In conclusion, the results of present study point to a synergism between Ce and Al cations, when co-substituted in siliceous MCM-41 during hydrothermal synthesis, resulting in increase in the concentration of both the Lewis and the Brönsted acid sites, compared to that in corresponding Al-MCM-41 and Ce-MCM-41 samples. The IR spectra of chemisorbed pyridine reveal that the dual-substituted samples contained at least two distinct Lewis acid sites, designated as L_2 and L_1, the

L_2/L_1 ratio increasing progressively with the Ce/Al atom ratio. The sites L_1, found in abundance in Al-MCM-41, are identified with the conventional Lewis acid sites related to the presence of Al^{3+} at defect sites. The L_2 sites, associated with weakly bound pyridine, are identified with the isolated Ce species in silicate network. The decrease in the intensity of the silanol groups (Si−OH) and the consequent increase in the concentration of Brönsted acid sites on Ce incorporation provide an evidence for creation of new Brönsted acid sites as hydrogen bonded polarized ≡Ce-OH or ≡Si-OH bonds in the vicinity of regular Brönsted acid sites (Bridged OH moieties). The ammonia TPD results (Figures 2.22 and 2.23, Chapter 2) indicate that not only the concentration but the strength of the Brönsted acid sites also increases as a result of Ce-substitution. This may be attributed to the presence of more electropositive character of Ce^{4+} vis-à-vis Si^{4+} in the vicinity of Al^{3+}. The over all acid character of Ce-Al-MCM-41 samples is in complete harmony with catalytic activity data, where the presence of Ce is found to enhance the catalytic activity for both the Lewis and the Brönsted promoted benzylation reactions.

3.1.5. REFERENCES

1. S. C. Laha, P. Mukharjee, S. R. Sainkar, R. Kumar, *J. Catal.* **2002,** 207, 213.

2. M. D. Kadgaonkar, S. C. Laha, R. K. Pandey, P. Kumar, S. P. Mirajkar, R. Kumar, *Catal. Today* **2004**, 97, 225.

3. W.Yao, Y.Chen, L.Min, H. Fang, Z. Yan, H. Wang, and J. Wang , *J. Mol.Catal. A: Chem.* **2005**, 246, 161.

4. S. Araujo, J. M. F. B. Aquino, M. J. B. Souza and A. O. S. Silva, *J. Solid State Chem.* **2003,** 171, 371.

5. P. Kalita, N. M. Gupta, R. Kumar, *J. Catal.* **2007,** 245, 338.

6. G. A. Olah, *Friedel-Crafts Chemistry*, Wiley, New York, **1973**.

CHAPTER 3: Part B

3.2. METHODOLGY FOR THE PREPARATION OF 1,5-DICARBONYL COMPOMUNDS BY MUKAIYAMA-MICHAEL REACTION OVER Ce-MCM-41, Al-MCM-41 AND Ce-Al-MCM-41 CATALYSTS

3.2.1. INTRODUCTION

In 1974-1976, Mukaiyama and co-workers[1-3] introduced a version of the Mukaiyama-Michael addition reactions involving the conjugate addition of silyl enol ether or silyl ketene acetals to α, β-unsaturated carbonyl compounds. These so called Mukaiyama-Michael reactions via nucleophilic carbon-carbon bond formation have now become a powerful method for the preparation of 1, 5-dicarbinyl compounds, and are known to be catalyzed by Lewis acid catalysts.[4-8] Several authors have reported the reaction between enol silanes with α, β-unsaturated carbonyl compounds using several homogeneous Lewis acid such as $TiCl_4$, $SnCl_4$, Ti $(O-iPr)_4$,Ti $(OEt)_4$, stoichiometric amounts and at lower temperatures.[3,9] The utility of bifluorides such as $(Me_2N)_3S^+Me_3SiF_2^{4-}and(Me_2N)_3S^+Me_3SiF_2^{6-}$,[9-11] and the per chlorate Ph_3CClO_4[12] in the homogenous condition for the Michael and aldol type reactions has also been highlighted. Among the heterogeneous catalyst, solid acid catalysts such as amorphous $SiO_2 -Al_2O_3$ and zeolites are also known to be the potential candidates for the promoting C-C bond formation[13-17] However, only a few heterogeneous catalysts and inorganic salts, like CsF and Al-clay montmorillonite,[18-19] have shown the low temperature catalytic activity for such reactions. Recently, the Mukaiyama-Michael reactions of silyl enol ether / silyl ketene acetal with α, β-unsaturated carbonyl compounds using microporous titanium silicate (TS-1) have been reported. [20,21] These Michael products have demand in the field of pharmaceuticals as they are used in the total synthesis of the antitumor diterpenoid bruceantin and the cytotoxic natural product sesbanimide A.[22,23] Michael addition is extremely important in the organic synthesis and preparation of bridged- or fused-ring bicyclic ketone.[24] The Michael product of 1, 5-dicarbonyl compounds can also serve as starting materials for preparing many heterocyclic compounds,[25-28] and polyfunctional compounds.[29-30]

The present section deals with the studies on the catalytic application of Ce-MCM-41, Al-MCM-41 and Ce-Al-MCM-41 catalysts in Mukaiyama-Michael reaction. To explore the catalytic activity of these catalysts, 1-phenyl-1-(trimethylsilyloxy) ethylene and 2-cyclohexen-1-one was chosen as starting reactant for this particular reaction as shown in reaction Scheme 3.2.1.
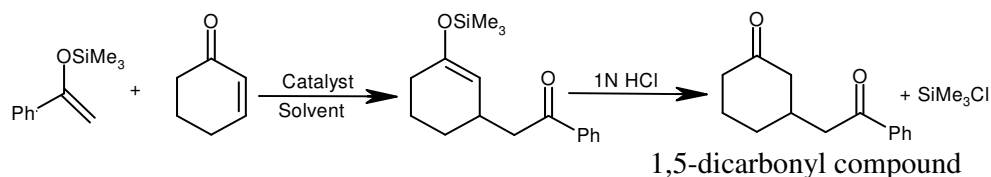
Scheme 3.2.1. Mukaiyama-Michael reaction of 1-phenyl-1-(trimethylsilyloxy) ethylene and 2-cyclohexen-1-one.

3.2.2. GENERAL PROCEDURE FOR MUKAIYAMA-MICHAEL REACTION

The catalytic reaction was performed in liquid-phase, under N_2 atmosphere using two necked round bottom flask. The samples were activated at 423 K under vacuum prior to their use as catalyst. In a typical procedure, the 10 mmol of substrate (e.g. 1-phenyl-1-(trimethylsilyloxy) ethylene / 2-cyclohexen-1-one) was added in dry dichloromethane (DCM) and catalyst (0.2 g) was added to the reaction vessel and the reaction mixture was stirred magnetically at 313 K for 9 h. The progress of the reaction was monitored over the period of 24 h by gas chromatography (Varian model-CP-3800) equipped with capillary column and flame ionization detector (FID) as well as by thin layer chromatography (TLC). After completion of the reaction, the catalyst was filtered out and the filtrate was diluted with DCM and then washed with 1N HCl and finally washed with water. The organic layer was separated and dried with anhydrous Na_2SO_4. The solvent was removed by rotary evaporator and the product was purified through column chromatography using silica gel (100-200 mesh), petroleum ether: ethyl acetate (3:1) and confirmed through GC, GC-MS, [1]H

NMR, ^{13}C NMR techniques. The product (Entry 1, Table 3.2.4) got 85 % isolated yield. M.P. 71-73 °C, R_f 0.32 (petroleum ether: ethyl acetate = 3:1); ^{1}H NMR (200 MHz, $CDCl_3$) δppm: 7.91-7.89 (m, 2H), 7.56-7.48 (m, 1H), 7.45-7.40 (m, 2H), 3.05-2.80 (m, 2H), 2.53-1.98 (m, 7H), 1.75-1.59 (m, 1H), 1.47-1.35 (m, 1H); ^{13}C NMR (50 MHz, $CDCl_3$) δ 209.52, 197.52, 136.27, 132.33, 127.85, 127.2, 46.85, 43.83, 40.35, 34.06, 30.27, 24.11; C, H, and N analysis C 78%, H 8% (calculated), C 77.78%, H 7.58 % (observed).

3.2.3. RESULTS AND DISCUSSION

3.2.3.1. Effect of Reaction Time

Figure 3.2.1 shows the catalytic efficiency of various Ce-Al-MCM-41 samples having different Ce-contents at comparable Si/Al ratio for the condensation of 2-cyclohexen-1-one (α, β-unsaturated compounds) with 1-phenyl-1-(trimethylsilyloxy) ethylene (silyl enol ether) to produce the corresponding 1,5-dicarbonyl compound (Michael 1,4-addition, Scheme 3.2.1.). Although, the reaction was carried out for 24 h, there was only marginal increase after 9 hours of the reaction. The trend of the product yield obtained over different catalyst was: Ce-MCM-41 < Al-MCM-41 < Ce-Al-MCM-41. Among Ce-Al-MCM-41 samples having comparable Al content and varying Ce contents, the conversion / product yield followed the order: D< E < F ≈ G.

From Figure 3.2.1, it is observed that the catalytic activity of Ce-MCM-41 and Al-MCM-41 samples was only marginally different; a significant increase in the Michael product yield was observed when both Ce and Al were present together in a sample. Thus, the conversion / product yield obtained over Ce-Al-MCM-41 samples was found to be higher than that obtained using Ce-MCM-41 or Al-MCM-41 samples. This enhancement of catalytic activity may be attributed to the increase in total acidity (Table 2.4, Chapter 2), as reported in our recent paper.[31]
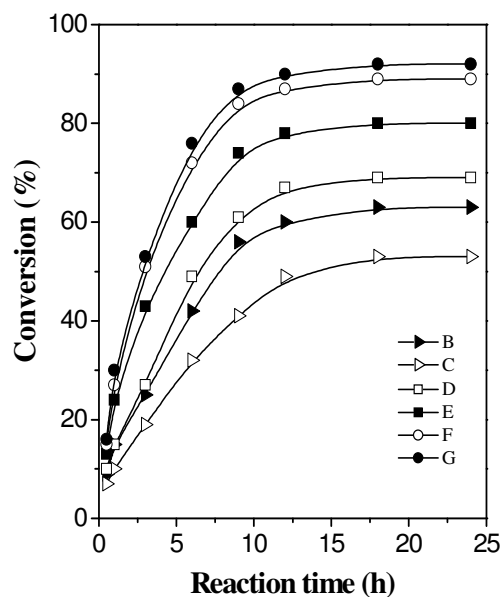
Figure 3.2.1. Effect of reaction time on conversion over various Ce-Al-MCM-41

catalysts. The sample notations as per Table 2.1 (Chapter 2).

A direct correlation was found (Figure 3.2.2) between the conversion obtained

over different catalyst samples (B-G) and the ratio of the intensity of certain IR bands

i.e. 1444/1452 cm^{-1} bands (L_2/L_1, curve a) and 1545/1444 cm^{-1} bands (B/L_2, curve b)

on one hand and the total acidity, as measures by the TPD ammonia measurements,

(curve c) on the other. As the Ce content in Ce-Al-MCM-41 samples increases, the

conversion also increases progressively. Almost linear correlation between the

conversion and intensity ratios of B/L_2 as well as L_2/L_1 bands (of Ce-Al-MCM-41

samples having comparable Al and increasing Ce contents) clearly indicates that both

the Lewis acid sites, generated due to Ce and Al incorporation, may play an important

role in catalyzing the Michael reaction. It is further supported by similar direct

correlation between the conversion and the total acidity of the samples (curve c,

Figure 3.2.2). As observed in Figure 2.23 (Chapter 2), the total acidity of these

samples, as obtained by ammonia TPD, is plotted against their mole fraction of Ce

and Al [(Ce+Al)/(Si+Ce+Al)]. As expected, here also direct correlation was observed

between Ce contents in Ce-Al-MCM-41 samples and the total acidity of the samples.

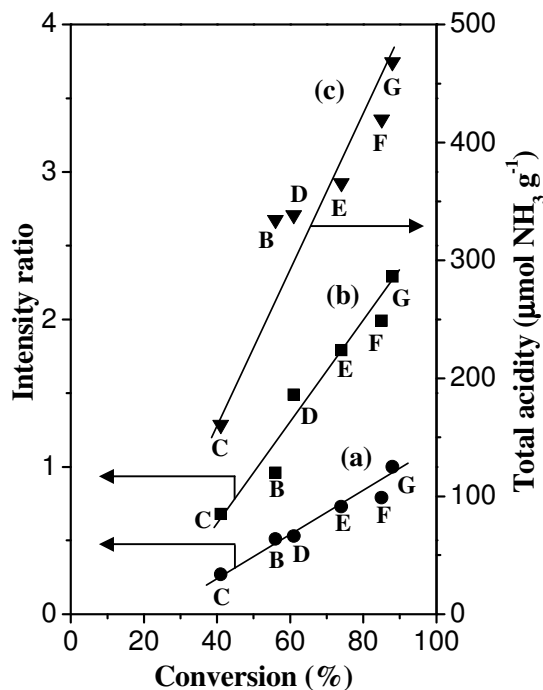**Figure 3.2.2.** Plots of conversion / yield vs intensity ratio and total acidity (μmol NH_3

g^{-1}) of Ce-Al-MCM-41 samples. Curves (a) 1545/ 1444(B/L_2); (b) 1444/1452 (L_2/L_1)

for adsorption at 420 K and (c) total acidity (μmol NH_3 g^{-1}). The sample notations as

per Table 2.1, Chapter 2.

However, it will be pertinent to compare the intrinsic activity of these catalysts

samples with respect to per mole of Ce, Al and Ce + Al in different samples. In Table

3.2.1, the conversion and the corresponding TON values obtained over samples B-G

using DCM as solvent at 313 K and 9 h of reaction time are reported. The TON was

calculated with respect to Ce and Al individually as well as Ce+Al present in the Ce-

Al-MCM-41 samples. Since, the Al contents were comparable in samples B and D-G,

it is interesting to compare the TON of these samples with respect to their Al contents.

The TON (with respect to Al) increased in the order: B > D > E > F > G in

accordance with increasing Ce-content in the samples, as expected. However, when

the TON of the sample C to G calculated with respect to Ce-contents in these samples is compared, quite different trend (C << D > E > F > G) was observed. The Ce contents of the samples D-G follow the opposite trend (D < E < F < G) at comparable Al content, indicating that as the concentration of Ce is increased, more and more Ce gets buried inside the walls of MCM-41 and therefore not available for the reaction. This is further supported by the fact that almost comparable values of TON were obtained for all the samples, when both Ce and Al were taken into consideration for TON calculations (Table 3.2.1). The catalyst Ce-Al-MCM-41 (Si/Ce = 59, Si/Al = 33, sample F) was chosen for the detailed activity measurements by using different solvents and different substrates.

Table 3.2.1. Mukaiyama-Michael reaction of 1-phenyl-1-(trimethylsilyloxy) ethylene and 2-cyclohexen-1-one over different MCM- 41 materials.[a]
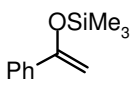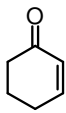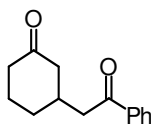
Sample	Catalyst	Mole ratio		Conv. [b] (mole %)	TON [c]		
		Si/Ce	Si/Al		Ce	Al	Ce+Al
B	Al-MCM-41	0	30	56	-	52.0	52.0
C	Ce -MCM-41	30	0	41	40.4	-	40.4
D	Ce-Al-MCM-41	108	32	61	202.8	60.3	46.5
E	Ce-Al-MCM-41	80	32	74	183.9	73.2	52.3
F	Ce-Al-MCM-41	59	33	85	158.5	87.4	56.3
G	Ce-Al-MCM-41	38	34	88	107.8	92.4	49.7

[a] Reaction Condition: 10 mmol of 1-phenyl-1-(trimethylsilyloxy) ethylene, 10 mmol of 2-cyclohexen-1-one, catalyst amount = 200 mg, 10 ml of dry DCM , reaction time 9 h, reaction temperature 313 K. [b]Conversion (Conv.) with respect to 2-cyclohexen-1-one and based on GC analysis, products isolated by column chromatography using solvent ethyl acetate: petroleum ether (1:3), and confirmed by GC-MS, ^{1}H NMR and ^{13}C NMR. [c]TON with respect to moles of 2-cyclohexen-1-one converted per mole of single metal (Al or Ce) or total metal content (Al + Ce).

3.2.3.2. Effect of Solvent and Temperature

Various authors have reported for the Mukaiyama-Michael reaction between silyl enol ether and enone in the presence of different organic solvents with a variety of homogeneous and heterogeneous catalysts.[3,9-11,19] The catalytic activity of Ce-Al-MCM-41 (sample F) catalyst for Mukaiyama-Michael reaction of 1-phenyl-1-(trimethylsilyloxy) ethylene with 2-cyclohexen-1-one with various solvent was measured. These results are given in Table 3.2.2. Each reaction was continued for 9 h at 313 K. It is important to note that the Michael product was always found to be ~100 %; regardless of the conversion level and the rest is an essentially unconverted starting material. Michael products were obtained by hydrolyzing the product with 1N HCl, extracted by dichloromethane (DCM) and purified by column chromatography. The Mukaiyama-Michael reaction was carried out at room temperature (298 K) and at 313 K. Furthermore, all the reactions were performed under perfectly dry conditions at 313 K. Among the investigated solvents, dichloromethane (DCM) was found to be the superior solvent for this particular reaction as can be seen in Table 3.2.2. According to Hughes-Ingold Rules[32] of solvent effects, the transition state is capable of greater solvation and then the reaction rate will be increased by more polar solvent with higher solvation leading to the lowering of required activation energy.

Table 3.2.2. Effect of solvent and temperature in Mukaiyama-Michael reaction between 1-phenyl-1-(trimethylsilyloxy) ethylene and 2-cyclohexen-1-one over Ce-Al-MCM-41 (Si/Ce = 59, Si/Al = 33, sample F) catalyst.[a]

Silyl enol ether	α, β- unsaturated carbonyl compound	Solvent	Temp. (K)	Conv.[f] (mole %)	TON[g]	Product
		DCM[b]	298	59	39.1	
		DCM[b]	313	85	56.3	
		THF[c]	313	72	47.7	
		MeCN[d]	313	73	48.4	
		MeNO$_2$[e]	313	75	49.7	

[a] Reaction condition: 10 mmol of 1-phenyl-1-(trimethylsilyloxy) ethylene, 10 mmol of 2-cyclohexen-1-one, catalyst = 200 mg, 10 ml of dry DCM, reaction time 9 h, reaction temperature 298-313 K. [b] Dry dichloromethane (DCM), [c] Dry tetrahydrofuran (THF), [d] Dry acetonitrile (MeCN), [e] Dry nitromethane (MeNO$_2$), [f] Conversion (Conv.) with respect to 2-cyclohexen-1-one and based on GC analysis, [g] TON with respect to moles of cyclohexenone converted per mole of combine metal (Al + Ce).

3.2.3.3. Recyle Studies

The stability of the heterogeneous catalysts was evaluated by recovering them from the hot reaction mixtures by filtration. In the Figure 3.2.3 the conversion and TON obtained during recycle studies of the catalyst Ce-Al-MCM-41 (Ce+Al, sample F) are plotted as a function of number of recycles at identical reaction condition. The same catalyst sample was used for four consecutive cycles without any activation. While, the conversion decreased progressively from *ca.* 85 to 78 % in 4th cycle, the rate of decrease was more in the case of first two recycles and then almost stabilized

at *ca.* 78% during 3rd and 4th recycle. This decrease in the conversion during first few

recycles was mainly due to partial leaching of Ce and Al, which was confirmed by the

AAS analysis of Ce and Al in the filtrate obtained by separating the solid catalyst

after the reaction (Table 3.2.3). The TON, calculated on the basis of remaining Ce and

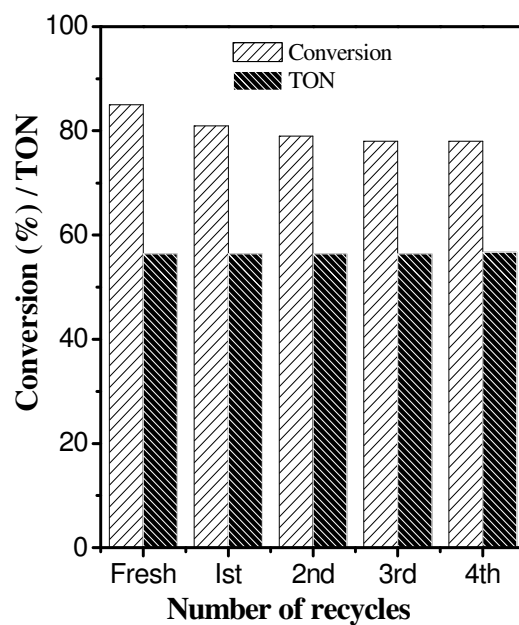Al contents in the solid catalysts, remained unchanged during course of the recycles,

as expected.

Figure 3.2.3. Effect of conversion / yield and turn over number (TON, Ce+Al) vs

number of catalyst recycles for Mukaiyama-Michael reaction.

Table 3.2.3. Recycle studies Mukaiyama-Michael reaction of 1-phenyl-1-(trimethylsilyloxy) ethylene and 2-cyclohexen-1-one over Ce-Al-MCM-41 (Si/Ce=59, Si/Al=33, sample F) catalyst.

| Recycle No	Catalyst amount (g)	Molar ratio [a]		Conv. [b] (mole %)	TON [b]		
		Si/Ce	Si/Al		Ce	Al	Ce+Al
Fresh	0.20	59.3	33.3	85	158.5	87.7	56.3
Ist	0.19	59.7	33.7	81	158.1	87.6	56.4
2nd	0.18	60.5	34.8	79	156.1	88.2	56.3
3rd	0.17	61.4	35.2	78	156.4	88.0	56.3
4th	0.16	62.2	36.1	78	156.0	89.1	56.7

[a]Solid product calculated by AAS, [b] Conversion with respect to 2-cyclohexen-1-one and based on GC analysis, [b]TON with respect to moles of 2-cyclohexen-1-one converted per mole of combine metal (Al + Ce).

3.2.3.4. Effect of Different Substrates

The conversion of different α, β-unsaturated carbonyl compounds with 1-phenyl-1- (trimethylsilyloxy) ethylene to give corresponding Mukaiyama-Michael product is given in Table 3.2.4 (Scheme 3.2.2). Entry 1 and 2 compare the reactivity of cyclic ketones, where six membered 2-cyclohexen-1-one gave slightly higher conversion (Entry 1) than that obtained when five membered 2-cyclopenten-1-one is taken as substrate (Entry 2). While 2-cyclohexen-1-one can aquire more stable chair conformation, 2-cyclopenten-1-one can aquire less stable envelop form.

A number of acyclic α, β-unsaturated ketones were investigated (Entry 3-8, Table 3.2.4) for the Mukaiyama-Michael reaction using Ce-Al-MCM-41 (sample F) catalyst in the identical reaction condition. Among the various substrates, the highest conversion was obtained for the reaction of 1-phenyl-1- (trimethylsilyloxy) ethylene

and benzylideneacetophenone (Entry 5, Table 3.2.4). However, slightly less conversion was observed for benzalacetone (Entry 6) because of the negative mesomeric (-I) effect. Due to phenyl group (Entry 5), the beta carbon in enone possesses more electropositive character, so, attack of nucleophile to electrophlile will be easier at beta carbon in enone to get Michael product. Since, electron-withdrawing group on the beta carbon in enone increases the electrophilicity by delocalization of electron results in facile nucleophilic reactions. In the other case, the conversion / yield of Michael product decreases with increasing with electron donating groups or increasing carbon chain length in a parent enones because electron donating groups attached with beta carbon in enone decrease electropositive character as observed for entries 3, 4 and 7, 8 (Table 3.2.4).
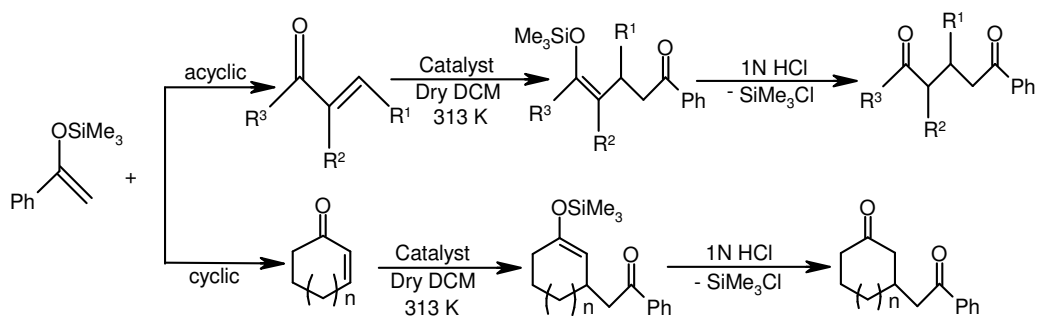
Scheme 3.2.2. Mukaiyama-Michael reaction of 1-phenyl-1-(trimethylsilyloxy) ethylene with different α, β-unsaturated carbonyl compounds.

Where, n = o, (2-cyclopenten-1-one) and n = 1, (2-cyclohexen-1-one).

The catalytic activity of Ce-Al-MCM-41 (sample F) was examined for the Mukaiyama-Michael addition of silyl enol ether with different α, β-unsaturated esters (Entry 9-14, Table 3.2.4) in the identical reaction condition. This reaction is very difficult and thermodynamically disfavored in the presence of homogeneous catalyst.[33,34] In the case of methyl acrylate (Entry 9), the slightly high conversion was

obtained than that of methylmethacrylate (Entry 10). This is due to the extra methyl group (electron donating group, +I effect) is substituted in β-carbon. This makes β-carbon less electropositive and it leads the lower conversion / yield of Michael product. Slightly higher conversions were observed for ethyl crotonate and ethyl cinnamate (Entry 12, 14) than methyl crotonate and methyl cinnamate (Entry 11, 13), probably due to the presence of more electron-withdrawing groups such as ethyl ester (-COOEt) and phenyl group. Since, ethyl ester (-COOEt) and phenyl group have more electron-withdrawing power than methyl ester (-COOMe) and methyl groups.

Table 3.2.4. Mukaiyama-Michael reaction of 1-phenyl-1-(trimethylsilyloxy) ethylene (silyl enol ether) with different α, β- unsaturated carbonyl compounds over Ce-Al-MCM-41 (Si/Ce = 59, Si/Al = 33, sample F) catalyst.

Entry	α, β- Unsaturated carbonyl compounds	Silyl enol ether	Product	Time (h)	Conv.[b] (mole %)
1	2-Cyclohexen-1-one			9	85
2	2-Cyclopenten-1-one			9	77
3	Methyl vinyl ketone			7	70
4	Ethyl vinyl ketone			6	73
5	Benzylideneacetophenone			2	97
6	Benzalacetone			3	90
7	3-Methylpent-3-en-3-one			7	65

8	3-Nonen-2-one		7	62
9	Methyl acrylate		9	69
10.	Methylmethacrylate		9	63
11.	Methyl trans-crotonate		9	62
12.	Ethyl crotonate		9	66
13.	Methyl trans-cinnamate		8	71
14.	Ethyl cinnamate		8	74

[a] Reaction condition: 10 mmol of silyl enol ether,10 mmol of α,β- unsaturated carbonyl compounds, catalyst = 200 mg, 10 ml of dry dichloromethane (DCM), reaction temperature 313 K, reaction time 2-9 h.

[b] Conversion (Conv.) with respect to ketone/ester and based on GC analysis.

3.2.4. CONCLUSIONS

Cerium-containing Al-MCM-41 mesoporous materials are promising catalysts for Mukaiyama-Michael reactions of silyl enol ether and α, β-unsaturated carbonyl compounds. The increased in Michael product yield may be due to simultaneous incorporation Ce and Al in Ce-Al-MCM-41 lead to increased acidity. The Ce-Al-MCM-41 samples showed higher catalytic activity for the Mukaiyama-Michael reactions reactions, as compared to the Ce-MCM-41 and Al-MCM-41 catalysts

having comparable Ce or Al contents. The product yield (75-85 %) was slightly influenced by the nature of the solvent employed as reaction medium. The best result was obtained by using dichloromethane as solvent. For Mukaiyama-Michael reactions, the substrate reactivity increases when phenyl group (electron-withdrawing group) is attached with α, β-unsaturated carbonyl compounds and decreases with increasing electron donating groups or increasing carbon chain length in a parent enones. Moreover, ketones showed comparatively high conversion than esters. The reusability of the catalysts enables its use several times without substantial decrease in activity.

3.2.5. REFRENCES

1.   K. Narasaka, K. Soai, T. Mukaiyama, *Chem.Lett.* **1974**, 1223.

2.   K. Saigo, M. Osaki, T. Mukaiyama, *Chem. Lett.* **1976**, 163.

3.   K. Narasaka, K. Soai, Y. Aikawa, T. Mukaiyama. *Bull. Chem. Soc. Jpn*. **1976**, 49, 779.

4.   T-P. Loh, L-L. Wei, *Tetrahedron* **1998**, 54, 7615.

5.   X. Wang, S. Adachi, H. Iwai, H. Takatsuki, K. Fujita, M. Kubo, A. Oku, T. Harada, *J. Org. Chem.* **2003**, 68, 10046.

6.   S. Kobayashi, M. Murakami, T. Mukaiyama, *Chem. Lett*. **1985**, 953.

7.   S. Kobayashi. *Eur. J. Org. Chem*. **1999**, 1, 15.

8.   T. Harada, H. Iwai, H. Takatsuki, K. Fujita, M. Kubo, A. Oku, *Org. Lett.* **2001**, 3, 2101.

9.   C. H. Heathock, M. H. Norman, D. E. Uehling, *J. Am. Chem. Soc*. **1985**, 107, 2797.

10. O. W. Webster, W. R. Hertler, D. Y. Sogah, W. B. Farnham, T. V. Rajan Babu, *J. Am. Chem. Soc.* **1983**, 105, 5706.

11. T. V. Rajan Babu, *J. Org. Chem*. **1984**, 49, 2083.

12. S. Kobayashi, M. Murakami, T. Mukaiyama, *Chem. Lett*. **1985**, 953.

13. R. Noyori, I. Nishida, J. Sakata, *J. Am. Chem. Soc*. **1983**, 105, 1598.

14. C. R. Brindaban, S. Manika, B. Sanjay, *Tetrahedron Lett*. **1993**, 34, 1989.

15. M. T. Reetz, D. Giebel, *Angew. Chem. Int. Ed*. **2000**, 39, 2498.

16. H. Mitshuhashi, M. Tanaka, H. Nakamura, K. Arata, *Appl.Catal. A: Gen.* **2001**, 208, 1.

17. D. L. Gin, W. J. Zhou, W. Gu, *Chem. Mater.* **2001**, 13, 1949.

18. J. Boyer, R. J. P. Corriu, R. Perez, C. Reye, *Tetrahedron* **1983**, 39, 117.

19. M. Kawai, M. Onaka, Y. Izumi, *J. Chem. Soc. Chem. Commun*. **1987,** 1203.

20. M. Sasidharan, R. Kumar, *Catal. Lett.* **1996**, 38, 251.

21. M. Sasidharan, R. Kumar, *J. Catal.* **2003**, 220, 326.

22. R. A. Bunce, M. F. Schlecht, W. G. Dauben, C. H. Heathcock, *Tetrahedron Lett.* **1983**, 24, 4943.

23. P. A. Grieco, R. J. Cooke, K. J. Henry, J. M. Vander Roest, *Tetrahedron Lett.* **1991**, 32, 4665.

24. D. Liu, S. Hong, E. J. Corey, *J. Am. Chem. Soc*. **2006**, 105, 1598.

25. Z. S. Arigan, H. Suschitiky, *J. Chem. Soc.* **1961**, 2242.

26. S. S. Hisrch, W. J. Bailey, *J. Org. Chem.* **1978**, 43, 4091.

27. F. Krohnke, *Synthesis* **1976**, 1.

28. E. C. Constable, A. M. W. Cargill Thompson, *J. Chem. Soc. Dalton Trans.* **1992**, 2947.

29. I. R. Butler, S. J. Mcdonald, *Polyhedron* **1995**, 14, 529.

30. N. S. Gill, K. B. James, F. Lions, K. T. Potts, *J. Am. Chem. Soc.* **1952**, 74, 4923.

31. P. Kalita, N. M. Gupta, R. Kumar, *J. Catal.* **2007,** 245, 338.

32. S. Isaacs, *Physical Organic Chemistry, ELBS,* Longman group UK Ltd. **1987**, p. 171.

33. M. Yasuda, Y. Shigeyoshi, I. Shibata, A. Baba, *Synthesis* **2005**, 233.

34. M. Yasuda, K. Chiba, N. Ohigashi, Y. Katoh, A. Baba, *J. Am. Chem. Soc.* **2003**, 125, 7291.

3.3. **METHODOLOGY FOR THE PREPARATION OF β-HYDROXY CARBONYL COMPOUNDS BY MUKAIYAMA-ALDOL CONDENSATION UNDER SOLVENT FREE SYSTEM OVER Ce-MCM-41, Al-MCM-41 AND Ce-Al-MCM-41 CATALYSTS**

3.3.1. INTRODUCTION

The Mukaiyama-aldol condensation of silyl ketene acetal / silyl enol ether and aldehyde is a facile method for the Lewis acid–catalyzed C–C bond formation under the homogeneous conditions and at sub–ambient temperatures.[1-5] These reactions have been investigated in heterogeneous mode using solid Lewis acid catalysts, such as clays, naffion-117, amorphous silica-alumina and zeolites.[6-11] Further, solid bases, such as zeolites substituted with alkali or alkaline earth metals, alkaline earth oxides, hydrotalcites and AlPOs have also been utilized for the nucleophilic reactions, e.g. Michael, Aldol, and Knoevenagel type condensation reactions involving carbonyl compounds.[12] The Mukaiyama-type aldol and Michael reactions of silyl ketene acetal with aldehydes and α, β-unsaturated carbonyl compounds have been reported using microporous materials[13-15] and mesoporous materials such as Sn-MCM-41[16] and Ti-MCM-41[17].

In the present section, the catalytic properties of Ce-substituted Al-MCM-41 samples were examined for Mukaiyama-aldol condensation. For catalytic model reaction, methyl trimethylsilyl dimethylketene acetal and benzaldehyde were taken as staring materials (Scheme 3.3.1). Although, the effect of organic solvent was studied using different solvents by keeping all other reaction conditions the same, the reactions were also carried out under solvent free condition. The effect of various aldehydes and silyl enol ethers on the conversion and the selectivity of these reactions have also been investigated in detail.

β-hydroxy carbonyl compound
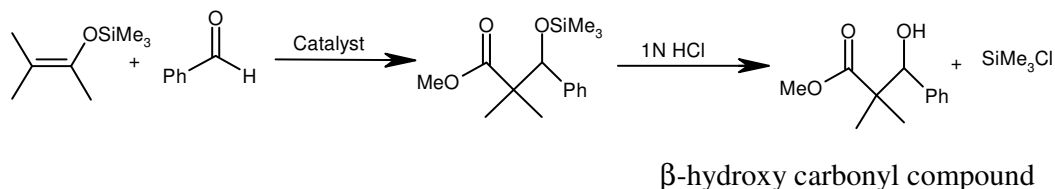
Scheme 3.3.1. Mukaiyama-aldol condensation of methyl trimethylsilyl dimethylketene acetal with benzaldehyde.

3.3.2. GENERAL PROCEDURE FOR MUKAIYAMA-ALDOL CONDENSATION

The catalytic liquid-phase reaction was performed under N_2 atmosphere using a two-necked continuously stirred round bottom flask, equipped with a water condenser. The catalyst was pre-activated at 423 K in a vacuum oven and the reactions were carried out under dry condition. In a typical procedure, the methyl trimethylsilyl dimethylketene acetal (10 mmol) in dry dichloromethane (DCM) was added to a pre-activated catalyst (0.21 g), followed by addition of benzaldehyde (10 mmol) to reaction vessel which was maintained at 313 K. The reactions under solvent free conditions (neat substrate) were also carried out at 373 K. The progress of the reaction was monitored over the period of 24 h by gas chromatography (Varian model-CP-3800) equipped with capillary column and flame ionization detector (FID) as well as by thin layer chromatography (TLC). After completion of the reaction, the catalyst was filtered out and the filtrate was diluted with DCM and then washed with 1N HCl and finally washed with water. The organic layer was separated and dried with anhydrous Na_2SO_4. The solvent was removed by rotary evaporator and the product was purified through column chromatography using silica gel (100-200 mesh), petroleum ether : ethyl acetate (3:1) as eluent and products confirmed through GC, GC-MS, ^{1}H NMR, ^{13}C NMR techniques. White powder; M. P. 66-67 °C, ^{1}H NMR (200 MHz, CDCl$_3$) δppm: 1.12 (s, 3H), 1.17 (s, 3H), 3.29 (d, 1H), 3.72 (s, 3H), 4.91 (d, 1H), 7.22-7.44 (m, 5H). ^{13}C NMR (50 MHz, CDCl$_3$) δ 19.0, 23.2, 47.7, 52.5, 78.4, 127.6, 139.9, 178.2.

3.3.3. RESULTS AND DISCUSSION

3.3.3.1. Effect of Reaction Time

In Figure 3.3.1, the conversion or yield (as selectivity is 100%) obtained on Al-MCM-41 (sample B), Ce-MCM-41 (sample C) and Ce-Al-MCM-41 (samples D-

G) in the Mukaiyama-type aldol condensation of methyl trimethylsilyl dimethylketene acetal with benzaldehyde (Scheme 3.3.1) to produce corresponding beta-hydroxy ester using dichloromethane as a solvent are plotted as a function of reaction time. Although, the reaction was continued for 24 h, there was only marginal increase after 6 hours of the reaction. The trend of the product yield obtained over different catalyst was: Ce-MCM-41 < Al-MCM-41 < Ce-Al-MCM-41. Among Ce-Al-MCM-41 samples having comparable Al content and varying Ce contents, the product yield followed the order: D < E < F $\leq$ G, where the Ce contents in the sample also follow the same order. This enhancement of catalytic activity may also be attributed to the increase in total acidity (Table 2.4, Chapter 2) due to the simultaneous incorporation of Ce and Al in MCM-41.

Similar to the case of Michael reaction (Part 3B of this chapter), here also a direct correlation was observed between the conversion obtained over different catalyst samples (B-G) and their intensity ratios: 1444/1452 cm^{-1} bands (L_2/L_1, curve a, Figure 3.3.2) and 1545/1444 cm^{-1} bands (B/L_2, curve b, Figure 3.3.2) on one hand and the total acidity, as measures by the TPD ammonia measurements, (curve c, Figure 3.3.2) on the other. As the Ce content in Ce-Al-MCM-41 samples increased, the conversion also increased progressively. Almost linear correlation between conversion and intensity ratios of B/L_2 as well as L_2/L_1 bands of Ce-Al-MCM-41 samples having comparable Al and increasing Ce contents is interesting and clearly indicates that both Lewis acid sites, generated due to Ce incorporation, play important role in catalyzing the aldol condensation. It is further supported by similar direct correlation between conversion and the total acidity of the samples (Figure 3.3.2).
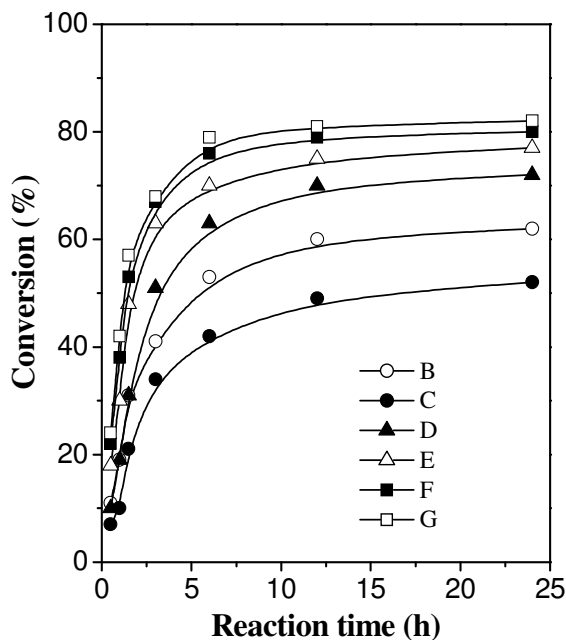
Figure 3.3.1. Plots of conversion vs reaction time for Mukaiyama-aldol condensation over different Si/Ce ratio in Ce-Al-MCM-41 samples. The sample notations as per Table 2.1, Chapter 2.

After establishing the overall 'acidity-activity' correlation of these Ce-Al-MCM-41 samples, it is worthwhile to find out the intrinsic activity (turn-over numbers) of these samples per mole of Ce, Al and Ce+Al present in the amount of the catalyst taken. In Table-3.3.1, the conversion and the corresponding TON values obtained over samples B-G using DCM as solvent at 313 K and 6 h of reaction time are reported. The TON was calculated with respect to Ce and Al individually as well as Ce+Al present in the Ce-Al-MCM-41 samples. Since, the Al contents were comparable in samples B and D-G, it is interesting to compare the TON of these samples with respect to their Al contents. The TON increased in the order: B > D > E > F > G in accordance with increasing Ce-contents in the samples, as expected. However, when the TON of the sample C to G calculated with respect to Ce-contents in these samples are compared, quite different trend (C << D > E > F > G) was

observed. The Ce contents of the samples D-G follow the opposite trend (D < E < F < G) at comparable Al content, indicating that as the concentration of Ce is increased, more and more Ce gets buried inside the walls of MCM-41 and therefore not available for the reaction. The catalyst Ce-Al-MCM-41 (Si/Ce = 59, Si/Al = 33, sample F) was chosen for the detailed activity measurements under solvent free condition as well as by using different solvents and different substrates.
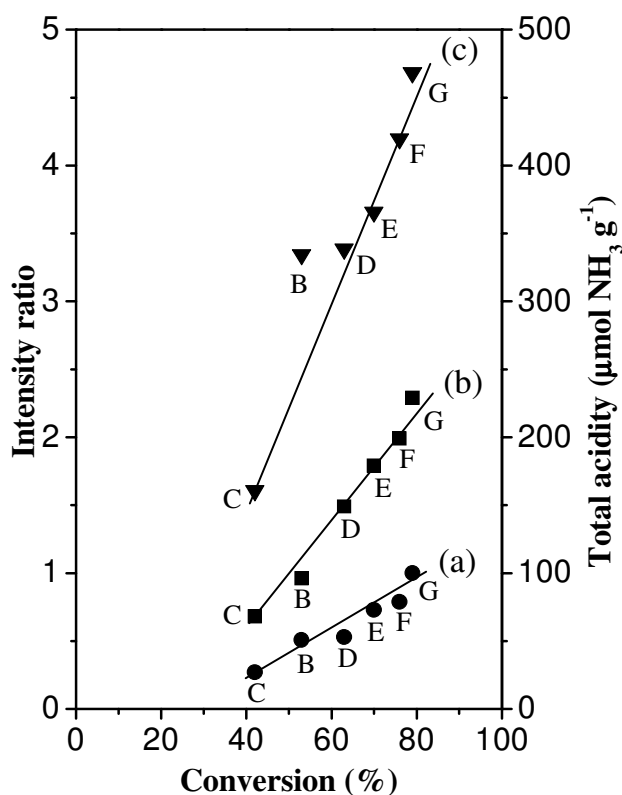
Figure 3.3.2. Plots of conversion/yield vs intensity ratio and total acidity (μmol NH$_3$ g^{-1}) of Ce-Al-MCM-41 samples. Curve (a) 1545/ 1444(B/L$_2$); (b) 1444/1452 (L$_2$/L$_1$) for adsorption at 420 K and (c) total acidity (μmol NH$_3$ g^{-1}). The sample notations as per Table 2.1, Chapter 2.

Table 3.3.1. Mukaiyama-aldol condensation of methyl trimethylsilyl dimethylketene acetal with benzaldehyde over different Ce-Al-MCM- 41 catalyst. [a]

Sample	Catalyst	Mole ratio		Conv.[b] (mole %)	TON [c]		
		Si/Ce	Si/Al		Ce	Al	Ce+Al
B	Al-MCM-41	0	30	53	-	46.9	46.9
C	Ce -MCM-41	30	0	42	39.4	-	39.4
D	Ce-Al-MCM-41	108	32	63	199.5	59.4	45.7
E	Ce-Al-MCM-41	80	32	70	165.7	66.0	47.2
F	Ce-Al-MCM-41	59	33	76	134.9	74.4	47.9
G	Ce-Al-MCM-41	38	34	79	92.2	79.0	42.5

[a] Reaction Condition : 10 mmol of methyl trimethylsilyl dimethylketene acetal and, 10 mmol of benzaldehyde, catalyst = 0.21 g , 10 ml of dry DCM , reaction time 24 h, reaction temperature 313 K.

[b] Conversion (Conv.) with respect to benzaldehyde and based on GC analysis.

[c] TON with respect to moles of benzaldehyde converted per mole of single metal (Al or Ce) or total metal content (Al + Ce).

3.3.3.2. Effect of Solvent

Mukaiyama-aldol condensation was found to depend upon the nature of the solvent employed for a reaction.[5, 14, 17, 21-25] Therefore, this reaction was carried out in the presence of different solvents using the Ce-Al-MCM-41 (Si/Ce = 59, Si/Al = 33, sample F) catalyst and the data obtained are given in Figure 3.3.3.

Among the various solvents tried out in this study, the highest conversions were obtained using dichloromethane (DCM) for this particular reaction (Table 3.3.2) at 313 K reaction temperature. Whereas, considerably low activity was observed in the presence of acetone, tetrahydrofuran (THF) and 1, 4-dioxane, the conversions

obtained with DMF (N, N-dimethylformamide) and acetonitrile (MeCN) solvents were comparable. As mention earlier, according to Hughes-Ingold hypothesis of solvent effects,[26] the transition state is capable of greater solvation than the reagents, so the reaction rate will be increased by a more solvating solvent and lowers the activation energy.
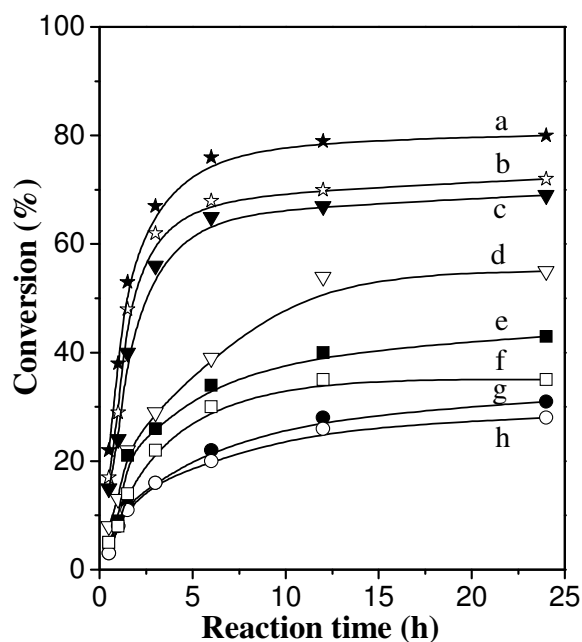
Figure 3.3.3. Plots of conversion vs reaction time for Mukaiyama-aldol condensation using different solvents over Ce-Al-MCM-41 (Si/Ce = 59, Si/Al = 33, sample F), (a) DCM, (b) MeCN, (c) DMF, (d) Toluene, (e) Diethyl ether (DEE), (f) THF, (g) 1,4-Dioxane and (h) Acetone.

Table 3.3.2. Mukaiyama-aldol condensation of methyl trimethylsilyl dimethylketene acetal and benzaldehyde with different solvents over Ce-Al-MCM-41 catalyst (Si/Ce = 59, Si/Al = 33, sample F).[a]

Entry	Solvent	Conv.[c] (mole %)	TON [d]
1	DCM	76	47.1
2	Toluene	39	24.2
3	DMF	65	40.3
4	THF	30	18.6
5	Diethyl ether	34	21.1
6	Acetonitrile	68	42.2
7	Acetone	20	12.4
8	1,4-Dioxane	22	13.6
9	No solvent	71	44.0
10 [b]	No solvent	95	59.9

[a] Reaction Condition : 10 mmol of methyl trimethylsilyl dimethylketene acetal, 10 mmol of benzaldehyde, catalyst = 0.21 g, 10 ml of solvent, reaction time 6 h, reaction temperature 313 K.

[b] Reaction temperature 373 K.

[c] Conversion (Conv.) with respect to benzaldehyde and based on GC analysis.

[d] TON with respect to moles of benzaldehyde converted per mole of (Al + Ce).

3.3.3.3. Effect of Different Catalysts and Reaction Temperatures

The Mukaiyama-aldol condensation under the solvent-free reaction condition was also studied. The results are summarized in Table 3.3.3. Under solvent free condition, low volatility of the solvent used posed no constraint in carrying out the reaction at higher temperature. The reactions were conducted at two different temperatures, viz. 313 and 373 K. These results obtained for a typical Mukaiyama-

aldol reaction involving methyl trimethylsilyl dimethyketene acetal and benzaldehyde
are plotted in Figure 3.3.4. For comparison, the data obtained for this reaction at 313
K in the presence of DCM as solvent are also included in this figure (curve b). Sample
F gave considerably higher yields (~ 95 %) in a solvent free system by raising the
temperature to 373 K, keeping all other experimental conditions same.
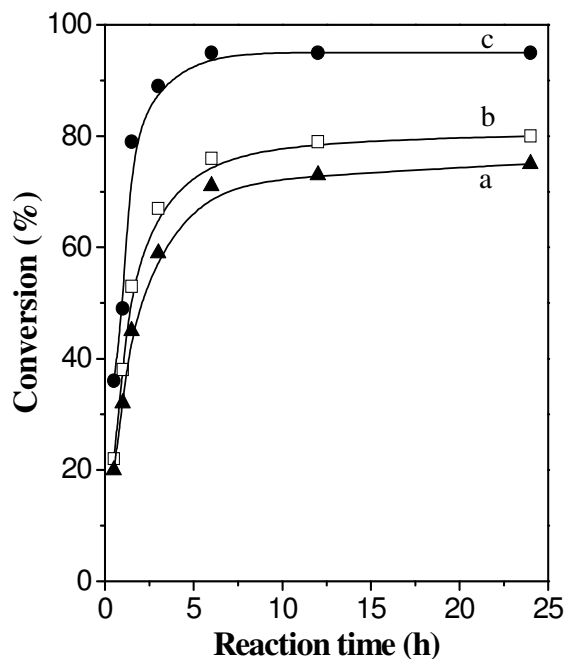
Figure 3.3.4. Plots of conversion vs reaction time for Mukaiyama-aldol condensation
(a) no solvent at 313 K, (b) DCM as solvent at 313 K and (c) no solvent at 373 K over
Ce-Al-MCM-41 catalyst (Si/Ce = 59, Si/Al = 33, sample F).

Table 3.3.3. Solvent free Mukaiyama-aldol condensation of methyl trimethylsilyl dimethylketene acetal with benzaldehyde over different catalysts.[a]

Sample	Catalyst	Temp. (K)	Conv.[b] (mole %)	TON[c] Ce	Al	Ce+Al
B	Al-MCM-41	313	49	-	43.4	43.4
		373	65	-	57.5	57.5
C	Ce-MCM-41	313	40	37.5	-	37.5
		373	59	55.4	-	55.4
F	Ce-Al-MCM-41	313	71	126.1	69.5	44.8
		373	95	168.7	93.1	59.9

[a] Reaction condition: 10 mmol of methyl trimethylsilyl dimethylketene acetal, 10 mmol of benzaldehyde, catalyst = 0.21 g, reaction time 6 h, reaction temperature 313-373 K.

[b] Conversion (Conv.) with respect to benzaldehyde and based on GC analysis.

[c] TON with respect to moles of benzaldehyde converted per mole of single metal (Al or Ce) or total metal content (Al + Ce).

3.3.3.4. Recycle Studies

In Figure 3.3.5, the conversion and TON obtained during recycle studies of the catalyst Ce-Al-MCM-41 (sample F, Ce+Al) are plotted as a function of number of recycles under solvent-free condition at 373 K for 6 h. The same catalyst sample was used for six consecutive cycles. While, the conversion decreased progressively from 95 % to *ca.* 80 % up to 6th cycle (5th recycle), the rate of decrease was more in the case of first three recycles and then almost stabilized at *ca.* 80% during 4th and 5th recycle. This decrease in the conversion during first few recycles was mainly due to partial leaching of Ce and Al, which was confirmed by the AAS analysis of Ce and Al in the filtrate obtained by separating the solid catalyst after the reaction (Table 3.3.4). The

TON, calculated on the basis of remaining Ce and Al contents in the solid catalysts,

remained unchanged during course of the recycles.
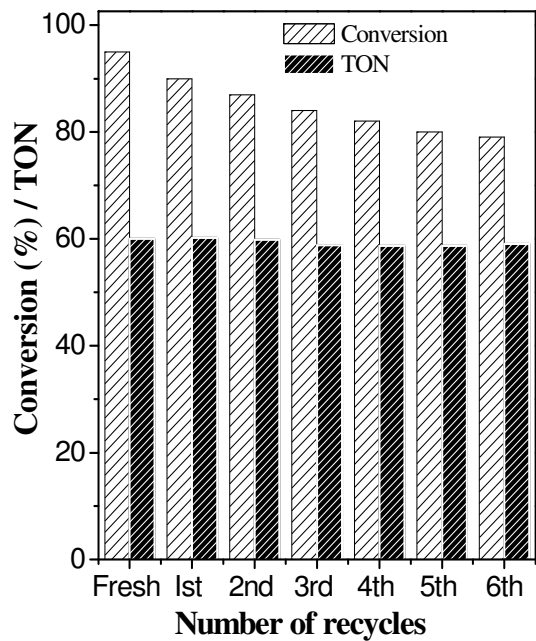
Figure 3.3.5. Effect of conversion and turn over number (TON, Ce+Al) on number

recycles of catalyst for Mukaiyama-aldol condensation.

Table 3.3.4. Recycle studies of solvent free Mukaiyama-aldol condensation of methyl

trimethylsilyl dimethylketene acetal with benzaldehyde over Ce-Al-MCM-41

(Si/Ce = 59, Si/ Al = 33, sample F) catalyst.

Recycle No	Catalyst amount (g)	Molar ratio [a]		Conv.[b] (mole %)	TON [c]		
		Si/Ce	Si/Al		Ce	Al	Ce+Al
Fresh	0.21	59.3	33.3	95	168.7	93.1	59.9
1st	0.20	62.7	36.0	90	166.8	94.1	60.1
2nd	0.19	63.4	37.4	87	163.4	94.4	59.8
3rd	0.18	64.6	38.1	84	160.2	92.8	58.7
4th	0.17	65.1	39.4	82	157.5	93.6	58.7
5th	0.16	66.8	40.4	80	157.5	93.6	58.7
6th	0.15	67.1	40.7	79	156.2	93.1	58.3

[a] Solid product calculated by AAS.

[b] Conversion (Conv.) with respect to benzaldehyde and based on GC analysis.

[c] TON with respect to moles of benzaldehyde converted per mole of single metal (Al

or Ce) or total metal content (Al + Ce).

3.3.3.5. Reaction of Different Silyl Ketene Acetal or Silyl Enol Ether with

Benzaldehyde

The Mukaiyama-aldol condensations were investigated for the different silyl

ketene acetals or silyl enol ethers with benzaldehyde (Scheme 3.3.2) at 373 K under

solvent free condition and the results obtained are presented in Table 3.3.5. The

reaction of ester derivative of silyl enol ether (Entry 1, 2 and 3) with benzaldehyde

was faster than the ketone (Entry 4 and 5) derivative of silyl enol ether due to (+)

mesomeric effect. Since, the β-carbon associated with the electron donating (+ I

effect) group, hence the nucleophilic addition is more preferable as seen with Entry 1,

2 and 3 in Table 3.3.5. Lower conversion was observed when electron withdrawing groups were attached with β-carbon at silyl enol ether as seen with Entry 4 and 5 (Table 3.3.5). The product selectivity was found to be 100 % in each silyl enol ether / silyl ketene acetal.
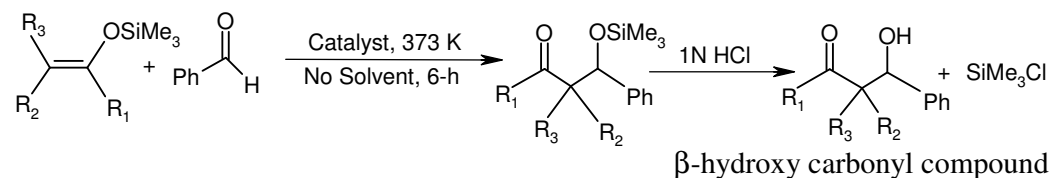
Scheme 3.3.2. Mukaiyama-aldol condensation of different silyl ketene acetal or silyl enol ether with benzaldehyde.

Where, entry 1 R_1= OMe R_2, R_3 = Me

       entry 2 R_1 = OPh R_2 = H, R_3 = Me

       entry 3 R_1 = OMe R_2, R_3 = H

       entry 4 R_1 = Ph R_2, R_3 = H

and   entry 5 R_1 = Ph R_2 = H, R_3 = Me

Table 3.3.5. Solvent free Mukaiyama-aldol condensation of different silyl ketene acetal / silyl enol ether with benzaldehyde over Ce-Al-MCM-41 (Si/Ce = 59, Si/ Al = 33, sample F) catalyst.[a]

Entry	Silyl enol ether / Silyl ketene acetal	Conv.[b] (mole %)
1.	Me, OSiMe₃ / Me, OMe	95
2.	Me, OSiMe₃ / H, OPh	87
3.	H, OSiMe₃ / H, OMe	81
4.	H, OSiMe₃ / H, Ph	75
5.	Me, OSiMe₃ / H, Ph	78

[a] Reaction Condition: 10 mmol of silyl ketene acetal / silyl enol ether, 10 mmol of benzalaldehyde, catalyst amount = 0.21 g, reaction time 6 h, reaction temperature 373 K. [b] Conversion with respect to benzaldehyde and based on GC analysis.

3.3.3.6. Reaction of Methyl Trimethylsilyl Dimethylketene Acetal with Different Adehydes
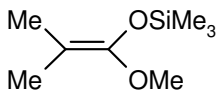
The conversions obtained in condensation of different aldehydes with methyl trimethylsilyl dimethylketene acetal (Scheme 3.3.3) at 373 K under solvent free condition are shown in Table 3.3.6.

β-hydroxy carbonyl compound
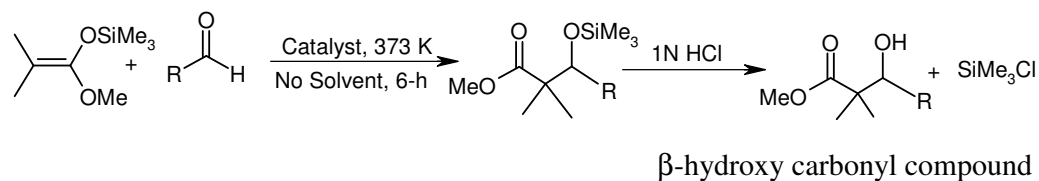
Scheme 3.3.3. Mukaiyama-aldol condensation of methyl trimethylsilyl dimethylketene acetal with different aldehyde.

The reactivity of aldehydes can be explained on the basis of their +I effect. As the electron density on carbonyl carbon increases, the reactivity of aldehyde decreases. Since, the order of +I is increasing from top to bottom (Entry 1 to 8, Table 3.3.6), the conversion also follows the reverse order, as expected.

Table 3.3.6. Solvent free Mukaiyama-aldol condensation of methyl trimethylsilyl dimethylketene acetal with different aldehydes over Ce-Al-MCM-41 (Si/Ce = 59, Si/Al = 33, sample F) catalyst.[a]

Entry	Aldehydes	Methyl trimethylsilyl dimethylketene acetal	Conv.[b] (mole %)
1.	4-Nitrobenzaldehyde		98
2.	4-Cyanobenzaldehyde		96
3.	Benzaldehyde		95
4.	4-Methoxybenzaldehyde		85
5.	Furfuraldehyde		83
6.	Propionaldehyde		80
7.	Isobutyraldehyde		76
8.	Octyldehyde		72

[a] Reaction condition: 10 mmol of methyl trimethylsilyl dimethylketene acetal, 10 mmol of aldehydes, catalyst amount = 0.21 g, reaction time 6 h, reaction temperature 373 K. [b] Conversion with respect to aldehyde and based on GC analysis.

3.3.4. CONCLUSIONS

The cerium containing Al-MCM-41 samples can be used as efficient solid catalyst for carbon-carbon bond formation reaction such as Mukaiyama-aldol condensation as compared to the Ce-MCM-41 and Al-MCM-41 catalysts having comparable Ce or Al contents. Quite high conversions could be obtained even under

solvent free condition by raising the reaction temperature. The silyl ketene acetal showed better activity than silyl enol ether. Further, higher conversions were observed when aromatic aldehydes containing an electron-withdrawing (-I effect) group in para-position of the benzene ring. Aliphatic aldehydes are less active than aromatic aldehydes due to electron-releasing effect of the alkyl groups attached to –C=O groups. The high conversion can be explained by total acid strength of Ce-containing Al-MCM-41 samples.

3.3.5. REFERENCES

1.   Z. G. Hajos, R. L. Augustine, *In Carbon-Carbon Bond Formation*, Vol. 1, Marcel Dekker, New York, Chap. **1979**, 1, 1.

2.   A. T. Nielsen and W. J. Houlihan, *Organic Reactions*, **1968,** 16, 1.

3.   H. Yamamoto and K. Oshima, *Main Group Metals in Organic Synthesis*, **2002,** 2, 409.

4.   T. Mukaiyama, K. Narasaka, K. Banno, *Chem. Lett*. **1973**, 1011.

5.   T. Mukaiyama, K. Banno, K. Narasaka, *J. Am. Chem. Soc*. **1974,** 96, 7503.

6.   S. Kobayashi, *Eur. J. Org. Chem.* **1999**, 1, 15.

7.   L. Teck-Peng, L. Xu-Ran, *Tetrahedron* **1999,** 55, 10789.

8.   C. R. Brindaban, S. Manika, B. Sanjay, *Tetrahedron Lett.* **1993**, 34, 1989.

9.   M. T. Reetz, D. Giebel, *Angew. Chem. Int. Ed.* **2000**, 39, 2498.

10.   H. Mitshuhashi, M. Tanaka, H. Nakamura, K. Arata, *Appl. Catal. A: Gen.* **2001,** 208, 1.

11.   D. L. Gin, W. J. Zhou, W. Gu, *Chem. Mater*. **2001**,13, 1949.

12.   H. Hattori, *Chem. Rev*. **1995**, 95, 537.

13.   M. Sasidharan, R. Kumar, *Catal. Lett.* **1996,** 38, 251.

14.   M. Sasidharan, S. V. N. Raju, K. V. Srinivasan, V. Paul, R. Kumar, *Chem. Comm.* **1996**, 129.

15.   M. Sasidharan , R. Kumar, *J.Catal.* **2003**, 220, 326.

16.   T. Gaydhankar, P. N. Joshi, P. Kalita, R. Kumar, *J. Mol. Catal. A: Chem.* **2006,** 265, 306.

17.   R. Garro, M. T. Navarro, J. Primo, A. Corma, *J. Catal.* **2005**, 233, 342.

18.   S. C. Laha, P. Mukharjee, S. R. Sainkar, R. Kumar, *J. Catal.* **2002,** 207, 213.

19.   M. D. Kadgaonkar, S. C. Laha, R. K. Pandey, P. Kumar, S. P. Mirajkar, R. Kumar, *Catal. Today* **2004**, 97, 225.

20.   P. Kalita, N. M. Gupta, R. Kumar, *J. Catal*. **2007**, 245, 338.

21.   M. Kawai, M. Onaka, Y. Izumi, *Bull. Chem. Soc. Jpn*. **1988**, 61,1237.

22.   T. Nakagawa, H. Fujisawa, Y. Nagata, T. Mukaiyama, *Bull. Chem. Soc. Jpn*. **2004**, 77, 1555

23.   H. Hagiwara, H. Inoguchi, M. Fukushima, T. Hoshi, T. Suzuki, *Tetrahedron Lett*. **2006,** 47, 5371.

24.   Y. Mori, K. Manabe, S. Kobayashi, *Angew. Chem. Int. Ed*. **2001**, 40, 2816.

25.   S. Kobayashi, S. Nagayama, *J. Am. Chem. Soc*. **1998**, 120, 2985.

26.   N. S. Isaacs, *Physical Organic Chemistry*, ELBS, Longman group UK Ltd **1987**.

CHAPTER 4

CHAPTER 4: Part A

4.1. MICHAEL-ADDITION OF INDOLES TO α, β-UNSATURATED CARBONYL COMPOUNDS OVER TRIFLIC ACID LOADED Zr-TMS CATALYSTS

4.1.1. INTRODUCTION

Indole derivatives have attracted considerable attention from both the synthetic and medicinal chemists. For example, the indole alkaloids such as harmicine and tryptophan have been investigated for their therapeutic use covering a wide range of medicinal applications.[1] The electrophilic substitution of 3-substitued indoles to α,β -unsaturated ketones is used to prepare important building blocks for the synthesis of biologically active compounds and natural products.[2] Also, nitrogen-containing compounds are of significant importance in biologically active substances, dyes, and fine chemicals.[3] Further, the β-amino carbonyl group is a common moiety in a large variety of biologically active compounds such as alkaloids and polyketides.[4] They serve as attractive precursors in the preparation of γ-amino alcohol, β-lactums, β-amino acid derivatives and chiral auxiliaries,[5] many of which serve as antibiotics or other drugs.[6] Moreover, indoles can undergo two types of reactions: at NH (Michael reaction) and at C3 (Michael as well as Friedel-Crafts reactions).

The Michael-addition of α, β -unsaturated carbonyl compound to indoles has been attempted in the presence of various Lewis acids such as $FeCl_3$, $LiCl$, $HgCl_2$,[7] lanthanide salts (Ln= La, Sm, Yb),[8] $InCl_3$ and $InBr_3$,[9] Pd,[10] $CeCl_3$,[11] $Bi(NO_3)_3$,[12] $Bi(OTf)_3$,[13] $Sc(DS)_3$,[14] copper salts,[15] and acidic clays[16] etc. Again, acid catalyzed reaction of indoles requires careful control of the acidity to prevent unwanted side reactions, such as dimerization and polymerization.[17]

Although, Michael-addition of indole to enone has been reported under solvent free condition, the yield of C-adduct product was lower.[18,12a,b] Solvent-free reactions have many advantages such as reduced pollution, lower costs and simplicity.

The present section deals with carbon-carbon bond formation reaction such as Michael-addition of indole to α,β -unsaturated carbonyl compound using

trifluoromethanesulfonic acid (triflic acid, TFA) functionalized on Zr-TMS (Zr-TMS-zirconia based transition metal oxide mesoporous molecular sieves) catalyst. The reactions were carried out under solvent free condition. For a model catalytic reaction, 3-methylindole and cyclohexenone were chosen as starting materials as shown in Scheme 4.1.1. The effects of various reaction conditions, such as different loadings of triflic acid over Zr-TMS, different amount of catalyst, effect of temperature, recyclibilty of the catalyst, effect of different indole and α, β -unsaturated ketone, have been studied.
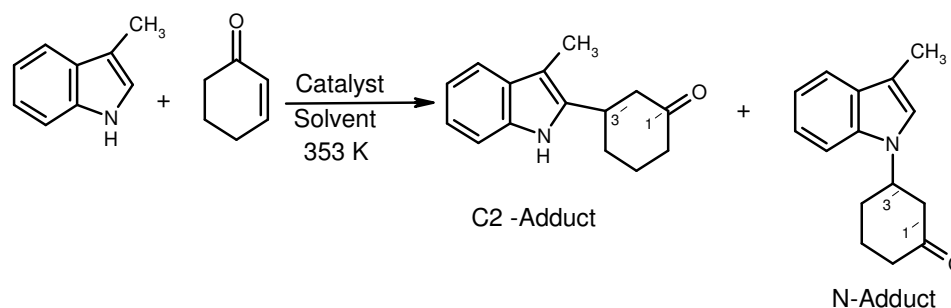
Scheme 4.1.1. Michael-addition of 3-methylindole and cyclohexenone.

4.1.2. GENERAL PROCEDURE FOR MICHAEL-ADDITION OF INDOLES TO α, β-UNSATURATED CARBONYL COMPOUNDS

The catalytic liquid-phase reaction was performed in a two-necked round bottom flask equipped with a water condenser and accompanied by vigorous stirring (magnetic) under N_2 atmosphere. The catalyst was pre-activated at 393 K in vacuum oven and was used for the reactions under extremely dry condition. In a typical procedure, a mixture of indole (10 mmol) and α,β -unsaturated carbonyl compound (10 mmol) was added to a preactivated catalyst (0.1 g). The reaction mixture (Scheme 4.1.1) was stirred magnetically at 353 K for 2 h. The progress of the reaction was monitored by gas chromatography (Varian model-CP-3800) equipped with capillary column and flame ionization detector (FID) as well as by thin layer

chromatography (TLC). After completion of the reaction, the catalyst was separated by filtration. The filtrate was diluted by dichloromethane (DCM), washed with 1N HCl twice and finally washed with water three times. The organic layer was separated and dried with anhydrous Na_2SO_4. The solvent was removed by rotary evaporator to produce crude product and then the corresponding product was purified through column chromatography using silica gel (100-200 mesh), petroleum ether: ethyl acetate = 3:1) The formation of the product was confirmed by employing GC, GC-MS, ^{1}H NMR, and ^{13}C NMR techniques.

The ^{1}H NMR spectrum of C2-adduct is shown below

Product: 3-(3-methyl-1H-indol-2-yl) cyclohexanone
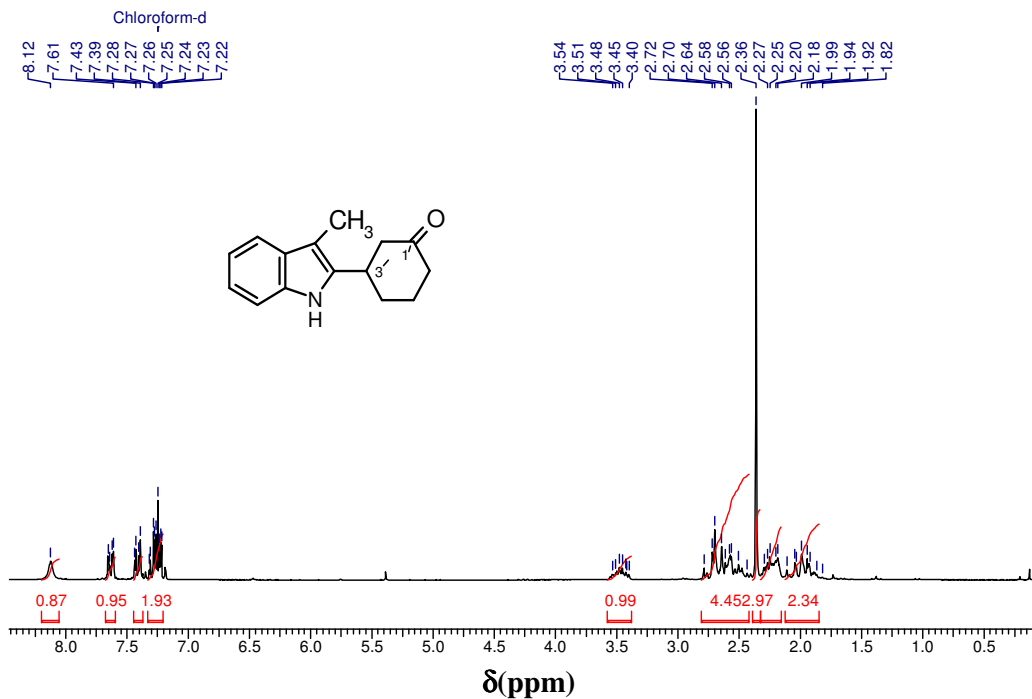
The ^{1}H NMR spectrum of N-adduct is shown below

Product: 3-(3-methyl-1H-indol-1-yl) cyclohexanone
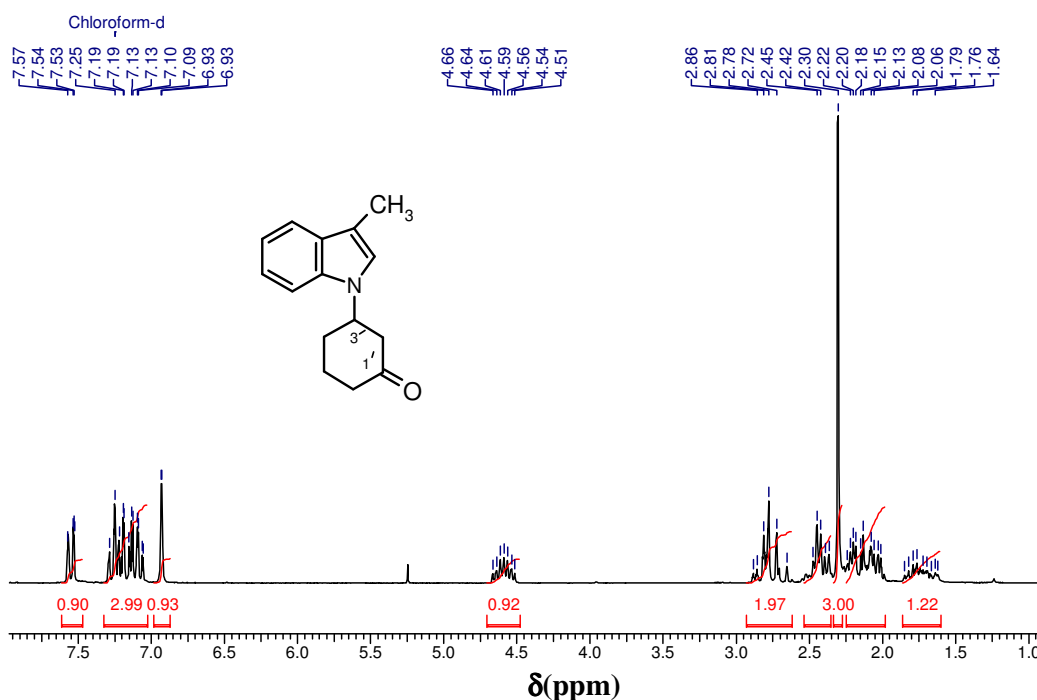
4.1.3. RESULTS AND DISCUSSION

4.1.3.1. Effect of Loading of Triflic Acid over Zr-TMS Materials

The catalytic activity of the samples for different loading of triflic acid (TFA) on Zr-TMS was examined for the reaction between 3-methylindole and cyclohexenone (Scheme 4.1.1). These results are plotted as a function of reaction time in Figure 4.1.1. The conversion of 3-methylindole was found to increase from 38 to 87 % with increasing loading of triflic acid on Zr-TMS from 5 to 25 wt% (Table 4.1.1). The selectivity of C2-adduct was also found to increase with increasing loading of triflic acid, with a consequent decrease in the selectivity of N-adduct (Table 4.1.1). This trend finds correlation with the increase in the number of acid site on functionalization of the Zr-TMS by triflic acid. The Michael products of N-adduct

and C2-adduct were successfully isolated and characterized by ^{1}H NMR spectroscopy.

• N-adduct δ ~ 4.72-4.57 (m) and C2-adduct δ ~ 3.47-3.34 (m).

These differences are comparable with the changes in the methyl chemical shift noted in N-methyl and C2-methyl indoles. Analogous differences were also observed in the ^{13}C NMR spetra :

• N-adduct C3$^{/}$ ~ 54.8 ppm; C2-adduct C3$^{/}$ ~ 36.9 ppm

• N-adduct C1$^{/}$ ~ 209.6 ppm; C2-adduct C1$^{/}$ ~ 211.7 ppm.

The catalytic activities of amorphous Zr-TMS-TFA-A (sample Q) and pure triflic acid (sample R) are also shown in the Table 4.1.1 for reaction between 3-methylindole and cyclohexenone. It was observed that the pure triflic acid (homogeneous condition) gives rise to slightly higher conversion compared to that obtained over amorphous Zr-TMS-TFA-25-A (~ 81 %, sample Q) catalyst. However, the selectivity of C2-adduct was considerably lower with a consequent increase in N-adduct selectivity over sample R *vis-à-vis* sample Q. Under the similar reaction conditions, the conversion of 3-methylindole over Zr-TMS-TFA-25 (sample P) catalyst is found to be higher (87 %) when compared to that obtained over sample Q (81 %). However, the selectivity of C-adduct over Zr-TMS-TFA-25 (sample P, 95 %) is quite high as compared to Zr-TMS-TFA-A (sample Q, 77 %).

The Michael-addition of 3-methylindole to cyclohexenone has also been carried out by Ce-Al-MCM-41(Si/Ce = 38, Si/Al = 34) catalyst under identical reaction condition for comparison purpose (curve G, Figure 4.1.1). However, the conversion of 3-methylindole was found to be significantly lower than that of Zr-TMS-TFA-25 catalyst (Table 4.1.1). The low conversion of 3-methylindole over Ce-Al-MCM-41 sample can be explained by total acidity of Ce-Al-MCM-41 and Zr-

TMS-TFA catalyst. The total acidity of Ce-Al-MCM-41 (sample G, Table 2.1) catalyst was found to be rather low than Zr-TMS-TFA-25 (sample P, Table 2.5) catalyst. Hence, this result reveals that Michael-addition of 3-methylindole to cyclohexenone needs high acidity in the catalyst. All further reactions were examined over the Zr-TMS-TFA-25 (sample P, Table 2.5) catalyst.
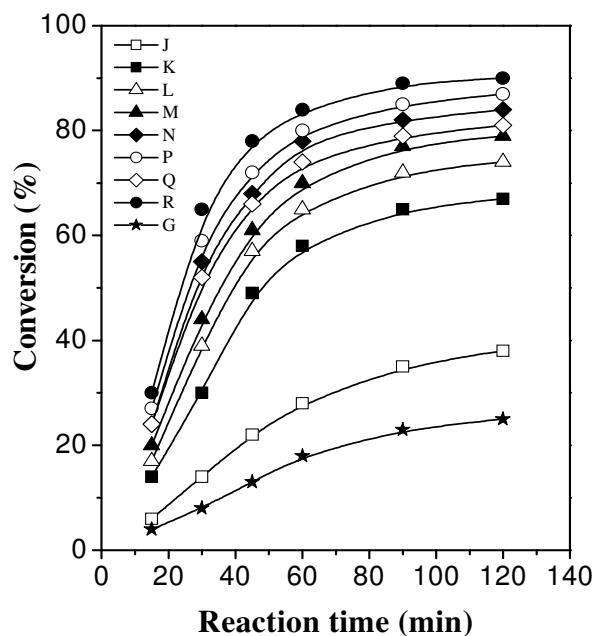
Figure 4.1.1. Plot of conversion vs reaction time for Michael-addition of 3-methylindole and cyclohexenone using different loading of triflic acid over Zr-TMS catalyst.The sample notations as per Table 2.1 and 2.5, Chapter 2.

Table 4.1.1. Michael-addition of 3-methylindole with cyclohexenone over different

Zr-TMS and MCM-41 catalysts (Table 2.1 and 2.5, Chapter 2).[a]

Sample	Catalysts	Conv.[d] (mole %)	TON [e]	Selectivity (%)	
				C-adduct	N-adduct
J	Zr-TMS	38	-	74	24
K	Zr-TMS-TFA-5	67	238.2	78	22
L	Zr-TMS-TFA-10	74	131.5	86	14
M	Zr-TMS-TFA-15	79	93.6	89	11
N	Zr-TMS-TFA-20	83	73.7	93	7
P	Zr-TMS-TFA-25	87	56.8	95	5
Q	Zr-TMS-TFA-25-A [b]	81	50.5	77	23
R	CF$_3$SO$_3$H [c]	90	-	70	30
G	Ce-Al-MCM-41 (34, 38)	25	28.2	95	5

[a] Reaction condition: 3-methylindole (10 mmol), cyclohexenone (10 mmol), catalyst

amount = 0.1g, reaction time 120 min (2 h), reaction temperature 353 K.

[b] Amorphous material, [c] Triflic acid taken 0.05g

[d] Conversion (Conv.) with respect to 3-methylindole and based on GC analysis.

[e] TON is given as moles of 3-methylindole transformed per mole of sulfur.

4.1.3.2. Effect of Catalyst Amount

The effect of catalyst amount on conversion of 3-methylindole was studied for

2 h at 353 K as Zr-TMS-TFA-25 (sample P) catalyst. From Figure 4.1.2, it is seen that

the conversion increases with increasing catalyst amount (curves a-d). The reaction

showed only marginal increase in the conversion as escalating catalyst amount from

0.08 to 0.1 gram (curves c and d). There is no significant difference for the selectivity

of C-adduct and N-adduct with increasing amount of catalyst from 0.04 to 0.1 gram

(Table 4.1.2).
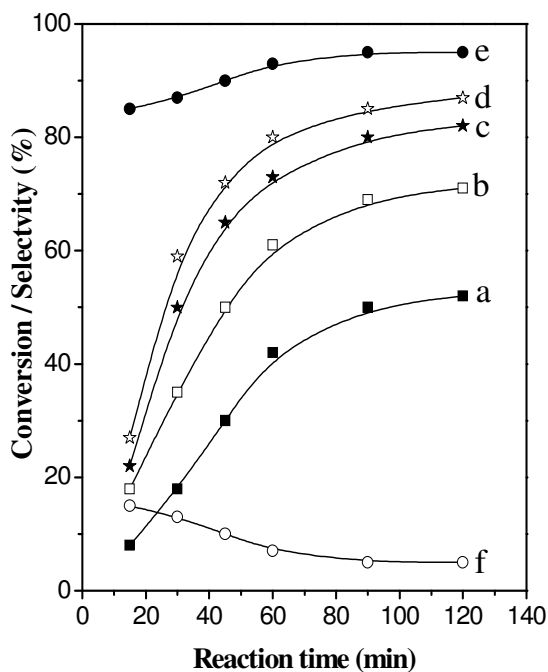
Figure 4.1.2. Plot of conversion vs reaction time for Michael-addition of 3-methylindole and cyclohexenone using Zr-TMS-TFA-25 catalyst (sample P) for different amount of catalyst. Curves (a) 0.04 g, (b) 0.06 g, (c) 0.08 g, (d) 0.1g, (e) C-adduct (0.1g catalyst, 353 K) and (f) N-adduct (0.1g catalyst, 353 K).

Table 4.1.2. Michael-addition of 3-methylindole with cyclohexenone for different amount of catalyst Zr-TMS-TFA-25 (sample P, Table 2.5, Chapter 2).[a]

Catalyst Amount	Conv. [b]	Selectivity (%)	
(gram)	(mole %)	C-adduct	N-adduct
0.04	52	92	8
0.06	71	93	7
0.08	82	95	5
0.1	87	95	5

[a] Reaction condition: 3-methylindole (10 mmol), cyclohexenone (10 mmol), reaction time 120 min (2 h), reaction temperature 353 K.
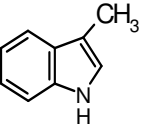
[b] Conversion (Conv.) with respect to 3-methylindole and based GC analysis.

4.1.3.3. Effect of Temperature

The triflic acid (TFA) functionalized Zr-TMS-TFA-25 (sample P) catalyst was used to study the effect of temperature in Michael-addition of 3-methylindole to cyclohexenone under solvent free condition for 2 h. From Figure 4.1.3, it is seen that the temperature has remarkable effect for conversion of 3-methylindole. The conversion of 3-methylindole was increased with increasing temperature from 298 to 353 K (curves a-c), as expected. The conversion increases with increasing temperature upto 353 K and then remained almost unchanged (Table 4.1.3). The selectivity of C-adduct however remained quite high (88-95 %, Table 4.1.3)
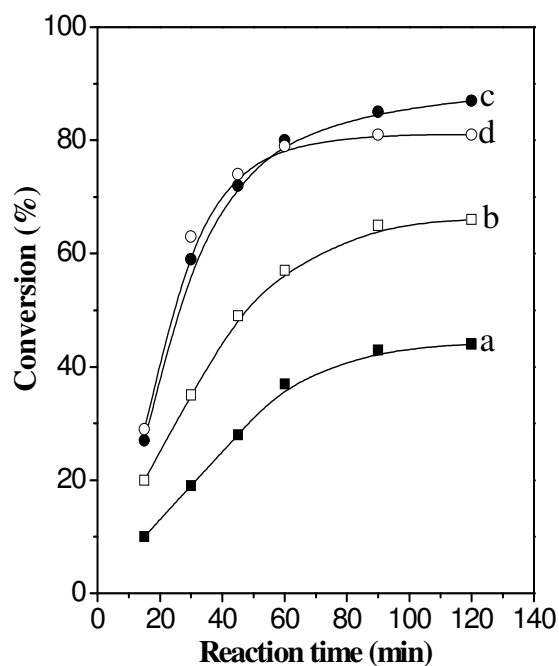
Figure 4.1.3. Plot of conversion vs reaction time for Michael-addition of 3-methylindole and cyclohexenone using Zr-TMS-TFA-25 (sample P) catalyst at different temperature. Curves (a) 298 K, (b) 333 K, (c) 353 K and (d) 373 K.

Table 4.1.3. Michael-addition of 3-methylindole with cyclohexenone at different temperature over Zr-TMS-TFA-25 (sample P, Table 2.5, Chapter 2) catalyst.[a]

Temperature	Conv. [b]	Selectivity (%)	
(K)	(mole %)	C-adduct	N-adduct
298	44	88	12
333	66	93	7
353	87	95	5
373	81	90	10

[a] Reaction condition: 3-methylindole (10 mmol), cyclohexenone (10 mmol), catalyst amount = 0.1 g, reaction time 120 min (2 h), different reaction temperature.

[b] Conversion (Conv.) with respect to 3-methylindole and based GC on analysis.

4.1.3.4. Recycle Studies

The conversion and turn over number (TON) obtained for various cycles of test runs using the Zr-TMS-TFA-25 catalyst (sample P) for Michael-addition of 3-methylindole with cyclohexenone under solvent-free condition at 353 K for 2 h, are plotted in Figure 4.1.4. After the reaction, the catalyst was filtered from hot reaction mixture and the same catalyst was reused for four times without any activation. The conversion decreased slowly from 87 to 77 % (4th recycle) as shown in Table 4.1.4. The selectivity of C-adduct and N-adduct remained almost same. Marginal decrease in the conversion during recycle studies was mainly due to partial leaching of triflic acid. This was confirmed by chemical analysis for C and S (Table 4.1.4) of the fresh and used catalyst after each cycle. However, the turn over number (TON), calculated on the basis of sulfur content in the solid catalyst, and was found to be nearly the same from the first to fourth recycle.
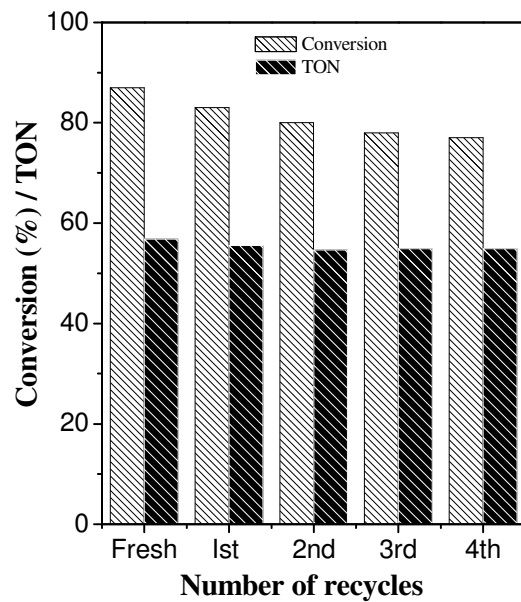
Figure 4.1.4. Conversion / turn over number (TON) when Michael-addition of 3-methylindole and cyclohexenone was carried out on a catalyst sample for four consecutive cycles.

Table 4.1.4. Recycle studies of Zr-TMS-TFA-25 catalyst for the Michael-addition of 3-methylindole with cyclohexenone under solvent free system.

Recycle No	Elemental analysis (wt%)		Conv.[a] (mole %)	Selectivity (%)		TON [b]
	C	S		C-adduct	N-adduct	
Fresh	1.91	4.90	87	95	5	56.8
I[st]	1.83	4.76	83	95	5	55.5
2nd	1.76	4.67	80	94	6	54.6
3rd	1.70	4.55	78	93	7	54.8
4th	1.65	4.52	77	93	7	54.8
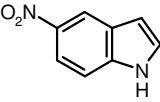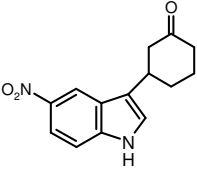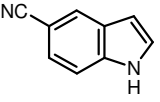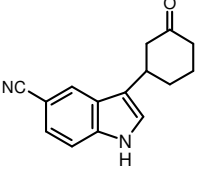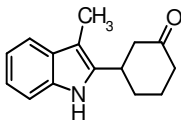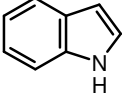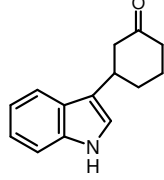
[a] Conversion with respect to 3-methylindole and based on GC analysis.

[b] TON is given as moles of 3-methylindole transformed per mole of sulfur.

4.1.3.5. Michael-Addition of Different Indoles with Cyclohexenone

The results obtained for the Michael-addition of different substituted indoles with cyclohexenone in the absence of any organic solvent are presented in Table 4.1.5. Among the various substrates investigated, 5-nitroindole (Entry 1) shows better activity than other indoles. This may be due to presence of strong electron-withdrawing (-NO$_2$ group) group in the 5-position of indole.

Table 4.1.5. Michael-addition of substituted indoles with cyclohexenone over Zr-TMS-TFA-25 catalyst (sample P).[a]

Entry	Indole	C-adduct Product	Conv.[b] (mole %)	Selectivity (%) C-adduct	Selectivity (%) N-adduct
1.			98	100	0
2.			94	97	3
3.			87	95	5
4.			79	90	10
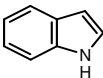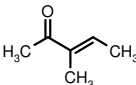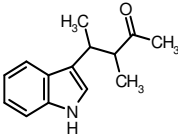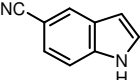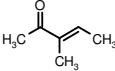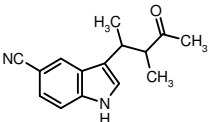
[a] Reaction Condition: 10 mmol of indole, 10 mmol of cyclohexenone, catalyst amount = 0.1 g, no solvent, reaction temperature 353 K, reaction time 120 min (2 h).
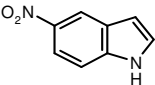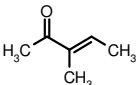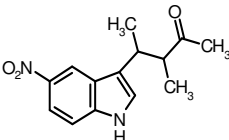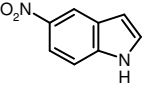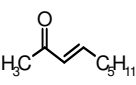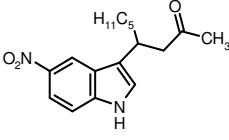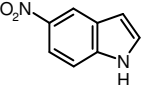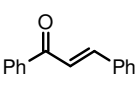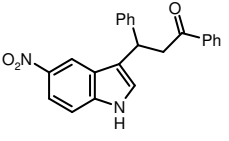
[b] Conversion (Conv.) with respect to indole and based on GC analysis.

4.1.3.6. Michael-Addition of Different Indoles with Different α, β -Carbonyl Compounds

The Michael-addition of different indoles with different α, β -unsaturated carbonyl compounds have been carried out under the identical reaction condition, and the results are summarized in Table 4.1.6. The compounds having electron-withdrawing group in 5-position of indole, generate more Michael product than other indole as obtained in Table 4.1.5 (Entry 1, 2) and Table 4.1.6. (Entry 2 and 3). The high conversion of Michael product of C-adduct was obtained for the reaction between 3-methyl pent-3-ene-2-one and 5-nitroindole (Entry 3, Table 4.1.6) rather than with 3-nonen-2-one (Entry 4, Table 4.1.6). This is because of the only methyl group which is present at β-carbon in the enone of 3-methyl pent-3-ene-2-one (Entry 3, Table 4.1.6). However, in case of 3-nonen-2-one (Entry 4, Table 4.1.6), with longer carbon chain leads to less electrophilicity. Less conversion was obtained for the reaction between 5-nitroindole and chalcone (Entry 5, Table 4.1.6) because of the presence of two bulkier groups attached to α,β-unsaturated ketone.

Table 4.1.6. Michael-addition of different indoles with different   α, β-unsaturated carbonyl compounds over Zr-TMS-TFA-25 catalyst (sample P).[a]

Entry	Indoles	α, β-Unsaturated carbonyl compounds	C-adduct Product	Conv.[b] (mole %)	Selectivity (%)	
					C-adduct	N-adduct
1.				85	92	8
2.				92	95	5

.				98	100	0
4.				91	100	0
5.				64	100	0

[a] Reaction Condition: 10 mmol of indole, 10 mmol of α, β-unsaturated ketone, catalyst = 0.1 g, no solvent, reaction temperature 353 K, reaction time 120 min (2 h).

[b] Conversion (Conv.) with respect to indole and based on GC analysis..

4.1.4. CONCLUSIONS

In conclusion, a methodology has been developed for the Michael-addition of indole to α,β-unsaturated ketone by using triflic acid functionalized Zr-TMS as a catalyst. The conversion and selectivity of C-adduct increases with the increase in the triflic acid loading from 5 to 25 wt %. Further, high Michael adduct (C-adduct, 100 %) was observed in the reaction between 5-nitroindole and 3-methyl pent-3-ene-3-one. Based on these observations, the observed catalytic activity trend can be explained on the basis of the total acid strength of triflic acid functionalized Zr-TMS catalysts. The total acidity of the catalyst is found to increase with increasing loading of triflic acid, as confirmed by TPD-ammonia measurements (Table 2.5, Chapter 2).

4.1.5. REFERENCES

1. (a) R. J. Sundberg, *The Chemistry of Indoles; Academic*: New York, **1996**, p. 113. (b) R. Livingstone, In Ansell, M. F., Ed. *Rodd's Chemistry of Carbon Compounds;* Elsevier: Oxford, **1984**, Vol. 4.

2. (a) V. Snieckus, *The Alkaloids,* Vol. 11, Academic, New York, **1968**. (b) G. W. Gribble, *Comprehensive Heterocyclic Chemistry,* Vol. 2, 2nd ed., Pergamon, New York, **1996**, p. 203. (c) R. Gibe, M. A. Kerr, *J. Org. Chem.* **2002**, 67, 6247.

3. (a) M. S. Gibson, in: S. Patai (Ed), *The Chemistry of Amino Group, Interscience*, New York, **1968**, p. 61. (b) J. March, *Advanced Organic Chemistry,* 4th ed., Wiley, New York, **1992**, p. 768.

4. (a) R. Baltzly, E. Lorz, P. B. Russell, F. M. Smith, *J. Am. Chem. Soc*. **1955**, 77, 624. (b) C. B. Pollard, G. C. Mattson, *J. Am. Chem. Soc*. **1956**, 78, 4089. (c) P. Traxler, U. Trinks, E. Buchdunger, H. Mett, T. Meyer, M. Muller, U. Regenass, J. Rosel, N. Lydon, *J. Med. Chem*. **1995**, 38, 2441. (d) J. Staunton, B.Wilkinson, *Top. Curr. Chem*. **1998,** 195, 49.

5. (a) M. Tramontini, *Synthesis* **1973**, 703. (b) Y. F. Wang, T. Izawa, S.Kobayashi, M. Ohno, *J. Am. Chem. Soc*. **1982,** 104, 6465. (c) G. I. Georg (Ed), *The Organic Chemistry of β-Lactams,* VCH Publishers, New York, **1993**. (d) Y. Hayashi, J. J. Rode, E. J. Corey, *J. Am. Chem. Soc*. **1996,** 118, 5502. (e) S. Kobayashi, H. Ishitani, *Chem. Rev*. **1999**, 99, 1069.

6. (a) G. Cardillo, C. Tomasini, *Chem. Soc. Rev*. **1996,** 117. (b) A. Graul, J. Castaner, *Drugs Future* **1997**, 22, 956. (c) E. Juaristi, H. Lopez-Ruiz, *Med. Chem*. **1999,** 6, 983.

7. (a) J. Cabral, P. Laszlo, L. Mahe, M. T. Montaufier, S. L. Randriamahefa, *Tetrahedron Lett*. **1989,** 30, 3969. (b) M. Perez, R. Pleixats, *Tetrahedron* **1995**, 51, 8355.

8. (a) S. Matsubara, M. Yoshioka, K. Utimoto, *Chem. Lett.* **1994**, 827. (b) G. Jenner, *Tetrahedron Lett*. **1995**, 6, 33. (c) Z.-P. Zhan, R.-F. Yang, K. Lang, *Tetrahedron Lett*. **2005**, 46, 3859.

9. (a) J. S. Yadav, S. Abraham, B. V. S. Reddy, G. Sabitha, *Synthesis* **2001**, 265. (b) T. P. Loh, L.-L. Wei, *Synlett*, **1998**, 75. (c) M. Bandini, P. G. Cozzi, M. G. Giacomini, P. Melchiorre, S. Selva, A. Umani-Ronchi, *J. Org. Chem.* **2002**, 7, 3700.

10.   M. Kawatsura, J. F. Harwig, *Organometallics* **2001,** 20, 1960.

11.   G. Bartoli, M. Bosco, E. Marcantoni, M. Pertini, L. Sambri, E. Torregiani, *J. Org. Chem.* **2001**, 66, 9052.

12.   (a) N. Srivastava, B. K. Banik, *J. Org. Chem.* **2003**, 68, 2109. (b) B. K. Banik, M. Fernandez, C. Alvarez, *Tetrahedron Lett.* **2005**, 46, 2479. (c) S. Leitch, Jennifer Addison-Jones, A. McCluskey, *Tetrahedron Lett.* **2005**, 46, 2915

13.   (a) R. Varala, M. M. Alam, S. R. Adapa, *Synlett* **2003**, 720. (b) M. M. Alam, R. Varala, S. R. Adapa, *Tetrahedron Lett.* **2003,** 44, 5115.

14.   K. Manabe, N. Aoyama, S. Kobayashi, *Adv. Synth. Catal.* **2001**, 343, 174.

15.   L. W. Xu, J. W. Li, C. G. Xia, S. L. Zhou, X. X. Hu, *Synlett* **2003**, 2425.

16.   N. S. Shaikh, V. H. Deshpande, A. V. Bedekar, *Tetrahedron* **2001**, 57, 9045.

17.   (a) M. Chakrabarty, R. Basak, N. Ghosh, *Tetrahedron Lett.* **2001**, 41, 8331. (b) I. Komoto, S. Kobayashi, *Org. Lett.* **2002**, 4, 1115.

18.   H. Firouzabadi, N. Iranpoor, M. Jafarpour, A. Ghaderi, *J. Mol. Catal A: Chem.* **2006**, 252, 150.
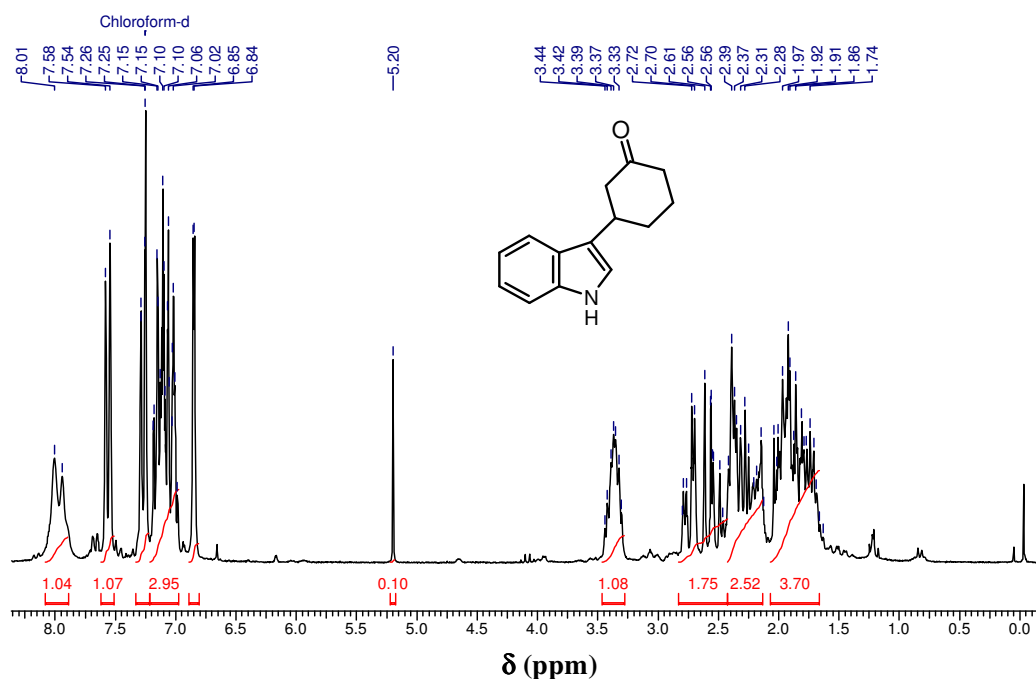
4.1.6. ^{1}H NMR SPECTRA

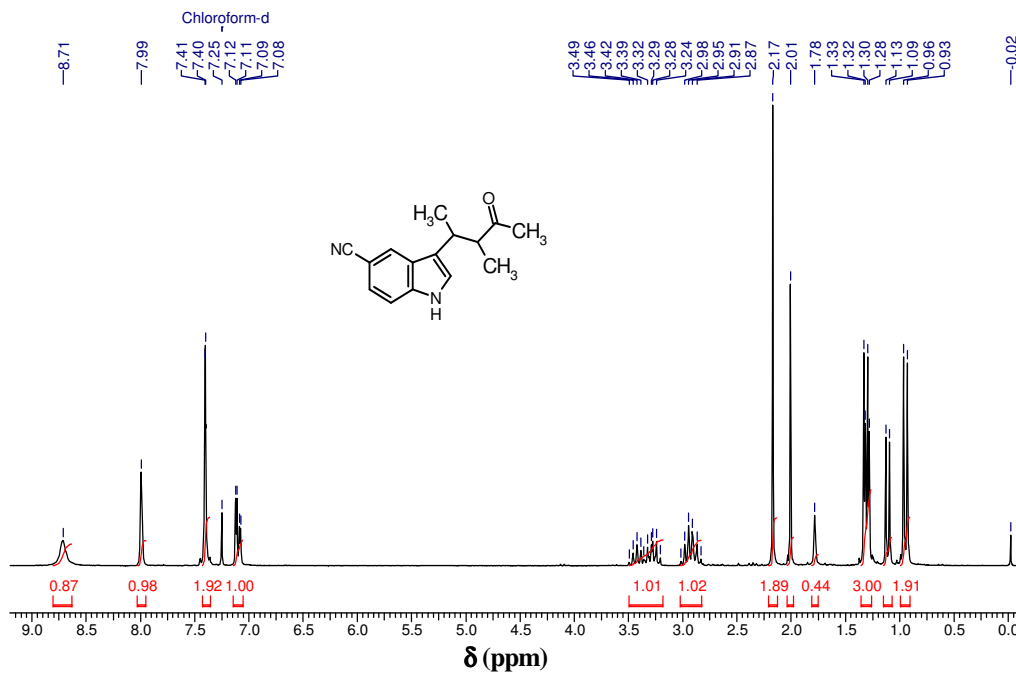The representative ^{1}H NMR spectra are given below

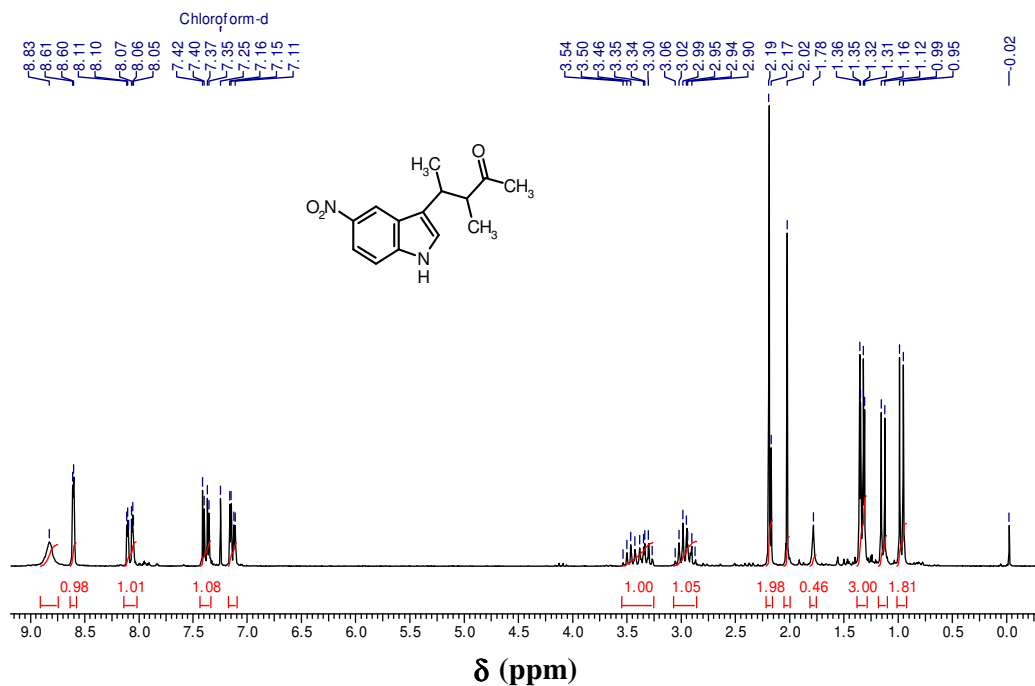**Product (Table 4.1.5, Entry 1): 3-(5-nitro-1H-indol-3-yl) cyclohexanone**
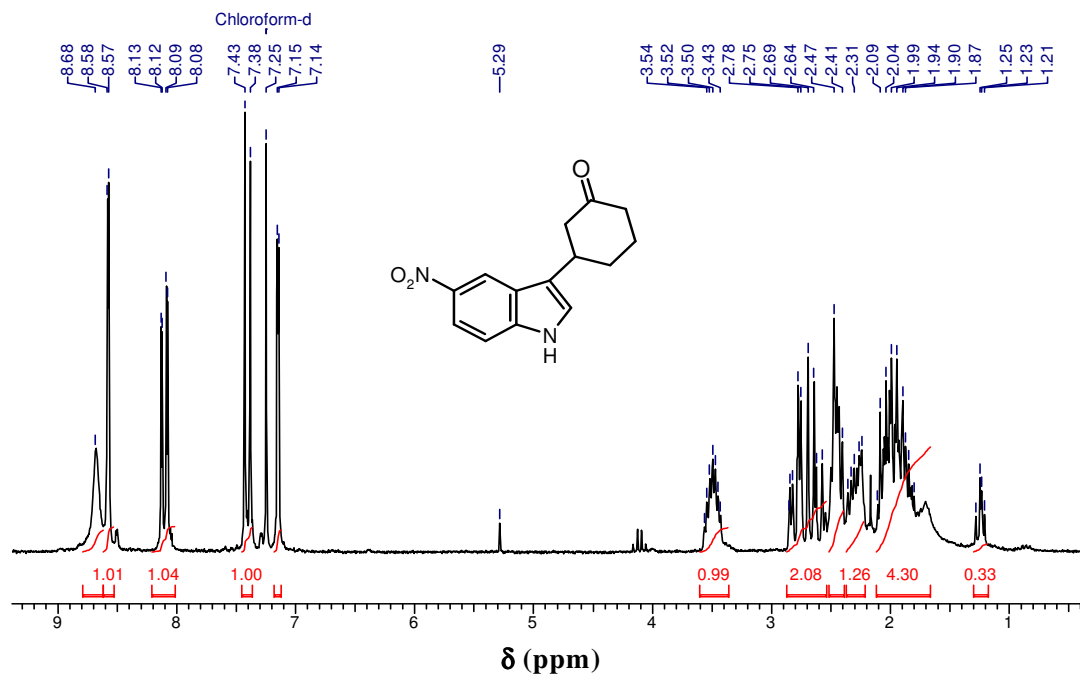
Product (Table 4.1.5, Entry 4): 3-(1H-indol-3-yl) cyclohexanone

Product (Table 4.1.6, Entry 2): 3-(3-Methyl-4-oxopentan-2-yl)-1H-indol-5-

carbonitrile

Product (Table 4.1.6, Entry 3): 3-Methyl-4-(5-nitro-1H-indol-3-yl) pentan-2-one

4.2.1. INTRODUCTION

Coumarin and its derivatives have been attracting great interest because of their importance in synthetic organic chemistry. Coumarins are structural units of several natural products,[1] and feature widely in pharmacologically and biologically active compounds.[2.] They have been used widely: as anticoagulants,[3] as additives in food and cosmetics,[2] and in the preparation of insecticides, optical brighteners,[4] dispersed fluorescent and laser dyes.[5] Coumarin can be synthesized by using various name reactions such as Pechmann,[6] Perkin,[7] Knoevenagel,[8] Reformatsky,[9] and Wittig reaction[10] by using acidic as well as basic catalysts.[11,12] However, the conventional methods for coumarin synthesis requires drastic reaction conditions. For example, 4-methyl-7-hydroxycoumarin has been prepared by stirring a mixture of resorcinol and ethyl acetoacetate in concentrate H_2SO_4 for 12-24 h,[13] where 7-hydroxy-4-methylcoumarin is used as a starting material for the preparation of an insecticide such as hymecromone. This process results in the formation of several byproducts, requires long reaction time, and encompasses corrosion related problems. Heterogeneous catalysts have also been used for the synthesis of coumarins and some examples of these catalysts are Nafion,[14,15] amberlyst 15,[16] montmorillonite clay,[17] ionic liquids,[18] and solid acid W/ZrO_2.[19] Recently, synthesis of 7-hydroxycoumarin and their derivatives via the Pechmann reaction has been reported by using solid acid catalysts (e.g. zeolite H-beta).[20]

Due to the growing concern for the adverse influence of the organic solvents on the environment, organic reactions without use of organic solvents have attracted the attention of chemists. Green chemistry as applied to chemical processes can be considered as a series of reductions (energy, auxiliaries, waste, *etc*.) and should always lead to the simplification of the process in terms of the number of chemicals

and steps involved. Here, solvent-free procedures are described for the synthesis of compounds having commercial value.

The present section deals with the carbon-carbon bond formation reaction such as Pechman reaction of phenol and β-ketoester for the synthesis of coumarins and their derivatives. For the model catalytic reaction, ethyl acetoacetate (β-ketoester) and resorcinol (1,3-dihydroxy phenol) were chosen as starting materials as shown in Scheme 4.2.1. The effect of loading of different amout of trifluoromethanesulphonic acid (triflic acid, TFA) over Zr-TMS catalyst (Zr-TMS-zirconia based transition metal oxide mesoporous molecular sieves), different amount of catalyst, effect of temperature, effect of different β-ketoester and phenol, and recyclibilty of the catalyst, have been studied.


Where R = C_2H_5 or CH_3 7-Hydroxy-4-methyl coumarin
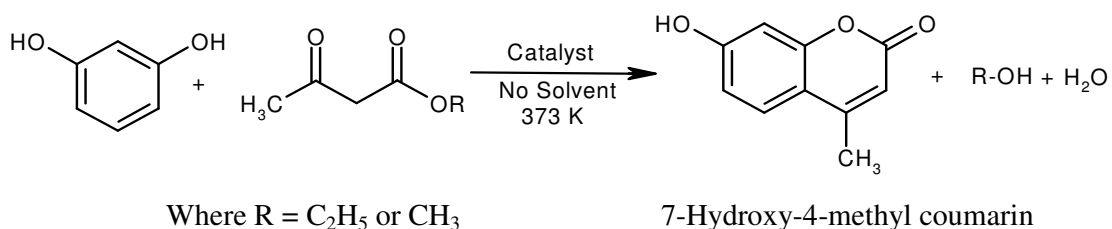
Scheme 4.2.1. Pechmann reaction of resorcinol and β-ketoester.

4.2.2. GENERAL PROCCEDURE FOR PECHMANN REACTION

The catalytic liquid-phase reaction was performed in a two-necked round bottom flask, equipped with a water condenser and accompanied by vigorously stirring under N_2 atmosphere. Prior to the reaction, catalyst was activated at 393 K in a vacuum oven and was used for the reactions under dry conditions. In a typical procedure, a mixture of resorcinol (10 mmol) and ethyl acetoacetate (10 mmol) was added to a preactivated catalyst (0.1 g). The reaction mixture (Scheme 4.2.1) was stirred magnetically at 373 K for 12 h. The progress of the reaction was monitored by gas chromatography (Varian model-CP-3800) equipped with capillary column and

flame ionization detector (FID) as well as by thin layer chromatography (TLC). After completion of the reaction, the catalyst was separated by filtration and then filtrate was diluted by dichloromethane (DCM), washed with 1N HCl for two times and finally washed with water for three times. The organic layer was separated and dried with anhydrous Na_2SO_4. The solvent was removed by rotary evaporator to obtain the crude product, which was then purified through column chromatography using silica gel (100-200 mesh), petroleum ether: ethyl acetate = 3:1). The product was identified and confirmed through GC, GC-MS, ^1H NMR, ^{13}C NMR techniques. Product 7-Hydroxy 4-methyl coumarin: M. P. 186-189 °C, (petroleum ether: ethyl acetate = 2:1), ^1H NMR (200 MHz, $CDCl_3$ + 4-drops of d_6-DMSO) δppm: 9.68 (s, 1H), 7.29-7.33 (m, 1H), 6.68-6.72 (m, 2H), 5.92-5.95 (m, 1H), 2.27 (s, 3H).^{13}C NMR (100 MHz, $CDCl_3$) δ 161.20, 161.12, 154.97, 153.04, 125.70, 112.99, 110.43, 102.6, 18.38.

Product: 7-Hydroxy-4-methyl coumarin
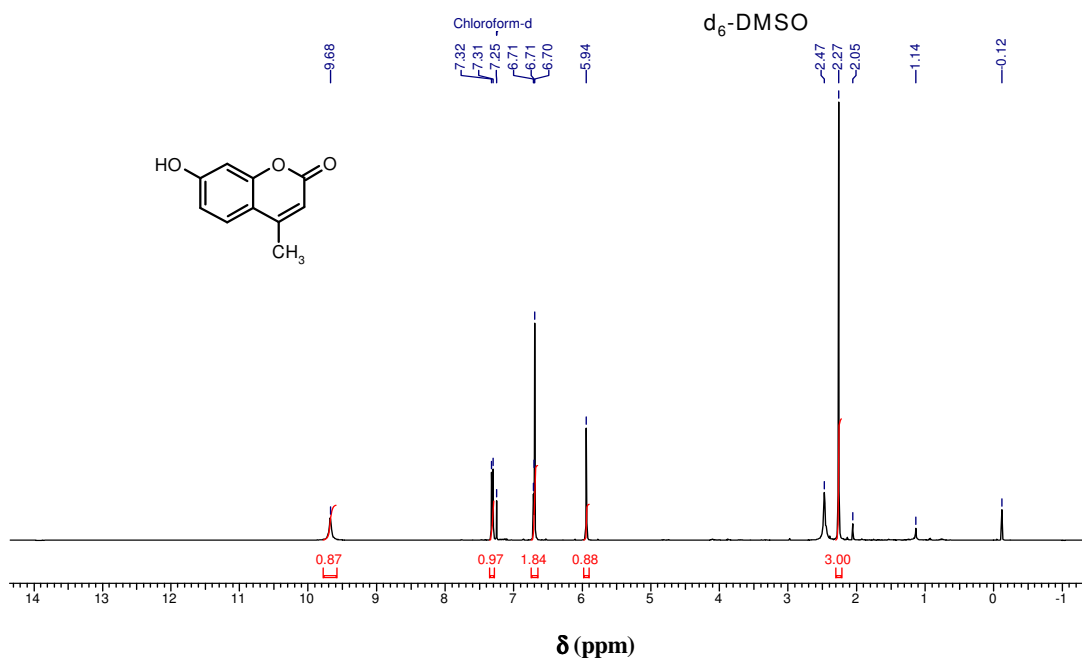
4.2.3. RESULTS AND DISCUSSION

4.2.3.1. Effect of Loading of Triflic Acid over Zr-TMS Materials

Figure 4.2.1 shows the time dependenent conversion of the Pechmann reaction of resorcinol and ethyl acetoacetate to produce corresponding 7-hydroxy-4-methyl coumarin, using different amount of triflic acid (TFA) loaded on Zr-TMS as catalysts. Although, the reaction was continued for a period of 12 h at 373 K, there was only marginal increase after 9h. The conversion of resorcinol was found to be only ~ 38% in the case of Zr-TMS catalyst. The conversion was found to increase as the loading of triflic acid on Zr-TMS increased from 5-25 wt %. The product selectivity was always found to be ~ 100 % in each system (Table 4.2.1.). The product (7-hydroxy-4-methyl coumarin) has been successfully isolated (Scheme 4.2.1.) and confirmed by ^{1}H and ^{13}C NMR spectroscopy.
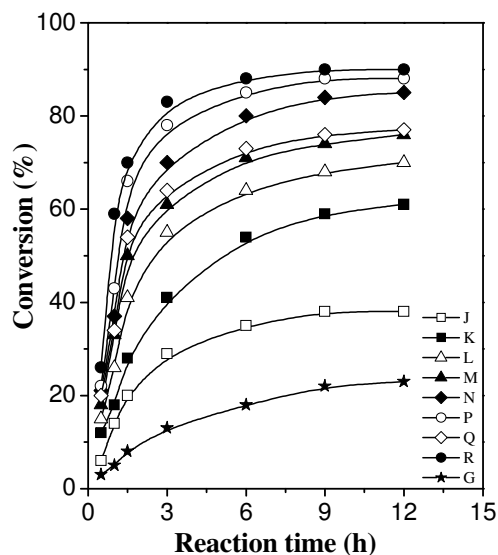

Figure 4.2.1. Plot of conversion vs reaction time for Pechmann reaction of resorcinol and ethyl acetoacetate for different loading of triflic acid over Zr-TMS catalyst. The sample notations as per Table 2.1 and 2.5, Chapter 2.

Table 4.2.1. Synthesis of coumarin by Pechmann reaction of resorcinol and ethyl acetoacetate over catalysts containing different loading of triflic acid on Zr-TMS and MCM-41 catalysts (Table 2.1 and 2.5, Chapter 2).[a]

Sample	Catalyst	Conv.[d] (mole %)	TON [e]	Selectivity (%)
J	Zr-TMS	38	-	100
K	Zr-TMS-TFA-5	59	209.7	100
L	Zr-TMS-TFA-10	68	120.8	100
M	Zr-TMS-TFA-15	74	87.7	100
N	Zr-TMS-TFA-20	84	74.6	100
P	Zr-TMS-TFA-25	88	57.4	100
Q	Zr-TMS-TFA-25-A [b]	81	50.5	100
R	CF_3SO_3H [c]	90	-	85
G	Ce-Al-MCM-41 (38,34)	23	26.0	100

[a] Reaction condition: 10 mmol of resorcinol, 10 mmol of ethyl acetoacetate, catalyst amount = 0.1 g, no solvent, reaction temperature 373 K, reaction time 9 h.

[b] Amorphous material.

[c] Triflic acid taken 0.05 g.

[d] Conversion (Conv.) with respect to resorcinol and based on GC analysis.

[e] TON is given as moles of resorcinol transformed per mole of sulfur.

The same reaction was carried out by using an amorphous catalyst Zr-TMS-TFA-25-A (sample Q) that contained a loading of 25 wt % of triflic acid. The conversion was obtained ~ 81 % to be compared with 88 % on catalyst P. This can be explained by the non-uniform pore size, low porosity, and low surface area of the amorphous Zr-TMS-TFA-25-A catalyst. On the other hand, the conversion of resorcinol was observed almost 90 % by use of pure triflic acid (sample R) under

homogeneous system. The product selectivity was found to be only *ca.* 85 %. This may be attributed to the selective nature of unsupported triflic acid. The results are given in Table 4.2.1. Similarly, the turn over number (TON) of Zr-TMS-TFA-25 (sample P) catalyst was also found to be more than that of the amorphous Zr-TMS-TFA-25-A (sample Q) catalyst.

The catalytic activity of Ce-Al-MCM-41(Si/Ce = 38, Si/Al = 34, sample G, Table 2.1) was also examined for the Pechmann reaction of resorcinol and ethyl acetoacetate under the identical reaction condition for comparison purpose as shown in Figure 4.2.1 (curve G). The catalyst shows lower conversion. It may be recalled that similar observation were made in case of Michael-addition of 3-methylindole to cyclohexenone. This lower activity of Ce-Al-MCM-41 vis-à-vis Zr-TMS-TFA catalyst can be attributed to lower acidity of Ce-Al-MCM-41 over Zr-TMS based catalyst. This result reveals that Pechmann reaction needs stronger acidity. Further, all the reactions were examined over the Zr-TMS-TFA-25 (sample P, Table 2.5) catalyst.

4.2.3.2. Effect of Catalyst Amount

To optimize the amount of catalyst for the synthesis of coumarin by Pechmann reaction of resorcinol and ethyl acetoacetate (Scheme 4.2.1) was carried out under solvent free condition over Zr-TMS-TFA-25 (sample P, Table 2.5) catalyst. The reaction was stirred for a period of 12 h at 373 K. From Figure 4.2.2**,** it is seen that the conversion is increases progressively with increasing catalyst amount (curves a-d). The product selectivity of coumarin was found to be *ca.* 100 % in each case.
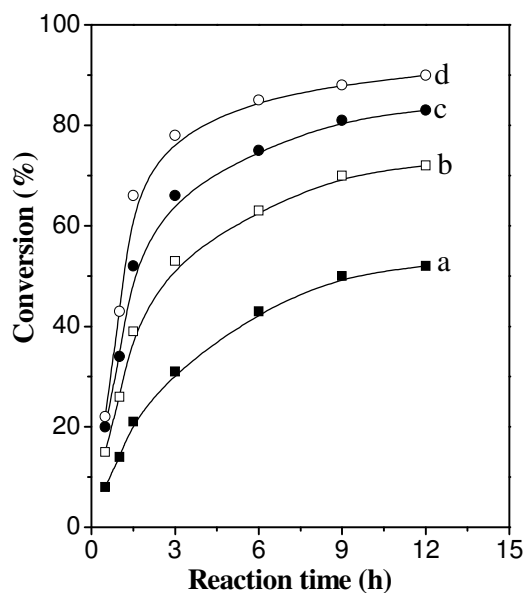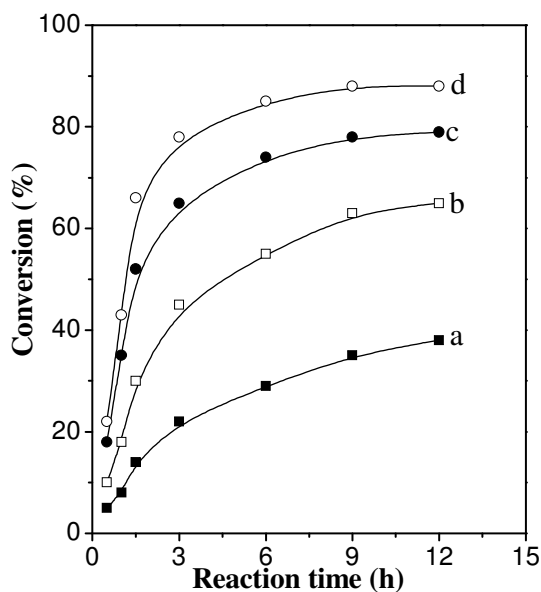
Figure 4.2.2. Plot of conversion vs reaction time for Pechmann reaction of resorcinol and ethyl acetoacetate using Zr-TMS-TFA-25 (sample P, Table 2.5) catalyst for different amount of catalyst. Curves (a) 0.04 g, (b) 0.06 g, (c) 0.08 g and (d) 0.1g.

4.2.3.3. Effect of Temperature

The synthesis of coumarin by Pechmann reaction of resorcinol and ethyl acetoacetate was carried out for different temperature under solvent free condition using Zr-TMS-TFA-25 (sample P, Table 2.5) catalyst for 12 h. The product selectivity of coumarin was found to be *ca*. 100 % at each temperature. As expected, the conversion increases by increasing the temperature from 298 to 373 K (Figure 4.2.3, curves a-d).

Figure 4.2.3. Plot of conversion vs reaction time Pechmann reaction of resorcinol and ethyl acetoacetate using Zr-TMS-TFA-25 (sample P, Table 2.5) catalyst for different temperature. Curves (a) 298 K, (b) 333 K, (c) 353 K and (d) 373 K.

4.2.3.4. Recycle Studies

The synthesis of coumarin by Pechmann reaction, as mentioned above, was carried out on Zr-TMS-TFA-25 catalyst (sample P, Table 2.5) for four consecutive reaction recycles. The conversion and turn over number (TON) observed in these experiments, conducted under solvent free condition at 373 K for 9 h, are shown in Figure 4.2.4. After the reaction, the catalyst was filtered from hot reaction mixture and reused for four successive test runs without any activation. The conversion was found to decrease slowly after each cycle reaching to 78 % in 4th recycle of the reaction. These data are shown in Table 4.2.2. The decrease in the conversion can be ascribed to the decrease in the carbon and sulfur content in solid catalyst due to partial leaching / breaking of the TFA as confirmed by elemental analysis (Table 4.2.2). The turn over number (TON) was however found to be nearly the same for all the four

cycles of test runs. The TON, values given in the Table 4.2.2 is calculated on the basis of the sulphur content in the solid catalyst. As seen in the data given in Table 4.2.2, the product selectivity for formation of 7-hydroxy-4-methyl coumarin is ~100 % in each recycle.
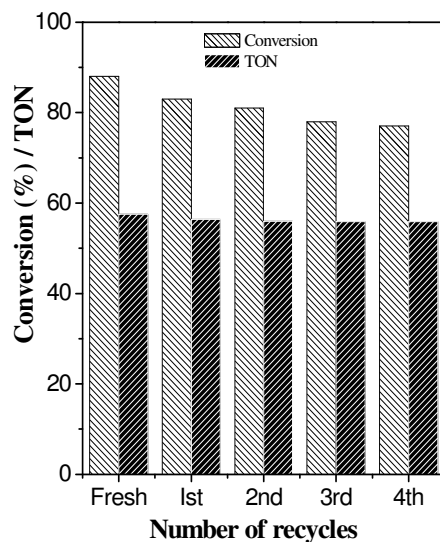
.

Figure 4.2.4. Conversion / turn over number (TON) observed during the consecutive test runs using a Zr-TMS-TFA-25 catalyst for Pechmann reaction of resorcinol and ethyl acetoacetate.

Table 4.2.2. Recycle studies of Zr-TMS-TFA-25 catalyst for Pechmann reaction of resorcinol and ethyl acetoacetate under solvent free system.

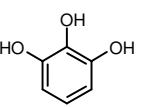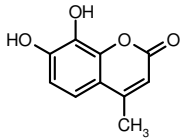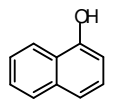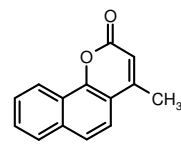| Recycle No	Elemental analysis (wt %)		Conv.[a] (mole %)	Selectivity (%)	TON[b]
	C	S			
Fresh	1.91	4.90	88	100	57.4
I[st]	1.83	4.76	83	100	56.3
2nd	1.75	4.63	81	100	55.9
3rd	1.69	4.52	79	100	55.9
4th	1.61	4.47	78	100	55.8
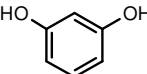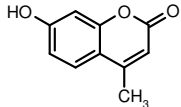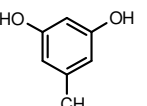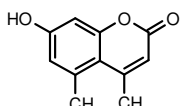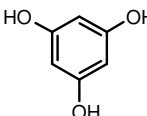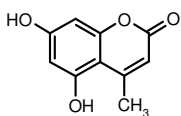
[a] Conversion (Conv.) with respect to resorcinol and based on GC analysis.

[b] TON is given as moles of resorcinol transformed per mole of sulfur.

4.2.3.5. Effect of Different Substrates

The different substrates were examined for the Pechmann reaction and the results are summarized in Table 4.2.3. All the reactions were performed under the solvent free condition by using Zr-TMS-TFA-25 (sample P, Table 2.5) as catalyst at temperature of 373 K for 9 h. The Pechmann reactions were carried out with different phenol and β-ketoester (e.g. ethyl acetoacetae and methyl acetoacetate) as shown in Table 4.2.3. Same products are obtained in both the cases. It is seen that the slightly higher conversion was obtained for methyl acetoacetate compared to that obtained for ethyl acetoacetate. This is because of the more electron-donating group (-OEt group) is attached with ethyl acetoactate which result less electropositive of β-keto carbonyl group. Hence, the attack of nucleophile to ethyl acetoactate will be less facile than methyl acetoacetate. The higher conversions were found for the reaction of 1, 3, 5-trihydroxybenzene (Entry 3) with ethyl acetoacetate and methyl acetoacetate than other substituted phenols. This is mainly because of the presence of three hydroxyl groups in the benzene ring and it helps in activating the aromatic ring for hydroxyalkylation. However, in case of 1, 3-dihydroxy-5-methylbenzene (Entry 2), the significantly low conversion was observed than that of other phenols. This may be due to the presence of methyl group meta to the position of hydroxyalkylation.

Table 4.2.3. Synthesis of coumarin derivatives by Pechmann reactin under solvent free condition over Zr-TMS-TFA-25 catalyst (sample P).[a]

Entry	Phenols	β-ketoesters, Conv. [b] (mole %)		Product
		Ethyl acetoacetate	Methyl acetoacetate	
1.		88	91	
2.		71	74	
3.		93	96	
4.		82	87	
5.		85	90	

[a] Reaction condition: 10 mmol of phenol, 10 mmol of β-ketoester, no solvent, reaction temperature 373 K, catalyst amount = 0.1 g, reaction time 9 h.

[b] Conversion (Conv.) with respect to phenol and based on GC analysis.

4.2.4. CONCLUSIONS

In conclusion, a methodology has been developed for the synthesis of coumarin and its derivatives by Pechmann reaction by using triflic acid functionalized over Zr-TMS catalyst under solvent free condition at 373 K. The conversions were found to increase with increasing loading of triflic acid from 5 to 25 wt %. The product selectivity was always found to be ~ 100 %. Further, the higher conversion was observed in the reaction between 1, 3, 5-trihydroxybenzene and

methylacetoacetate. The recycling studies support the stability of the catalyst at the reaction temperature. The catalytic activities are explained on the basis of the total acid strength of triflic acid functionalized Zr-TMS catalysts and the total acidity of the catalysts increasing with increasing loading of triflic acid, as confirmed by TPD-ammonia measurements (Chapter 2, Table 2.5).

4.2.5. REFERENCES

1. R. D. H. Murray, *Prog. Chem. Org. Nat. Prod.* **1991,** 58, 84.

2. R. O'Kennedy, R. D. Thornes, *Coumarins: Biology, Applications and Mode of Action,* Wiley and Sons, Chichester, **1997**.

3. L. A. Singer, N. P. Long, *J. Am. Chem. Soc.* **1966**, 88, 5213.

4. M. Zahradnik, *The Production and Application of Fluorescent Brightening Agents*, Wiley, New York, **1992**.

5. R. D. H. Murray, J. Mendez, S. A. Brown, *The Natural Coumarins, Occurrence, Chemistry and Biochemistry*, Wiley, New York, **1982**.

6. H. Von Pechmann, C. Duisberg, *Chem. Ber.* **1884**, 17, 929.

7. J. R. Johnson, *Org. React.* **1942**, 1, 210.

8. (a) G. Jones, *Org. React*. **1967**, 15, 204. (b) G. Brufola, F. Fringuelli, O. Piermatti, F. Pizzo, *Heterocycles* **1996**, 43, 1257.

9. R. L. Shirner, *Org. React*. **1942**, 1, 1.

10. I. Yavari, R. Hekmat-Shoar, A. Zonouzi, *Tetrahedron Lett.* **1998**, 39, 2391.

11. A. Ramani, B. M. Chanda, S. Velu, S. Sivansaker, *Green Chem.* **1999**, 1, 163.

12. F. Bigi, L. Chesini, R. Maggi, G. Sartori, *J. Org. Chem*. **1999**, 64, 1033.

13. E. C. Horning, *Organic Synthesis, Coll. Vol. III*, John Wiley & Sons, New York, **1955**, p. 281.

14. M. C. Laufer, H. Hausmann, W. F. H¨olderich, *J. Catal*. **2003**, 218, 315.

15. D. A. Chaudhari, *Chem. Ind*. **1983**, 568.

16. E. A. Gunnewegh, A. J. Hoefnagel, H. van Bekkum, *J. Mol. Catal. A: Chem.* **1995**, 100, 87.

17. (a) S. Fr`ere, V. Thi´ery, T. Besson, *Tetrahedron Lett*. **2001**, 42, 2791. (b) T. Li, Z. Zhang, F. Yang, C. Fu, *J. Chem. Res*. **1998**, 38.

18. Y. Gu, J. Zhang, Z. Duan, Y. Deng, *Adv. Synth. Catal*. **2005**, 347, 512.

19. B. M. Reddy, V. R. Reddy, D. Giridar, *Synth. Commun*. **2001**, 31, 3603.

20. A. J. Hoefnagel, E. A. Gunnewegh, R. S. Downing, and H. van Bekkum, *J. Chem. Soc., Chem. Commun*. **1995**, 225.
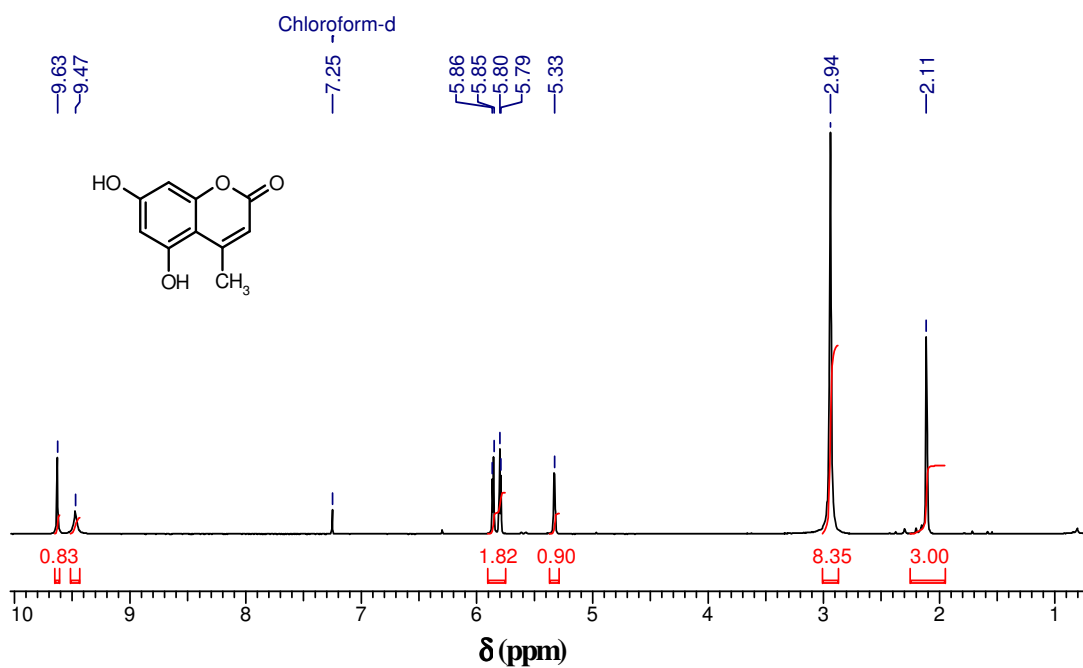
4.2.6. ^{1}H NMR SPECTRA
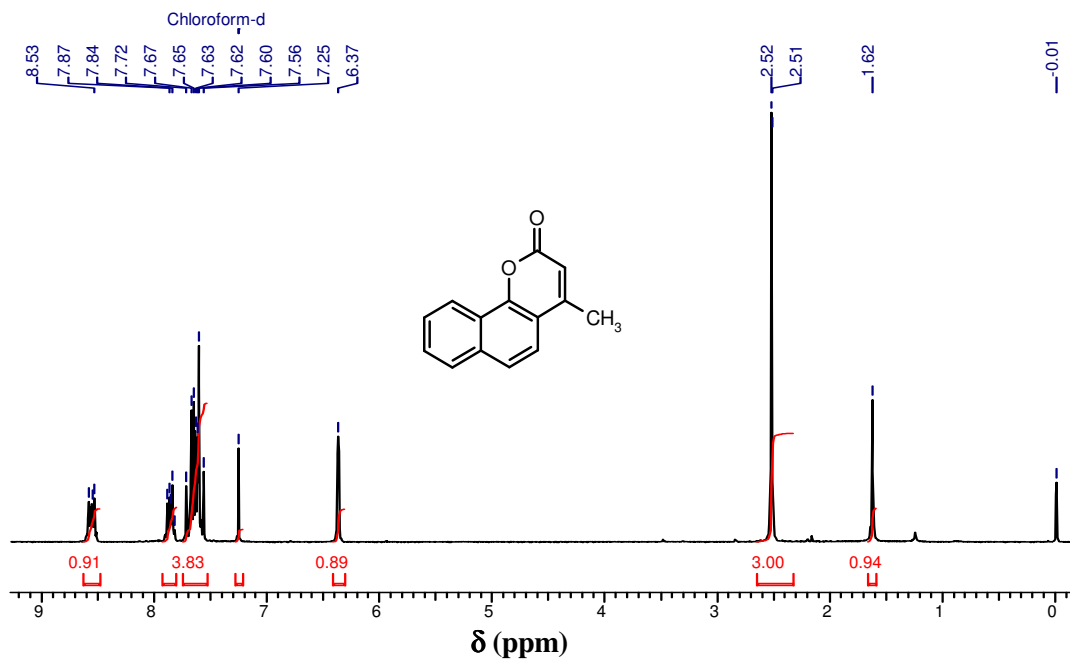
The representive ^{1}H NMR spectra are given below

Product (Table 4.2.3, Entry 2): 4, 5-Dimethyl-7-hydroxy coumarin
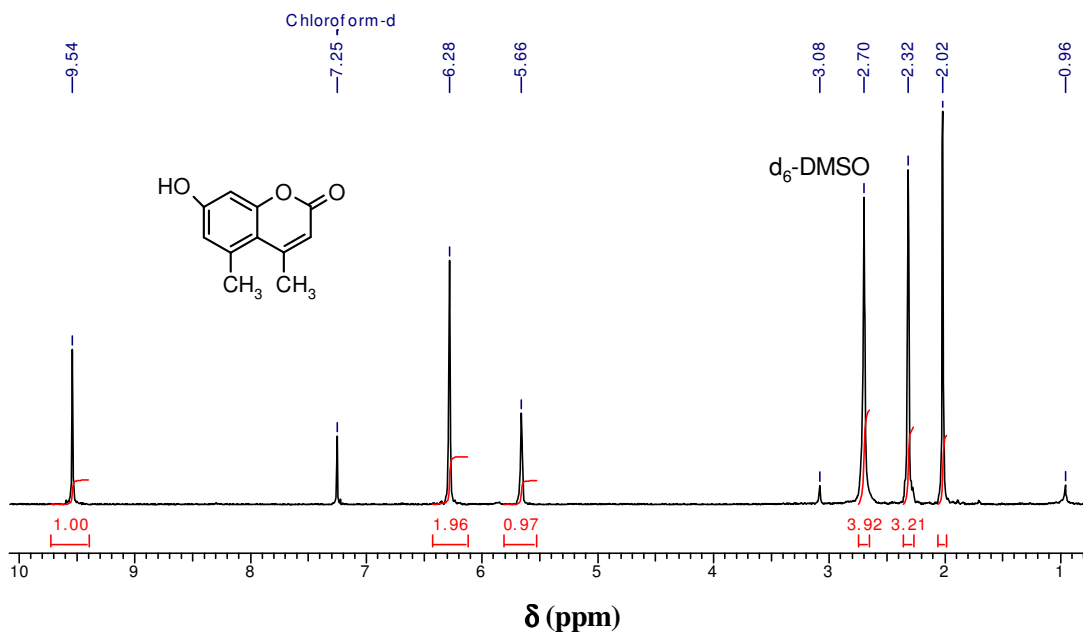
Product (Table 4.2.3, Entry 3): 4-Methyl-5, 7-dihydroxy coumarin

Product (Table 4.2.3, Entry 5): 4-Methyl-2H-benzo [h] chromene-2-one

5. **MICHAEL-ADDITION OF β-NITROSTYRENE TO MALONATE OVER STRONGLY BASIC GUANIDINE MODIFIED MCM-41/SBA-15 MATERIALS**

5.1. INTRODUCTION

There are many organic superbases such as 1,5,7-triazabicyclo [4.4.0] dec-5-ene (TBD), 3,4,6,7,8-hexahydro-1-methyl-2H-pyrimido [1,2-a] pyrimidine (MTBD), 1,4-diazabicyclo [2,2,2] octane (DABCO), 1,8-diazabicyclo [5.4.0] undec-7-ene (DBU) and tetramethylguanidine (TMG) etc. Among the various organic superbases, 1,5,7-triazabicyclo [4.4.0] dec-5-ene (TBD) has been widely utilized in organic synthesis because of its high pKa value. For example, TBD promote various organic reactions such as Wittig reaction,[3] nitroaldol (Henry) reaction,[4] dialkyl phosphate addition to carbonyl compounds[4] and the addition of azoles to α, β-unsaturated nitriles and esters,[5] and Baylis–Hillman reactions.[6]

Several authors have reported Michael-addition of β-nitrostyrene to malonates,[7] 1, 3-dicarbonyl compounds,[8] ketones,[9] aldehydes,[10] N-heterocycles[11] and indoles,[12] using homogeneous catalyst. The Michael-addition to nitroalkenes has been developed as a powerful tool in organic synthesis, because Michael adducts are versatile building blocks for agricultural and pharmaceutical compounds. For example, the Michael-addition of β-nitrostyrene to diethyl malonates produced Michael adducts.

This chapter deals with an effort towards developing green protocol for synthesis of diethyl 2-(3-nitro-phenylethyl) malonate and its derivatives by Michael-addition of β-nitrostyrene (nitro-alkene) and malonate using TBD immobilized mesoporous MCM-41/SBA-15 catalysts. The use of single step solventless conditions in combination with heterogeneous catalysts represents one of the main aspects of green chemical methods. For catalytic model reaction, β-nitrostyrene and diethyl malonate was chosen as starting material as shown in reaction Scheme 5.1. To the best of my knowledge, this is the first example of solid base heterogeneous catalyst

for Michael-addition of β-nitrostyrene to malonate. The effect of different mesoporous materials as support, effect of amount of catalyst; effect of temperature, recyclability of the catalyst and different substrates have been studied in this chapter. The product was successfully isolated by column chromatography and identified by ^{1}H NMR spectroscopy.
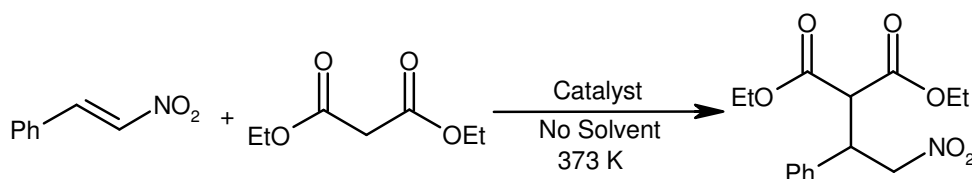
Scheme 5. 1. Michael-addition of β-nitrostyrene and diethyl malonate.

## 5.2. GENERAL PROCEDURE FOR MICHAEL-ADDITION OF β-NITROSTYRENE TO MALONATE

The catalytic liquid-phase reaction was performed in a two-necked round bottom flask with a water condenser under vigorously stirring in N_2 atmosphere. The catalyst was preactivated at 393 K in a vacuum oven and subsequently used for the reactions under dry conditions. In a typical procedure, a mixture of β-nitrostyrene (10 mmol) and diethyl malonate (10 mmol) was added to a preactivated catalyst (0.2 g). The reaction mixture was stirred magnetically at 373 K for a period of 12 h. The progress of the reaction was monitored by gas chromatography (Varian model-CP-3800) equipped with capillary column and flame ionization detector (FID) as well as by thin layer chromatography (TLC). After completion of the reaction, the catalyst was separated by centrifugation and then filtrate was diluted with dichloromethane (DCM), washed with 1N HCl for two times and finally washed through water for three times. The organic layer was separated and dried with anhydrous Na_2SO_4. The solvent was removed by rotary evaporator to the produce crude product and then corresponding product was purified through column chromatography using silica gel

(100-200 mesh), petroleum ether: ethyl acetate (3:1) and confirmed through GC, GC-MS, ^{1}H NMR, ^{13}C NMR. The ^{1}H NMR spectra were recorded in a 200 MHz using CDCl$_3$ as solvent.

^{1}H NMR (200 MHz, CDCl$_3$) δppm: 1.03 (t, 3H), 1.25 (t, 3H), 3.84 (d, 1H), 4.04 (q, 2H), 4.16–4.26 (m, 3H), 4.88-4.98 (d q, 2H), 7.20-7.31 (m, 5H).

^{13}C NMR (100 MHz, CDCl$_3$) δppm: 13.7, 13.9, 42.9, 54.9, 61.9, 62.1, 77.2,77.6, 128.0, 128.3, 128.9, 136.2, 166.8, 167.4.

Product: Diethyl 2-(2-nitro-1-phenylethyl) malonate
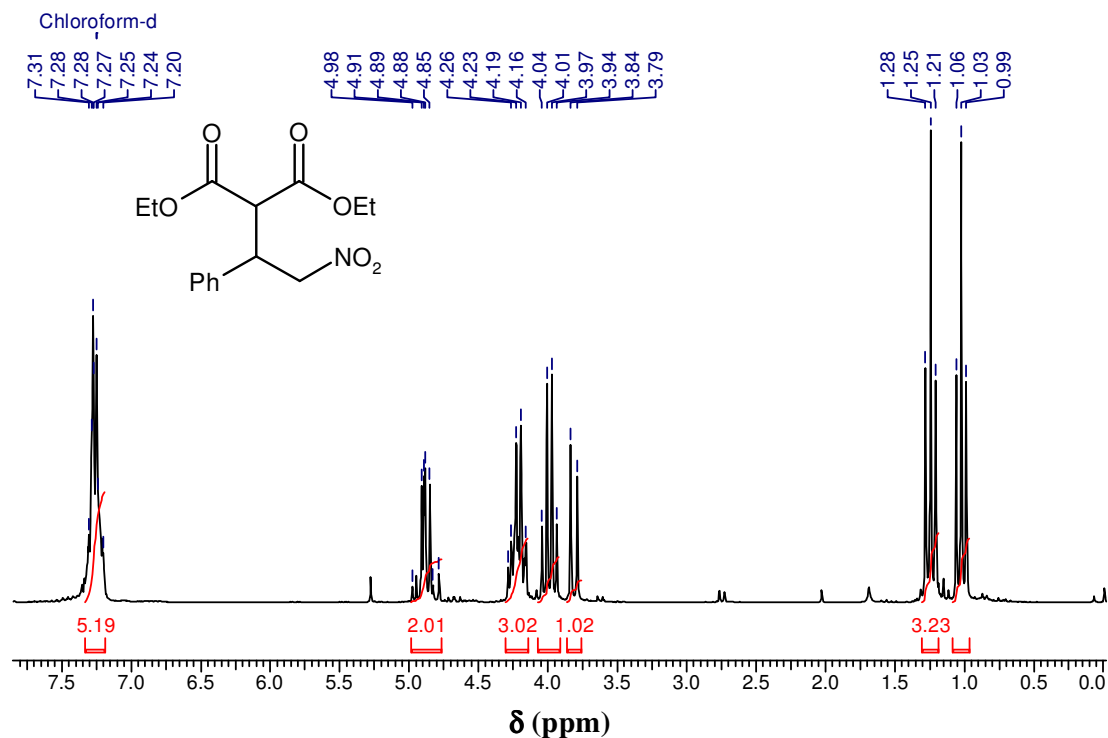
5.3. RESULTS AND DISCUSSION

5.3.1. Effect of Reaction Time

Figure 5.1 A shows the effect of reaction time on conversion of β-nitrostyrene over MCM-41-TBD and SBA-15-TBD catalyst in Michael-addition of β-nitrostyrene with diethyl malonate (Scheme 5.1) to produce corresponding diethyl 2-(2-nitro-1-phenylethyl) malonate. Ethanol (EtOH) was used as a solvent in these experiments at 353 K. Although, each experiment was continued for ca. 12 h, there was only marginal increase in the conversion after 9 hours of the reaction. The individual experiments were performed for MCM-41-TBD and SBA-15-TBD catalyst under N_2 atmosphere. It was observed that the conversion of β-nitrostyrene was reached 65 and 71 % within 9-h over the MCM-41-TBD and SBA-15-TBD catalyst, respectively (Figure 5.1 A).

The catalytic activity was also examined for Michael-addition of β-nitrostyrene and diethyl malonate over (a) MCM-41-TBD and (b) SBA-15-TBD catalyst under solvent free system at 353 K. The reaction data are plotted as function of time in Figure 5.1 B. Under solvent free system, 67 and 75 % conversion of β-nitrostyrene were obtained within 9-h over the MCM-41-TBD and SBA-15-TBD catalyst, respectively (Figure 5.1B). The selectivity towards the product over both catalysts was found to be 100 %. It was observed that there was marginal increase in the conversion of β-nitrostyrene under solvent free condition (vis-à-vis in the presence of solvent, ethanol) over the MCM-41-TBD and SBA-15-TBD catalyst (Table 5.1). Since, SBA-15-TBD catalyst exhibited higher activity compared to that of MCM-41-TBD under same reaction (Table 5.1); further studies were carried out using SBA-15-TBD catalyst.
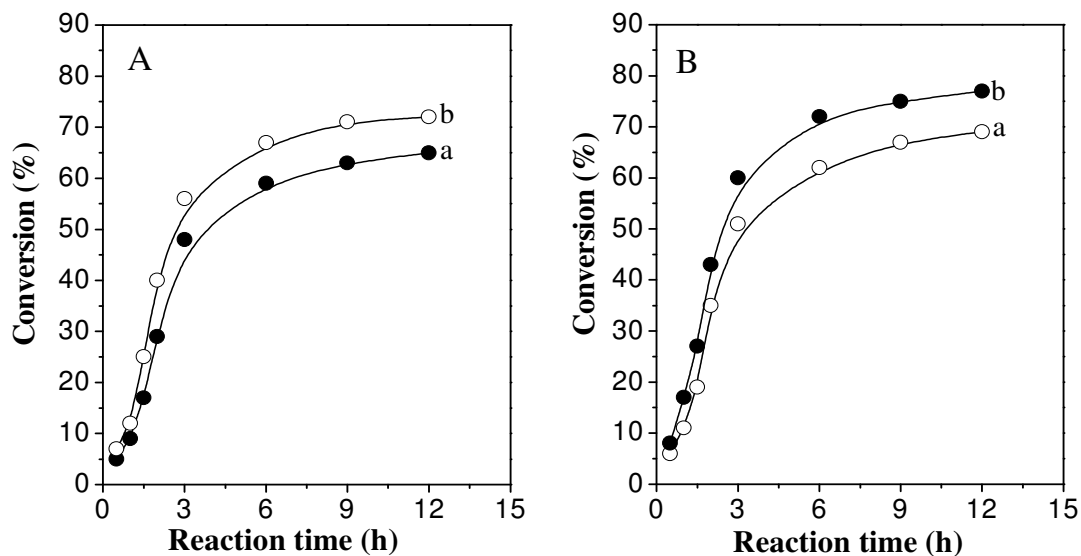
Figure 5.1. Effect of reaction time on conversion for Michael-addition of β-nitrostyrene and diethyl malonate over (a) MCM-41-TBD and (b) SBA-15-TBD catalyst with (A) ethanol as solvent and (B) no solvent at 353 K.

Table 5.1. Michael-addition β-nitrostyrene with diethyl malonate over MCM-41-TBD and SBA-15-TBD catalyst at different temperature.[a]

Catalysts	Solvent	Temperature (K)	Conv.[b] (mole %)	TON[c]
MCM-41-TBD	Ethanol	353	63	33.9
MCM-41-TBD	No solvent	353	67	36.0
SBA-15-TBD	Ethanol	353	71	36.3
SBA-15-TBD	No solvent	353	75	38.4
SBA-15-TBD	No solvent	373	81	41.4
SBA-15-TBD	No solvent	333	50	25.6
SBA-15-TBD	No solvent	298	23	11.7

[a]Reaction condition: β-nitrostyrene (10 mmol), malonate (10 mmol), reaction temperature 298-373 K, reaction time 9 h, catalyst amount = 0. 2 g.

[b] Conversion (Conv.) with respect to β-nitrostyrene and based on GC analysis.

[c] TON is given as moles of β-nitrostyrene transformed per mole of nitrogen.

5.3.2. Effect of Catalyst Amount

To optimize the amount of catalyst for the Michael-addition of β-nitrostyrene with diethyl malonate, the reaction was carried out under solvent free condition over SBA-15-TBD catalyst for 12 h using varying amount of catalyst (3.5 to 13.3 wt % with respect to β-nitrostyrene). The conversion of β-nitrostyrene was found to increase when catalyst amount was increased from 0.05 (3.3 wt %) to 0.2 g (13.3 wt %) (Figure 5.2, curves a-d). The product selectivity was always obtained ca. 100%. About 10 wt % catalyst is required amount for significant Michael-addition of β-nitrostyrene with diethyl malonate.
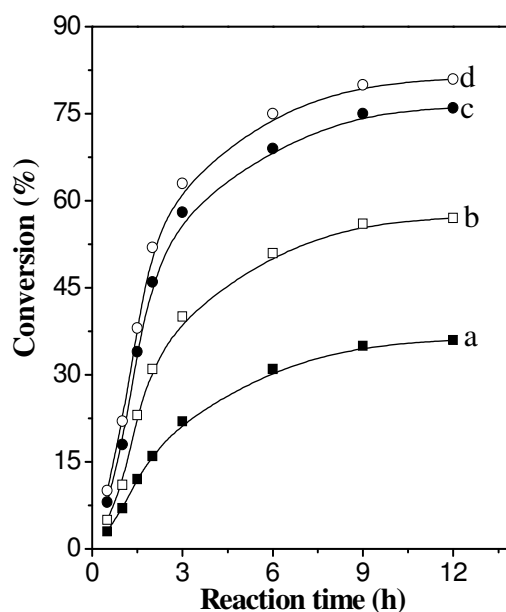

Figure 5.2. Plot of conversion vs reaction time for Michael-addition of β-nitrostyrene with diethyl malonate using different amount of SBA-15-TBD catalyst under solvent free condition at 373 K. Curves (a) 0.05 g (3.3 wt %), (b) 0.1 g (6.6 wt %), (c) 0.15 g (10 wt %) and (d) 0.2 g (13.3 wt %).

5.3.3. Effect of Temperature

The effect of temperature was examined for Michael-addition of β-nitrostyrene with diethyl malonate under solvent free condition over the SBA-15-TBD catalyst for 12 h (Figure 5.3). Individual experiments were performed at each temperature under identical reaction conditions. The rate of β-nitrostyrene conversion was increased with increasing temperature from 298 to 373 K as expected (curves a-d). However, there was no significant change in conversion as further increasing temperature from 353 to 373 K (Figure 5.3, curves c and d) and these data are presented in Table 5.1.
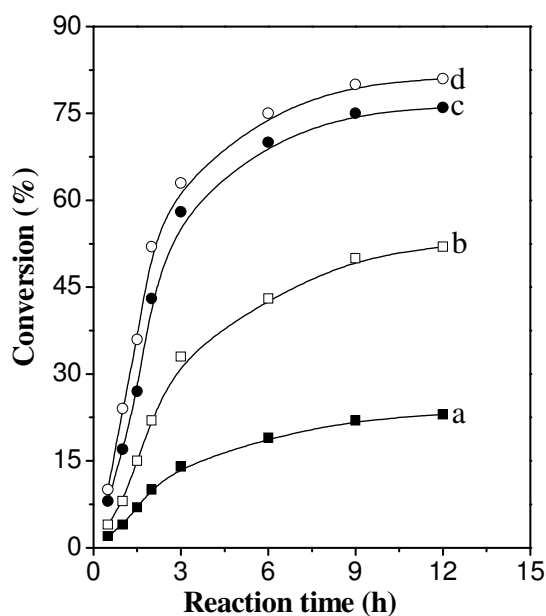

Figure 5.3. Plot of conversion vs reaction time for Michael-addition of β-nitrostyrene with diethyl malonate over SBA-15-TBD catalyst at different temperature.

Curves (a) 298 K, (b) 333 K, (c) 353 K and (d) 373 K.

5.3.4. Recycle Studies

In order to check the recyclibility and stability of the catalyst, the Michael-addition of β-nitrostyrene with diethyl malonate was carried out for three consecutive reaction cycles using SBA-15-TBD catalyst. After the reaction, the catalyst was filtered from hot reaction mixture, washed with dichloromethane and used for three successive times without any further activation. The conversion and turn over number (TON) obtained for the period of recycle studies of the SBA-15-TBD catalyst are plotted as a function of number of recycles under solvent-free condition at 373 K for 12 h (Figure 5.4). The conversion was decreased from 81 to 76 % in the first recycle, and then it decreases slowly upto 69 % (3rd recycle) as shown in Figure 5.4. The conversion decreased due to loss of nitrogen content (due to leaching) in the solid catalyst as confirmed by elemental analysis (Table 5.2). Nevertheless, the TON was found to remain unchanged when calculated on the basis of the N remaining in the solid catalysts after these consecutive test runs.
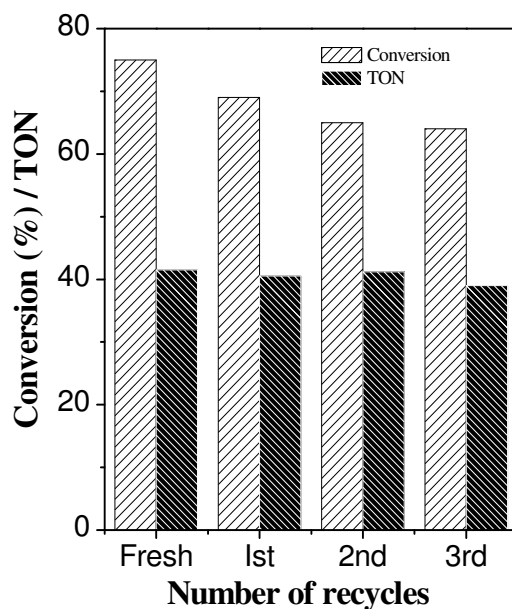

Figure 5.4. Conversion and turn over number (TON) during successive recycles of a catalyst sample for Michael-addition of β-nitrostyrene and diethyl malonate at 373 K.

Table 5.2. Recycle studies of SBA-15-TBD catalyst for Michael-addition of β-nitrostyrene and diethyl malonate under solvent free condition.

Recycle No	Elemental analysis (wt%)			Conv.[a] (mole %)	TON [b]	Selectivity (%)
	C	H	N			
Fresh	16.0	3.8	4.1	81	41.4	100
1st	15.4	3.6	3.9	76	40.5	100
2nd	14.3	3.1	3.6	71	41.1	100
3rd	11.9	2.8	3.2	69	39.0	100

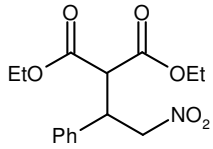[a] Conversion (Conv.) with respect to β-nitrostyrene and based on GC analysis.

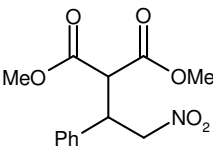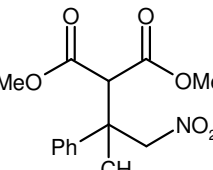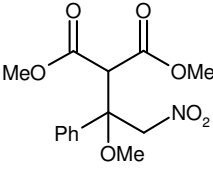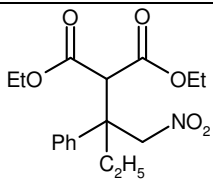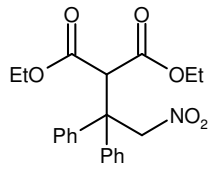[b] TON is given as moles of β-nitrostyrene transformed per mole of nitrogen.

5.3.5. Michael-Addition of β-Nitrostyrene with Different Malonates

The different substrates were examined for the Michael-addition of β-nitrostyrene with different malonates over SBA-15-TBD catalyst. All the reactions were performed under solvent free condition at 373 K for 9 h in N_2 atmosphere. The corresponding results are summarized in Table 5.3. The product selectivity of all the reactions was observed *ca.* 100 %. As compared to dimethyl malonate (Entry 2), less conversion was obtained when diethyl malonate was used (Entry 1). This is because of the less electron delocalization in diethyl malonate (Entry 1) and due to the more electron donating nature of ethoxy group in it which results in the less electronegative α-substituted malonate. Hence, the attack of nucleophile to electrophile will be less facile in diethyl malonate than dimethyl malonate. Slightly less conversion was obtained in the case of dimethyl methylmalonate (Entry 3) than dimethyl methoxymalonate (Entry 4). This is mainly because of the more electron-donating group (-OMe group) present in dimethyl methoxymalonate (Entry 4). Since, methoxy

group (-OMe) is more electron-donating than methyl group, so, the formation of nucleophile in α-substituted malonate will be more in dimethyl methoxymalonate (Entry 4) than dimethyl methylmalonate (Entry 3). In the case of Entry 5, the significantly low conversion was obtained for the reaction of β-nitrostyrene and diethyl ethylmalonate. However, no conversion was observed for the reaction of β-nitrostyrene with diethyl phenylmalonate (Entry 6, 0 %) even after the reaction was carried out for 24 h. This is mainly because of the presence of more sterically hindered phenyl group in α-substituted malonate (Entry 6). Hence, it is not possible to make nucleophilic center in α-substituted malonate. Therefore, attack of nucleophile to electrophile did not occur in this reaction.

Table 5.3. Michael addition of β-nitrostyrene with different malonate over SBA-15-TBD catalyst.[a]

Entry	Malonate	Conv.[c] (mole %)	Product
1.	Diethyl malonate	81	
2.	Dimethyl malonate	84	
3.	Dimethyl methylmalonate	86	
4.	Dimethyl methoxymalonate	89	

5.	Diethyl ethylmalonate	65	
6.[b]	Diethyl phenylmalonate	0	

[a] Reaction condition: β-nitrostyrene (10 mmol), malonate (10 mmol), no solvent, reaction temperature 373 K, reaction time 9 h, , catalyst amount = 0. 2 g.
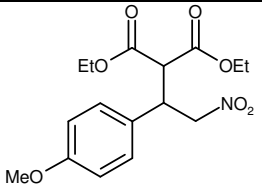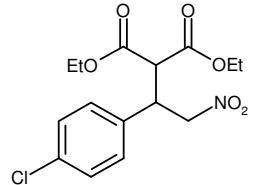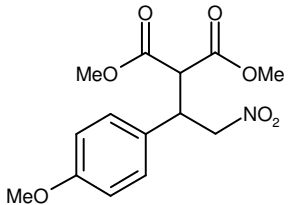
[b] Reaction time 24 h.

[b] Conversion (Conv.) with respect to β-nitrostyrene and based on GC analysis.

5.3.6. Michael-Addition of Different Nitrostyrenes with Different Malonates

The Michael-addition was also carried out with different nitrostyrenes and different malonates under identical reaction condition and these results are summarized in Table 5.4. The conversion obtained was 79 and 84 % for the reactions of diethyl malonate with p-OMe-NO$_2$ styrene (Entry 1) and p-Cl-NO$_2$ styrene (Entry 2), respectively. Similarly, the reaction of dimethyl malonate with p-OMe- NO$_2$ styrene (Entry 3) and p-Cl-NO$_2$ styrene (Entry 4) gave conversion of 84 and 91%, respectively. High conversion was observed when the reaction was carried out with p-Cl-NO$_2$ styrene (Entry 2, 4) and diethyl malonate as well as with dimethyl malonate. This is mainly because of the presence of electron-withdrawing group (-Cl) in the 4-position of nitrostyrene (Entry 2 and 4). Since, chlorine has more electron-withdrawing power than methoxy (-OMe) group, so, the electropositive character will be high at β-carbon in nitro styrene. Hence, attack of nucleophile to electrophile will be more facile which leads to the more conversion of the reaction.

Table 5.4. Michael-addition of different nitrostyrene with different malonate over SBA-15-TBD catalyst.[a]

Entry	Malonate	Nitrostyrene	Conv. [b] (mole %)	Product
1.	Diethyl malonate	p-OMe-NO$_2$ Styrene	79	
2.	Diethyl malonate	p-Cl-NO$_2$ Styrene	84	
3.	Dimethyl malonate	p-OMe-NO$_2$ Styrene	84	
4.	Dimethyl malonate	p-Cl-NO$_2$ Styrene	91	

[a] Reaction condition: nitrostyrene (10 mmol), malonate (10 mmol), no solvent, reaction temperature 373 K, reaction time 9 h, catalyst amount = 0. 2 g.
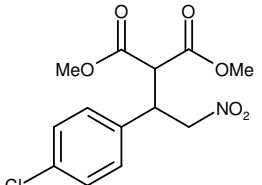
[b] Conversion (Conv.) with respect to β-nitrostyrene and based on GC analysis.

5.4. CONCLUSIONS

To conclude, a well-organized and environmentally friendly catalyst has been successfully synthesized by a facile two-step route immobilization and a methodology has been developed for carbon-carbon bond formation reaction such as Michael-addition of β-nitrostyrene to malonate. This methodology is applicable to wide range

of substrates making it a useful addition reaction for the organic chemists. Since, 1,5,7-triazabicyclo [4.4.0] dec-5-ene (TBD) is inexpensive and commercially available, so converting homogeneous TBD into heterogeneous TBD catalyst is a better option as it can be easily filtered as well as can be recycled for several times. The loss of activity is observed to some extent after three recycles which may be because of the decrease of nitrogen content and loss of crystallanity of the SBA-15-TBD catalyst.

5.5. REFERENCES

1.   (a) D. H. R. Barton, J. D. Elliott, S. D. Ge´ro, *J. Chem. Soc*. *Perkin Trans*. **1982,** 1, 2085. (b) Schmidtchen, F. P. *Chem. Ber.* **1980**, 113, 2175.

2.   (a) B. Kovacˇevic´, Z. B. Maksic´, *Org. Lett*. **2001**, 3, 1523. (b) I. Kaljurand, T. Rodima, A. Pihl, V. Maemets, I. Leito, I. A. Koppel, M. Mishima, *J. Org. Chem.* **2003**, 68, 9988.

3.   (a) D. Simoni, M. Rossi, R. Rondanin, A. Mazzali, R. Baruchello, C. Malagutti, M. Roberti, F. P. Invidata, *Org. Lett.* **2000**, 2, 3765. (b) M. G. Edwards, J. M. J Williams, *Angew. Chem. Int. Ed*. **2002**, 41, 4740.

4.   D. Simoni, R. Rondanin, M. Morini, R. Baruchello, F. P. Invidiata, *Tetrahedron Lett*. **2000**, 41, 1607.

5.   A. Horva´th, *Tetrahedron Lett*. **1996**, 37, 4423.

6.   V. K Aggarwal, A. Mereu, *Chem. Commun*. **1999**, 2311.

7.   M. Watanabe, A. Ikagawa, H. Wang, K. Murata, T. Ikariya*, J. Am. Chem. Soc.* **2004**, 126, 11148.

8   (a) J. Ji, D. M. Barnes, J. Zhang, S. A. King, S. J. Wittenberger, H. E. Morton, *J. Am. Chem. Soc*. **1999**, 121, 10215. (b) D. M. Barnes, J. Ji, M. G. Fickes, M. A. Fitzgerald, S. A. King, H. E. Morton, F. A. Plagge, M. Preskill, S. H. Wagaw, S. J. Wittenberger, J. Zhang, *J. Am. Chem. Soc*. **2002**, 124, 13097. (c) J. Wang, H. Li, W. Duan, L. Zu, and W. Wang, *Org. Lett*. **2005**, *7*, 4713

9.   (a) N. Mase, K. Watanabe, H. Yoda, K. Takabe, F. Tanaka, C. F. Barbas, *J. Am. Chem. Soc.* **2006**, 128, 4966. (b) S. H. McCooey and S. J. Connon, *Org. Lett.* **2007**, 9, 599.

10   L. Zu, J. Wang, H. Li, W. Wang, *Org. Lett*. **2006,** *8*, 3077.

11.   J. Wang, H. Li, L. Zu, W. Wang, *Org. Lett.* **2006**, 8, 1391.

12.   (a) Y-X. Jia, S-F. Zhu, Y. Yang, Q-L Zhou, *J. Org. Chem.* **2006**, *71*, 75. (b) S-F. Lu, D-M. Du, J. Xu, *Org. Lett.* **2006**, 8, 2115. (c) C. Lin, J. Hsu, M.N.V. Sastry, H. Fang, Z. Tu, J-T Liu, Y. C-Fa, *Tetrahedron*, **2005**, 61, 11751.

5.6. ^{1}H NMR SPECTRA

The representative Michael products of ^{1}H NMR spectra are given in the following

Product (Table 5.3, Entry 2): Dimethyl 2-(2-nitro-1-phenylethyl) malonate
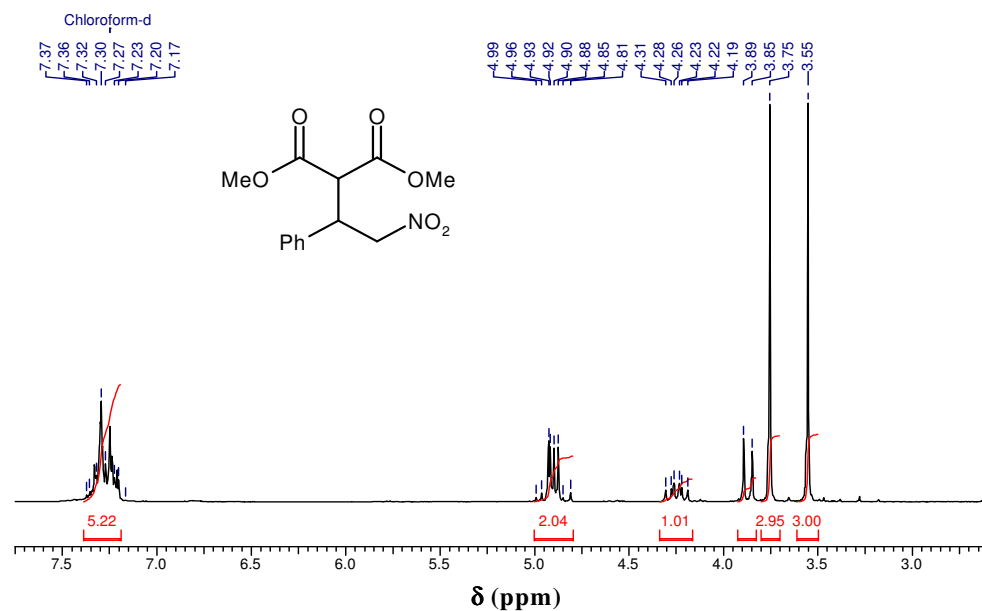
Product (Table 5.4, Entry 1): Diethyl 2-(1-(4-methoxyphenyl)-2-nitroethyl) malonate
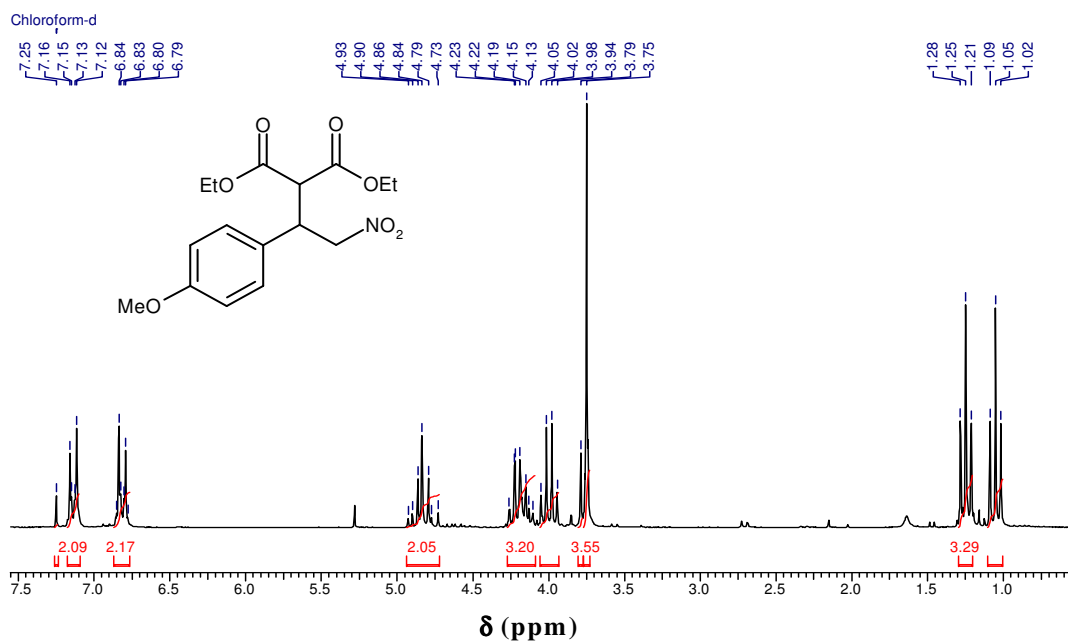
Product (Table 5.4, Entry 3): Dimethyl 2-(1-(4-methoxyphenyl)-2-nitroethyl) malonate
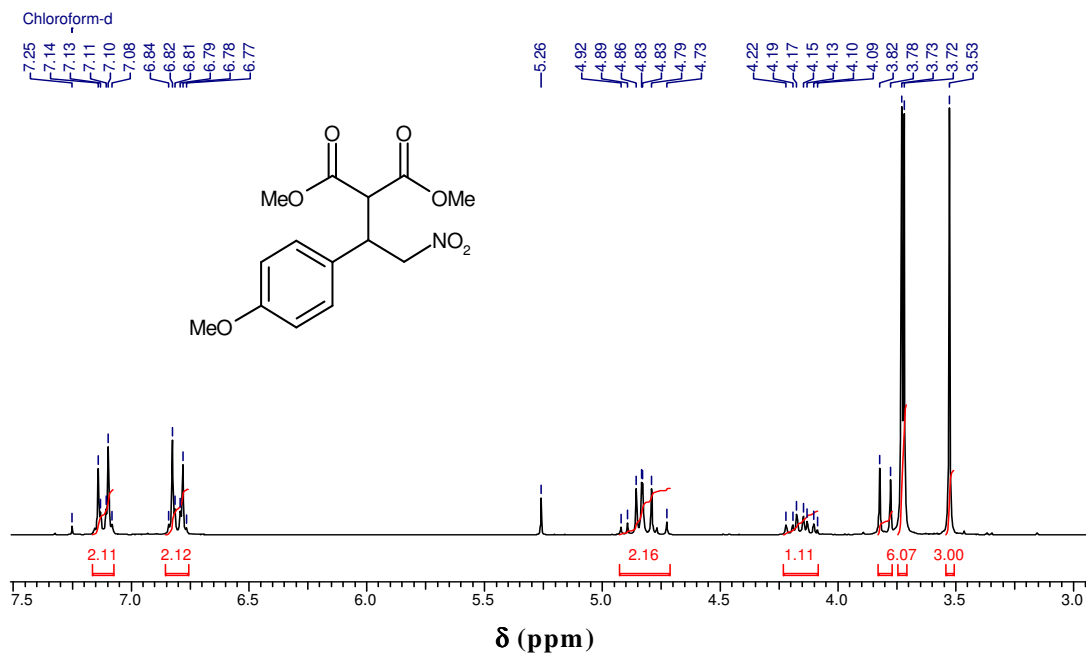
Product (Table 5.4, Entry 4): Dimethyl 2-(1-(4-chlorophenyl)-2-nitroethyl) malonate
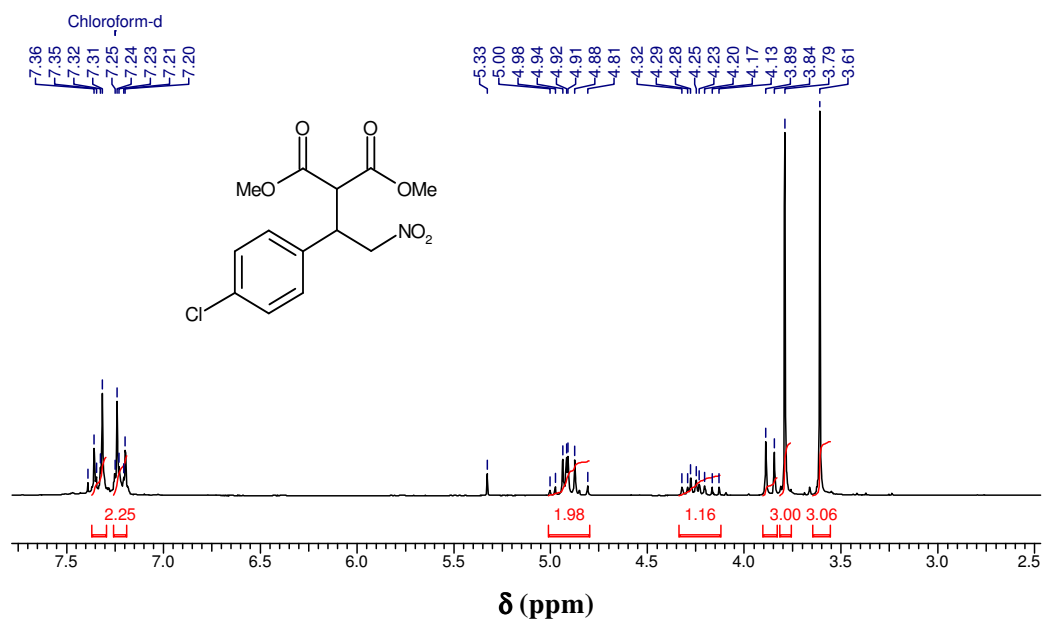
CHAPTER 6

6. SUMMARY AND CONCLUSIONS

6.1. SUMMARY

The present thesis is divided into six chapters including the present on as follows:

Chapter 1 presents a general introduction about various aspects of mesoporous materials and organic-inorganic hybrid mesoporous materials. Different factors influencing their formation, synthesis mechanism, approaches for surface-functionalization and commonly used characterization techniques are briefly presented. The applications of these materials for different carbon-carbon bond formation reactions are also discussed. A detailed review of the work done on the above aspect is also presented here in this chapter. Finally the scope and objectives of the present work have been outlined at the end of this chapter.

Chapter 2 describes the detailed synthesis of (i) Cerium-containing Al-MCM-41samples by the direct substitution method, (ii) Zr-TMS (mesoporous transition metal oxides) along with its functionalization by trifluoromethanesulfonic acid (triflic acid, TFA), and (iii) SBA-15 catalyst with immobilization of 1,5,7-triazabicyclo [4.4.0] dec-5-ene (TBD) by post-synthesis route. Different physico-chemical properties of these catalysts were characterized by powder XRD, N_2-adsorption, SEM, TEM, FT-IR spectroscopy, ^{29}Si CP MAS NMR, ^{13}C CP MAS NMR, ^{27}Al MAS NMR, UV-Vis, and TPD (ammonia). The acidic nature of MCM-41 with different extent of substitution by Ce was investigated using *in situ* FT-IR spectroscopy of pyridine adsorption.

Chapter 3 describes the catalytic activity of carbon-carbon bond formation reactions using Ce-Al-MCM-41 catalyst. The chapter is divided into three sections:

3.1. Friedel-Crafts benzylation of toluene by benzyl chloride and benzyl alcohol.

3.2. Mukaiyama-Michael reaction between silyl enol ether and α, β-unsaturated carbonyl compound.

3.3. Mukaiyama-aldol condensation of aldehyde with silyl ketene acetal / silyl enol ether.

Chapter 4 presents the catalytic activity of carbon-carbon bond formation reactions by using organo-functionalized Zr-TMS-TFA catalyst. This chapter includes the following two sections:

4.1. Michael-addition of indole to α,β-unsaturated carbonyl compound.

4.2. Synthesis of coumarin by Pechmann reaction.

Chapter 5 presents the catalytic activities of carbon-carbon bond formation reaction such as Michael-addition of β-nitrostyrene to malonate catalyzed by SBA-15-TBD.

Chapter 6 provides summary and conclusion

6.2. CONCLUSIONS

6.2.1. Synthesis and Characterization

❖ Highly ordered Ce-Al-MCM-41 catalyst was synthesized using hydrothermal method. N_2 adsorption experiments showed type IV isotherms characteristics of mesoporous materials. X-ray diffraction patterns confirmed the formation of MCM-41 structure and no CeO_2 phase was found in all the Ce-containing samples such as Ce-MCM-41 and Ce-Al-MCM-41 samples. Further, all the Ce-Al-MCM-41 samples were found to be EPR inactive, indicating the incorporation of Ce as Ce^{4+} ions and not as Ce^{3+} ions. The oxidation state of Ce^{4+} was also confirmed by XPS and DRIFT UV-*Vis* measurements. The solid state ^{29}Si CP MAS NMR spectra of Ce-Al-MCM-41 samples showed the presence of more Q^4 than Q^3 species. The solid state ^{27}Al MAS NMR spectra

of Al-MCM-41 and different Ce-Al-MCM-41 samples revealed the presence of Al in tetrahedral position and the absence of octahedrally coordinated Al sites. The detailed quantitative Lewis and Brönsted acid sites of Ce-Al-MCM-41 samples were calculated by pyridine-FTIR spectroscopy and the total acidity of the Ce-Al-MCM-41 samples was determined by TPD-ammonia.

❖ Zr-TMS catalysts have been synthesized by sol-gel method. The template was extracted from the synthesized materials by using ethanol and HCl at 353 K. The extracted Zr-TMS was further successfully functionalized with triflic acid (TFA) by post synthesis treatment to obtain covalently-bonded Zr-TMS-TFA catalysts. Dfferent amount of triflic acid was loaded over Zr-TMS catalyst (Zr-TMS-TFA). Functionalized amorphous (Zr-TMS-TFA-A) catalyst was also synthesized and characterized for comparison. All the samples in general were found to be in agreement with previous values reported for mesoporous ZrO_2 and show type IV isotherm characteristics of mesoporous materials. The TPD-ammonia (TPD-NH_3) measurements showed that the catalysts were highly acidic. The solid state ^{13}C CP MAS NMR and FTIR revealed that the $–CF_3$ group remained intact in the material. The XPS measurement showed peak broadening and shift in the binding energies of zirconium 3d, silicon 2p, carbon 1s, sulfur 2p (both sulfide and sulfate sulfur) lines in the case of Zr-TMS-TFA catalysts.

❖ Organic-inorganic hybrid materials such as immobilization of 1,5,7-triazabicyclo [4.4.0] dec-5-ene (TBD) over SBA-15 materials have been successfully synthesized by a facile two-step route. The XRD and isotherm shows the presence of mesoporosity SBA-15-TBD samples. The presence of Q^4, Q^3 and T^2, T^3 species in solid state ^{29}Si CP MAS NMR indicates complete

immoblizatioin of 1,5,7-triazabicyclo [4.4.0] dec-5-ene group on mesoporous materials. The FT-IR and solid state ^{13}C CP MAS NMR spectra of SBA-15-TBD sample shows that coordination of TBD with SBA-15 material. The microscopy studies also reveal that the morphology and hexagonal structure of mesporous SBA-15-TBD catalyst remain unchanged.

6.2.2. Catalytic Activities

❖ Friedel-Crafts benzylation (alkylation) reaction was carried out using Ce-Al-MCM-41 samples. The benzylation of toluene with benzyl chloride and benzyl alcohol was chosen as a model catalytic reaction for distinguishing the Lewis and Bronsted acidity in the Ce-Al-MCM-41 catalysts where benzyl chloride and benzyl alcohol were used as alkylating agent. Both the reactions were carried out in the solvent free system. The main products in both the cases are 1, 4-methyldiphenylmethane (1, 4-MDPM) and 1, 2-methyldiphenylmethane (1, 2-MDPM). However, in the case of Lewis acid catalyzed route (using benzyl chloride) the small amount of 1-benzyl-3- (4-methyl benzyl) benzene (BMBB) and methylphenylbenzyl chloride (MPBC) is also obtained. In the case of Brönsted acid catalyzed benzylation of toluene with benzyl alcohol the main side product formed is dibenzyl ether (DBE) along with minor amount of methylphenylbenzyl alcohol (MPBA). In both the cases, the total (benzyl chloride or benzyl alcohol) conversion and selectivity of MDPM was found to increase with temperature. The selectivity of BMBB and DBE was decreased with the increasing temperature. Similarly, there was no selectivity observed in MPBC and MPBA at higher temperature. The interesting result is that no conversion was obtained on Ce-MCM-41 for Brönsted acid catalyzed benzylation of toluene with benzyl alcohol. Further, this result is supported by

pyridine-IR study, where no Brönsted peak was found in the Ce-MCM-41 sample.

❖ The catalytic activities were examined in Mukaiyama-Michael reaction by using Ce-Al-MCM-41 sample. The Mukaiyama-Michael reaction of 1-phenyl-1-(trimethylsilyloxy) ethylene and 2-cyclohexen-1-one was chosen for model catalytic reaction. The product selectivity was found to be ~ 100 %. The different solvents were employed for this particular reaction at 313 K and among them dry dichloromethane showed better activity. Effect of different substrates were also examined and among them high conversion was obtained for reaction between 1-phenyl-1-(trimethylsilyloxy) ethylene and benzylideneacetophenone. In the recycle study, the conversion decreases from 85 to 81 % in 1st recycle and then it was stabilized *ca.* 78 % in the 4th recycle.

❖ Ce-containing Al-MCM-41 samples exhibit promising catalytic activity in Mukaiyama-aldol condensation of methyl trimethylsilyl dimethylketene acetal with benzaldehyde in the liquid-phase system. The product selectivity was found to be ~ 100 %. The different solvents were employed for this particular reaction at 313 K and among them dry dichloromethane showed better activity. The Mukaiyama-aldol condensation of methyl trimethylsilyl dimethylketene acetal with benzaldehyde was also carried out under solvent free condition at 313 and 373 K. Out of these two temperatures, the highest activity was observed at 373 K. The catalyst was successfully used for six consecutive times with no significant loss in catalytic activity. Various substrates were examined for Mukaiyama-aldol condensation. Among them, reaction between methyl trimethylsilyl dimethylketene acetal and 4-nitrobenzaldehyde produced more aldol product.

❖ Michael-addition of indole to enone was performed on Zr-TMS and Zr-TMS-TFA catalysts under solvent free system at 353 K. The Michael product of C-adduct and N-adduct could be differentiated by ^{1}H NMR spectroscopy. The high selectivity of C-adduct was obtained at higher loading of triflic acid over Zr-TMS catalyst. For comparison purpose, Michael-addition of 3-methylindole with cyclohexenone was carried out over amorphous Zr-TMS-TFA-25-A catalyst and homogeneous triflic acid under identical reaction condition. In both cases, less selectivity was observed towards the C-adduct product compared to Zr-TMS-TFA ordered mesoporous materials. The stability and recyclibility of the catalyst was checked in the Michael-addition of 3-methylindole with cyclohexenone by using Zr-TMS-TFA-25 catalyst. The catalyst was used for four consecutive times. The conversion and the product selectivity for C-adduct marginally decreased during catalyst recycle, mainly due to partial leaching / breaking of the TFA. The Michael-addition was also examined for different substrates on Zr-TMS-TFA-25 catalyst in the identical reaction condition. Among investigated substrates, the highest conversion was obtained for Michael-addition of 5-nitroindole and 3-methyl pent-3-ene-2-one under solvent free system over Zr-TMS-TFA-25 catalyst. In this case, the selectivity of C-adduct product was found to be ~100 %.

❖ Pechmann reaction of phenol and ethyl acetoacetate was carried for the synthesis of coumarin over Zr-TMS and Zr-TMS-TFA catalysts under solvent free system at 373 K. The high conversion was obtained at the higher loading of triflic acid over Zr-TMS catalyst. The product selectivity of coumarin was found to be ~ 100 % in each case while less than 100 % was observed in the case of triflic acid. The catalyst (Zr-TMS-TFA-25) was used successfully for

four consecutive recycle with marginal loss of catalytic activity along with 100 % product selectivity. The highest conversion was obtained for Pechmann reaction of 1, 3, 5-trihydroxy phenol and methyl acetoacetate over Zr-TMS-TFA-25 catalyst under solvent free system under identical reaction condition.

❖ SBA-15-TBD sample exhibit promising catalytic activity in Michael-addition of β-nitrostyrene to diethyl malonate in the liquid-phase system at 373 K. The catalyst (SBA-15-TBD) was used successfully for three consecutive recycles with no significant loss of catalytic activity and also retaining 100 % product selectivity. The highest conversion was obtained for Michael-addition of p-Cl-nitrostyrene with dimethyl malonate over SBA-15-TBD catalyst under solvent free system in the identical reaction condition.

PUBLICATIONS /

SYMPOSIA /

CONFERENCES

LIST OF PUBLICATIONS

1. Synergistic role of acid sites in the Ce-enhanced activity of mesoporous Ce-Al-MCM-41 catalysts in alkylation reactions: FT-IR and TPD-ammonia Studies.

    P. Kalita, N. M. Gupta, R. Kumar, **J. Catal. 245 (2007) 338-247.**

2. Optimal synthesis parameters and application of Sn-MCM-41 as an efficient catalyst in solvent-free Mukaiyama-type aldol condensation.

    T. Gaydhankar, P. N. Joshi, **P. Kalita,** R. Kumar, **J. Mol. Catal. A: 265 (2006) 306-315.**

3. Ce-Al-MCM-41: An efficient catalyst for Mukaiyama-Michael reaction

    P. Kalita, R. Kumar, **Stud. Surf. Sci. Catal. 170 (2007)1161-1166.**

4. Hydrothermal synthesis, characterization and catalytic application of mesoporous Sn-MCM-48 molecular sieves in solvent-free Mukaiyama-type aldol condensation reaction.

    U. S.Taralkar, **P. Kalita,** P. N. Joshi, R. Kumar, **(Revision submitted to J. Mol. Catal. A).**

5. Mukaiyama-aldol condensation catalyzed by Ce-Al-MCM-41 mesoporous materials under solvent free condition.

    P. Kalita, N. M. Gupta, R. Kumar **(Communicated to J. Catal.).**

6. Michael addition of Indole to α,β -unsaturated carbonyl compound over organofunctionalized heterogeneous system in solvent free system.

    P. Kalita and R. Kumar **(To be communicated).**

7. Synthesis of coumarins by Pechmann reaction under organofunctionalized heterogeneous system in solvent free system.

    P. Kalita and R. Kumar **(To be communicated).**

8. Base catalyzed Michael-addition of β-nitro styrene to malonate under solvent free system.

    P. Kalita and R. Kumar **(To be communicated).**

195

PAPER PRESENTED AT NATIONAL / INTERNATIONAL SYMPOSIA / CONFERENCES

1. Ce-enhanced catalytic activity of mesoporous Ce_xAl_yMCM-41for alkylation of toluene: Role of acid sites.

   Pranjal Kalita, Narendra M. Gupta, R. Kumar

   Catalysis for Future Fuels"18th National symposium & Indo-US Seminar on Catalysis, 16 – 18 April 2007, Indian Institute of Petroleum (IIP), Dehradun. (Poster Presentation).

2. Ce-Al-MCM-41: An efficient catalyst for Mukaiyama-Michael reaction

   Pranjal Kalita and Rajiv Kumar, **15th International Zeolite Conference**

   12-17 August 2007, Beijing, China. (Accepted for Oral Presentation).

3. Study of mesoporous Ce_xAl_yMCM-41 catalyst by pyridine-IR and TPD: Catalytic acitivity for alkylation of toluene.

   Pranjal Kalita, Narendra M. Gupta, R. Kumar.

   Organized by "**NCL in Science Day", 22nd February 2007, National Chemical Laboratory, Pune, India (Poster presentation).**

4. Cerium containing Al-MCM-41: An efficient catalyst for Mukaiyama-Michael reaction.

   Pranjal Kalita and Rajiv Kumar.

   Organized by **"NCL in Science Day ", 27-28th February 2006, National Chemical Laboratory, Pune, India (Poster presentation).**

5. Enantioselective hydrogenation of carbonyl compounds by "heterogenized" transition metal   Complexes.

   Anirban Ghosh, **Pranjal Kalita** and Rajiv Kumar.

   7th National Symposium in Chemistry, Organized by **"Chemical Research Society of India", 4-6th February 2005, Indian Association for the Cultivation of Science, Calcutta, India (Poster presentation).**

6. "International Conference on Catalysis in Organic Synthesis New horizons"

   3rd to 4th August, 2004, Indian Institute of Chemical Technology, Hyderabad, India.